ERRATUM

Title of ETD:

Mechanical and Morphological Characterization of Full-Culm Bamboo

Name of Author:

Yusuf Akinbade

Description of Correction(s):

Due to an error in data curation, some values of beta in the dissertation were reported incorrectly as follows:

Table F4: Sample PE2E2; beta = 0.75
Table F11: PB2C2, PB1C9 and PB3E5: beta = 0.75
Table F15: PN3C1: beta = 0.75
Table F19: PM2A3, PM2E3, PM3F1, PM3F9, PM1B1 and PMIC8: beta = 0.75
Table F23: BS1D7 and BS2E1: beta = 0.75
Table F23: BS3D11 and BS3E4: beta = 0.80

These corrections result in the need to revise some entries in Table 3.2 and to replot Figure 3.7. The corrections have only a marginal impact on the reported data and no impact on the trends, discussion and/or conclusions of the work.

Original dissertation: http://d-scholarship.pitt.edu/38530/

Christy Kohser 9/16/21

Graduating School Approval Date Initialed

Amanda Godley/JLW 10/15/21

Office of the Provost Approval (Month/Day/Year) Date Initialed

University of Pittsburgh

Mechanical and Morphological Characterization of Full-Culm Bamboo

by

Yusuf Akintayo Akinbade

BEng, University of Southampton, UK 2010

MSCE, Purdue University, USA 2011

Submitted to the Graduate Faculty of

Swanson School of Engineering in partial fulfillment

of the requirements for the degree of

Doctor of Philosophy

University of Pittsburgh

2020

UNIVERSITY OF PITTSBURGH

SWANSON SCHOOL OF ENGINEERING

This dissertation was presented

by

Yusuf Akintayo Akinbade

It was defended on

March 6, 2020

and approved by

Dr. Christopher M. Papadopoulos, Ph.D., Professor, Department of Engineering Sciences and Materials, University of Puerto Rico, Mayagüez

Dr. John Brigham, Ph.D., Professor, Department of Engineering, Durham University, UK

Dr. Amir H. Alavi, Ph.D., Assistant Professor, Department of Civil and Environmental Engineering

Dr. Ian Nettleship, Ph.D., Associate Professor, Department of Mechanical Engineering and Materials Science

Dissertation Director: Dr. Kent A. Harries, Ph.D., Professor, Department of Civil and Environmental Engineering

Mechanical and Morphological Characterization of Full-Culm Bamboo

Yusuf Akintayo Akinbade, Ph.D.

University of Pittsburgh, 2020

Full-culm bamboo that is bamboo used in its natural, round form used as a structural load-bearing material, is receiving considerable attention but has not been widely investigated in a systematic manner. Despite prior study of the effect of fiber volume and gradation on the strength of bamboo, results are variable, not well understood, and in some cases contradictory. Most study has considered longitudinal properties which are relatively well-represented considering bamboo to be a unidirectional fiber reinforced composite material governed by the rule of mixtures. Despite the dominance of transverse failure (splitting) of bamboo in load-bearing applications, very little study of bamboo transverse properties has been conducted. The objective of this work is therefore to develop a framework and the tools required to evaluate the material and mechanical properties of full-culm bamboo. The study focuses on transverse properties and recognizes that bamboo is a heterogeneous highly orthotropic functionally graded material rather than a homogeneous fiber-reinforced composite as is often assumed. This framework brings together work conducted in the area of bamboo geometric, morphologic and material characterization to develop a correlation with mechanical properties. The effect of fiber volume ratio and gradation in the bamboo cross-section in the characterization is studied and used as a basis to establish materials- and mechanics-based constitutive models for the behavior of full-culm bamboo. The impact of material variability and uncertainty in the mechanical behavior of the full-culm is investigated and included in the presented models. Experimental, imaging and numerical results from this study indicate that considering the

transverse behavior of bamboo as a fiber-reinforced material, governed by the rule of mixtures, is not appropriate. The scope of the work focuses on materials test specimens. This is believed to be the scale at which internal heterogeneity of the bamboo effects experimentally determined data and is also a scale at which complex modeling is still appropriate. The models developed in this work have two primary and related uses: 1) providing a platform for researchers to better understand the results of bamboo material property tests; and 2) providing a platform against which to validate macroelement models suitable for structural evaluation and design.

This is a correction to the original version. For information about the changes made, please see the erratum.

Table of Contents

List of Tables

List of Figures

Acknowledgement

Surely, it is only a journey that has not begun that would not come to an end someday. The end of one is however only a beginning to another. First and foremost, I would like to dedicate this particular journey to Almighty Allah who has made it possible for me to complete this chapter of my life.

My greatest appreciation goes to Dr. Kent Harries who has been more than an advisor but also a mentor to me during the progress of this work. His untiring support and guidance has pushed me to continuously seek excellence in all actions. I would like to also appreciate the advice and support received from my committee members, Dr. Nettleship, Dr. Papadopoulos, Dr. Brigham and Dr. Alavi. It was great to know that I could always count on them.

A special thank you goes to my wife, Mujeebat, for her utmost support, love and patience as I navigated through this journey. I appreciate my parents for their prayers and advice, which has constantly steered me on the right path. I cherish my friends and siblings who stood by me and kept me motivated during the tough times. It has been a pleasure working alongside great friends and colleagues in the laboratory as well. A special thank you to Charles Hager, Abdullah Alabdulkarim, Chelsea Flower, Shawn Platt, Tianqiao Liu, Chuyuan Zheng and Chase Rogers for their contributions along the way.

1.0 Introduction

1.1 Motivation

Full-culm bamboo – that is, bamboo used in its natural, round form rather than being processed into an engineered material – used as a structural load-bearing material is receiving considerable attention but has not been widely investigated in a systematic manner. Nonetheless, over one billion people are estimated to live in 'traditional' or vernacular bamboo housing while another 2.5 billion people depend economically in some way on bamboo [FAO 2007]. The use of bamboo in modern construction ranges from use in its natural full-culm form to its use in engineered materials including laminated lumber and panels, and 'strand' boards. Van Der Lugt *et al.* [2003] suggested that bamboo, as a fast-growing renewable material with a simple production process, is a sustainable alternative to more conventional materials like concrete, steel and timber. Despite its availability, sustainability and, in some cases, superior mechanical properties, bamboo is rarely considered by engineers as a building material. This is largely due to the significant gap in data availability and understanding of the material properties and behavior of bamboo; this gap serves as a primary motivation for this study.

1.2 Bamboo as a Natural Resource for Construction

The application of bamboo as a structural material has varied across species. Two of the most common commercially available species are *Phyllostachys Edulis* (Moso) in China and *Guadua Angustifolia Kunt* (Guadua) in Latin America. However, other locally available species have been used traditionally as structural members in one-storey houses, short span foot bridges, long span roofs and construction platforms in countries with plentiful bamboo resources [Chung and Yu 2002]. The mechanical properties of bamboo in many construction applications are believed to be similar to, if not superior to those of structural timber. Structural use of bamboo, however, is limited by the lack of design guidance and standards. Standards bring together mechanical properties and structural adequacy for use as a modern construction material. Despite the lack of formal design documents, bamboo is gaining interest as a material which could successfully serve as a substitute for structural timber [Chung and Yu 2002].

One major advantage which could contribute to the adoption of bamboo is its quick time of growth to full strength which has been reported to be as short as 3 to 6 years from cultivation to harvest [Lo *et al.* 2004; Yu *et al.* 2003; Yu *et al.* 2011a]. Woody bamboos have characteristics that make them unique and a potentially important non-timber resource suitable for structural load-bearing applications. In order to better highlight the unique characteristics of bamboo, it is compared with trees, i.e. (wood) in Table 1.1 [Clark *et al.* 2015].

Table 1.1: Comparison between bamboo and trees (wood) [Clark *et al.* 2015].

Bamboo	Trees (wood)
Underground parts consisting of rhizomes	Underground parts consisting of roots
Culms (stems) usually hollow and segmented	Stems solid and not segmented
The hardest part of the culm is the periphery	The hardest part of the stem is in the center
There is no vascular cambium so the culm does not increase in diameter with age	A vascular cambium is present so the stem increases in diameter with age
The conducting tissues, phloem and xylem, are together inside each vascular bundle	The conducting tissues, phloem and xylem, are separated by the vascular cambium
Culms lack bark	Stems have bark (cork + 2° phloem)
No radial (lateral) communication in the culms except at the nodes	Radial (lateral) communication throughout the stem
Culms grow extremely fast (to as much as 36 m tall at 6 months), reaching full height in one growing season	Stems grow slowly in height and diameter over many seasons
Culms grow in an association from a network of rhizomes, such that each culm depends on the others and the harvest of a culm directly affects the rest of the community	Each stem usually grows as an independent individual, and the harvest of a stem does not directly affect the rest of the community
Entire community flowers once (typically after decades of growth) and the entire community dies	Individuals typically flower annually without affecting the community

1.3 Taxonomy of Bamboo

Bamboo forms a unique part of the group of giant grasses, which are native to all continents except Europe and Antarctica. Most of the identification keys are based on floral characteristics, which only occur at the end of a bamboo plant's lifespan of about 20 to 40 years [Liese 1987].

Bamboo belongs to the subfamily *Bambusoideae*, one of 12 in the grass family *Gramineae (Poaceae)*, and has about 90 genera [FAO 2007]. A recent survey reported that there are more than 1600 species, widely distributed in tropical and subtropical regions of the world [Vorontsova *et al.* 2016; Clark *et al.* 2015]. According to the BPG [2012], bamboos can be subdivided into three tribes: *Arundinarieae* (temperate woody bamboos), *Bambuseae* (tropical woody bamboos), and *Olyreae* (herbaceous bamboos). However, the relationships between these three lineages are not known with certainty.

The division into tribes is the result of continuing work of research dating back to the first reported uses of bamboo in arts and technology by early Chinese scholars at a time when taxonomic studies were dominated by the Western world [Soderstrom 1985]. The first modern classification of bamboo came with Holttum [1956], who proposed a classification scheme for bamboos based on perceived evolutionary trends. This was followed by the work of McClure [1966], which pointed out that all parts of the vegetative and the flowering structures should be used for bamboo classification. Clark *et al.* [2015] reviewed the evolution of bamboo classification up until the use of molecular sequence data.

DNA sequence data in combination with morphological and anatomical studies form the basis of the most recent comprehensive and phylogenetically-based classification system for bamboos. In more recent times, there have been several compendiums of bamboos from various parts of the world. This includes bamboo from China [Zhu *et al.* 1994 and Yi *et al.* 2008], India [Seethalakshmi and Kumar 1998], the Americas [Judziewicz *et al.* 1999], Malaysia and South East Asia [Dransfield 1992, 1998; Dransfield and Widjaja 1995; Stapleton 1994a, 1994b, 1994c; Widjaja 1987 and Wong 1993, 1995, 2005] and of the world [Ohrnberger 1999]. Canavan *et al.* [2017] reported the distribution of bamboo species found in countries and islands with highest

bamboo diversity in the world (Figure 1.1). Canavan *et al.* excluded regions with less than 15 species and classified the findings into species being native, introduced or invasive to the location.

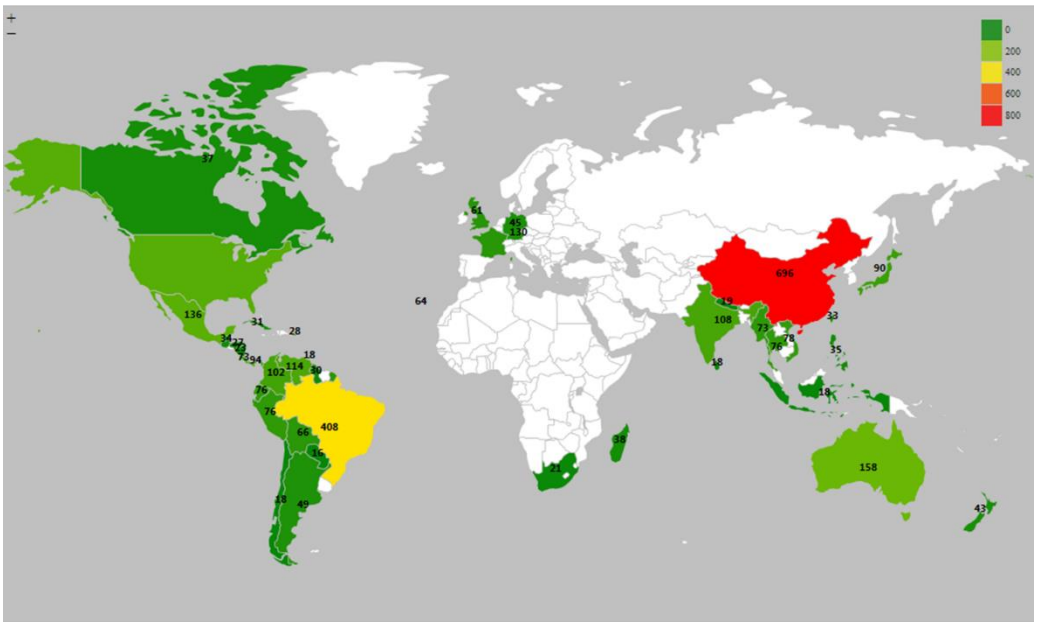

Figure 1.1: Number of bamboo species found in 52 countries and islands with the highest bamboo diversity. Data from Canavan *et al.* [2017]

1.4 Bamboo Morphology and Microstructure

Bamboo macrostructure consists of a hollow cylindrical shoot, known as the culm (Figure 1.2a). The culm is divided by solid nodes, which are oriented transversely through its cross section, into internodes consisting of a hollow tube (surrounding the lacuna) with axially oriented cells. At each node, a diaphragm is formed at the interior of the culm while the culm-sheath and branches form at the exterior.

Culm development occurs in two phases: first, new, unbranched shoots bearing culm leaves develop to their full diameter and height; culm leaves provide protection and initial support for the

unlignified culm. Culm lignification and branch development with production of foliage then takes place [Liese and Kohl 2015]. It is only after the second phase – through lignification – that bamboo attains material properties suitable for load-bearing applications.

Bamboo is a functionally graded hierarchical bio-composite [Amada *et al.* 1996; Ghavami *et al.* 2003] comprising three fundamental tissues: epidermis, vascular bundles and parenchyma ground tissue. The epidermis is a silica-rich layer comprising the outer wall of the bamboo, which provides environmental protection to the plant (and causes considerable wear on tool blades used to process bamboo). The vascular bundles are the longitudinal tissues supporting the culm, and the ground parenchyma occupies the rest of the culm section [Habibi and Lu 2014]. The majority of a bamboo culm section is a composite of vascular bundles embedded in a matrix of parenchyma cells [Liese 1998].

The vascular bundles are composed of metaxylem vessels and sheaths of sclerenchyma fibers. These can be visibly distinguished from the surrounding parenchyma ground tissue in which they typically appear dark in contrast. Micrographic images of a typical [*P. edulis*] bamboo culm wall with its different constituents are shown in Figures 1.2b-d. The sclerenchyma fibers are the main longitudinal load-carrying component determining the mechanical characteristics of bamboo. The parenchyma tissue takes the role of the composite matrix: providing stability to the fibers and transmitting load between them. In the vascular bundle, the phloem vessels transport sugars and nutrients and the xylem and metaxylem vessels transport water. In view of macro-mechanical behavior, bamboo is most often described as a unidirectional fiber reinforced composite material. Its mechanical properties depend on the mechanical characteristics of its components, as well as on its microstructural characteristics, such as the volume fraction and distribution of sclerenchyma fibers, and the interface properties of the various bamboo components [Shao *et al.* 2010].

An important aspect of bamboo morphology is the graded nature of the fiber distribution in the culm wall as seen in Figure 1.2b. Gradation of constituent materials and material properties are a focus of this work and are described at length in Chapter 3.

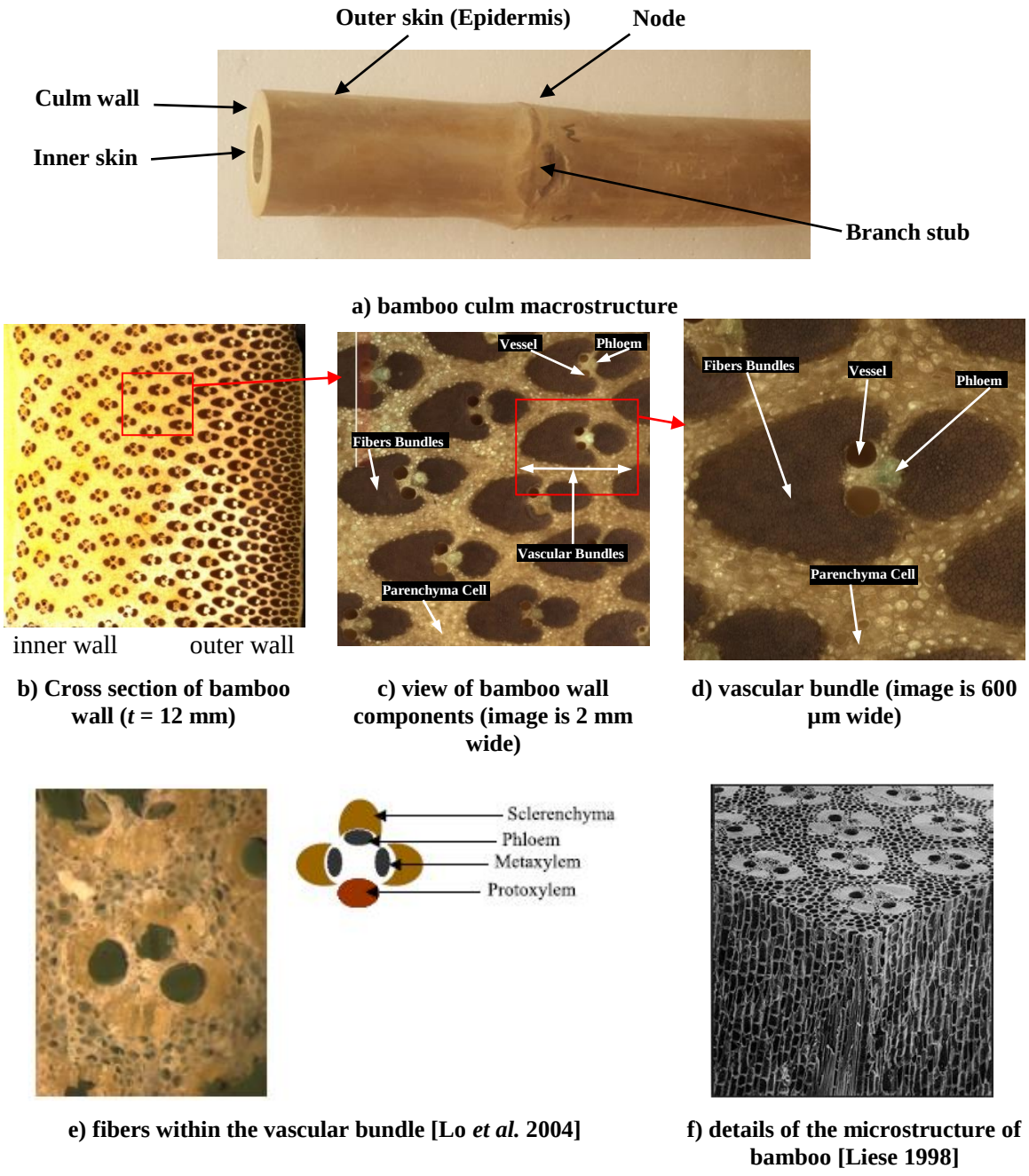

a) bamboo culm macrostructure

b) Cross section of bamboo wall (*t* = 12 mm)

c) view of bamboo wall components (image is 2 mm wide)

d) vascular bundle (image is 600 µm wide)

e) fibers within the vascular bundle [Lo *et al.* 2004]

f) details of the microstructure of bamboo [Liese 1998]

Figure 1.2: Structure of a bamboo culm

1.5 Numerical Study and Modelling of Bamboo

Study of bamboo using the finite element method (FEM) is limited. Much work in the area of modeling natural materials and natural fibers tends to focus on simplified analytical models; that is, using macroelements that capture the bulk behavior of the material. This approach is likely appropriate when considering engineering structures but may be inadequate when considering materials test methods which use small specimens and are influenced by multiple local effects [e.g., Richard and Harries 2015].

In general, Amada *et al.* [1996] suggested that bamboo can be modeled as a fiber-reinforced composite cylinder with a hollow cross section having circular discs inserted as nodes. The function of the nodes is reported to be the prevention of culm-wall buckling. Additionally, the nodes also play the role of arresting longitudinal cracks; i.e., preventing splitting cracks from propagating across multiple internodes.

FE have been used to model bamboo for different applications. Tan *et al.* [2011] applied a 2-D model in *ABAQUS* (using CPE8 eight-node plane strain elements) to calculate the energy release rate for single edge notched flexural specimen crack growth. The actual load, crack length and varying values of Young's Modulus (obtained from nanoindentation) were used in the modelling. The values of Young's Modulus were found to decrease with radial distance from the outside surface of the culm wall. The results however were not validated and a conclusion indicating the need for further study to better understand the behavior of many species of tropical and subtropical bamboo was made. The author of this dissertation has some reservations regarding the utility of the nanoindentation technique to measure Young's modulus considering the soft nature of the parenchyma cells in the wall structure shown in Figure 1.2. This will be discussed further in Chapter 3.

Silva *et al.* [2006] used FE and homogenization to investigate the structural behavior of bamboo. They concluded that such an approach could not predict the effects of local features such as stresses near supports suggesting that their approach is unsuited to modeling materials test specimens. They identify the need to model the fiber volume gradient, suggesting that it was necessary to employ a numerical procedure that accurately models material gradients through the culm wall. Kim and Paulino [2002] had proposed to model a functionally graded material using graded elements, which incorporate actual material properties at integration points and continuous material distribution into the numerical simulation leading to smoothly varying and more accurate stresses Modelling bamboo in this manner will be described in greater detail in Chapter 6.

No known studies have addressed the uncertainty associated with modeling bamboo – a natural, and therefore highly variable material. This study will attempt to address this shortcoming using a random fields approach [Alder and Taylor 2010] which has been applied to a number of engineering problems which exhibit high variability and spatial gradation, including pavement [Caro *et al.* 2014], soils [Kim 2005] and ground water modelling [El-Kadi and Williams 2000]. This will be described in Chapter 5.

1.6 Objective and Organization of Study

Despite prior study of the effect of fiber volume ratio and gradation on the strength of bamboo, results are variable, not well understood, and in some cases contradictory. Additionally, most work has been conducted on a limited number of bamboo species, requiring extrapolation and judgement to extend results to other bamboo species or even to the same species harvested in a different location. The objective of this study is therefore to develop a framework and the tools

required to evaluate the material and mechanical properties of bamboo in its full-culm form. This framework will bring together work conducted in the area of bamboo characterization to develop a correlation with the mechanical properties.

Bamboo characterization is studied focusing on culm-wall geometry and composition and its effect on mechanical properties and characterization (Chapter 2). The effect of fiber volume distribution on the characterization will be studied (Chapter 3) and used as a basis to establish materials and mechanics-based constitutive models for the behavior of full-culm bamboo (Chapter 6). The impact of material variability (Chapter 4) and uncertainty (Chapter 5) in modeling the mechanical behavior of the full-culm will be investigated and is included in the proposed models. Each chapter contains a review of relevant literature.

The scope of the work presented focuses on materials test specimens. This is believed to be the scale at which internal heterogeneity of the bamboo affects experimentally-determined data and is also a scale at which complex modeling is still appropriate. The models developed in this work will have two primary and related uses: 1) providing a platform for researchers to better understand the results of bamboo material property tests; and 2) providing a platform against which to validate macroelement models suitable for structural evaluation and design.

This dissertation identifies gaps in the present knowledge of bamboo and its use as a construction material. The framework and tools this study aims to generate are expected to be made globally available in the research community such that they will fill gaps in knowledge and provide a new tools with which bamboo can be identified and represented going forward. Achieving this relies upon having an adequate understanding and the resources needed to simplify the processes. It is of great importance to the author that the output of this work creates a platform

that simplifies the characterization of full-culm bamboo in a way that can be used in the field and by anyone with minimal training.

1.7 Nomenclature

The following nomenclatures are used throughout this dissertation. Figure 1.3 defines some of the parameters and culm orientation.

a	shear span of the flat ring flexure test specimen
A	cross sectional area of the culm calculated from the average diameter, D
$\mathbf{A}$	covariance matrix of the random field (Eq. 5-2)
b	function of the location of the strip within the culm wall (Eq. 4-1)
$\mathbf{C}$	lower triangular autocorrelation matrix obtained from **A** (Eq. 5-2)
D	average culm diameter
D_1	major axis culm diameter (oval culm shape)
D_2	minor axis culm diameter (oval culm shape)
d_o	ovality (Table 6.1)
$d^r_{i,j}$	radial component of distance between points i and j
E_f	modulus of elasticity of bamboo fiber
EI	flexural stiffness of full-culm bamboo (i.e., modulus multiplied by moment of inertia)
E_i	flexural modulus at the innermost layer of bamboo strip
E_L	modulus of elasticity in longitudinal direction
E_m	modulus of elasticity of bamboo matrix (parenchyma)
$E_{m,90}$	circumferential modulus of elasticity perpendicular to the fibers
E_o	flexural modulus at the outermost layer of bamboo strip
E_T	modulus of elasticity in transverse direction
$\mathbf{E_{T,mean}}$	mean vector of experimentally measured E_T for the discretized space
$\mathbf{E_{T,rand}}$	vector containing the values of E_T for the discretized space considered
$f_{c,0}$	compression strength parallel to culm longitudinal axis
$f_{m,90}$	apparent bending strength perpendicular to the fibers

$f_{mC,90,EW}$	bending strength perpendicular to the fibers at the inner culm wall in E-W quadrant
$f_{mC,90,NS}$	bending strength perpendicular to the fibers at the outer culm wall in N-S quadrant
$f_{mT,90,EW}$	bending strength perpendicular to the fibers at the outer culm wall in E-W quadrant
$f_{mT,90,NS}$	bending strength perpendicular to the fibers at the inner culm wall in N-S quadrant
f_r	transverse modulus of rupture
$f_{r\alpha}$	transverse modulus of rupture of control sample
f_v	in-plane shear strength
G	shear modulus
h	estimate of neutral axis location for a curved beam in flexure (Eq. 2-12)
H	specimen length (height) in culm longitudinal direction
k	fitting factor for the gradation of volume fraction (Eq. 3-6)
k_1	factor accounting for axial stress and shear deformation in circumferential compression test (Eq 2-6)
k_2	factor accounting for axial stress deformation in circumferential compression test (Eq 2-7)
K	stiffness matrix elasticity tensor
L_r	correlation distance or length
m	variation of the fiber volume through the strip dimension x (Eq. 4-1)
MC	moisture content
M_{EW}	bending moment in circumferential compression test E-W quadrant (Eq. 2-8)
M_{NS}	bending moment in circumferential compression test N-S quadrant (Eq. 2-10)
n	no. of samples
N[0,1]	vector of normally distributed random values between 0 and 1
P_{20}	applied load at $0.2P_{ult}$
P_{60}	applied load at $0.6P_{ult}$
P_{ult}	ultimate applied load
$R = 0.5(D-t)$	radius at the centreline of the culm wall
$R_i = 0.5D - t$	radius at the inner surface of the culm wall
$R_o = D/2$	radius at the outer surface of the culm wall
$S = 0.85D$	Flat ring flexure test span
t	average culm wall thickness
t_N	wall thickness at North quadrant of culm

t_S	wall thickness at South quadrant of culm
V_f	volume fraction of fibers
W	weight of test specimen
x	normalised culm wall thickness ($x = 0$ at inner culm wall surface)
α	fraction of thickness of clipped bamboo at North and South quadrants
β	fraction of wall thickness removed at outer culm wall in clipped flat-ring flexure
γ	fraction of wall thickness removed at inner culm wall in clipped flat-ring flexure
δ	displacement of the applied load
Δ_{20}	relative vertical deflections between the loaded points (N-S) of the circumferential compression test determined at $0.2P_{ult}$
Δ_{60}	relative vertical deflections between the loaded points (N-S) of the circumferential compression test determined at $0.6P_{ult}$
ε_{xx}	strain measured in horizontal direction
ε_{yy}	strain measured in vertical direction
ξ	Halpin-Tsai empirical constant (Eq. 3-5)
ρ_{12}	density of bamboo normalized for 12% moisture content
ρ_{ij}	autocorrelation function between each couple of spatial points i and j
σ	standard deviation
σ_f	strength of bamboo fiber
σ_m	strength of bamboo matrix (parenchyma)
σ_{xx}	stress measured in horizontal direction
σ_{yy}	stress measured in vertical direction

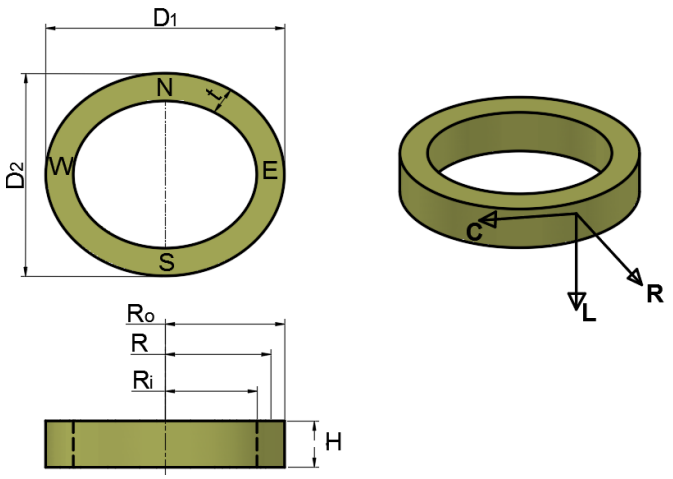

Figure 1.3: Full-Culm specimen geometry notation

2.0 Mechanical Characterization of Full-Culm Bamboo

2.1 Materials Tests for Bamboo

There are different test methods used to determine the mechanical properties of bamboo. Harries *et al.* [2012] summarized existing well-established tests, most of which are included in the newly revised International Organization for Standardization (ISO) model standard, ISO 22157:2019 *Bamboo structures – Determination of physical and mechanical properties of bamboo culms*. Characteristic material properties[1] are then adopted in the bamboo structural design standard ISO 22156:2004 *Bamboo - Structural design*[2]. Current ISO 22157:2019 standard tests for mechanical properties include: compression parallel to fibers, tension parallel and perpendicular to fibers, shear parallel to fibers, bending parallel and perpendicular to fibers. There are limitations to each test method [Harries *et al.* 2012] and the methods are being continually refined (e.g., Richard and Harries [2015] impact on 2019 revisions of tension test method). An important aspect to consider when specifying tests is the ease with which they may be conducted in the field and/or in less developed regions where bamboo is harvested and used. Tension-based tests are not as easy to conduct as compression-based testing which usually requires simpler fixtures and no complex gripping methods [Harries *et al.* 2012].

[1] Characteristic strength properties for bamboo are presently defined as the 5th percentile capacity determined with 75% confidence. Characteristic modulus is defined as the mean modulus determined with 75% confidence [ISO 22156:2004 and :2019].

[2] ISO 22156:2004 is in the process of complete revision. Dr. Harries leads this effort. Where possible, reference to the revised version will be made in this dissertation and designated ISO 22156 [2019]. The revision is not likely to be published before late 2021.

Longitudinal splitting is a dominant failure mode of bamboo. Such failures are associated with bamboo carrying flexure, compression or tension loads and are exacerbated by many common connection details [Sharma 2010]. Transverse culm behavior has not been fully addressed in existing ISO standard tests and the need for additional work in this area was identified by Janssen [1981] who noted the compressive modulus perpendicular to the fiber as being very low and unknown. Proposals for a split-pin transverse tension test [Mitch *et al.* 2010] and a circumferential compression test [Amada *et al.* 1996; Sharma *et al.* 2013] were aimed at addressing the issue of splitting resistance and identifying material properties transverse to the culm longitudinal axis. Both tests have been adapted into the 2019 revisions of ISO 22157. Other tests aimed at capturing interlaminar shear [Moreira 1991] and perpendicular shear [Cruz 2002] have also been proposed in the literature. Variations of shear tests have also been proposed by a number of researchers [Sharma 2010].

Recently, Virgo *et al.* [2017] proposed a flat ring flexure test that is believed to be a simple method to assess the fundamental capacity associated with bamboo splitting. Revision, validation and formal standardization of this method is a secondary objective of the present study. It is hypothesized that the flat ring flexure test and the ISO 22157 shear parallel to culm test (bowtie test), together, will describe the splitting dominant behavior of bamboo. The flat ring test results in an essentially pure Mode I response, while the bowtie test affects a Mode II behavior[3]; both modes are relative to the culm longitudinal axis.

To satisfy the major aim of this study on the mechanical characterization of bamboo it was important to study various properties of full-culm bamboo using different species. Bamboo is known to be an anisotropic material [Amada *et al.* 1997; Amada and Untao 2001; Ghavami, 2005;

[3] Reference to Modes I and II are in relation to classical fracture mechanics in which Mode I refers to perpendicular in-plane ‘peeling’ forces and Mode II refers to forces resulting in ‘in-plane shear’.

García *et al.* 2012] with different properties in its longitudinal, transverse and circumferential directions. As a natural non-homogenous material, there is a large variation in mechanical properties. Properties vary radially through the thickness of the culm wall as well as along the length of the culm. Culms are also not necessarily symmetric and section properties can vary circumferentially around a culm. Variations in physical properties, such as material density and moisture content, also effect mechanical properties. This study focuses on the determination of mechanical properties at a section and the variation of these primarily in the radial direction. The results of this study will provide a better understanding of the varying mechanical properties of bamboo with the aim of representing these with relatively simple parameters such as the variation of fiber volume in the culm section. Combining this with the inclusion of uncertainties (Chapter 5), a numerical simulation will be demonstrated (Chapter 6).

The mechanical characterization was conducted using four established test methods with some modifications made to better understand the test methods. A related study [Gauss *et al.* 2019] provides detailed analyses of the test methods themselves, including precision data, but was carried out using only a single species (*P. edulis*; reported as *P. edulis*-B in this study). The four tests include: circumferential compression test (ISO 22157:2019), shear parallel to culm ('bowtie' test) (ISO 22157:2019), full-culm compression (ISO 22157:2019) and the flat ring flexure (Virgo *et al.* 2017). Two modifications of the flat ring flexure test intended to obtain focused data for the present study are described further in Chapter 3.

2.2 Specimen Preparation

Chinese-sourced *P. edulis* is likely the most-reported species in the literature and is the most commercially valuable species in the world [Shao *et al.* 2010; Fang *et al.* 2018]. Ninety percent of *P. edulis* on earth is grown in China [Zhang 2003], representing approximately 56% of the bamboo forests in China [Zhou *et al.* 2006]. Including *P. edulis* from two different sources, six different species from three genera have been used in this study based on their availability to the laboratory: *Phyllostachys edulis*, *Phyllostachys bambusoides*, *Phyllostachys meyeri*, *Phyllostachys nigra*, *Bambusa stenostachya*, and *Dendrocalamus barbatus*. All are thin-walled (*D/t* generally greater than 8) except *B. stenostachya* which is a thick-walled species (designations proposed by Harries *et al.* 2018).

Two batches of *P. edulis* are reported. *P. edulis*-C is Chinese sourced bamboo obtained through a commercial importer; this material was water treated and kiln dried. *P. edulis*-B is Brazilian sourced bamboo obtained directly from a commercial supplier in Brazil and shipped to Pittsburgh. *P. edulis*-B specimens were part of another study – reported by Gauss *et al.* [2019]. *P. edulis*-B specimens were treated in one of two ways: a) with chromated copper borate (CCB) in a pressure chamber; or b) by immersion in 8% disodium octaborate tetrahydrate (DOT). No statistically significant difference was observed in material properties of the specimens treated in the different manners and the data from both treatments is combined in this study (as it was in Gauss *et al.*). Testing of the *P. edulis*-B specimens followed all protocols reported here and inclusion of this additional data supports the objectives of the present study.

All other *Phyllostachys* culms were obtained from a commercial importer and were water treated and kiln dried. The *B. stenostachya* and *D. barbatus* were commercially imported from Vietnam and both were borax treated. *D. barbatus* is the most commercially viable species native

to Vietnam. A limitation of this study is that since all specimens (except *P. edulis*-B) are commercially imported, it is not possible to document such factors as growing environment, age, etc.; thus, this study intentionally focuses on the mechanics of the bamboo behavior rather than the reporting of characteristic material properties; care should be taken making inferences on structural capacity from the data presented.

In all cases, sampling for testing followed a protocol intended to extract adjacent specimens for different tests so as to limit the along-culm and culm-to-culm variation of data. The following paragraphs report the protocol followed for all but *P. edulis*-B and *D. barbatus* specimens. The *P. edulis*-B sampling protocol is reported by Gauss *et al.* [2019] and the *D. barbatus* sampling varied slightly from what is reported here due to the need for specimens suitable for screw connection tests for which the culms were obtained and which are reported elsewhere.

Culms were selected at random from those available. Test specimens consisting of cylinders of length 1.0*D* and rings of length 0.2*D* (where *D* is the average nominal diameter of the culm) test specimens are cut in an alternating fashion from each culm always within 2 m of each other in order to limit along-culm variation. An example of a full-culm cut schedule is shown in Figure 2.1.

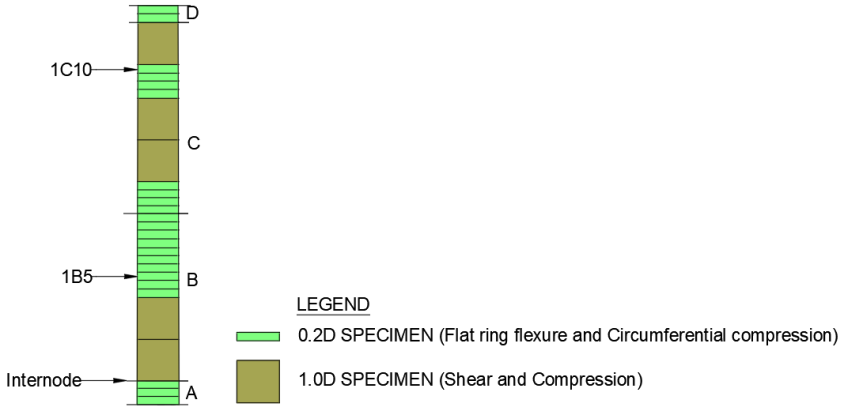

Figure 2.1: Typical full-culm specimen cut schedule.

Average culm diameter (*D*), wall thickness (*t*), specimen length (height) (*H*), and the weight (*W*) of each test specimen were measured and recorded. The diameter was measured in both the longer and shorter axes of the cross section (see Figure 1.3) and averaged for each specimen [ISO 22157:2019]. The specimen heights and culm wall thickness were measured at the four quadrants of each specimen, labelled North, East, South, and West (see Figure 1.3) and averaged for each specimen [ISO 22157:2019]. Depending on the test method, average culm dimensions or specific quadrant dimensions are used; this is described for each test method in the sections below. All measurements were made using a digital calliper having a precision of 0.01 mm. A summary of average specimen dimensions is given in Table 2.1.

Table 2.1: Culm dimensions of bamboo used in this study.

species	ρ_{12} (kg/m^3)		*D* (mm)		*t* (mm)	
	mean	COV	mean	COV	mean	COV
P. edulis-C	896	0.01	117.0	0.06	10.07	0.10
P. edulis-B[1]	767	0.06	78.7	0.04	7.25	0.10
P. bambusoides	818	0.04	95.5	0.05	8.20	0.22
P. nigra	907	0.02	93.5	0.03	6.74	0.19
P. meyeri	840	0.04	65.3	0.12	6.67	0.10
B. stenostachya	616	0.03	77.5	0.06	14.45	0.32
D. barbatus	689	0.24	79.4	0.04	10.02	0.28
[1] Gauss et al. [2019]						

Bamboo density normalized for 12% moisture content, ρ_{12}, was determined from few random specimens of each available culm and is reported in Table 2.1. Dry density is determined using the oven-dry method of ISO 22157:2019 and subsequently corrected for 12% moisture content as is conventionally reported and permitted by ISO 22157:2019. Specimens were stored in a laboratory environment for some time prior to testing. The moisture content (MC) of all

specimens at time of testing was measured with an electronic (pin-type) moisture meter [ISO 22157:2019] and typically found to be between 10% and 15%.

Full-culm compression and shear specimens were prepared using a belt sander to ensure that ends were smooth, parallel to each other, and perpendicular to the culm longitudinal axis. Sulphur capping compound was placed on both ends of the compression specimens to ensure uniform application of load [ISO 22157:2019].

In order to limit – to the extent possible – material variation for the flat ring flexure tests, multiple 0.2*D* specimens were extracted adjacent one another (Figure 2.1). In particular, adjacent specimens were used for control and clipped specimens reported in Chapter 3.

2.3 Test Methods

2.3.1 Full-Culm Compression Parallel to Fibers

In order to place the materials in the context of the broader literature, standard longitudinal compression tests (Figure 2.2a) of all species were conducted as specified in ISO 22157:2019. A 60 kN-capacity servo-mechanical test frame (Figure 2.2b) was used in most cases although a 600 kN-capacity computer controlled servo-hydraulic test frame was used for some tests reported. In either case, the lower platen is fixed while the upper platen is equipped with a spherical bearing to ensure specimen alignment [ISO 22157:2019]. Load is applied using displacement control at a rate that results in specimen failure in between 3 and 7 minutes [ISO 22157:2019] – approximately 1 mm/min in this study. A minimum of five specimens of each species were tested. An image of a

test in the 60 kN machine is shown in Figure 2.2b; the capping of the bamboo specimen can be seen.

Compression strength parallel to the culm longitudinal axis, $f_{c,0}$, is determined as:

$$f_{c,0} = \frac{P}{A} \tag{2-1}$$

where P is the applied load at specimen failure and A is the cross sectional area of the culm calculated from the average diameter, D and culm wall thickness, t, of the specimen:

$$A = \frac{\pi}{4}(D^2 - (D - 2t)^2) \tag{2-2}$$

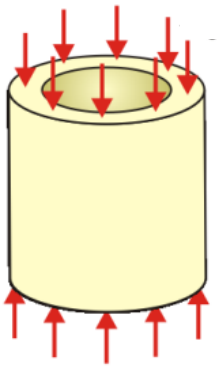

(a) Schematic of test set-up **(b) Image of compression test set-up.**

Figure 2.2: Full-culm compression test.

2.3.2 Full-Culm Shear Parallel to Fibers

The full-culm shear or "bow-tie" shear test was performed in accordance with ISO 22157:2019. In this test, the loading plates at the ends of the specimen are bow-tie shaped and offset 90^o to one another resulting in four shear planes being developed when compression is applied to the specimen (Figure 2.3a). A typical failure along one shear plane is shown in Figure 2.3c. The same 60 kN-capacity servo mechanical machine was used and load is applied using displacement control at a rate that results in specimen failure in between 3 and 7 minutes [ISO 22157:2019] – approximately 1 mm/min in this study. A minimum of five specimens were tested for each species. The Mode II in-plane shear strength (f_v) is calculated as follows:

$$f_v = \frac{P}{4tH} \tag{2-3}$$

where P is the applied load at specimen failure, t is the average culm wall thickness and H is the average specimen length (height).

Because the failure is unlikely to occur at all four planes simultaneously, f_v is interpreted to be a lower bound shear strength for the specimen [ISO 22557:2019].

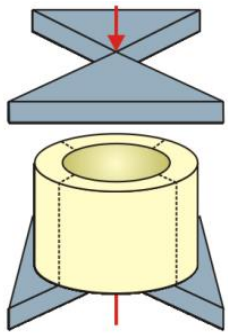

(a) Schematic of test set-up

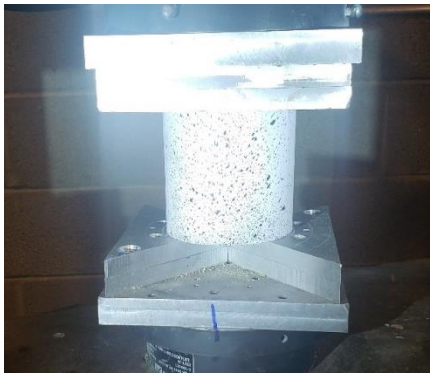

(b) Image of test set-up

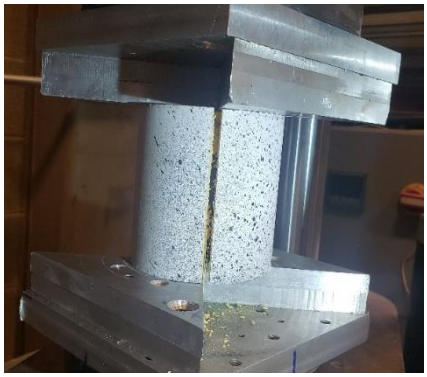

(c) Typical specimen failure at shear plane

Figure 2.3: Bow-tie shear test.

2.3.3 Flat Ring Flexure

The flat ring flexure test [Virgo *et al.* 2017][4] assesses the tendency of bamboo to fail via longitudinal cracks using a full cross-sectional specimen that is $H \approx 0.2D$ in length. The specimen is subjected to either four-point (preferred) or three-point flexure depending on the specimen diameter; only four-point flexure tests are reported in this study. The four-point flexure test schematic is shown in Figure 2.4a. The desired failure for this test occurs in the constant moment region. Tests with failures occurring outside of this region (i.e., in the shear span of a four-point test) are recorded as outliers. The flat ring flexure test gives the apparent modulus of rupture of the specimen (f_r) which, due to specimen geometry, is related to the transverse tension capacity of the bamboo. The modulus of rupture is calculated from the test results as:

$$f_r = 3Pa/(t_N + t_S)H^2 \quad (2\text{-}4)$$

[4] Virgo *et al*. provide an Appendix in which the flat-ring flexure test is prescribed in a manner consistent with ISO 22157:2019. This proposed test method is followed in this study.

where P is total load applied to specimen; a is the shear span; t_N and t_S are culm wall thickness at the failure locations on either side of the culm; and H is the length of culm section tested (i.e., the flexural depth of specimen).

A practical test span is found to be approximately $S = 0.85D$ and the shear span should be at least $0.33S$. Oval-shaped columns are tested such that the test span is the major axis of the oval. By convention, the constant moment region always spans the N and S quadrants of the specimen (Figure 1.3). This test is easily translated to a field setting, requiring only two loading plates, four pins, and free weights, rather than a hydraulic press.

(a) schematic of test set-up (Virgo *et al.* 2017) **(b) test set-up**

Figure 2.4: Flat ring flexure test set-up

In this study, all tests were carried out in a 45 kN-capacity precision gear driven test frame. Due to the very small displacements involved, tests are conducted in displacement control at a rate of crosshead travel of 0.76 mm/min resulting in failure in between 1 and 5 minutes. Loads are obtained using a load cell with a precision of ± 0.4N. A specimen loading apparatus (Figure 2.4b) is used to ensure accurate and repeatable specimen alignment. With this apparatus, test span and shear span can be varied independently in increments of 5 mm [Virgo *et al.* 2017].

Prior to this study, the flat-ring flexure test has been used on only full-culm cross sections. Such full-culm cross section specimens are referred to in this work as the control specimens and the modulus of rupture thus obtained is denoted $f_{r\alpha}$. Modifications to specimen geometry intended to extract specific through culm thickness data for this study are reported in Chapter 3.

2.3.4 Circumferential Compression Test

Only limited circumferential compression tests were conducted – primarily to obtain DIC data as described in subsequent sections. These tests serve as validation cases for the finite element study presented in Chapter 6.

The circumferential compression test was recently adopted into ISO 22157:2019. This test applies diametric compression across a short (H = 0.2D) full-culm specimen (Figure 2.5a). Quadrants are designated N-E-S-W as shown in Figure 2.5a and the load is applied across the N-S diameter. The failure mechanism involves the formation of a pair of multi-pinned arches resulting from the hinges forming at the locations of maximum moment around the circumference – the N-E-S-W points – of the culm section. From this, the culm wall bending properties may be determined [Sharma 2010; Moran *et al.* 2017]. Specifically, the culm wall modulus of rupture is a measure of the transverse tension capacity of the culm wall and therefore should be correlated with the splitting behavior. Values of interest from the experiment are the modulus of rupture perpendicular to the fibers, $f_{m,90}$, and the corresponding average circumferential modulus of elasticity, $E_{m,90}$, calculated as follows [Young *et al.* 2002, ISO 22157:2019 and Moran *et al.* 2017].

$$E_{m,90} = \frac{12R^3(P_{60} - P_{20})}{Ht^3(\Delta_{60} - \Delta_{20})}\left(\frac{\pi k_1}{4} - \frac{2k_2^2}{\pi}\right) \tag{2-5}$$

$$k_1 = \left(1 - \frac{t^2}{12R^2} + \frac{1.2Et^2}{12GR^2}\right) \approx 1 + \frac{t^2}{6R^2} \tag{2-6}$$

$$k_2 = 1 - \frac{t^2}{12R^2} \tag{2-7}$$

Typically, failure occurs at the E or W locations on the culm. The moment at these locations is given by Eq. 2-8 and the peak compressive (inner culm wall) stress and tensile (outer wall) stress are given by Eqs 2.9a, and 2.9b, respectively:

$$= \left(\frac{P_{ult}R}{\pi}\right)\left(1 - \left(\frac{t^2}{12R^2}\right)\right) - \frac{P_{ult}R}{2} \tag{2-8}$$

$$f_{mC,90,EW} = \frac{M_{EW}}{Hth}\frac{(R - R_i - h)}{R_i} - \frac{P_{ult}}{2Ht} \tag{2-9a}$$

$$f_{mT,90,EW} = \frac{M_{EW}}{Hth}\frac{(R - R_o - h)}{R_o} - \frac{P_{ult}}{2Ht} \tag{2-9b}$$

If failure occurs at the N or S locations on the culm, Eqs 2.10 and 2.11 apply and the peak compressive and tensile stresses occur at the outer and inner culm walls, respectively:

$$M_{NS} = \left(\frac{P_{ult}R}{\pi}\right)\left(1 - \left(\frac{t^2}{12R^2}\right)\right) \tag{2-10}$$

$$f_{mC,90,NS} = \frac{M_{NS}}{Hth}\frac{(R - R_o - h)}{R_o} \quad (2\text{-}11a)$$

$$f_{mT,90,NS} = \frac{M_{NS}}{Hth}\frac{(R - R_i - h)}{R_i} \quad (2\text{-}11b)$$

In Eqs 2.9 and 2.11, h is an estimate of neutral axis location for a curved beam in flexure corresponding to any of the four 90° arc segments between the principal quadrants [Young *et al.* 2002]:

$$h = R - \left(t/\ln\left(\frac{2R + t}{2R - t}\right)\right) \quad (2\text{-}12)$$

In Eqs 2.8 through 2.12, P_{ult} is the applied ultimate load; M_{NS} and M_{EW} are the bending moments perpendicular to the fibers at the N-S and E-W quadrants, respectively; H is the length of the specimen; t is the wall thickness at the failure quadrant; $R = 0.5(D\text{-}t)$ is the radius of the centreline of the culm wall; $R_i = 0.5D - t$ is the radius of the inner culm wall; $R_o = D/2$ is the radius of the outer surface of the culm wall; D is the mean outside diameter of the culm; P_{20} and P_{60} are the applied loads, at $0.2P_{ult}$ and $0.6P_{ult}$, respectively; and, Δ_{20}, Δ_{60} are the relative vertical deflections between the loaded points (N and S) of the compressed culm, determined at P_{20} and P_{60}.

As reported by Moran *et al.* [2017], the circumferential compression test can also be conducted in tension – pulling the ring specimen apart rather than compressing it (Figure 2.5b) and revising signs as appropriate in the previous equations. Although no difference in test results is expected or observed [Moran *et al.* 2017] based on test orientation, the different arrangements

permit more versatility when using digital image correlation (DIC) to obtain full strain fields (see Section 2.3.5).

Both compression and tension tests were conducted in a 45 kN-capacity precision gear driven test frame using a load cell having 0.4N precision. Due to the very small strains involved, tests are run in displacement control at a rate of 0.76 mm/min.

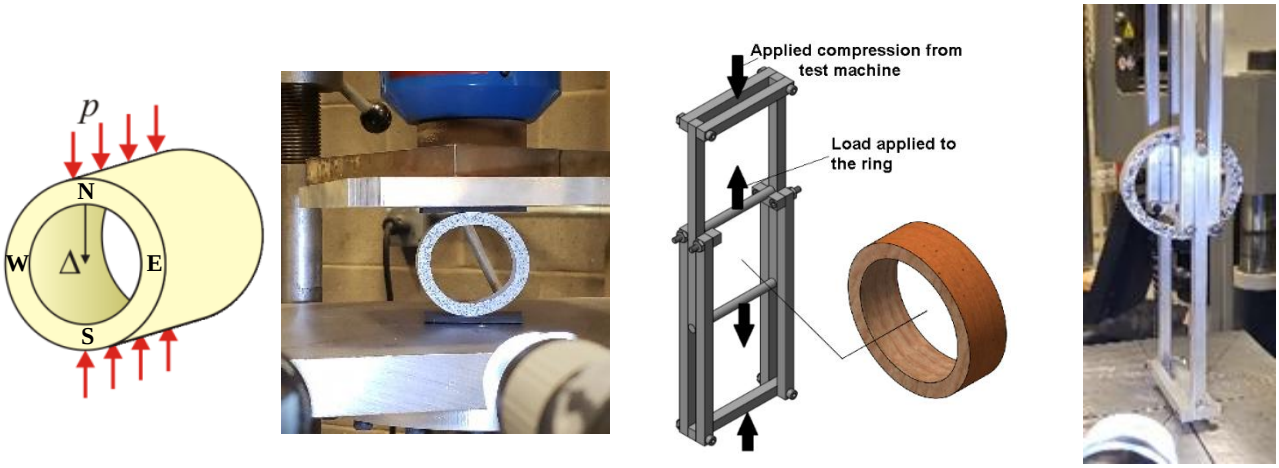

a) Compression loading **b) Tension loading**

Figure 2.5: Circumferential compression test.

2.3.5 Digital Image Correlation

To better understand the transverse behavior of full-culm bamboo, the use of Digital Image Correlation (DIC) together with the flat ring flexure and circumferential compression tests was conducted. A study that includes DIC analysis of other test methods is presented in Gauss *et al.* (2019). DIC combines the minimization methods of Coarse-fine and Newton-Raphson [Martínez-

Pañeda and Gallego 2015] and is used to measure the variation in in-plane displacement (from which strains are calculated) in the test specimens. DIC was used to capture the strain in both the longitudinal and transverse directions of the bamboo culm wall. Because DIC measures displacement, single location data can be confirmed and correlated using discrete displacements measured manually.

Surface strain fields on the bamboo specimens were obtained using a VIC-3D digital image correlation system (www.correlatedsolutions.com). The system takes consecutive high-resolution images of specimens prepared with painted speckle patterns (to provide high contrast) prior to testing. The sequential deformation is determined based on absolute and relative deformations of the speckle pattern. From these, strain fields may be calculated.

The DIC cameras were set up in order to capture the entire surface of the specimen area of interest during the experiment (see Figures 2.6 and 2.7). Only one image plane may be captured at a time; therefore the three image planes obtained for the flat ring flexure test (Figure 2.6a) are necessarily obtained from different tests. The DIC system uses two 5-megapixel CCD cameras having a 2448×2048 pixel field of view. The resulting resolution across a 10 mm wide image is 0.004 mm. Images taken from the two cameras simultaneously were stored on a PC with the VIC-3D software installed for later analysis. A representative specimen view of a flat-ring flexure test, as recorded from both the left and right cameras, is shown in Figure 2.7. Both cameras were positioned to have a clear view of the constant moment region (region between two upper rollers seen in Figure 2.7) of the flat ring flexure specimen where failure is expected to occur. Images were captured at an interval of 20 seconds from initiation of load to failure during the experiment except for tests that imaged the compression face which were captured at a 10 second interval.

Five *P. nigra* specimens were used for both the flat ring and the circumferential compression tests for each area of interest (20 tests using DIC in all).

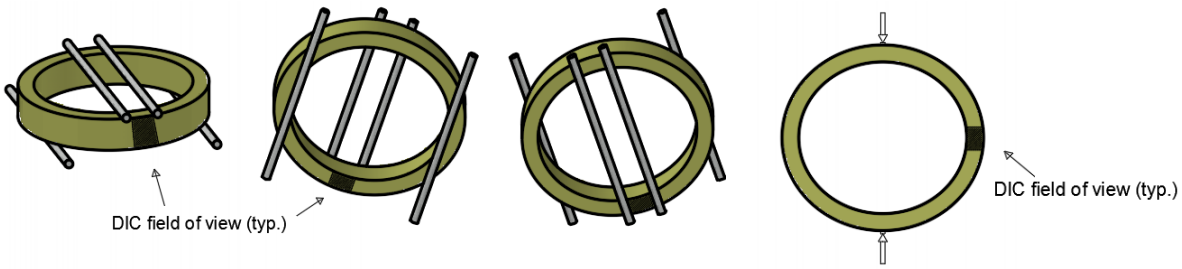

a) Flat ring flexure **b) Circumferential compression**

Figure 2.6: Illustration of DIC area of interest in selected tests

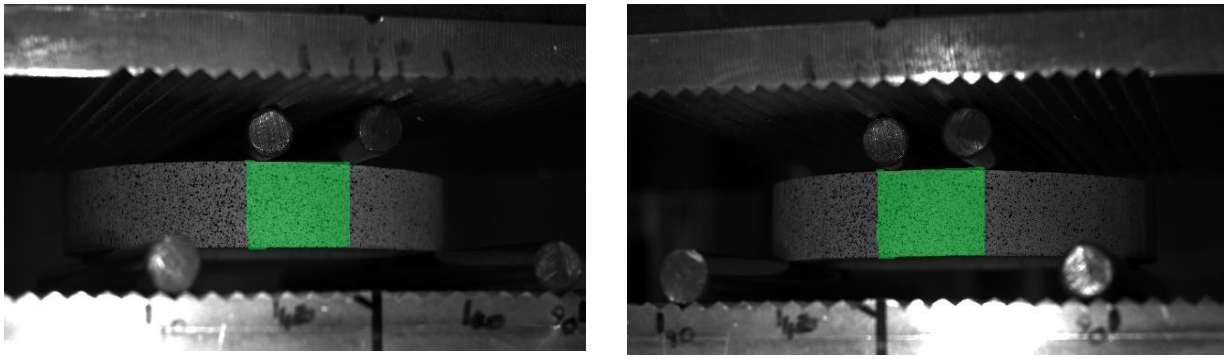

(a) View from left camera **(b) View from right camera**

Figure 2.7: DIC views from the two cameras during the flat-ring flexure tests showing the area of interest.

The specimen preparation involves the creation of random speckle pattern on the surface of interest on the specimen. It is expected that each speckle on the surface of the specimen should be imaged by at least 3 pixels to ensure minimal oversampling and good accuracy in the image correlation [Pan *et al.* 2009]. The bamboo surface was spray painted with a flat white RUST-OLEUM product, selected to avoid reflection of the lighting used. On top of the white, a similar

black paint was broadcast resulting in the high-contrast speckle patterns seen in Figures 2.3 and 2.5.

2.4 Mechanical Test Results

A summary and discussion of test results is given in this section. Descriptive statistics have been used for data analysis. The mean and coefficient of variation (COV) of each result have been reported to give a better estimation of the variation observed in the testing program.

2.4.1 Full-Culm Test Results

A summary of test results from the full-culm compression, shear parallel to fibers and flat-ring flexure is given in Table 2.2. The measured moisture content (MC) at time of testing and density at 12% moisture content [ISO 22157:2019] are also reported. Data for *P. edulis*-B has been reported previously by Gauss *et al.* [2019]. Data for *D. barbatus* was obtained by summer research interns working under the direction of the author. All other data was collected by the author.

Table 2.2: Full-culm mechanical properties of bamboo used in this study.

species	ρ_{12} (kg/m^3)		MC (%)	$f_{c,0}$ (MPa)			f_v (MPa)			$f_{r\alpha}$ (MPa)		
	mean	COV		n	mean	COV	n	mean	COV	n	mean	COV
P. edulis-C	896	0.01	14.0	8	48.1	0.20	6	15.1	0.11	33	17.3	0.18
P. edulis-B[1]	767	0.06	10.2	55	57.9	0.09	49	18.1	0.08	28	12.1	0.23
P. bambusoides	818	0.04	14.6	7	59.3	0.28	6	14.6	0.24	27	15.7	0.21
P. nigra	907	0.02	14.8	10	45.2	0.13	9	14.6	0.16	31	15.6	0.14
P. meyeri	840	0.04	13.7	10	55.8	0.11	9	16.2	0.06	49	20.0	0.16
B. stenostachya	616	0.03	13.0	9	46.0	0.12	7	9.9	0.12	39	9.4	0.13
D. barbatus	689	0.24	11.5	10	36.2	0.16	11	11.4	0.15	7	8.0	0.20
[1] Gauss et al. [2019]												

The compression and shear results reported in Table 2.2 are consistent with those reported in the literature. There is little available literature with which to compare flat ring flexure test values. A few observations can be made based on this data:

The single thick-wall species, *B. stenostachya* is both less dense and exhibits lower material strengths than the other thin-walled species. The properties related to transverse properties, f_v and $f_{r\alpha}$ are notably lower for the thick-wall species. Like timber, mechanical properties of bamboo are often correlated with density [e.g., Janssen 1981; Yu *et al.* 2008; Harries *et al.* 2017; Trujillo *et al.* 2017].

There is a significant difference in material properties of *P. edulis*-C and -B obtained from different sources. While no reasons can be given, this highlights the natural variation within a species and possibly the effects of growing and harvesting conditions on material properties.

All *Phyllostachys* tested, except *P. edulis*-B came from the same supplier and is believed to have similar origin. The properties determined for these different species from the same genus are, in some cases statistically indistinguishable. Direct comparison p-values for these specimens are shown in Table 2.3. The p-value is the probability that there is no statistically significant difference between the compared test output. While all the properties are shown to have comparable differences amongst species, the flat ring flexure tests show comparable transverse properties among species with the exception of *P. nigra* and *P. bambusoides* which are statistically similar. The highlighted data indicate data having a statistically significant ($p < 0.05$) difference.

Table 2.3: p-values for significance of *Phyllostachys* data.

	$f_{c,0}$					f_v					$f_{r\alpha}$				
	P. edulis-C	*P. edulis*-B	*P. bamb.*	*P. nigra*	*P. meyeri*	*P. edulis*-C	*P. edulis*-B	*P. bamb.*	*P. nigra*	*P. meyeri*	*P. edulis*-C	*P. edulis*-B	*P. bamb.*	*P. nigra*	*P. meyeri*
P. edulis-C	1					1					1				
P. edulis-B	0.00	1				0.00	1				0.00	1			
P. bamb.	0.12	0.65	1			0.76	0.00	1			0.07	0.00	1		
P. nigra	0.44	0.00	0.02	1		0.66	0.00	0.99	1		0.08	0.00	0.69	1	
P. meyeri	0.05	0.23	0.54	0.00	1	0.06	0.00	0.14	0.04	1	0.00	0.00	0.00	0.00	1

2.5 Flat Ring Flexure Test Results with DIC

All DIC tests were conducted using samples of *P. nigra*. The modulus of rupture, $f_{r\alpha}$, (Eq. 2-4) determined for the full-culm specimens is reported in Table 2.2. With the exception of *P. meyeri* and *P. edulis*-B, within the genus *Phyllostachys*, these values are mutually similar (Table 2.3) and all are notably greater than that observed for *B. stenostachya* and *D. barbatus*. The observed variation of test results is typical of bamboo and similar to that reported in Virgo *et al.* [2017]. Only specimens failing within the constant moment region (Figure 2.4) are included in the reported data (Virgo *et al.* 2017). Additionally, outliers defined as data falling outside 1.5 times the interquartile range (so called Tukey fences [Hoaglin 2003]), were also excluded from the reported data.

Figure 2.8 illustrates typical displacement and strain profiles obtained from the constant moment region (see Figures 2.6 and 2.7) of the flat-ring flexure test of Specimen PN5A1. Figure

2.8 shows the vertical displacement and horizontal strain plots at load levels of 50% of the failure load (left hand images) and just before failure (right). In Figure 2.8, the color scales are provided and are different for each image.

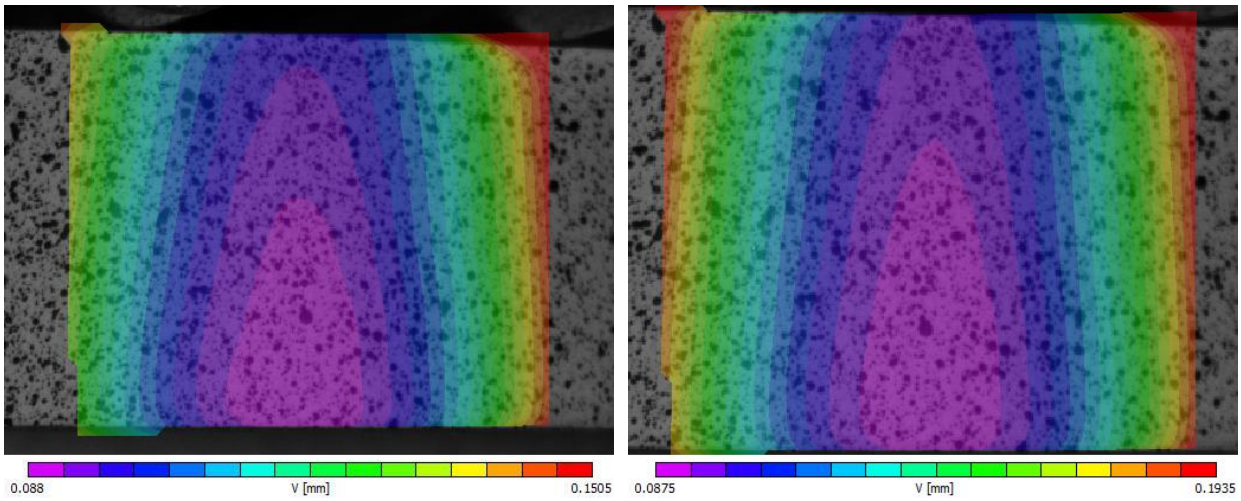

(a) Vertical displacement at 50% of failure load

(b) Vertical displacement at failure load

(c) Horizontal strain at 50% of failure load

(d) Horizontal strain at failure load

Figure 2.8: Displacement and strain fields from DIC at 50% and 100% of failure load of PN5A1

The flexural response of the specimen is evident from Figures 2.8a and b where the relative displacement between the load points (outer edges of images) and midspan is about 0.0625 mm and 0.106 mm at 50% peak load and at peak load, respectively[5]. The horizontal strain profile shown in Figures 2.8c and d show the horizontal bending strains as being essentially constant for given elevation/depth across the constant moment region as expected. The horizontal strain values are seen to vary essentially linearly through the depth of the cross section and a downward shift of the neutral axis can be inferred from the maximum strain values shown. This is described further below. The local effect of the right loading point is also evident.

The individual test results for each of the *P. nigra* specimens tested with DIC is shown in Table 2.4. Figure 2.9 illustrates the horizontal strain gradients for each specimen plotted against the normalized specimen height determined at the center of the constant moment region. All the figures show the bending strains (ε_{xx}) increasing during the test as expected with compression at the top face and tension on the bottom face of the specimen. All specimens exhibit near linear behavior at all load levels (i.e., plane sections remain plane). However, a shift in neutral axis toward the tension face (0H) to about 0.46H is seen in all cases; this shift is seen to increase marginally with applied load and is greatest at failure.

Table 2.4: Load and bending stress, f_r values from the Flat-Ring Flexure test with DIC

Specimen	MC	*D*	*t*	*H*	at failure				
					Applied load	f_r	ε_T,	ε_C,	neutral axis
	%	mm	mm	mm	N	MPa	με	με	location
PN5A1	10.4	92.7	8.05	19.6	1236	18.0	6503	6731	0.47*H*
PN5A2	9.7	92.4	8.17	17.3	920	17.0	6027	6456	0.48*H*
PN5A3	9.2	92.4	8.45	16.8	733	13.8	4613	4771	0.47*H*
PN5A5	10.1	92.4	8.05	19.3	537	8.7	2193	2122	0.46*H*

[5] DIC records absolute displacement relative to the camera location or initial field of view. Positive is upward. The lower platen of the test machine moves upward; thus the positive values for the entire displacement field.

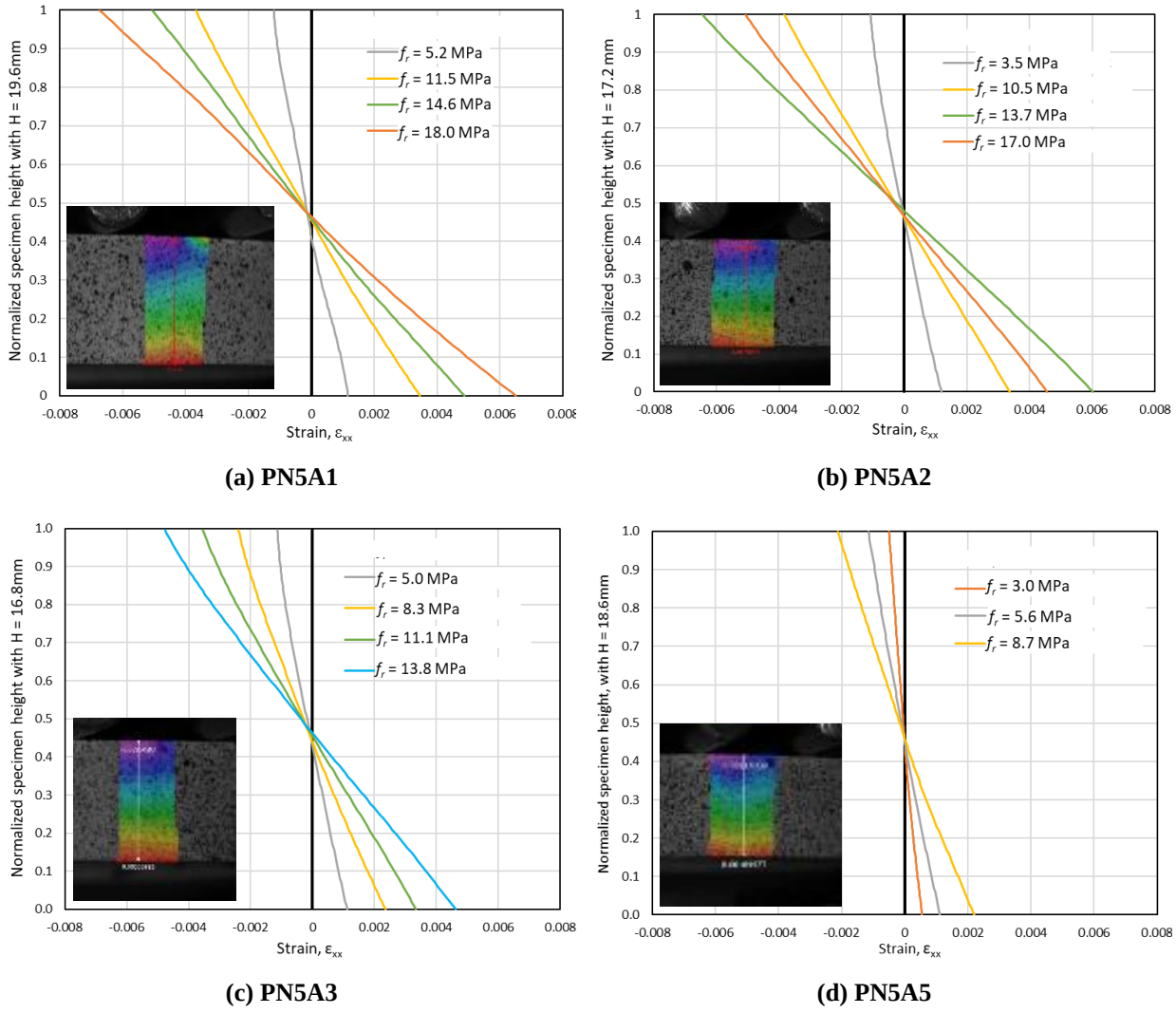

Figure 2.9: Horizontal strain, ε_{xx} against normalized specimen height for each of the tested specimens

Strain profiles from different specimens at similar stress levels (approximately 14 MPa) are shown overlaid in Figure 2.10. Nearly identical behavior is seen with the same shift in neutral axis to 0.46H at this load level.

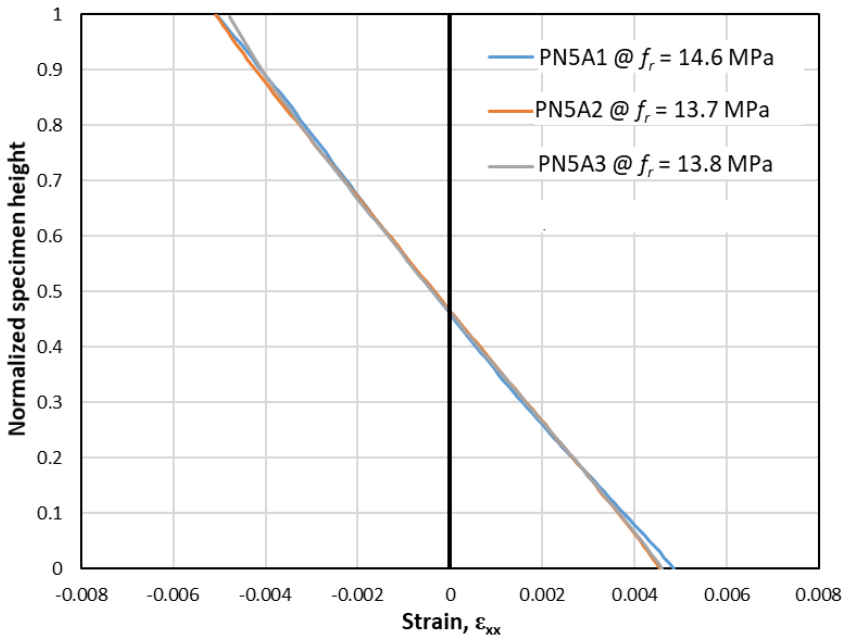

Figure 2.10: Horizontal strain, ε_{xx} against normalized specimen height at a bending stress of ~ 14 MPa.

In addition to the longitudinal ring face (elevation) analyzed with the DIC, the compression and tension faces of specimens were also imaged and analyzed in subsequent flat ring tests (Figure 2.6). To achieve this, the camera arrangement was changed to accommodate the new area of interest to be examined. A modified test set-up (Figures 2.11a and b) was required to permit imaging of the specimen faces; this resulted in a larger field of view (area of interest smaller in the image) and therefore reduced precision (Figures 2.11c and d). The revised DIC arrangement also meant that in order to image the compression face, the test orientation was inverted (Figure 2.11b); this should have no effect on results.

(a) Test template and camera placement

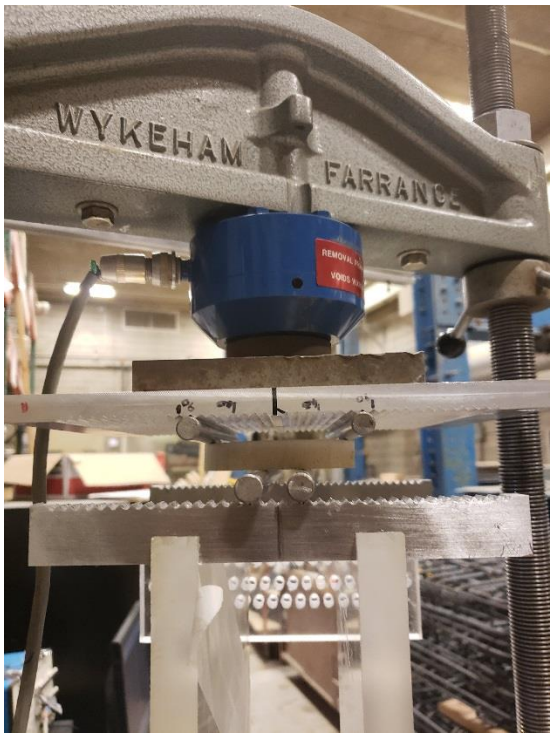

(b) Test set-up showing grooved plates

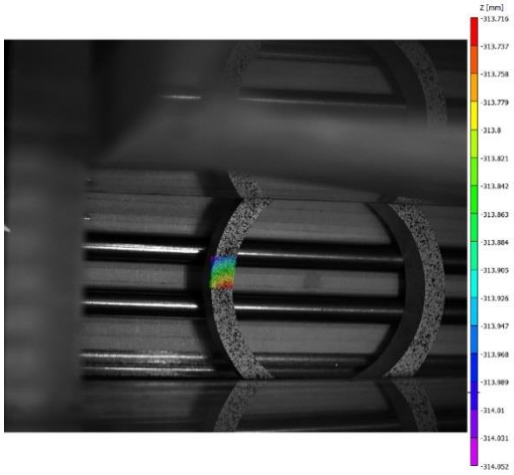

(c) Imaging tension face of specimen

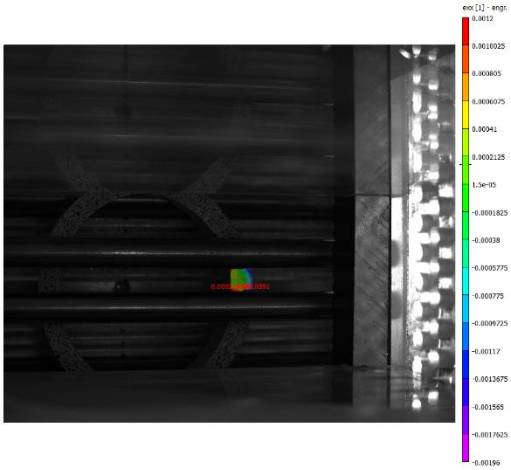

(d) Imaging compression face of specimen

Figure 2.11: Test set-up for imaging compression and tension faces of the flat-ring flexure test with DIC

Three *P. nigra* specimens were tested for each compression and tension face. The variation of longitudinal strain across the normalized specimen width (i.e., the culm wall thickness) at comparable values of stress is shown in Figure 2.12. Strain distributions for all three specimens at approximately the same stress level are overlaid in Figure 2.12d. Results are summarized in Table 2.5 with C and T in the specimen identifier signifying compression and tension.

Table 2.5: Output summary from compressive and tensile face DIC analysis

Specimen	MC	D	t	H	Applied load	f_r	Failure Strain με	
							Inner culm wall	Outer culm wall
	%	mm	mm	mm	N	MPa		
PN5D5C	11.3	85.3	7.94	17.4	884.7	13.8	-4570	-3960
PN5C7C	12.1	87.9	7.95	16.0	706.7	15.6	-4870	-3380
PN5A4C	12.0	92.4	8.05	19.3	1116.1	16.8	-7220	-6880
PN5A7T	10.4	91.2	7.90	18.3	662.2	11.3	2834	1954
PN5A8T	10.7	91.2	8.10	17.1	742.3	14.1	5818	3927
PN5A9T	10.3	91.2	7.90	17.4	871.4	16.3	5040	3979

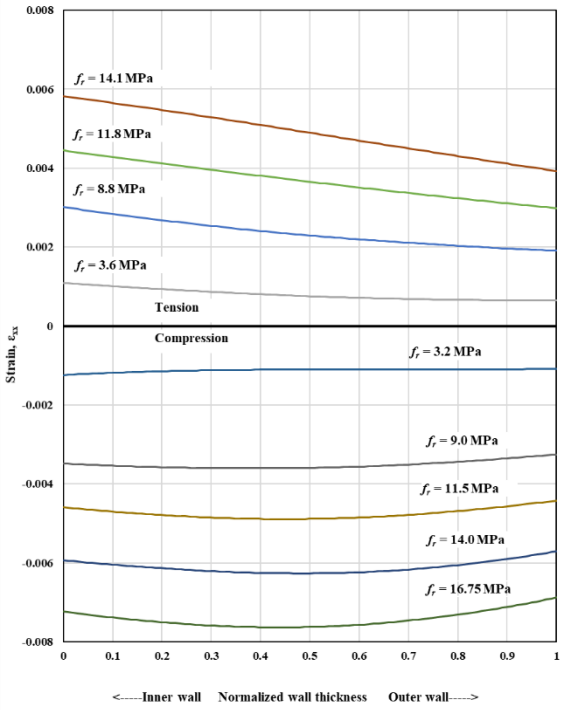

(a) PN5A8T (8.1mm) and PN5A4C (8.1mm)

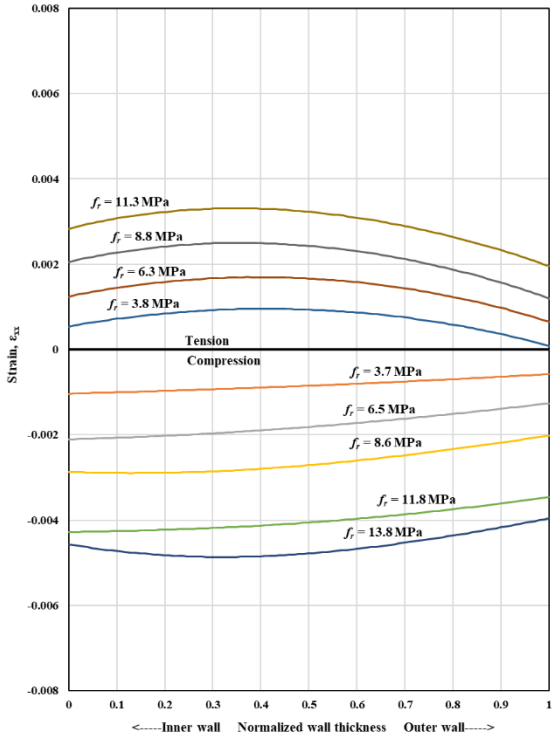

(b) PN5D5T (7.9mm) and PN5A7C (7.9mm)

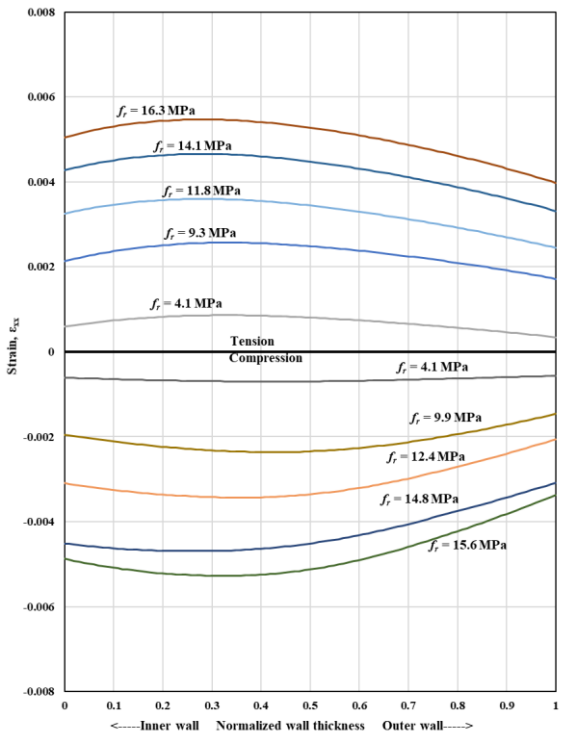

(c) PN5A9T (7.9mm) and PN5C7C (8.0mm)

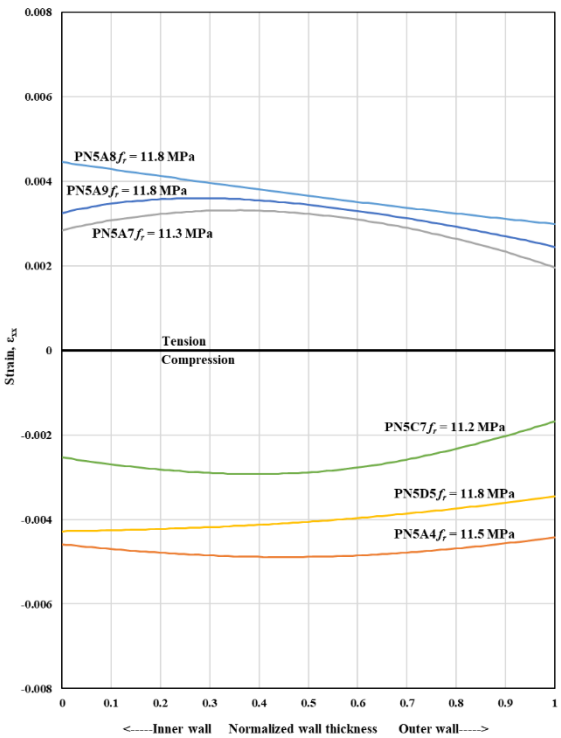

(d) All specimens at bending stress of ~ 11.5 MPa.

Figure 2.12: Plot of longitudinal strain, ε_{xx} against normalized culm wall thickness

An examination of the plots in Figure 2.12 shows an essentially elastic behavior of the tensile face of the specimen under the flat ring test; that is; the strain increases in proportion to the applied load. In all cases there is an apparent strain gradient across the specimen with absolute values of both tension and compression strains being larger nearer the inner culm wall in all cases. There is also a nonlinear gradient across the culm wall thickness as the stress level is increased, with peak strains apparently occurring at approximately 0.3*t*. The cause of this behavior is uncertain. The absolute strains being greatest near the inner culm wall regardless of test orientation would appear to confirm that the there is no torsion induced in the test specimen as has been suggested in (as yet unpublished) work by Moran.

From the experiments conducted, the range of tensile failure strain at the outer culm wall was from 1954 με to 3979 με and from 2834 με to 5818 με at the inner culm wall. Similarly, compression strains at failure ranged from 3380 με to 6880 με at the outer culm wall and 4570 με to 7220 με at the inner culm wall. The wide range in strain variation reflects the uncertainty associated with bamboo materials.

Finally, as shown in Figure 2.12 (especially 2.12d) compressive strains are marginally greater at similar stress levels resulting in a shift in the neutral axis toward the tension face as described previously.

2.6 Circumferential Compression Test Results with DIC

Similar to the flat ring flexure tests conducted with DIC, a limited number of circumferential compression tests were also conducted. Both conventional compression (Figure 2.5a) and specialized tension (Figure 2.5b; Moran *et al.* 2017) test orientations were conducted to

permit DIC imaging of both positive and negative culm wall bending away from the influence of the applied load. A summary of test results on the *P. nigra* specimens used is given in Table 2.6. The terms C and T at the ends of the specimen identifiers denote the loading condition of compression and tension respectively. All specimens tested in compression failed at the E-W positions (i.e. outer culm wall in tension) while all the tension loaded specimens failed at the N-S positions (also outer culm wall in tension). However only the E-W position was imaged. Thus, both cases in which the outer culm wall is in tension or compression may be investigated.

Table 2.6: Circumferential elastic properties at E-W quadrant from the circumferential compression test

Specimen identifier	MC	D	t	H	Failure location	P	Δ^1	$f_{mC,90,EW}$	$f_{mT,90,EW}$	$E_{m,90}$	neutral axis location
	%	mm	mm	mm		N	mm	MPa	MPa	MPa	
PN5B1C	9.3	91.4	8.50	19.0	E-W	591.8	3.35	-22.9	16.5	1983	0.50t
PN5B2C	9.1	91.0	8.35	17.2	E-W	382.7	2.09	-16.8	12.2	2623	0.52t
PN5B3C	9.3	90.8	8.40	18.2	E-W	560.7	3.27	-23.1	11.1	2354	0.53t
PN5B4C	8.2	90.5	8.10	19.3	E-W	413.8	2.07	-17.1	12.5	2658	0.50t
PN5C6T	12.3	88.0	7.56	15.6	N-S	254.1	1.24	-14.5	10.8	2649	0.59t
PN5C11T	12.5	87.3	7.62	19.8	N-S	329.9	2.26	-14.5	10.7	2039	0.63t
PN5C12T	11.7	87.3	7.51	15.5	N-S	325.4	2.26	-18.8	14.0	2503	0.56t

[1] Vertical deflection in the compression test is the measured relative difference between the North and South deflection while horizontal deflection in the tension test is twice the measured deflection at the East quadrant.

Circumferential strain at the E-W location determined from the DIC data exhibited essentially linear distributions (i.e. plane sections remain plane). A typical DIC image at maximum displacement and strain is shown in Figure 2.13. The strain profiles for all specimens are shown in Figures 2.14 and 2.15 for tests run in compression and tension, respectively. A shift of the neutral axis towards the outer culm wall is seen in all cases and appears to be more pronounced in the tension experiment. This shift in neutral axis location results from both the curvature of the specimen – captured by the value h given by equation 2-12 – and the effect of material property gradient.

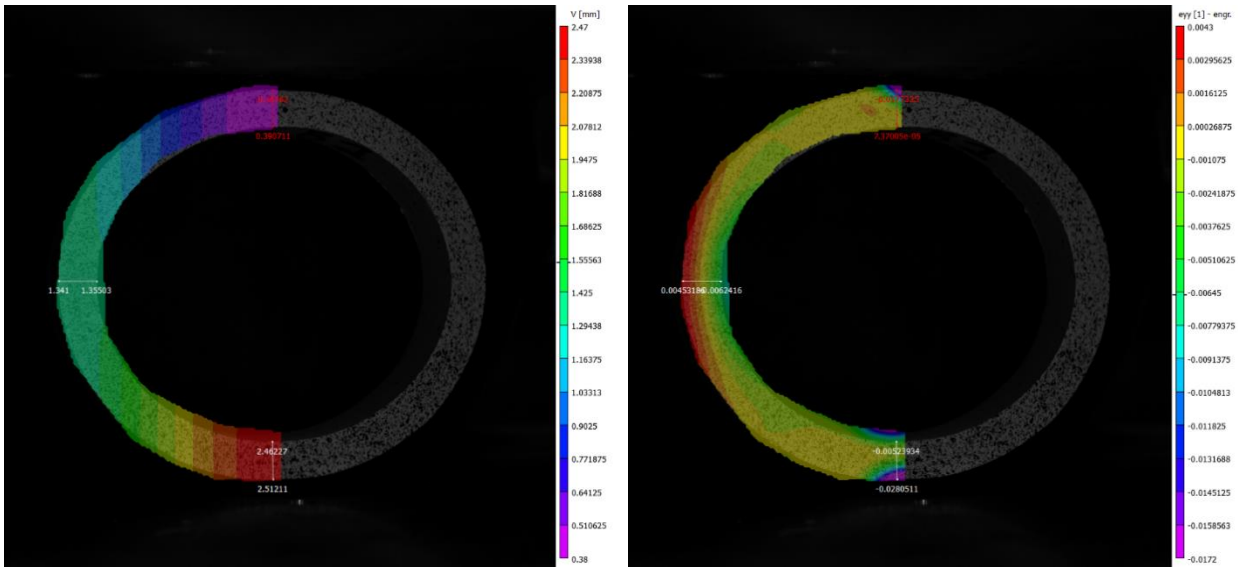

a.) Vertical displacement **b.) vertical strain**

Figure 2.13: Examples of maximum pricipal strain and vertical displacement (Specimen PN5B2C)

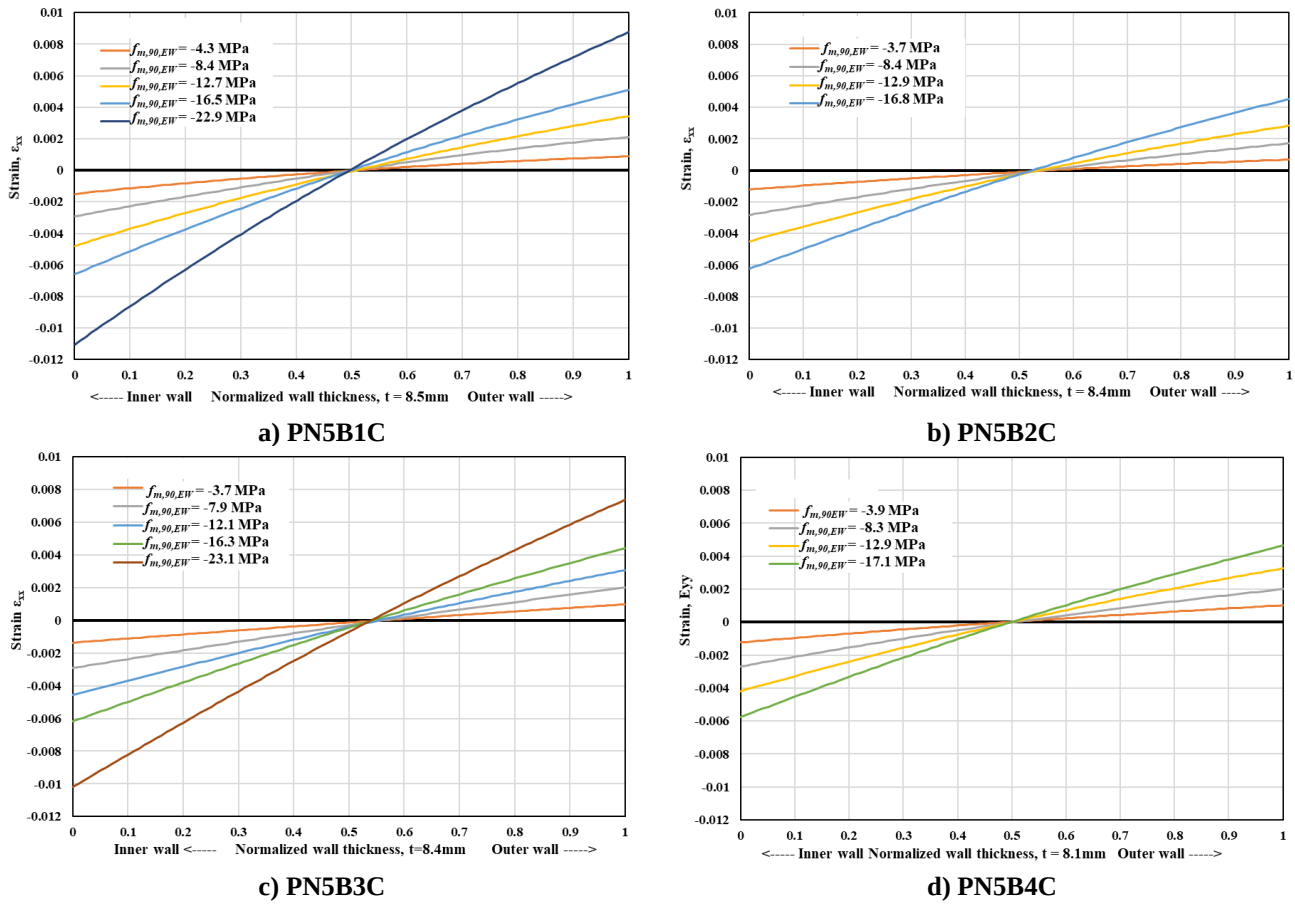

a) PN5B1C **b) PN5B2C**

c) PN5B3C **d) PN5B4C**

Figure 2.14: Plots of circumferential strain, ε_{xx} vs normalized wall thickness at E-W location for specimens under compression loading

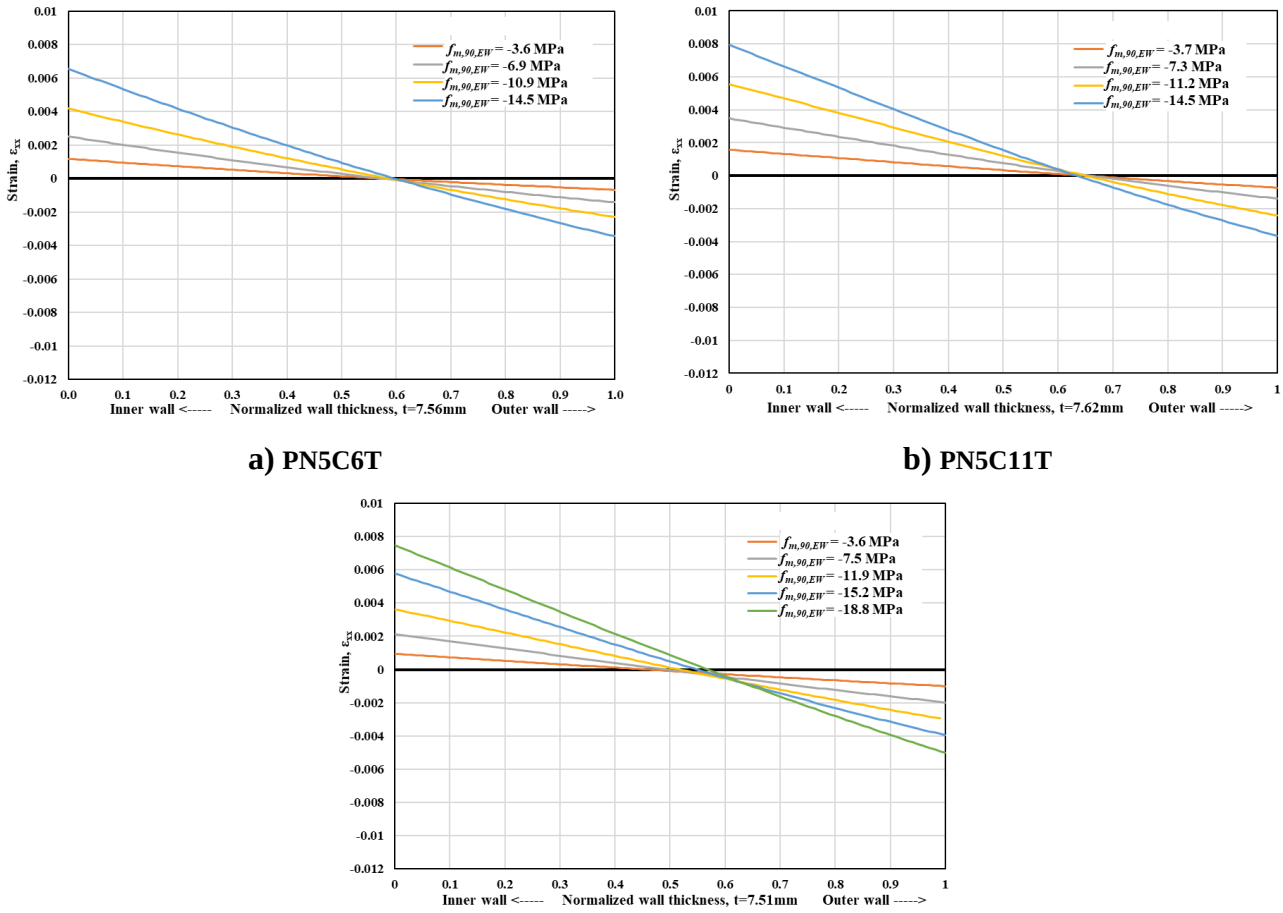

Figure 2.15: Plots of circumferential strain, ε_{xx} vs normalized wall thickness at E-W location for specimens under Tension loading

2.7 Summary

Four established test methods were conducted in order to quantify the mechanical properties of full-culm bamboo in different directions. Both the longitudinal direction parallel to fibers (full-culm compression, f_c and full-culm shear, f_v), and the transverse direction (flat ring flexure, $f_{r\alpha}$ and the circumferential compression test, $f_{m,90}$) were considered. Tests were conducted on a total of six species sourced from different locations. A sampling protocol was developed to

cut the specimens in both the 1D and 0.2D height required for the different tests while limiting the along-culm and culm-to-culm variation of data.

The material variation inherent in bamboo was evident. The compression strength parallel to the culm, f_c ranged from 36.2 MPa to 59.3 MPa with the lowest being the *D. barbatus* species. The average single species coefficient of variation over all compression tests was 16%. Similarly, the shear strength f_v ranged from 9.9 MPa for the thick-walled *B. stenostachya* to 18.1 for the *P. edulis*-C and an average single species coefficient of variation of 13% was observed over all species. The transverse modulus of rupture, $f_{r\alpha}$ from the flat ring flexure test also varied amongst species with values ranging from 9.4 MPa for the thick-walled *B. stenostachya* to 20 MPa for the thin walled *P. meyeri* with a 20% average single species coefficient of variation observed. Lower material strength was exhibited by the thick walled species in comparison to the thin walled species; this is partially attributed to the lower density of the thick-walled species.

The variation in mechanical properties from species to species was less significant within the same genus (*Phyllostachys*). However, significant differences were observed between *P. edulis*-B and *P. edulis*-C. This reinforces the hypothesis that mechanical property variation in bamboo occurs between species and even amongst the same species with different growth conditions.

P. nigra samples were selected for the circumferential compression test and flat ring flexure using DIC. Both strain and displacement values of different areas of interest were captured in order to better understand the behavior of the flexural response of the specimens under testing. All specimens in the flat ring flexure tests were found to exhibit linear behavior at all load levels (i.e. plane sections remain plane) and there was also an apparent shift in the neutral axis towards the tension face. The circumferential compression tests were conducted with both tension and

compression loading. A shift in the neutral axis location towards the outer culm wall was observed and was more pronounced in the tension loading tests in which the outer culm wall at the E-W quadrant is placed in compression.

The results of tests conducted in this section have given a better indication of the mechanical properties of bamboo and their variation. The aim of representing these with relatively simple parameters such as the variation of fiber volume in the culm section is considered in subsequent Chapters. This is combined with the consideration of uncertainties (Chapter 5), to demonstrate a numerical simulation (Chapter 6).

3.0 Bamboo Culm Wall Structure and Image Analysis

3.1 Background

In recent years, the structure and components of bamboo and its corresponding mechanical properties have been more widely studied [e.g., Obataya *et al.* 2007; Shao *et al.* 2010; Shao and Wang 2018; Wei *et al.* 2019]. Shao *et al.* [2009], proposed relationships between fiber volume fraction and mechanical properties. However, precise studies on the mechanical properties of bamboo fiber (sclerenchyma) and parenchyma ground tissue with respect to the fiber-reinforced composite structure of bamboo have not been reported sufficiently and relationships were often estimated from a small number of specimens [Shao *et al.* 2010]. Bamboo material properties depend on such factors as the density and diameter of fibers, thickness of the fiber cell walls and moisture content. In addition, bamboo is an orthotropic material with high strength and stiffness in the direction parallel to the fibers and significantly lower strength and stiffness perpendicular to the fibers [Low *et al.* 2006]. Although difficult to assess, ratios of longitudinal-to-transverse properties exceed 10 when they are reported [Richard 2013] and are more commonly reported as 20 or more [Janssen 2000; Archila *et al.* 2018].

Considering the distribution of fiber volume in bamboo, Amada *et al.* [1997] described the plant as a smart natural composite material which has developed through its evolution. Due to an optimized distribution of fibers and matrix, not just in the cross section but also along the culm length, bamboo is optimized to resist environmental loads the culm experiences in nature [Harries *et al.* 2017]. A large body of work [including Jain 1992; Li *et al.* 1994; Nogata and Takahashi 1995 and Amada 1995] confirms that the fiber distribution in the cross-section of the bamboo culm

is dense in the outer region of the culm wall and sparser in the inner region. This structure belongs to the class of materials known as functionally graded materials (FGM) [Rabin and Shiota 1995]. Figure 3.1 shows an example of the distribution of volume fraction of fibers (V_f) as a function of culm wall thickness with *n* representing the node number counted from the base of the culm [Amada *et al.* 1996]. The fiber volume ratio was reported to be about 15 ~ 20% at the inner surface and 60 ~ 65% at the outer surface of the culm wall. As a general trend, V_f increases marginally with height along the culm. Similar data has been reported by others; a summary is shown in Table 3.1.

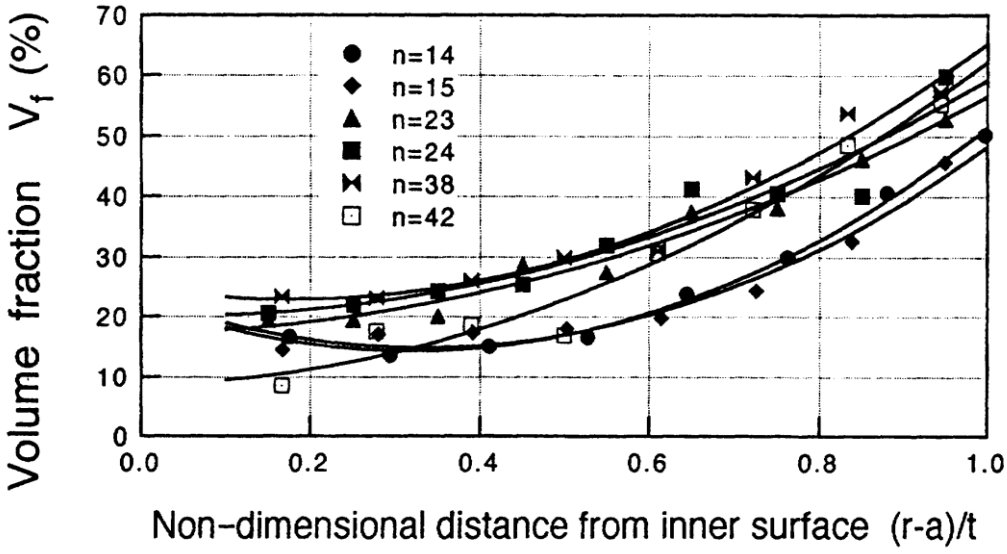

Figure 3.1: Variation of the volume fraction with non-dimentional distance from culm inner surface. [Amada *et al.* 1996]

In terms of volume fraction, the fibers and cellular parenchyma form the majority of the bamboo culm. For example, for *P. edulis,* fibers comprise 40–60% and parenchyma 20–60% depending on location, local climate, age, etc. Vessels and phloem make up the remaining 5-10%

[Palombini *et al.* 2016; Osorio *et al.* 2018]. The load-bearing mechanical properties of bamboo are mainly attributed to the fibers within the bamboo culm [Amada *et al.* 1996; Habibi and Lu 2014]. Lo *et al.* [2004] reports the sclerenchyma fibers, which were more densely packed at the top section of bamboo, resulted in a higher load carrying capacity and confirmed that fiber density is a good indicator of the strength capacity of bamboo. Based on specific strength, bamboo is comparable to structural steel; in terms of specific modulus, bamboo is comparable to conventional softwood. Combined, bamboo is most comparable to glass fiber reinforced polymer (GFRP) materials [Habibi and Lu 2014]. Table 3.1 reports the range of fiber volume (V_f) data reported in the literature. Table 3.1 also reports longitudinal modulus (E_L) which is less commonly reported and rarely correlated with V_f. Data from the present study (described below) is appended to the end of Table 3.1, placing this data in context. Finally, when reported, the modulus and strength of both the fibers and matrix are given in Table 3.1; this is described in Section 3.3. Throughout this study, all data is normalised by culm wall thickness such that $x = 0$ is the inner wall and $x = 1$ is the outer wall.

Table 3.1: Summary bamboo culm and fiber and matrix properties reported in literature

reference	method1[1]	species	BMT[2]	gross section		interior ($x = 0$)		exterior ($x = 1$)		proposed relationship for distribution through culm wall	fiber and matrix properties			
				V_f	E_L (GPa)	V_f	E_L (GPa)	V_f	E_L (GPa)		E_f (GPa)	E_m (GPa)	σ_f (MPa)	σ_m (MPa)
Janssen 1981; Vaessen and Janssen 1997	IA	general	nr	0.40	-	0.20	-	0.60	-	$V_f = 0.40x + 0.20$	35	1.8	-	-
Nogata and Takahasi 1995	V_f: IA E_L: RoM	*P. edulis*	B	-	9.1	0.09	2.5	0.77	22.6	exponential V_f $E_L = (E_{L,x=0})e^{2.2x}$	55	2	800	-
			T	-	13.7	0.11	3.8	0.88	33.8					
Amada *et al.* 1996	V_f: IA E_L: tens	*P. edulis*	B	0.25	-	0.17	4	0.50	29	exponential V_f and E_L	46	2	610	-
			M	0.28	-	0.18	6	0.56	30					
			T	0.34	-	0.10	6	0.60	32		-	-	-	-
Ghavami *et al.* 2003	IA	*P. edulis*	nr	0.28	-	0.12	-	0.62	-	$V_f = 0.49x^2 + 0.0066x + 0.12$	-	-	-	-
	IA	*D. giganteus*	B	0.42	-	0.29	-	0.53	-	$V_f = -0.09x^2 + 0.33x + 0.29$	-	-	-	-
			M	0.43	-	0.21	-	0.62	-	$V_f = 0.07x^2 + 0.29x + 0.26$	-	-	-	-
			T	0.43	-	0.19	-	0.60	-	$V_f = -0.12x^2 + 0.51x + 0.21$	-	-	-	-
Ghavami and Marinho 2005	V_f: SEM E_L: tens	*G. angustifolia*	B	0.26	16.0	0.19	-	0.62	-	$V_f = 0.83x^2 – 0.41x + 0.19$	-	-	-	-
			M	0.26	14.6	-	-	0.54	-	$V_f = -1.02x^3 + 2.61x^2 – 1.38x + 0.33$	-	-	-	-
			T	-	13.2	-	-	0.54	-	$V_f = -4.13x^4 + 9.68x^3 – 6.68x^2 + 1.71x – 0.04$	-	-	-	-
Shao *et al.* 2010	tens; RoM	*P. edulis*	M	-	-	0.12	4.5	0.54	21	$E_L = 40.13V_f + 0.22$	40.4	0.22	582	19
	FBT			-	-	-	-	-	-	-	33.9	-	-	-
Tan *et al.* 2011	nano	*P. edulis*	nr	-	-	-	6.5	-	13.8	-	-	-	-	-
Dixon and Gibson 2014	SEM	*P. edulis*	B	0.21	-	0.06	-	0.52	-	$V_f = (0.23x + 0.71)(0.09e^{1.83x})$	39.8	1.93	472	14.6
			M	0.23	-	0.06	-	0.58	-	$V_f = (0.23x + 0.71)(0.09e^{1.48x})$				
			T	0.26	-	0.06	-	0.69	-	$V_f = (0.23x + 0.71)(0.09e^{2.11x})$				
Dixon *et al.* 2015	V_f: SEM E_L: nano	*P. edulis*	nr	-	14.9	0.07	-	0.58	-	-	-	-	-	-
		G. angustifolia	nr	-	19.7	0.16	-	0.60	-		-	-	-	-
		B. stenostachya	nr	-	13.8	0.05	-	0.42	-		-	-	-	-
Habibi *et al.* 2015	flex; µtens	*P. edulis*	nr	-	8.7	-	2.8	-	15.2	$E_L = 12.43x^{0.43} + 2.78$	30.1	-	1000	-
	nano			-	-	-	-	-	-	-	22.8	3.7	-	-
Krause *et al.* 2016	V_f: SEM E_L: tens	*D. giganteus* at $x = 0.5$	M	-	-	0.38	17.6	0.55	30.7	culm wall divided into thirds	-	-	-	-
				-	-	0.45	27.3	-	-		-	-	-	-
Zhang *et al.* 2018	SFT	nr	nr	-	-	-	-	-	-	-	9.8	-	262	-
Yu *et al.* 2011b	SFT	*P. edulis*	nr	-	-	-	-	-	-	-	33.3	-	1560	-
Yu *et al.* 2014	SFT	11 species	nr	-	-	-	-	-	-	-	36.7	-	1550	-
Osorio *et al.* 2011	FBT	*G. angustifolia*	nr	-	-	-	-	-	-	-	43	-	800	-
Mannan *et al.* 2017	AS	*D. strictus*	nr	-	-	-	-	-	-	$E_L = 1.23e^{0.08x}$	15-29	3-7	-	-
Osorio *et al.* 2018	empirical	*G. angustifolia*	nr	-	-	-	-	-	-	-	50	-	-	-
Cousins *et al.* 1975	nano	nr	nr	-	-	-	-	-	-	-	-	3.3	-	-

Table 3.1 (continued)

reference	method1[1]	species	BMT[2]	gross section		interior ($x = 0$)		exterior ($x = 1$)		proposed relationship for distribution through culm wall	fiber and matrix properties			
				V_f	E_L (GPa)	V_f	E_L (GPa)	V_f	E_L (GPa)		E_f (GPa)	E_m (GPa)	σ_f (MPa)	σ_m (MPa)
Yu *et al.* 2007	nano	*P. edulis*	nr	-	-	-	-	-	-	-	16	5.8	365	230
Zou *et al.* 2009	nano	*P. edulis*	nr	-	-	-	-	-	-	-	5.9	-	391	-
Mannan *et al.* 2016	nano	*D. giganteus*	nr	-	-	-	-	-	-	-	10.4	3.4	490	440
this study	IA	*P. edulis*-C	B	0.29	-	0.12	-	0.67	-	$V_f = 1.41x^3 - 1.23x^2 + 0.50x + 0.10$	-	-	-	-
		P. bambusoides	B	0.32	-	0.14	-	0.65	-	$V_f = 0.96x^3 - 0.91x^2 + 0.57x + 0.10$	-	-	-	-
		P. nigra	B	0.26	-	0.07	-	0.64	-	$V_f = 0.94x^3 - 0.63x^2 + 0.36x + 0.06$	-	-	-	-
		P. meyeri	B	0.35	-	0.11	-	0.70	-	$V_f = 0.15x^3 + 0.34x^2 + 0.17x + 0.11$	-	-	-	-
		B. stenostachya	B	0.35	-	0.24	-	0.64	-	$V_f = 1.75x^3 - 1.98x^2 + 0.75x + 0.20$	-	-	-	-
		all four Phyllostachys	B	-	-	-	-	-	-	$V_f = 0.86x^3 - 0.61x^2 + 0.40x + 0.09$	-	-	-	-

x = normalized dimension through culm wall; V_f = fiber volume ratio; E_L = longitudinal tensile modulus of elasticity; E_f and σ_f = modulus and strength of fibers; E_m and σ_m = modulus and strength of matrix (parenchyma)

[1] methods of determining data: IA = image analysis; SEM = scanning electron microscope; RoM = rule of mixtures; tens = tension tests; μten = microtension; SFT = single fiber tension; FBT = fiber bundle tension; nano = nano-indentation; flex = flexural tests; AS = atomistic simulation

[2] locational along height of culm: B = bottom; M = middle; T = top; nr = not reported

Like timber, density of bamboo has been proposed as a basis for estimating mechanical properties [e.g., Janssen 1981; Lo *et al.* 2004; Trujillo *et al.* 2017]. It is widely accepted that density of bamboo depends on the size, quantity and distribution of fiber agglomerates around the vascular bundles. Fiber volume increases from the interior to the exterior portions of the culm wall and from the bottom of the culm to the top [Amada *et al.* 1996]. With decreasing thickness of the culm wall along the height of the culm, an increase in density and mechanical strength, especially of the inner parts of the culm wall, is reported. The outer parts of the culm wall vary less significantly [Sekhar and Bhartari 1960]. These trends can be seen in Figure 3.1 and the data presented in Table 3.1. Data developed in the present study will be used to further investigate the relationship between [normalized] wall thickness and fiber distribution. In addition to density, the age of bamboo at harvest is reported to lead to structural changes in the material. This is attributed to the degree of lignification that can be completed prior to harvest [Liese and Weiner 1996; Lo *et al.* 2004]. For bamboo species of a dimension suitable for load bearing structural applications (diameter greater than 50 mm) [ISO 22156-2019], culms are usually harvested at an age of 2 to 4 years. Earlier harvest leads to poor quality bamboo since lignification is not complete. Harvest after about 4 years leads to the properties of the bamboo beginning to deteriorate [e.g., Lu *et al.* 1985].

Reportage of the mechanical properties of bamboo fibers is lacking in literature. Although a considerable number of studies have focused on bamboo fiber variation, the correlation between bamboo fiber structure and mechanical properties, as well as bamboo growth mechanisms, are poorly understood. To explain the composition of the bamboo culm wall and its correlation with the strength of bamboo, Zou *et al.* [2009] studied the nanoscale structural details of the bamboo fiber cell wall of *P. edulis*. Figure 3.2 shows the hierarchical organization of bamboo fibers over different length scales. The presence of cobble-like polygonal cellulose particles (grains) with

diameters of 20–200 nm within the cell wall layers which constitute individual bamboo fibers was observed. From both transverse and longitudinal sections, it was seen that nanograins were oriented randomly in the fiber cell wall. It was concluded that the effect of these nanoproperties on the mechanical properties of bamboo is the same transversely and longitudinally [Zou *et al.* 2009]. The nanograin-structured bamboo fibers were found to be ductile in nature with nano-indentation hardness and elastic modulus values of the fiber cell wall measured to be 0.44 ± 0.09 GPa and 10.4 ± 1.8 GPa, respectively [Zou *et al.* 2009].

The use of nano-indentation in this application with bamboo is questionable because of the material structure. Looking at the structure shown in Figure 1.2d, one could argue that very different output would result if the nano-indentation is done on any of the vascular bundle components other than the fibers themselves. These concerns have also been raised in previous research and the method was suggested to either be in need of being refined for accuracy [Yu *et al.* 2007] or *in-situ* imaging would be needed during the testing to ensure that the indentation in the bamboo fiber cell wall are valid [Wang *et al.* 2013].

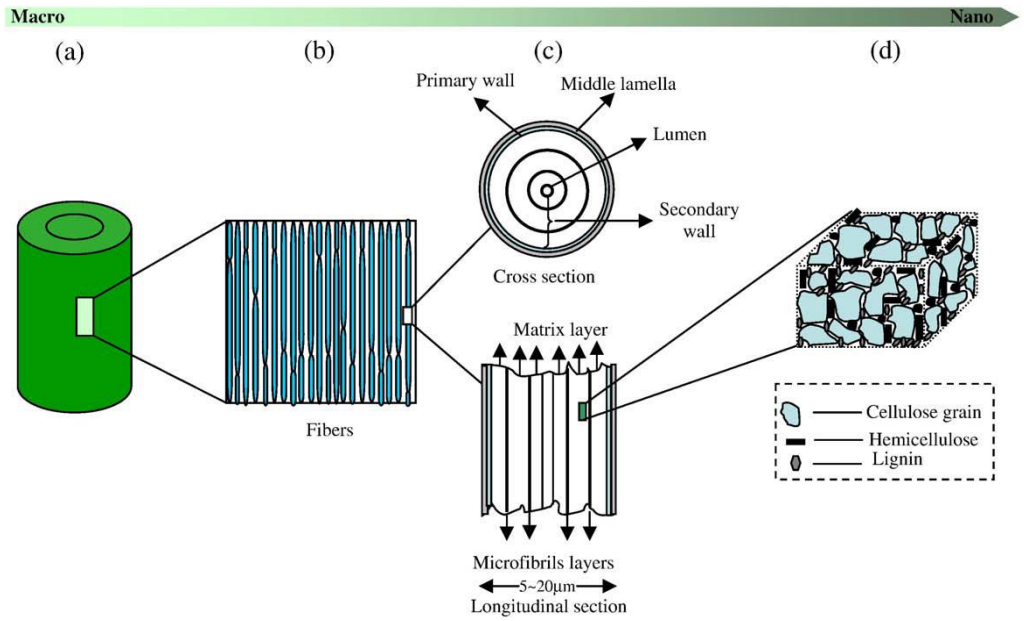

(a) Bamboo culm, in which bamboo fibers are distributed longitudinally along the culm. (b) The spindle-like short tiny fibers, tapered at both ends, are intercalated longitudinally each other along the culm. (c) The fiber cell wall exhibits a polylamellate structure with alternating broad and narrow lamellae. The middle lamella is the outer-most layer, followed by primary wall, and the secondary wall, as shown in the upper schematic in (c). The narrow layers consist of unidirectional microfibril layers, alternatively in transverse and longitudinal lamellae, with orientation 2–20°/85–90°; the broad layers are matrix, as shown in the lower schematic in (c). (d) Nanoscale cellulose grains with random orientation.

Figure 3.2: Hierarchical organization of bamboo fibers over different length scales [Zou *et al.* 2009].

3.2 Application of Rule of Mixtures to Bamboo Culm Wall Properties

In general, while highly variable, the longitudinal behavior of bamboo is relatively well understood in a qualitative sense. From an engineering perspective, the longitudinal behavior is most typically considered as a fiber-reinforced material in which longitudinal properties are obtained using a rule of mixtures approach. For example, gross section modulus, E_L, is estimated from:

$$E_L = V_f E_f + (1 - V_f) E_m \tag{3-1}$$

where V_f is the fiber volume ratio and E_f and E_m are the moduli of the fiber and matrix (parenchyma) phases, respectively.

Janssen (2000) reports typical values of E_f = 35 GPa and E_m = 1.8 GPa (these will be adopted in this study as described subsequently). Other researchers have reported different values as discussed in Section 3.3 and presented in Table 3.1.

The dominant failure mode of bamboo, however, is longitudinal splitting associated with bamboo carrying flexure, compression or tension loads, or as a result of using simple bolted connection details [Sharma *et al.* 2013]. Janssen [1981] describes the bending stresses in a culm as being characterized by the longitudinal compressive stress and transverse strain in the compression zone of the culm, with failure eventually occurring due to longitudinal splitting. This is ideally a Mode II longitudinal shear failure. However, in the presence of perpendicular stresses (as is the case wherever there is a non-zero shear-to-moment ratio), there is some Mode I component stress present which significantly reduces the Mode II capacity. Richard *et al.* [2017] demonstrate the effects of such mode mixity using longitudinal (bowtie) shear tests [ISO 22157:2019] which capture pure Mode II behavior, split pin tests [Mitch *et al.* 2010] which capture Mode I behavior, and notched full-culm bending tests of different spans resulting in different degrees of mode mixing. For two different species, thin walled *P. edulis* and thick-walled *B. stenostachya*, the split pin tests resulted in Mode I capacities equal to only 18% of the Mode II capacity determined from the longitudinal shear tests. Beam tests having mixed mode behavior exhibited shear capacities ranging from 40-70% of the Mode II capacity.

Both the Mode I and II behaviors are primarily functions of the transverse properties of the fiber-reinforced culm which are believed to be dominated by matrix (parenchyma) properties. Despite their importance in the dominant observed behavior of full-culm bamboo, there are few

studies of the transverse properties of the culm wall. In early work, Arce-Villalobos [1993] concluded that there is no correlation between the density of bamboo and its transverse tensile strength. Janssen [2000], based on flexural tests, reports that a transverse strain of 0.0013 results in transverse tensile failure of the culm wall (with no indication of species or other variation).

More recently, test methods have been proposed for obtaining transverse properties of bamboo culms [Mitch *et al.* 2010; Sharma *et al.* 2013; Virgo *et al.* 2017] although these have not yet been widely adopted to obtain material properties over a range of species and conditions. Sharma and Harries [2012] report a unique attempt to refine a circumferential compression test (see Section 2.3.4) to determine through culm-wall distribution of properties. In their study, the culm was cut using a water jet, into two or three concentric annular sections. Circumferential compression test results for each resulting 'ring' provided an improved measure of through-thickness transverse properties than could be obtained from a full-culm section. The approach, however, was limited to thicker culm walls, provided only two or three data points across the culm wall, and did not result in repeatable specimen preparation and was therefore abandoned.

Tan *et al.* [2011] conducted a micro-scale study on the crack growth and toughening mechanisms of *P. edulis*. The study revealed that toughening was inversely related to fiber density. The authors noted that their results suggest the need to account for the anisotropic strength and fracture properties of bamboo in the design of bamboo structures.

In order to understand the transverse behavior of bamboo, it is informative to consider the rule of mixtures for transverse properties:

$$E_T = [V_f/E_f + (1 - V_f)/E_m]^{-1} \tag{3-2}$$

Equation 3-2 is conventionally considered a lower-bound estimate of transverse properties since it does not account for the anisotropic nature of the fiber itself and, as a result, underestimates off-longitudinal properties [Mallick 2008]. Considering the work of Zou *et al.* [2009] reported in Figure 3.2, a similar hypothesis could be drawn for bamboo. The Halpin-Tsai correction to the transverse rule of mixtures is most often adopted to describe transverse behavior of fiber-reinforced composites [Halpin and Kadros 1976]:

$$E_T = E_m(1 + \xi n V_f)/(1 - n V_f) \tag{3-3}$$

$$n = (Ef/Em - 1)/(Ef/Em + \xi) \tag{3-4}$$

The value of ξ is an empirical constant fitted to the elasticity solution for a fiber geometry and confirmed by experimental data [Halpin and Kadros 1976]:

$$\xi = 2 + 40 V_f^{10} \tag{3-5}$$

When considering transverse properties of longitudinally reinforced fiber reinforced composites having V_f less than 0.50, it is conventional to assign $\xi = 2$ [Hewitt and de Malherbe 1970]. Halpin-Tsai is equally applicable to determining longitudinal properties. For longitudinal properties of long or continuous fiber composites (such as bamboo) however, Halpin-Tsai results in the same relationship as the rule-of-mixtures (Eq. 3-1). The Halpin-Tsai formulation given in Eq. 3-3 has been adopted in this study.

Figure 3.3 presents theoretical longitudinal and transverse modulus distributions determined using the rule of mixtures and Halpin-Tsai, respectively (Equations 3-1 and 3-3). The fiber volume distribution illustrated is that proposed by Dixon and Gibson [2014] for *P. edulis* and is representative of most distributions reported in Table 3.1. The modulus distributions shown are normalised by the average modulus for the culm wall which is what should be obtained when testing a full-culm specimen (i.e., the apparent modulus of the gross section). In addition to the variation in properties, a shift of the neutral axis of the section (the location at which the ratios equal unity) toward the outer culm wall is evident. This shift results in the increase in gross culm stiffness described by Janssen [2000] and Harries *et al.* [2017] (described below).

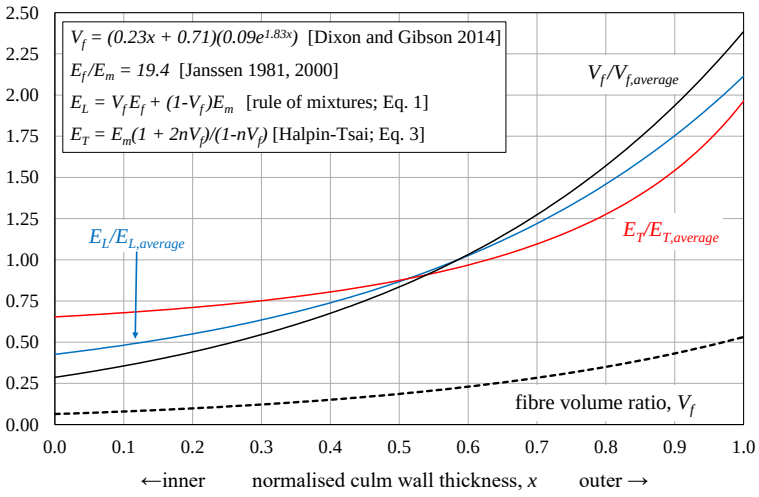

Figure 3.3: Distribution of fiber volume and modulus through culm wall based on rule of mixtures.

Habibi *et al.* [2015] introduced a numerical model, to predict the elastic flexural behavior of bamboo. The experimentally-derived flexural moduli was fitted to an exponential function treating a bamboo strip as a functionally graded beam having a through-depth gradation [Wakashima *et al.*1990].

$$E(x) = (E(0) - E(1))\left(x + \frac{1}{2}\right)^{k} + E(1) \tag{3-6}$$

where *E(0)* and *E(1)* are the flexural moduli at the innermost and outermost layers of the bamboo strips, respectively; *x* is the relative location through the wall having a thickness (*x* = 0 at inner face and *x* = 1 at outer face), and *k* is a factor fitting the gradation of the volume fraction of fiber through the thickness of the strips. The problem with this approach is the need to obtain *E(0)* and *E(1)* and that *k* is an empirical factor expected to vary considerably based on species, age, etc.

While many researchers report bamboo properties as gross section properties (and therefore as apparent average properties), considering the variation of the fiber volume through the culm wall thickness clearly represents an improvement in understanding the behavior of bamboo. Janssen [1981] proposed a 'rule-of-thumb' that the flexural stiffness of full-culm bamboo (*EI*) is in fact about 10% greater than one would obtained using measured geometry (*I*) and an apparent average modulus (*E*) obtained from a full-culm (i.e., gross section) test. Harries *et al.* [2017] refined this estimate to be an approximately 20% increase for thick-walled members (*D/t* < 8) and a 5% increase for thin-walled members. This study will attempt to refine this understanding and establish a standard basis for describing the functionally graded fiber volume in full-culm bamboo. In support of this, a database of existing empirical relationships for the variation of fiber volume ratio (and/or longitudinal modulus) of bamboo is summarized in Table 3.1.

An objective of the present study is to investigate the transverse material property gradient through the culm wall and to connect the mechanical results to physical observations and culm morphology, such as fiber volume. In this study, a modification to the flat-ring flexure [Virgo *et al.* 2017] test specimen, in which only portions of the culm wall cross-section are tested, is used

to obtain a measure of the transverse tensile capacity of the bamboo. Microscopy analyses are used to qualitatively describe the culm wall architecture and to quantitatively assess the failure modes observed through the culm wall thickness. Throughout this study, all data is normalized by culm wall thickness such that $x = 0$ is the inner wall and $x = 1$ is the outer wall.

3.3 Material Properties of Fibers and Matrix

To successfully apply the rule of mixtures formulation described above in modelling the effect of fiber volume on the mechanical property variation of the bamboo culm wall, the Young's modulus of both the fiber and parenchyma matrix needs to be estimated (E_f and E_m, respectively). Values reported in literature – summarized in the right-hand columns in Table 3.1 – have been derived using various techniques. The most commonly reported values were estimated using the rule of mixtures from results of experimental tests while many others were obtained from nano-indentation tests (which, as described above may not be entirely appropriate for bamboo).

One of the very first reports of Young's modulus of bamboo fibers, $E_f = 35$ GPa [Janssen 2000] was determined noting that that 50% of the cross section of a fiber was cellulose, which has a known modulus E = 70 GPa. Considering all the data shown in Table 3.1, this approximation stands up well and will be used in the analytical components of the present study (Chapters 5 and 6). Janssen [1981] reported that lignin – of which the parenchyma matrix is primarily comprised has Young's modulus of approximately $E_m = 1.8$ GPa having a Poisson's ratio of approximately 0.3; these values, too, are adopted in the analytical components of the present study.

Nogata and Takahashi [1995] and Amada *et al.* [1996] adopted the rule of mixtures to measured tension test results to estimate the Young's modulus of bamboo fiber to be E_f = 55 GPa and 46 GPa, respectively. Both report a matrix modulus, E_m = 2 GPa.

Yu *et al.* [2007] conducted longitudinal *in-situ* nano-indentation tests on bamboo fiber cell walls in both the longitudinal and transverse directions and recorded average values of 16.0 GPa and 5.9 GPa, respectively. The longitudinal modulus of the parenchyma cells measured in this study was 5.8 GPa and was inferred to be much closer to the actual value than the values measured for bamboo fibers using nano-indentation, suggesting that the method needed some improvement to yield accurate measurements. A limitation of the nano-indentation method is that it is based on the assumptions of isotropy and homogeneity, which are not appropriate for bamboo fibers and may not be appropriate for parenchyma cells.

Shao *et al.* [2010] conducted tensile tests on bamboo blocks and estimated the modulus of elasticity of fiber and parenchyma ground tissue to be 40.4 GPa and 0.22 GPa, respectively, using a parallel connection model. The study further carried out tensile tests on fiber bundles separated from the bamboo parenchyma ground tissue reporting E_f = 33.9 GPa. The difference in the two values was attributed to a possible redistribution of stresses between fibers by the parenchyma ground tissue, resulting in a greater apparent modulus when the fiber bundles were tested *in situ*.

Dixon and Gibson [2014] combined both experimental methods and rule of mixtures with nano-indentation tests carried out on fiber cell walls. Nano-indentation was performed on the sclerenchyma fiber bundles and the modulus was determined to be E_f = 14.9 ± 2.3 GPa. An extrapolation of the extreme density value in the experimental flexural Young's modulus data used to estimate the solid cell wall was assumed similar for both the fibers and parenchyma. The

reported values in the study were E_f = 39.8 GPa and E_m = 1.93 GPa respectively. Data from these and other studies are summarized in Table 3.1.

3.4 Digital Imaging to Obtain Fiber Volume Distribution

3.4.1 Background

A number of studies have used digital imaging techniques – many using Scanning Electron Microscopy (SEM) – to investigate the components and gradation of the bamboo wall section. Li and Shen [2011] used an optical microscope equipped with a digital camera. The outline of each vascular bundle was traced by hand, and the whole area of vascular bundles measured using CAD software to analyze the variation of fiber volume ratio, V_f, in the radial direction. Amada *et al.* [1996] captured an image of the cross section taken by a 484 x 252 pixel CCD camera. The image was processed into a binary image to separate the bundle sheaths from the culm tissues and the fiber volume was measured by counting pixels (results are summarized in Table 3.1). Due to the limited image size, the resolution and therefore precision of this method is limited. Other earlier studies reported by Amada *et al.* [1996] used similar approaches and many overestimated the fiber volume fraction due to low resolution images and some difficulty in distinguishing fiber from vessel in the vascular bundle (see Figure 1.2d). More recently, Habibi and Lu [2014] conducted a microstructural characterization on bamboo using Environmental Scanning Electron Microscopy (ESEM). The captured micrographs were processed using image analysis software to quantify the volume fractions of the different constituents of the culm wall (results are summarized in Table 3.1).

Based on the observed transverse section of the bamboo culm presented by Liese [1987], Ghavami *et al.* [2003] reports that bamboo is roughly constituted by the two distinct phases of cellulose fibers and the lignin matrix. This approximation allows bamboo to be considered as a simple two-component composite material for which well-established approaches such as the rule of mixtures, can be applied to account for the variability of the fiber gradation. Figure 1.2 shows labeled images of the microstructure of bamboo. Based on early image analysis studies, the reported fiber volume ratios are typically not reporting the ratio of structural or load-bearing fibers, but rather the ratio based on the entire vascular bundle (which includes the vessels). When considering gradation of properties, the approaches – including or excluding the vessels – have been reported interchangeably. Dixon and Gibson [2014], however, report the fiber volume ratio based on the vascular bundle followed by a relationship for the solids volume in the vascular bundle that also varies with wall thickness. In the current study when referring to 'fibers', only the fiber bundles in each individual vascular bundle is being described.

3.4.2 Image Analysis

Image analysis was used to characterize the culm wall fiber volume fraction. This was done by taking digital images of seven randomly selected full-culm cross sections of the bamboo species described in Chapter 2 (only four sections for *B. Stensostachya*). Each culm section was imaged at each of the four quadrants (N, E, S, and W). The quadrants are not in relation to the growth direction of the bamboo (which is unknown) but simply indicate four quadrants of the culm wall when cut into smaller pieces. Images were taken using a common digital camera to elaborate the possibility of repeating this procedure in the field with limited resources. The resulting images was

at least 640 x 480 pixels. For an image such as that shown in Figure 3.4, this results in a resolution on the order of 0.025 mm/pixel.

Using the purpose-written Matlab script given in Appendix A, based on image contrast, each square image (an example is shown in Figure 3.4a) was processed to produce a high contrast image allowing differentiation of the bamboo fiber bundles as seen in Figure 3.4b. The contrast imaging was able to discriminate between fiber bundle and vessels, excluding the latter from the vascular bundle. As a result, the fiber volume ratio, V_f is correctly reported.

Using the MatLab script, each full-culm wall thickness image was divided into ten equal sub images (each of thickness $t/10$) in the through-culm wall thickness (t) direction as shown in Figure 3.4b. The fiber components were extracted from the images and the fiber volume ratio determined for each sub image. From this analysis, the total fiber volume ratio of each strip, V_f, and the distribution as a function of location through the culm wall can be determined. An example of such output is shown in Figure 3.4c.

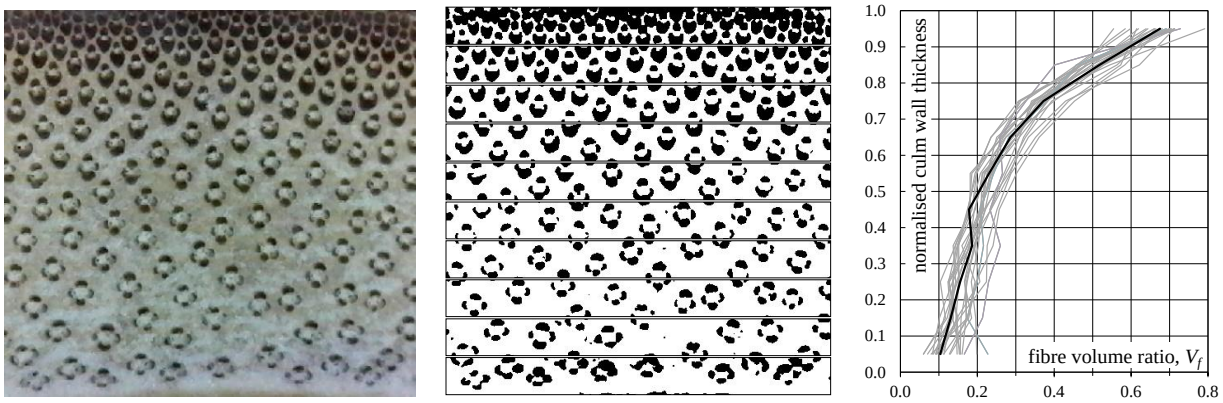

a) image of culm wall

b) MatLab pixel map of fibers divided into ten layers

c) fiber volume distribution for 28 *P edulis* specimens, Black line corresponds to image in figures a) and b)

Figure 3.4: Example of digital image analysis of culm wall (P. *edulis*-C specimen shown)

3.4.3 Fiber Volume Distribution

Using the analysis technique described in the previous section, the average fiber distribution (expressed as a third-order polynomial curve) is obtained for each species as shown in Figure 3.4. The distributions are reported at the bottom of Table 3.1 in terms of the normalized culm wall thickness, x ($x = 0$ is the inner culm wall and $x = 1$ is the outer culm wall). The coefficient of variation of measured fiber volume ratios was less than 0.18 for all but *P. nigra*, which exhibited a COV = 0.24. The 28 *P. edulis*-C specimens (4 quadrant images from each of 7 sections) shown in Figure 3.4c have a COV = 0.13. The best-fit equations representing fiber volume distribution reported in Table 3.1 all have a coefficient of determination $R^2 = 0.99$.

Figure 3.5a-e shows the fiber distribution with the range indicated for each species. As seen in Figure 3.5f, the fiber distribution among the four thin-wall *Phyllostachys* species is very similar. A single third-order polynomial relationship can be given for all four *Phyllostachys* species having $R^2 = 0.96$ as shown in Table 3.1. A marked difference in fiber distribution is observed in the thick-walled *B. stenostachya*. Thus, fiber distribution is observed to differ by genera (*Phyllostachys* and *Bambusa*) but less so among species in the same genera (*Phyllostachys*).

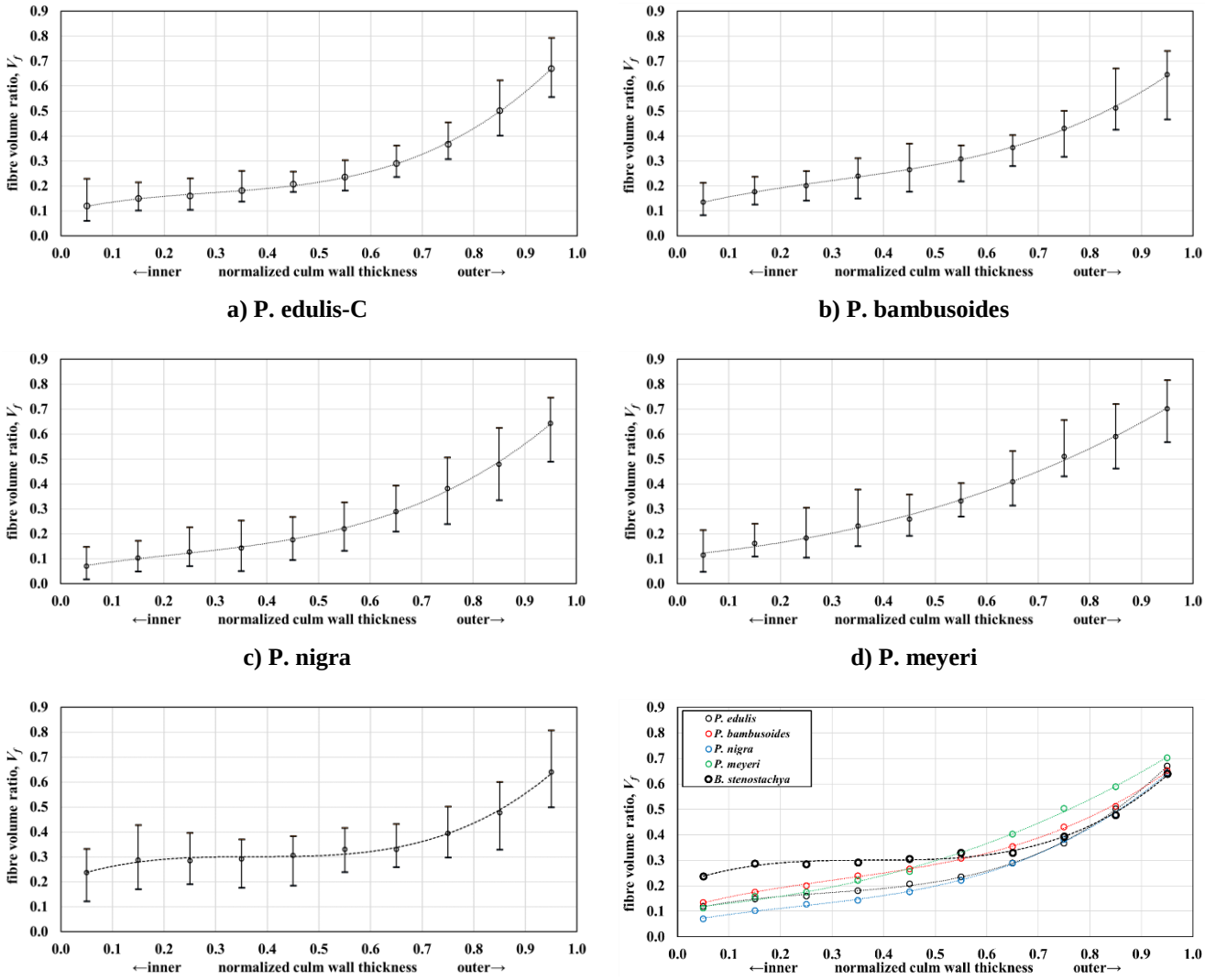

Figure 3.5: Third-order polynomial representations of fiber distributions obtained from image analysis.

3.5 Clipped Flat Ring Flexure Testing and Results

To investigate the variation of material properties through the culm wall thickness, a modification to the flat-ring flexure test method (Section 2.3.3) was developed in this study. The test specimens were modified such that only a specific part of the wall cross-section is tested. The

resulting specimens are described as being “clipped”. The intent of the modification is to determine the effect of the material property gradient through the culm wall and to connect the mechanical results to the fiber density reported in the previous section.

A number of methods were previously attempted to develop a test specimen which fails primarily in the constant or maximum moment regions. The most effective means found to produce the specimens was the use of an end mill to cut the inner and outer wall of the specimen, as described below. This method produced sufficient specimens of different (well-controlled) widths and consistently resulted in specimens that failed in the constant moment region.

3.5.1 Material and Specimen Preparation

The same five species used for the flat ring flexure test described in Chapter 2 were tested for the clipped cases. Average culm diameter, D, and wall thickness, t, for each group of specimens are reported with the summary of test results in Table 3.2. Each specimen was cut to a length of approximately 0.2D as described in Section 2.3.3. The specimens were then “clipped” using an end mill as shown in Figure 3.6a. As shown in Figure 3.6b, the specimens were cut through the culm wall thickness in increments of $0.2t$ or $0.25t$ depending on the overall thickness of the culm wall. The resulting specimens are relatively fragile and thinner specimen increments could not be consistently obtained. By using adjacent specimens along the culm length, each with a different clipped geometry, the transverse modulus of rupture can be obtained at four ($0.25t$ increments) or five ($0.2t$) locations through the culm wall.

The dimensions used for each clipped specimen included a fixed test segment width, α = 0.2 or 0.25, and varying β and γ dimensions which are cut from the outer and inner wall sections,

respectively. As shown in Figure 3.6b, the selection of β and γ locate the test segment α within the culm wall thickness and the sum $\alpha + \beta + \gamma = 1$, the culm wall thickness. This approach divides the culm wall into segments for which the modulus of rupture determined from each segment is calculated from Eq. 3-7 and is assumed to represent the average value for that segment; the value is then assigned to the centroid of the segment.

$$f_r = 3Pa/(\alpha t_N + \alpha t_S)H^2 \qquad (3\text{-}7)$$

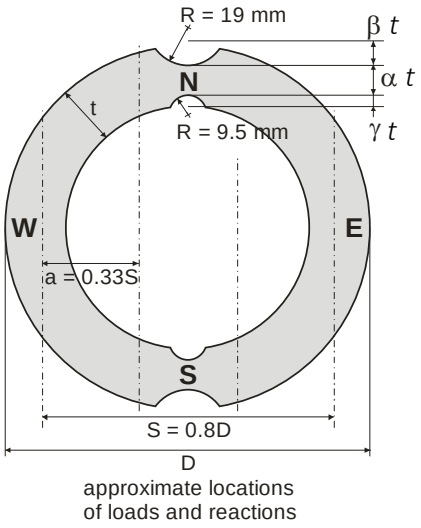

(a) End mill cutting of modified test specimens in operation (β = 0, α = 0.20 and γ = 0.80 shown)

(b) A typical finalized modified specimen schematic and dimensions.

Figure 3.6: Cutting process of modified test specimens and a typical specimen plan dimensions

For each chosen geometry in each species considered, at least two specimens were cut for the experiment. To achieve uniformity in all specimens, a 9.525 mm end mill was used to machine the inner region (γ) and a 19.05 mm end mill was used to machine the outer region (β). Although

care was taken to avoid loss of specimens during cutting or handling, some of the specimens were lost due to their fragile nature after being cut. This was particularly the case for the thinner walled species. With this study, the flat-ring flexure results with no cut (i.e., $\alpha = 1$) reported in Section 2.4 were used as the control specimens. The results from the control specimens represent the gross cross-section modulus of rupture, $f_{r\alpha}$, against which the clipped-specimen data is normalised. Apart from the specimen geometry, the test method was conducted in the same manner as described in Section 2.3.

3.5.2 Clipped Flat-Ring Flexure Test Results

A summary of the clipped flat-ring flexure test result is provided in Table 3.2. The clipped modulus is denoted as f_r to differentiate it from the full-culm wall thickness control specimens, $f_{r\alpha}$. With the clipped specimens, all failures occurred in the clipped region and no data was determined to be an outlier.

Table 3.2: Summary of clipped flat-ring flexure tests result (COV in parenthesis)

Species	D (mm)	t (mm)	n	β	α	x^a	f_r (MPa)	$f_r/f_{r\alpha}$	$f_r/f_{r\alpha}$	$\int \frac{f_r}{f_{r\alpha}} dx$
P. edulis-C	117 (0.06)	10.1 (0.10)	33	0.00	1		$f_{r\alpha}$ = 17.30 (0.18)		$4.0x^2 - 4.9x + 2.3$ ($R^2 = 0.842$)	1.18
	112 (0.05)	9.5 (0.09)	4	0.00	0.23	0.89	18.34 (0.17)	1.06		
			2	0.25	0.27	0.62	16.22 (0.28)	0.94		
			1	0.40	0.21	0.50	12.45	0.72		
			1	0.50	0.26	0.37	13.43	0.78		
			2	0.60	0.20	0.30	20.93 (0.14)	1.21		
			1	0.75	0.29	0.11	27.92	1.61		
			2	0.80	0.20	0.10	33.54 (0.01)	1.94		
P. bambusoides	95.5 (0.05)	8.2 (0.22)	27	0.00	1		$f_{r\alpha}$ = 15.70 (0.21)		$2.6x^2 - 2.5x + 1.5$ ($R^2 = 0.31$)	1.12
	94.8 (0.06)	8.1 (0.24)	4	0.00	0.25	0.88	21.60 (0.21)	1.37		
			2	0.25	0.25	0.63	12.60 (0.25)	0.80		
			1	0.4	0.21	0.50	12.40	0.79		
			1	0.5	0.28	0.36	19.09	1.22		
			2	0.6	0.19	0.31	18.67 (0.21)	1.19		
			2	0.75	0.29	0.10	15.78 (0.02)	1.00		
			2	0.8	0.2	0.10	22.98 (0.27)	1.46		
P. nigra	93.5 (0.03)	6.7 (0.19)	31	0.00	1		$f_{r\alpha}$ = 15.60 (0.14)		$0.7x^2 - 0.8x + 1.4$ ($R^2 = 0.08$)	1.23
	92.4 (0.01)	6.5 (0.14)	4	0.00	0.27	0.87	19.20 (0.16)	1.23		
			4	0.25	0.27	0.62	16.69 (0.22)	1.07		
			4	0.50	0.25	0.38	19.90 (0.05)	1.27		
			4	0.75	0.25	0.13	19.88 (0.17)	1.27		
P. meyeri	65.3 (0.12)	6.7 (0.10)	49	0.00	1		$f_{r\alpha}$ = 20.00 (0.16)		$2.4x^2 - 1.8x + 1.1$ ($R^2 = 0.59$)	1.00
	65.2 (0.09)	6.4 (0.11)	4	0.00	0.26	0.87	27.98 (0.11)	1.40		
			3	0.25	0.28	0.61	17.48 (0.28)	0.88		
			6	0.50	0.26	0.37	16.10 (0.25)	0.81		
			7	0.75	0.26	0.12	19.07 (0.19)	0.96		
B. stenostachya	77.5 (0.06)	14.4 (0.32)	39	0.00	1		$f_{r\alpha}$ = 9.44 (0.13)		$4.1x^2 - 3.6x + 1.6$ ($R^2 = 0.77$)	1.17
	75.4 (0.06)	14.7 (0.28)	4	0.00	0.23	0.89	15.75 (0.12)	1.67		
			2	0.20	0.19	0.71	12.00 (0.08)	1.27		
			2	0.25	0.27	0.62	8.80 (0.34)	0.93		
			2	0.40	0.19	0.51	8.27 (0.04)	0.88		
			1	0.50	0.28	0.36	7.53	0.80		
			2	0.60	0.19	0.31	8.87 (0.10)	0.94		
			2	0.75	0.26	0.12	10.31 (0.29)	1.09		
			2	0.80	0.19	0.11	13.75 (0.13)	1.46		

[a] $x = 1 - \beta - \alpha/2$
Reported data are averages and (COV)

Experimentally determined values of $f_r/f_{r\alpha}$ determined from the clipped tests are shown in Figure 3.7. The corresponding best fit second-order polynomial relationships are also shown and

reported in Table 3.2. Figure 3.7 shows that the modulus of rupture, f_r, varies through the culm wall thickness in a generally 'parabolic' manner: the modulus is greater at both the inner and outer walls and lower in the middle. The results illustrated in Figure 3.7 illustrate a similar trend although *P. nigra* specimens exhibit relatively little variation through the culm wall compared to the other species.

Integrating the $f_r/f_{r\alpha}$ best-fit curves (Table 3.2) from $x = 0$ to $x = 1$ should represent the gross modulus across the section; that is, the integral should equal unity. However, as shown in Table 3.2, with the exception of *P. meyeri*, the gross modulus obtained by integrating the clipped data exceeds unity by as much as 20%. A possible explanation for this behaviour – one in which the sum of the parts exceeds the capacity of the whole – is that failure of the full wall section control specimens is being initiated by a 'weak link'. A brittle failure of the outer layer of the culm wall initiating failure would explain this observation.

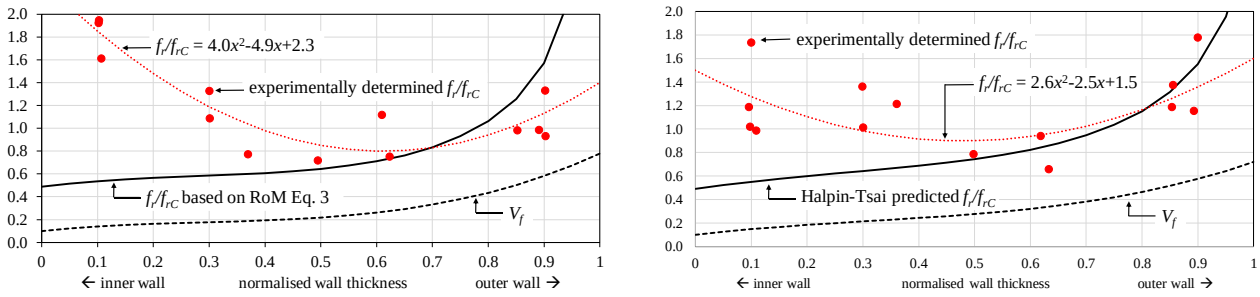

a) P. edulis-C

b) P. bambusoides

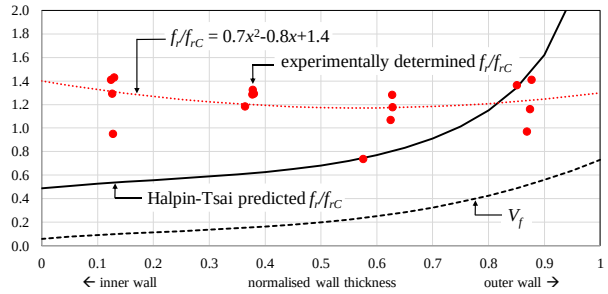

c) P. nigra

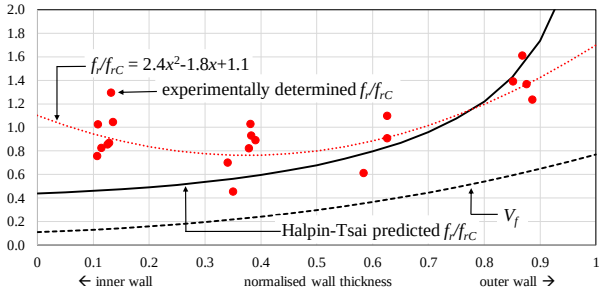

d) P. meyeri

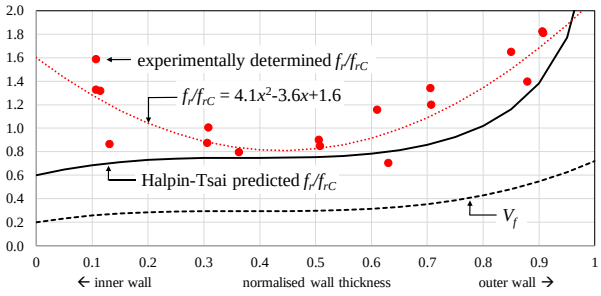

e) B. stenostachya

Figure 3.7: Variation of modulus of normalised rupture through culm wall section.

The fiber volume distributions, also shown in Figure 3.7 and given in Table 3.1, indicate a typically observed distribution having lower fiber volume at the inner wall and a greater fiber volume at the outer wall. Based on these fiber distributions, the predicted distribution of modulus of rupture using the Halpin-Tsai equation (Eq. 3-3) does not appear to capture the experimentally observed behavior, particularly in the inner half of the culm wall where fiber volumes are lowest.

Bamboo does not appear to be behaving as a classic fiber-reinforced composite material in the direction transverse to the fibers.

The observed behavior requires further study and may represent a material variation or morphological variation through the bamboo culm wall thickness. The observation may be a manifestation of the toughening effect reported by Tan *et al.* [2011] described in Section 3.2 To investigate this further, the failure planes of full-culm wall thickness control specimens were investigated using a scanning electron microscope (SEM) explained in Section 3.7.

3.6 Shaved Flat Ring Flexure

It is believed that the extreme outer layer of a bamboo culm which consists of a silica-rich outer skin (epidermis) and a thin region of densely packed fibers will be more brittle than the rest of the culm wall. This is hypothesized to initiate failures in specimens in which the outer wall is included. Therefore in the flat ring flexure specimen testing a question arises: *is the outer layer contributing disproportionately to the observed behavior, especially to the control and* $\beta = 0$ *tests*? To investigate this effect, additional specimens were tested having $\beta \approx 0.05$ and $\alpha \approx 0.95$ (i.e. $\gamma = 0$, see Figure 3.6b); essentially, these are full-culm sections with only the outer epidermal layer 'shaved' away. Figure 3.8 shows images of a shaved specimen before and after failure.

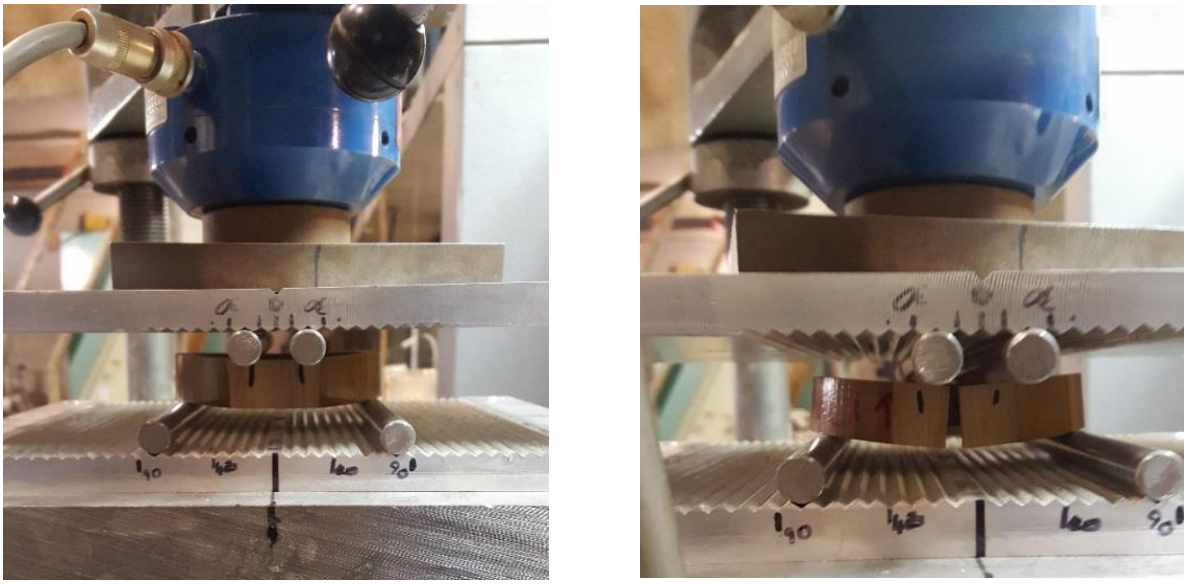

a.) Image of test set up **b.) Typical test set up at failure**

Figure 3.8: Flat ring flexure set up images of shaved specimens

Twenty new flat-ring flexure specimens were cut from comparable specimens of each species tested in the clipped flat-ring flexure test program (*P. edulis*-C was not included as there were no comparable specimens available). Alternating specimens along the culm were prepared using a belt sander. Resulting wall thicknesses in the constant moment region of the shaved flat ring flexure tests are reported in Table 3.3. Apart from specimen preparation, all tests were identical to those reported previously. To assess potential changes in specimen ductility, displacement of the applied load, δ, was measured and reported at failure of each specimen. Also shown in Table 3.3 is the p-value determined from an unpaired t-test for each set of 'shaved' and unshaved specimen. The p-value is the probability that there is no statistically significant difference between the compared conditions.

Table 3.3: Summary of results from specimens having outer layer removed (COV in parentheses).

Species	n	D	t	Modulus of rupture, f_r		Deflection, δ		f_r/δ	
		mm	mm	MPa	p	mm	p	MPa/mm	p
P. bambusoides	10	99.6 (0.01)	6.47 (0.09)	18.1 (0.08)	0.09	1.86 (0.13)	0.00	9.9 (0.14)	0.01
Outer layer removed	10	99.8 (0.01)	0.92t (0.04)	19.7 (0.12)		2.30 (0.16)		8.4 (0.08)	
P. nigra	10	96.0 (0.01)	8.44 (0.03)	26.4 (0.16)	0.75	2.10 (0.09)	0.59	12.6 (0.15)	0.99
Outer layer removed	9	95.8 (0.01)	0.95t (0.02)	26.0 (0.06)		2.06 (0.06)		12.6 (0.06)	
P. meyeri	4	62.8 (0.00)	6.58 (0.02)	22.5 (0.08)	0.22	0.95 (0.20)	0.06	25.0 (0.33)	0.09
Outer layer removed	5	62.9 (0.01)	0.95t (0.02)	21.0 (0.07)		1.21 (0.14)		17.6 (0.14)	
B. stenostachya	7	71.7 (0.02)	15.00 (0.03)	13.8 (0.10)	0.86	1.59 (0.22)	0.10	9.3 (0.30)	0.13
Outer layer removed	9	72.2 (0.02)	0.95t (0.04)	14.0 (0.09)		1.91 (0.18)		7.6 (0.17)	

It is seen from Table 3.3 that the modulus of rupture, f_r, is essentially unaffected by the removal of the outer layer. With the exception of *P. nigra*, the displacement at failure is observed to increase upon the removal of the outer layer. This increase is greater than can be attributed to the loss of 5% of the moment of inertia of the cross section (resulting from shaving the specimen) alone. To consider the observed behavior in a normalised fashion, the tangent 'stiffness', f_r/δ is also calculated. As seen in Figure 3.9, specimen stiffness (represented as linear best-fit line in Figure 3.9), falls between 15 and 30% (with the exception of *P. nigra*) despite the moment of inertia being reduced only 5%. The modulus of rupture itself remains unchanged

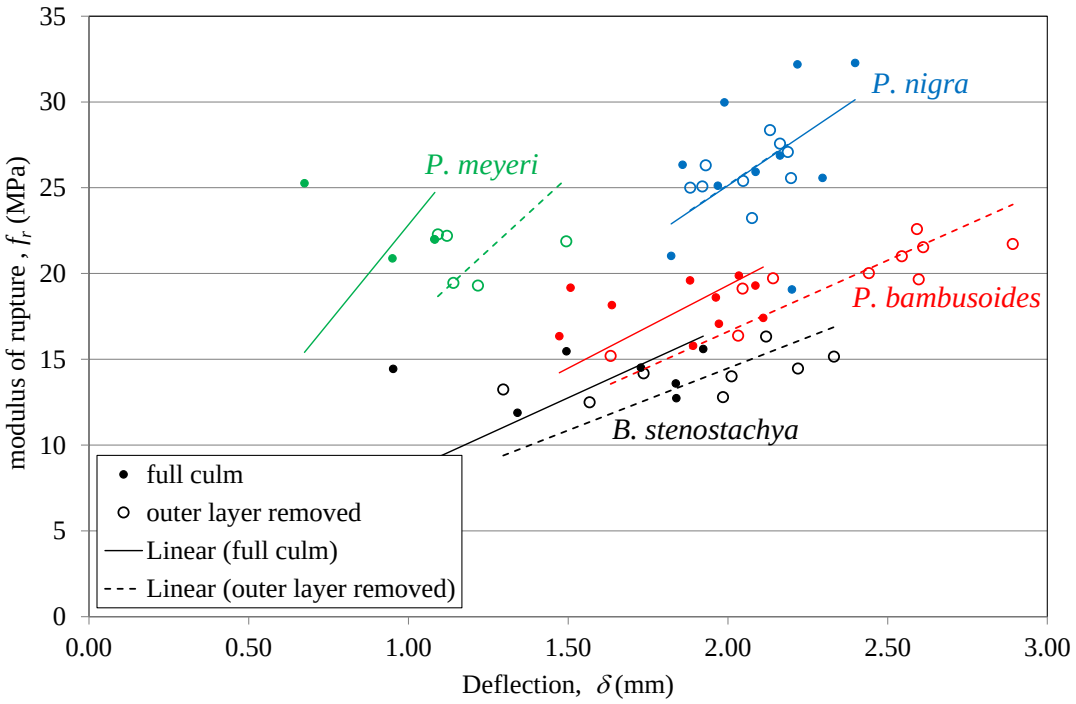

Figure 3.9: Comparison of full-culm specimens and those having only outer layer removed.

3.7 SEM Imaging of Flat-Ring Flexure Failure Surfaces

To further characterize the tested specimens, various specimens from the full-culm wall width flat-ring flexure tests were selected for microscopic evaluation. Both an optical microscope (OM) and a Scanning Electron Microscope (SEM) were used. Transverse culm sections and the failure planes created by the flat-ring flexure tests were investigated. This was aimed at giving a clearer understanding to the underlying mechanisms of bamboo behavior and to help explain the counterintuitive results shown in Figure 3.7 – especially nearer the inner culm wall.

3.7.1 Specimen Preparation for Imaging

To obtain images of the failure planes, no major surface preparation was needed other than cutting the cracked section into a smaller piece for mounting using a diamond cutting disc and sputter coating the surface to be imaged. The culm wall sections, however, required special preparation to attain clear images. The preparation of the transverse sections went through a number of iterations in order to obtain satisfactory images. The best practice developed is described here.

Except for the flat-ring flexure failure planes, which were imaged as close to their as-is condition as possible, specimen surfaces were cut smooth using a precision sectioning saw with a 0.5 mm thick diamond-cutting disc. The selection of a diamond disc is important as it ensures the surface is free from burn and distortion and that opposing surfaces are near parallel to each other. Simply cutting with a diamond disc was sufficient to obtain good quality images from optical microscopy.

For SEM imaging, the cut surface of the specimen being imaged was ground and polished using a *Buehler PlanarMet 300* bench top planar grinding machine. Due to the presence of small pores in the bamboo wall and behavior anticipated to be different from other materials, available cold mounting resin for impregnation could not be used. Therefore, a manual specimen placement was established which did not require direct mounting on the grinding machine. The apparatus used for the process includes the Buehler consumables (magnetic platen system, diamond grinding discs, diamond-polishing paste of different micron sizes), isopropyl alcohol and an ultrasonic cleaner filled with water. The process involves using the pastes in varying micron sizes ranging from 15 µm to polishing with a 3 µm paste followed by a 1µm paste. For each of the sizes, the

diamond polishing paste was spread on the Buehler grinding disc, which is glued to a platen system specific to the paste size. The setup is placed in the grinding machine and set to rotate at 50 rpm. No mount was used in this case; the specimens were carefully placed on the rotating disc by hand and pushed down gently for the grinding process. The grinding process lasted about five minutes while moving the specimen slowly in the direction opposing the rotating disc.

Upon completion of each step of the grinding process, the specimen was submerged in a beaker filled with isopropyl alcohol and subsequently placed in the ultrasonic cleaner for about 20 minutes. This process removes any excess polishing paste which might be trapped in the pores of the bamboo. The next process involved leaving the specimens to dry for about one hour at room temperature before a smaller micron size paste was used following the same procedure. The final specimen, after polishing with the 1 μm paste, was left to dry at room temperature for about 24 hours before SEM analysis. Before conducting the SEM analysis, each of the dried specimen surfaces was coated with palladium in a *Cressington Sputter Coater*.

3.7.2 Microscopic Images and Observations

The failure region from flat ring flexure tested specimens were further examined under OM and SEM in an attempt to understand the behavior identified from the clipped flat-ring flexure test series. A *Zeiss smartzoom 5* digital microscope (OM) and a *FEI Apreo Hi-vac FEGSEM* (SEM) were used in this study.

It was hypothesized that the high values of f_r observed in the inner culm wall region which differed from the predicted values (Figure 3.7) resulted from a different failure behavior than is conventionally seen in fiber reinforced composite materials. The propagation of cracks in bamboo

have been examined by various researchers [Low *et al.* 2006; Shao *et al.* 2009; Tan *et al.* 2011; Habibi and Lu 2014]. While most of the findings conclude that crack propagation occurs around the interface between the parenchyma and the schlerenchyma fibers, they do not fully explain what happens in regions of lower fiber volume.

Figure 3.10 shows SEM images of typical *P. edulis*- α vascular bundles (near the outer culm wall) showing the fiber bundles comprised of microfibrils surrounding the vessel and the parenchyma into which the bundle is embedded. In Figure 3.10, the fiber bundle can be seen to be penetrated by intra-fibril cracks whereas the interfaces between fibers and parenchyma appear quite intact. It is noted that the parenchyma cell walls are relatively thick indicating a relatively mature culm age at harvest [Liese and Weiner 1996]. The cracking of the fibers may therefore be a function of culm age (observed although not described by Liese and Weiner). The age at harvest of the bamboo used in this study is unknown and without comparative images, age cannot be estimated. Liese and Weiner (1996), however clearly describe, and Liese (1998) illustrates, the thickening of parenchyma cell walls with age.

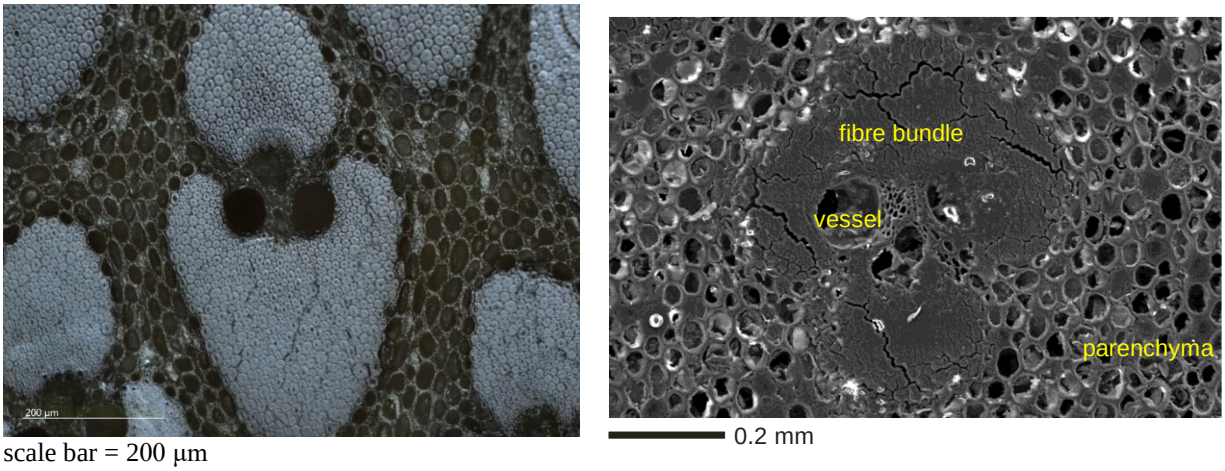

scale bar = 200 µm

Figure 3.10: OM and SEM images of *P. edulis*- α vascular bundles

A hypothesis is that these intra-fibril cracks formed as a result of shrinkage associated with drying (desiccation of the vessel) or treatment of the bamboo. Chen *et al.* [2018] clearly describes different behavior of the parenchyma and interaction between the parenchyma and fibers based on moisture content. On the other hand, Osorio *et al.* [2018] argues that these cracks result from extraction and preparation of the SEM specimen. Further study is required to address the source of these cracks – which are relatively commonly seen – as they represent a stress raiser in the adjacent parenchyma and may be the source of cracks in the parenchyma. Such an effect is shown in images in Habibi and Lu [2014] and Chen *et al.* [2018] although not described by the authors in either case.

Figure 3.11 shows SEM images taken from the failure plane of a flat-ring flexure test specimen. Each failure plane was divided into a grid and images of each region obtained, allowing the entire failure plane to be imaged.

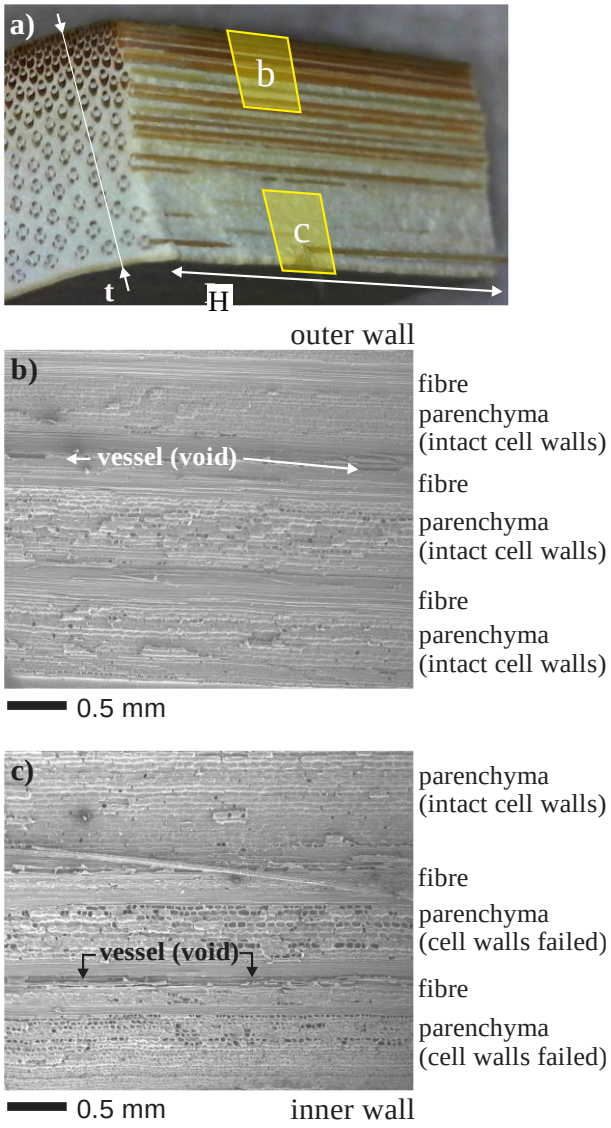

Figure 3.11: Images of culm wall showing failure surface across the wall thickness.

The images shown in Figures 3.11b and 3.11c are typical of images obtained at the outer and inner walls, respectively, of a *P. edulis*-C specimen obtained slightly above the neutral axis of the section in flexure (see Figure 3.11a). Image features did not vary considerably based on their location through the flexural depth of the specimen (dimension H in Figure 3.11a).

In Figures 3.11b and 3.11c, the failure plane can be seen to both follow the edge of the fiber bundles but also to go through the bundles themselves – presumably propagating along the

intra-fibril cracks observed in Figure 3.10. In some locations, the failure plane can be seen to expose the vessels (voids) surrounded by the fiber bundle. Where it is seen at the failure plane, the interface between the parenchyma and the fiber bundle appears intact. This supports the observation that the cracks in the fiber bundle initiate cracks in the parenchyma. In such a case, the failure plane represents the propagating crack and little damage would be expected at interfaces parallel to the crack plane. Similar behavior is reported by Chen *et al.* [2018] as propagation of cracks through the parenchyma then propagates around mircofibrils comprising the fiber bundle rather than around the fiber bundle itself (Figure 3.12).

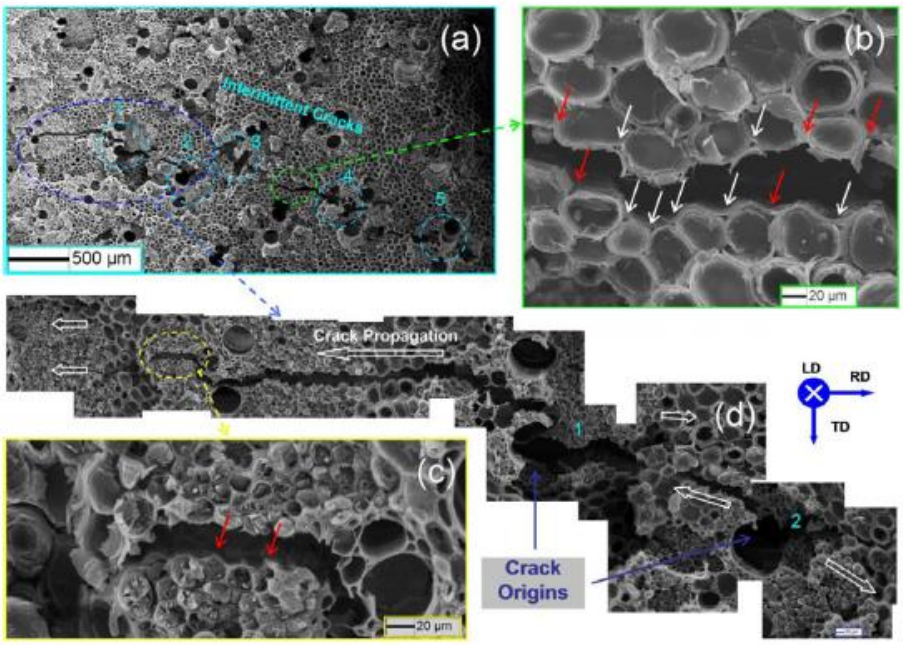

(a) Five intermittent cracks were observed; (b) Crack deflection in the parenchyma cells along RD, where the red and white arrows show the broken and intact triangular pores in the propagation paths; (c) Crack deflection along RD in the fiber bundles. The red arrows point out the neat deflection paths; (d) Origin and propagation analysis of the selected cracks, where the blue arrows point out the cracks origins, and the white hollow arrows show the crack propagation directions.

Figure 3.12: Tension-induced crack on the dry surface cross section Chen *et al.* [2018].

Additionally, the parenchyma shown in Figures 3.11b and 3.11c, appears to be behaving differently. Near the outer culm wall (Figure 3.11b), the failure appears to follow the interfaces between parenchyma cells (intact cell walls in Figure 3.11b). Near the inner culm wall (Figure 3.11c), the failure plane often appears to pass through the parenchyma cells (shown as non-intact cell walls in Figure 3.11c). This observation is typical of all images obtained in this study. Indeed, near the outer culm wall, the parenchyma is occasionally observed to fail in 'sheets' of intact cells as shown in Figure 3.13a.

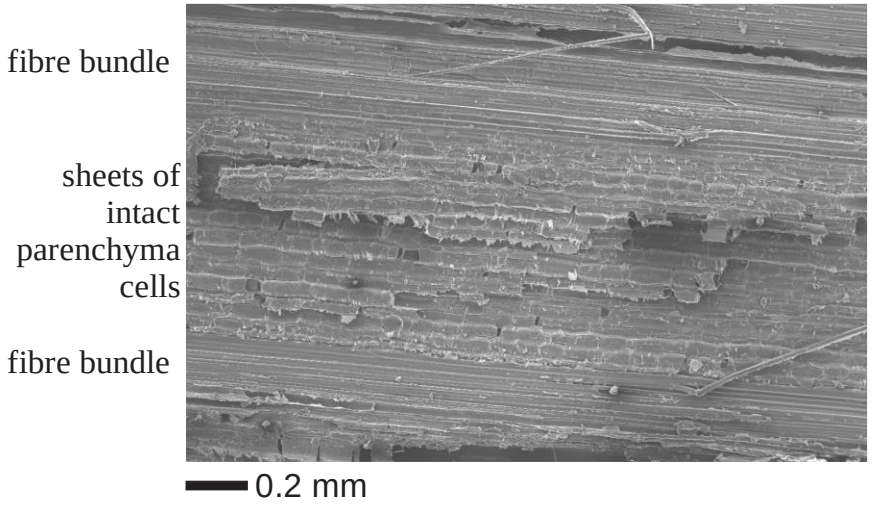

a) parenchyma between two fiber bundles near outer culm wall

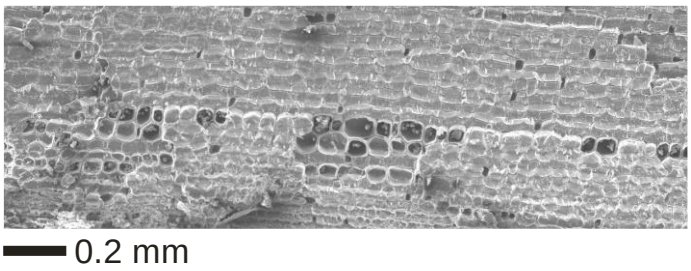

b) parenchyma near inner culm wall

Figure 3.13: SEM images of *P. edulis*-C parenchyma

In other images (Figure 3.13b) the intact parenchyma close to the inner culm wall appear ‘desiccated’: the intact cell wall appears to be ‘caving in’ or concave rather than being slightly convex as it is nearer the outer culm wall (Figure 3.13a). This observation may suggest a gradient in moisture content through the culm wall or a residual effect of moisture gradient during the drying process – recall that the *P. edulis*-C was kiln-dried. Such a gradient should be expected. The bamboo culm epidermis is relatively impermeable and resistant to wetting whereas the inner culm wall is permeable [Liese 1998, Yao *et al.* 2011]. The effects of moisture content, 0%, 6% and 20%, on parenchyma behavior of *P. edulis* has been recently reported by Chen *et al.* [2018] who correlate increased toughness – particularly of the parenchyma matrix – with increased moisture content.

The longitudinal aspect ratio of the parenchyma cells can be seen to be different in the outer (Figure 3.13a) and inner (Figure 3.13b) regions of the culm wall. In recent work, Zeng *et al.* [2019] identified significantly different morphology of parenchyma cell walls through the culm wall thickness of *P. edulis* specimens. Near the outer culm wall, parenchyma cell walls were tightly packed laminar structures with little pore space at interstices (Figure 3.14c). Nearer the inner culm wall, the laminar structure of the cell wall was separating and a larger triangular pore is present at parenchyma cell interstices (Figure 3.14a). It is unclear how these differences impact the behavior illustrated in Figures 3.11 and 3.13 but it is evident that parenchyma is not homogeneous through the cross section. Neither Zeng *et al.* [2019] nor Liese [1998] provide insight into the source of this inhomogeneity and the present author can only speculate on its cause, although it does appear to effect the through thickness mechanical behavior of the culm wall.

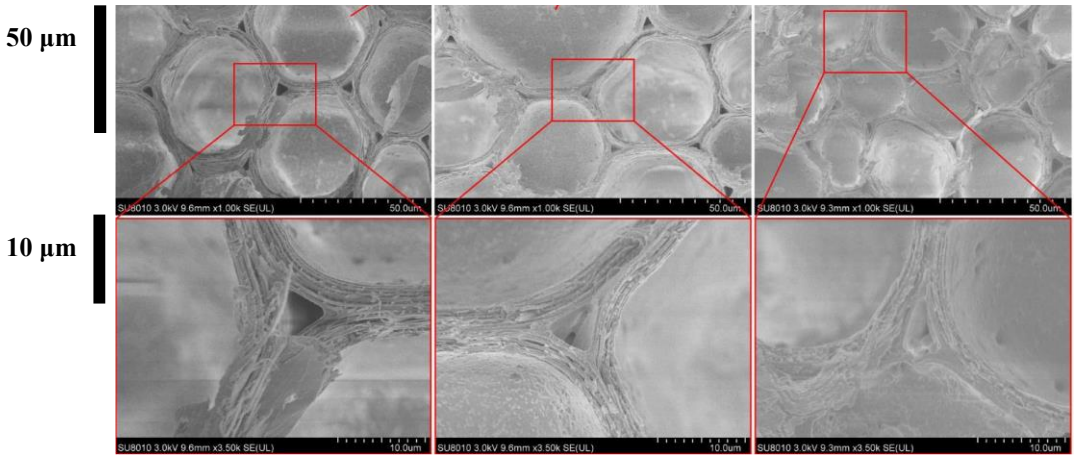

Figure 3.14: SEM images of parenchyma cell wall interstices [Zeng *et al.* 2019].

Similar observations to that of Zeng *et al.* [2019] and Liese [1998] were noticed in the OM images taken of tested specimens from this study. The images in Figure 3.15 show a typical *P. edulis*-C specimen at the outer and inner culm wall. At the outer culm wall (Figure 3.15b), the parenchyma cell walls exhibit distorted shapes resembling a flowing river path between the surrounding vascular bundles. This, when compared to the inner culm wall area (Figure 3.15a), suggested that the distortion is influenced by the increase in fiber volume present at the outer culm wall which constricts or constrains the parenchyma cells.

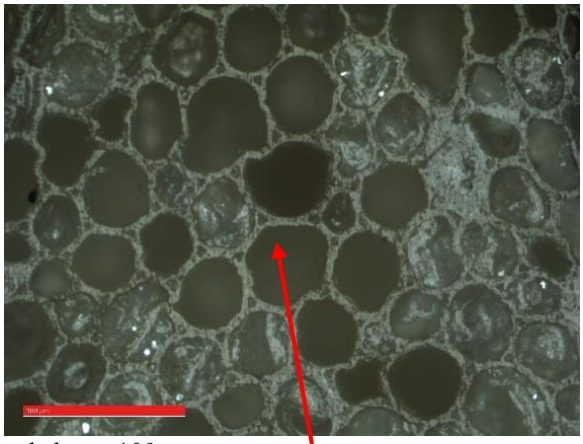

scale bar = 100 µm

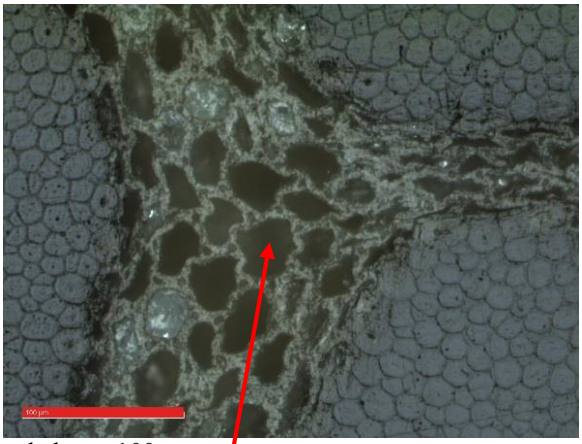

scale bar = 100 µm

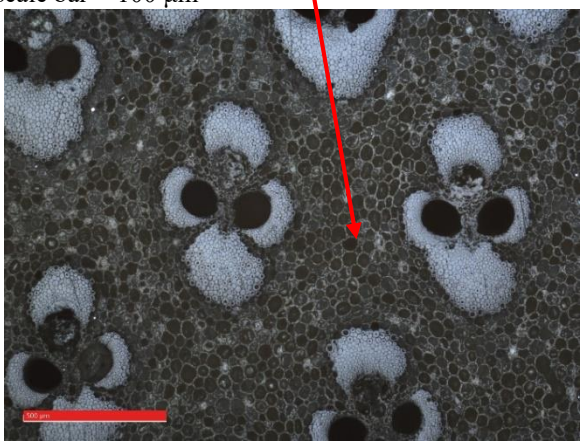

scale bar = 500 µm

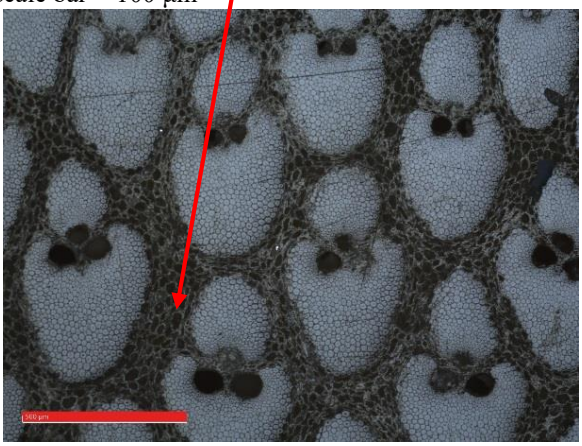

scale bar = 500 µm

a) near inner culm wall **b) near outer culm wall**

Figure 3.15: OM images of *P. edulis*-C showing the distortion of parenchyma cell features

Based on the observations made from the tests conducted and the failure plane imaging, it is evident that both the parenchyma cells and the fiber bundles play an important role in the mechanical property variation of bamboo through the culm wall thickness. The presence of moisture or the drying process of the bamboo could be a significant factor effecting the failure mechanism.

3.8 Summary

Bamboo is known to be a fiber reinforced material in which the longitudinal properties may be obtained from a rule of mixtures approach. The dominant failure mode of bamboo, however, is the longitudinal splitting with a mode II shear failure. In this study, the Halpin-Tsai rule of mixtures for the estimation of the transverse properties across the culm wall was considered. Image analysis together with a purpose-written MATLAB script was used to separate the bamboo fibers and conduct fiber volume calculations and analyses. The analysis indicated a fiber distribution having a third-order polynomial distribution through the culm wall and that culm-wall fiber distribution differs significantly among bamboo genera but less so among species in the same genera.

Modifications to the previously reported flat-ring flexure test were conducted to isolate portions of the culm wall cross-section to measure the transverse tensile capacity of the bamboo and investigate its variation through the culm wall thickness. Each specimen was produced with an end mill used to create reduced ("clipped") sections of $0.2t$ or $0.25t$ in the constant moment region. The modulus of rupture determined from the clipped tests, show a significant variation through the culm wall thickness. The variation had a generally parabolic shape with higher modulus at both the inner and outer walls compared to the middle of the culm wall. Comparison of this behavior to the fiber volume ratio and the predicted distribution of modulus of rupture using the Halpin-Tsai equation suggests that bamboo does not behave as a classic fiber-reinforced composite material in the transverse direction. This counterintuitive observation prompted further examination of the results using microscopic imaging techniques.

Similar to the clipped specimen test modifications, shaved specimens were also tested to examine the effect of the silica-rich outer epidermal layer of bamboo on culm mechanical properties. The results, when compared to the control test specimens, showed no significant change in the modulus of rupture but the displacement at failure was found to increase for all tested species except for *P. nigra.*

Full-culm control specimens were selected for further analysis using SEM. One of the first things noticed from the images was the presence of intra-fibril cracks within the fiber bundles. These cracks are hypothesized to be a result of shrinkage due to drying or treatment of the bamboo and to potentially be a source of eventual cracks through the parenchyma when the bamboo is under load. Although prior studies have shown the presence of such intra-fibril cracks, none was found that described their source. This phenomenon requires further investigation.

SEM images at the failure planes of full-culm control specimens indicated a clearly different morphology of the parenchyma through the culm-wall thickness. This observation may result from a variation of moisture content through the culm wall and also requires further investigation.

4.0 Characteristics of Bamboo Culm Wall

4.1 Background

While many studies have investigated the behaviour of engineered bamboo products, including glue-laminated bamboo, none have specifically investigated the nature of the constituent bamboo strips – the feedstock, as it were – used to fabricate the material. In particular, the expected variability inherent in the use of a natural material should be of interest to manufacturers of these products.

At the same time, in the realm of modelling bamboo material behaviour – relevant to the present work – it is necessary to understand the uncertainty inherent in ascribing material properties to a natural material. As a natural material, measured mechanical properties of bamboo are highly variable; coefficients of variation for many standard test methods are routinely reported on the order of 20 to 30% as shown in Chapter 2. Assessing the impact of this uncertainty on interpretation of test results, modelling, and the calibration of design equations will be critical if bamboo is to gain acceptance as an engineering material.

An approach to modelling bamboo by applying a random fields method [Alder and Taylor 2010] to a scale-independent functionally-graded material (FGM) model as a means of modelling uncertainty in full-culm bamboo behaviour is a primary focus of this study (Chapter 5). It is necessary to obtain and quantify relatively large amounts of data on both natural variation and spatial dependency of bamboo properties to achieve this. Laminated bamboo material provides an opportunity to investigate large data sets of individual culm wall data. At a minimum, the material

in a given glue-laminated member will be from the same species and, in most cases, from the same batch of bamboo. This provides some control for assessing statistical variation of properties within a relatively large batch size.

Image analysis as described in Section 3.2 is used to quantify the distribution of fiber volume ratio, V_f, in strips of *P. edulis* bamboo used in commercially available glue-laminated bamboo beams. High resolution images of cross sections of 58 glue-laminated bamboo beams were obtained. The images, produced and reported in a different context by Penellum *et al.* [2018], are 1200 dpi scans of the cross sections; an example is shown in Figure 4.1a.

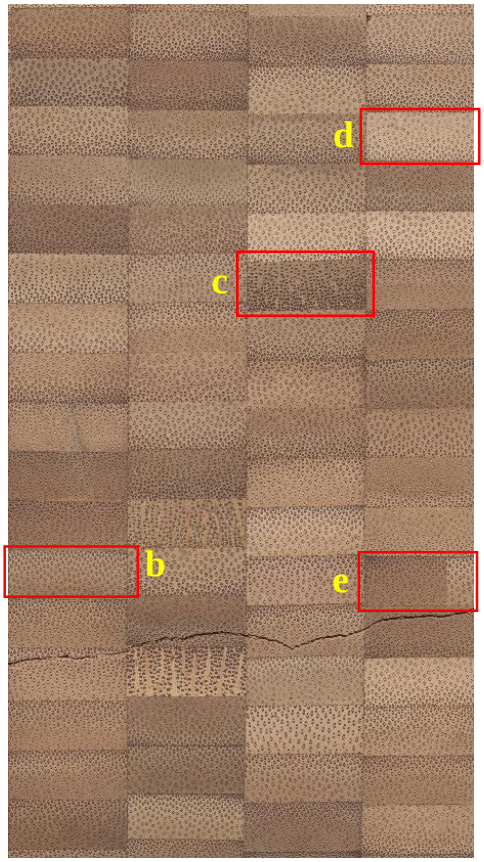

a) typical image of Batch M glue-laminated beam cross section; each strip is 19 x 6 mm. Horizontal crack is from original flexure test. Strips intersected by crack are excluded from analysis.

b) typical 19 x 6 mm strip image used for analysis

c) near-node strip section excluded from analysis

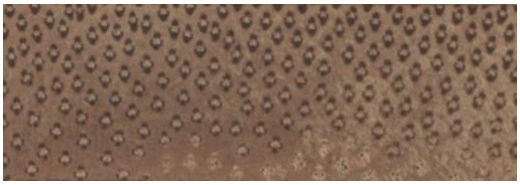

d) incomplete strip – likely due to cutting/polishing beam section excluded from analysis

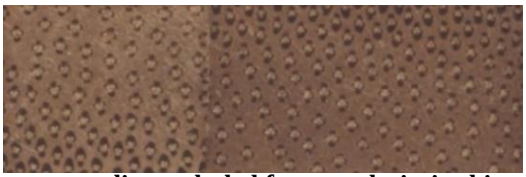

e) other anomalies excluded from analysis, in this case a strip composed of two smaller glued strips

Figure 4.1: Glue laminated bamboo beam and individuals strips extracted for image analysis.

4.2 Bamboo Material

The commercially produced beams – representing material obtained from two different manufacturers (designated batches M and P) – had been previously tested in flexure, as reported in a number of studies [Sharma *et al.et al.* 2015a, 2015b and 2017]. All material was *P. edulis* (Moso) bamboo originating in China. The beams were fabricated from 19 mm thick boards, with each board made of bamboo strips 19 mm wide and 6 mm thick in the direction through the culm wall.

The overall thickness of the source material culm wall is unknown, but in typical practice, 6 mm strips are taken from culms having a wall thickness on the order of 8 to 10 mm. The strips are therefore taken from the middle region of the culm wall as shown schematically in Figure 4.2. Image analysis of the full beam sections having the objective of determining the applicability of composite theory (i.e., rule of mixtures) to the glue-laminated members is reported by Penellum *et al.* [2018] who determined the fiber volume ratio, V_f, of the gross beam cross sections for both batches to be 0.21 (COV = 0.05).

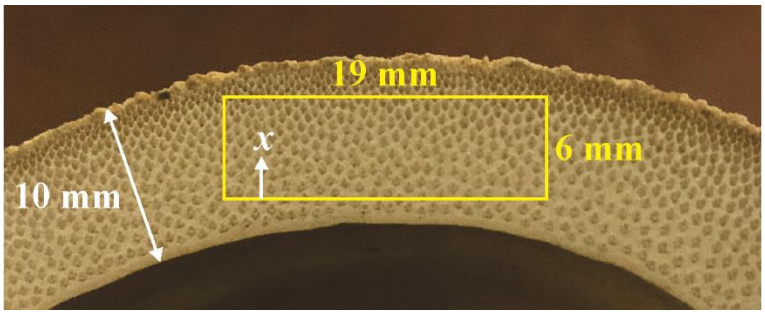

Figure 4.2: Image of strip location in a typical culm wall cross-section.

4.3 Image Extraction

Over 3500 individual images of the 19 x 6 mm strips (Figure 4.1b) were extracted from the 58 beam section images available (Table 4.1). Each image is approximately 900 x 300 pixels resulting in a pixel resolution of approximately 2400 pixels/mm^2. Following manual screening, approximately 13% of the extracted images were excluded from analysis due primarily to poor image quality or features unsuited to image analysis. Examples of excluded images are shown in Figures 4.1d-e. Additionally, approximately 3.5% of the strip sections were near the bamboo nodal region (Table 4.1 and Figure 4.1c). The varying fiber orientation and bamboo morphology in this region [Liese 1998] is also unsuitable for the analysis conducted and these strips were excluded from analysis. Following analyses of the remaining 2929 images (see below), 19 outliers determined using the interquartile rule were (Tukey fence [Hoaglin 2003])also excluded from further analysis – these outliers were attributed to additional anomalies affecting image analysis which were not identified in the initial screening.

Table 4.1: Summary of image analysis and autocorrelation test (COV in parentheses).

Batch		**M**	**P**
beam dimension (mm)		140 x 90	120 x 60
number of beams		38	20
19 x 6 mm strips in each beam		64 or 78	48 or 54
strips extracted		2590	927
strips analyzed		2309 of 2590 (89%)	601 of 927 (65%)
near-node strips		80 of 2590 (3.1%)	37 of 927 (4.0%)
fiber volume ratio, V_f		0.234 (0.12)	0.190 (0.19)
$V_f = mx + b$	m (mm^{-1})	0.025 (0.29)	0.032 (0.24)
	b	0.160 (0.21)	0.094 (0.46)
	MRE	0.125	0.214

4.4 Image Analysis

Using the purpose-written Matlab script given in Appendix A, based on image contrast, each image (Figure 4.3a) was processed to produce a high contrast image allowing differentiation of the bamboo fiber bundles as seen in Figure 4.3b. The high-contrast imaging was able to discriminate between fiber bundle and vessels, excluding the latter from the vascular bundle (see Figure 1.2). As a result, the fiber volume ratio, V_f is correctly reported.

Using the MatLab script, each full-culm wall thickness image was divided into ten equal sub images in the through-culm wall (6 mm) direction as shown in Figure 4.3b. The fiber components were extracted from the images and the fiber volume ratio determined for each sub image. From this analysis the total fiber volume ratio of each strip, V_f and the distribution as a function of location in the strip can be determined. Figure 4.4 shows examples of data obtained for M and P strips. In each image, 100 randomly selected fiber volume distributions are shown; the heavy black line indicates the average value obtained from all analysed strips (Figure 4.4).

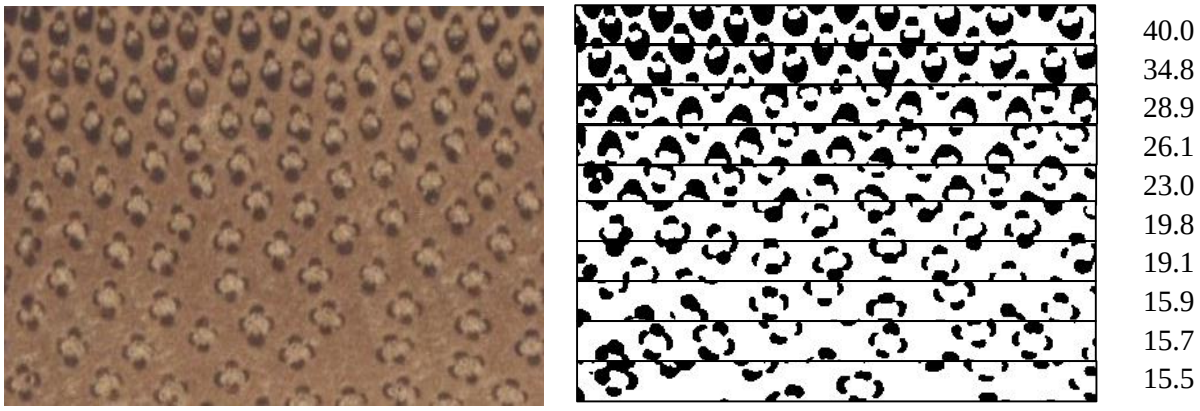

a) image of strip **b) ten-layer MatLab pixel map of fibers**

Figure 4.3: Example of digital image analysis of 6 mm thick strip (19 mm dimension cropped in this figure).

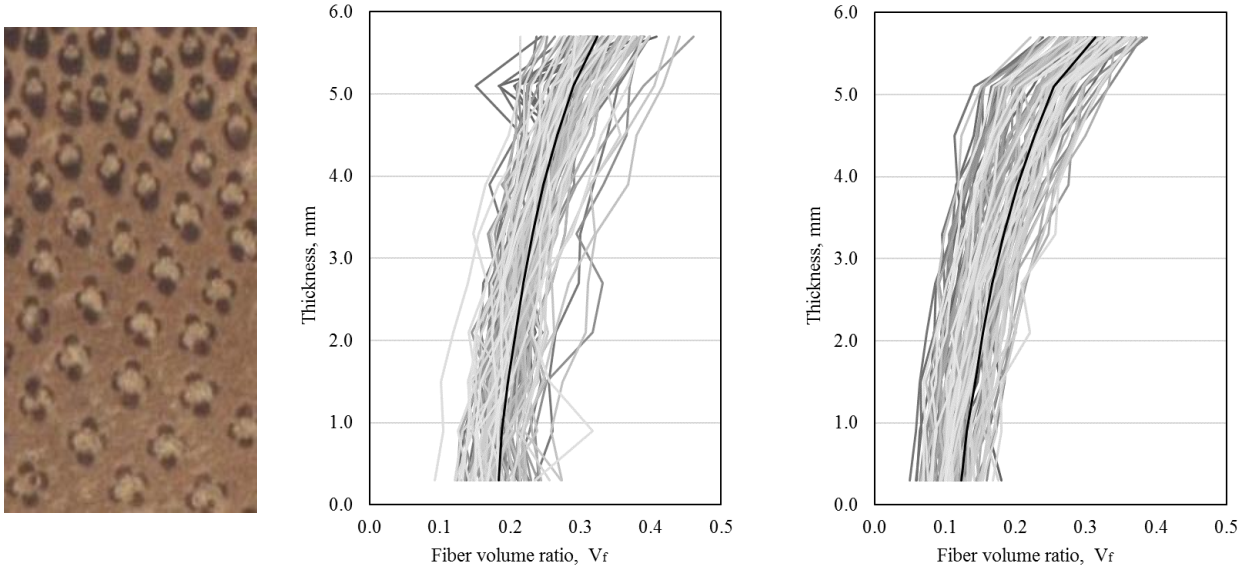

Figure 4.4: Representative fiber volume distributions from 100 strips.

Total fiber volume ratio, V_f, obtained from this analysis is given in Table 4.1 and is seen to differ between Batches P and M. The values are different from those reported by Penellum *et al.et al.* [2018] who report a value of 0.21 for both batches. The differences are believed to be an artefact of the different image analysis algorithms used. Specifically, Penellum *et al.*. imaged the entire beam rather than the individual strips. This therefore included the resin layers between strips. Looking at the processed images reported by Penellum *et al.*, it is believed that including the resin lines may have affected the resulting image 'thresholding' and therefore excluded some fibers in Batch M and included some of the vessels in Batch P. It is further noted that the coloring of the batches was different due to different treatment and caramelisation processes used in Batches M

and P. It is believed that the algorithm used in the present study overcame these issues by first converting to high contrast images and cropping to excluded the resin lines.

Additionally, by imaging the entire beam section, Penellum *et al.* did not exclude portions of the image that were unclear or contained nodal regions (Figure 4.1). This highlights an important aspect of similar digital analysis: that results and/or interpretation provided by different algorithms will vary. Therefore, comparisons relying on such image data must be internally consistent; that is, data must be collected using the same algorithm.

The measured distribution of fiber volume ratio through the culm wall thickness (Table 4.1) is not meaningful by itself since the location of the 6 mm specimen within the culm wall is unknown (Figure 4.2). Nonetheless, the nature of the distribution and its variation is a measure of the uncertainty inherent in ascribing geometric or material properties to bamboo. Each acquired fiber distribution was fitted to a linear relationship as described by Eq. 4-1.

$$V_f = mx + b \tag{4-1}$$

The value of m describes the variation of the fiber volume through the strip dimension x which ranges from 0 to 6 mm. The value b is a function of the location of the 6 mm strip within the culm wall (Figure 4.2) and is therefore not uniquely defined in this study. The values of m and b determined from regression analyses are given in Table 4.1. Additionally, the mean relative error (MRE) of equation 4-1 is shown. The statistical distributions of V_f and parameters, m and b, can be shown (with a confidence of 95%) to be Gaussian (normal) (Figure 4.5).

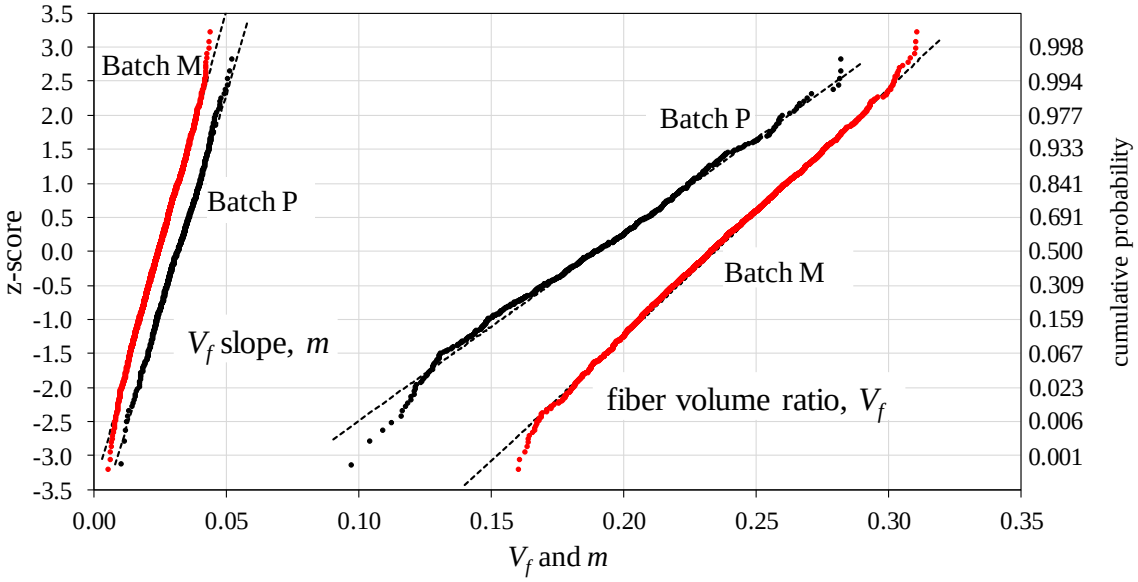

Figure 4.5: Probability plots showing data conforming to normal distribution.

A linear function was selected (Eq. 4-1) since this has been reported in the literature [Janssen 1981]. Exponential [Nogata and Takahasi 1995; Amada *et al.* 1996] functions were also obtained that yielded essentially identical MRE values; the discussion therefore considers only the simpler linear distribution. Others have reported polynomial distributions [Ghavami *et al.* 2003; Ghavami and Marinho 2005; Akinbade *et al.* 2019] across the full-culm wall thickness – including the results reported in Chapter 3 and Table 3.1. The strips considered, however, represent only a portion of the culm wall thickness and exclude both the extreme outer and inner fibers (see Figure 4.2); it is these regions that often require a higher order polynomial distribution to be used (see Chapter 3 and Figure 3.5). In the context of the numerical study (Chapters 5 and 6) however, the confirmed normality of the fiber volume distribution across the culm wall thickness is a valuable result which will help in further modelling processes.

4.5 Summary

Image analysis was used to quantify the distribution of fiber volume ratio, V_f, in strips of *P. edulis* bamboo obtained from two commercially available glue-laminated bamboo beam products. In total, 58 cross sections containing more than 3500 19 x 6 mm strips were analyzed. Simple digital manipulation techniques were found to work well in establishing fiber volume data from the 1200 dpi source images.

Although all bamboo was Chinese *P. edulis* and batches were likely from similar or identical source material (feedstock), variation was observed: the measured fiber volume ratio for each strip was 0.23 for Batch M and 0.19 for Batch P; the coefficient of variation observed was 12% and 19%, respectively. Both batches could be modelled as having a linear distribution of V_f through their thickness although the gradient was different in each case: 0.025/mm and 0.032/mm for Batch M and P, respectively. These observations indicate significantly different bamboo source material for the two batches. Indeed, many factors may affect the properties of strips used even by the same manufacturer. Bamboo suppliers, harvest conditions, and location of strips along the culm length all may result in variation of strip properties.

Additional analyses of the images with respect to the properties and behavior of the resulting glue-laminated beams is presented in Akinbade *et al.* [2020]. This additional analysis is not related to the present study – it addresses QA/QC issues for the engineered bamboo community – and is therefore not expanded upon in this dissertation.

5.0 Uncertainty in Bamboo Materials Characterization

Bamboo is a functionally graded material, evolved according to the need to resist external loads and internal stresses resulting from its natural environment [Amada and Untao 2001]. Nogata and Takahashi [1995], for instance, showed a variation in vascular bundle arrangement of bamboo grown on steep ground. The study showed that the deformed contour shape of the bamboo stem and the asymmetric shape of the fiber bundles were a reflection of a biased loading condition in the sloped growth environment. Other studies have considered the effects of intentionally shaping bamboo culms [Ghavami *et al.* 2003; Vittouris and Richardson 2011] and the section morphology of [naturally-occurring] "square bamboo", *Chimonobambusa quadrangularis* [Shigematsu 1958]. These studies show marked differences in fiber bundle distribution around the perimeter of the artificial or natural polygonal shaped bamboo, especially at corners. This all suggests the importance of growth conditions on the volume of fibers and their distribution from the mechanical and morphological points of view. This observation also opens the possibility of 'training' bamboo; that is, optimizing bamboo for a structural purpose by growing it under similar conditions of stress. While not the objective of this study, this is an area having strong potential for further research which may benefit from the models developed in this study.

Prior research showed that age at harvesting is also an important factor when considering the strength of bamboo. Sekhar and Bhartari [1960] noted that strength of bamboo increases with age as the plant lignifies, peaks at 2.5–4 years (likely species and growth condition dependent) and then decreases following maturity (reported to be older than about 6 years). *Neosinocalamus affinis* bamboo tested by Low *et al.* [2006] indicated a contrary trend, exhibiting modulus of elasticity,

strength, and fracture toughness to be all greater in a one year old sample than a matured, five year old sample. This serves to highlight the variability of bamboo species and the uncertainty associated with attributing general behaviors or trends to bamboo as a whole. Other properties of bamboo reported to be affected by the age of the culm at harvesting include the density, moisture content, and modulus of elasticity.

However, Correal and Arbelaez [2010] considered the effect of age on *Guadua angustifolia* and found no correlation between age and modulus of elasticity in bending or compression. It was noticed however that the top portion of the culm showed the maximum strength and modulus of elasticity compared to the lower two portions[6]. This was attributed to the greater density of the top portion of bamboo having more influence on compressive and bending strength than on other mechanical properties. A significant discussion of the variation of geometric and mechanical properties with height along the culm is provided by Harries *et al.* [2017].

The extent of variation and uncertainties in bamboo is further illustrated by the compressive tests carried out by Lo *et al.* [2004] to determine the effect of diameter and age of bamboo on compressive strength. It was determined that the compressive strength of *P. heterocycla* and *B. pervariabilis* decreased significantly with an increase in outer diameter. This matched previous findings [Liese 1986 and Sattar *et al.* 1990] that the compressive strength tends to increase with culm height (diameter decreases with height).

Similar to wood, moisture content (MC) affects the properties of bamboo. Also like wood, conventionally, properties of bamboo are normalized at 12% moisture content. The knowledge of the correlation between MC and mechanical properties of bamboo is limited compared to that of

[6] By convention, bamboo culms are typically 6 m or 9 m in length and are divided into thirds; labeled bottom (B), middle (M) and top (T) [ISO 22157-2019].

wood. Limited research has been conducted in this area other than a record of the moisture content at the time of test in earlier work. Xu *et al.* [2014], in a study focusing on bamboo scaffolding, demonstrated that the mechanical properties of previously dried *P. edulis* were observed to degrade significantly with increased MC up to about MC = 30%, a value close to the fiber saturation point (FSP)[7]. Like timber, for MC greater than the FSP, further degradation of mechanical properties, while apparent, was less significant. Xu *et al.* report that for specimens at their FSP, compressive strength and modulus were approximately 75% of the air-dry (MC = 12%) value and longitudinal shear and transverse tension capacities were approximately 90% of the air-dry values. Data presented by Limaye [1952] who tested both dry bamboo and green bamboo (having a moisture content greater than the FSP) shows a decrease in strength with increasing MC. The ratios of oven-dry to green strength and modulus of *P. edulis* have been shown to be approximately 2.2 and 2.0, respectively [Ota 1952]. The ratio of compression modulus of *D. strictus* tested at 12% moisture content to that in the green condition has been shown to vary based on age at harvest but to not exceed approximately 1.6 [Limaye 1952]. Similarly, the compressive and flexural strengths of *D. strictus* tested at 12% moisture content are approximately 1.9 times those tested in the green condition, regardless of age of harvesting [Limaye 1952].

Wang *et al.* [2013] carried out mechanical tests at both the cellular and macroscopic levels on *P. edulis* at different MC and found a similar correlation in the compressive modulus of elasticity (CMOE), indentation modulus of elasticity (EIT), and hardness (HIT). The CMOE was found to be more sensitive to a change in MC than the EIT and it was hypothesized that the

[7] For bamboo, the fiber saturation point is defined by ISO 22156 as: "moisture level in the bamboo solid material whereby no free liquid water remains in the cell cavities but the cell wall structure is fully 'saturated' by chemically bound water molecules; the maximum content of bound water in bamboo tissue is approximately 30% by weight of the fully dried tissue."

parenchyma cells in bamboo are more sensitive to changes in MC than are the bamboo fibers. Further tests are required to prove the hypothesis.

Chinese Standard JG/T 199-2007 'normalizes' mechanical properties to a moisture content of 12%[8]. Recognizing that standard tests will be conducted over a range of moisture contents, the Chinese standard specifies correction factors applied to the experimentally determined mechanical properties to 'convert' these to equivalent strength or modulus properties at a moisture content of 12%. The Colombian NSR-10 [AIS 2010] Standard also prescribes correction for mechanical properties normalized at 12% MC.

Still unpublished data from the work of Mateo Gutierre Gonzalez at the University of Queensland [personal correspondence] is quantifying the combined effects of MC and ambient temperature on bamboo mechanical properties. This work is showing that bamboo mechanical properties generally are reduced at higher MC and at higher ambient temperatures.

Mechanical properties of full-culm bamboo can be highly variable, affected by culm geometry, age at harvest, storage, treatment and service conditions (i.e. moisture content and temperature). A limitation of the present study is the lack of control over most of these variables; thus the focus is on morphology, mechanics and A-B comparisons, rather than reporting specific values of mechanical properties. Data is not corrected for MC although all tests are conducted at values of MC quite near 12%.

[8] Translation of this document has been undertaken by Dr. Harries and his colleagues at SRIBS in Shanghai; additional assistance has been provided by Dr. Tianqiao Liu, previously at Pitt, now at Tsinghua University.

5.1 Random field Methodology and Application

In order to consider the effects of uncertainty in the characterization of bamboo mechanical properties, the random field methodology, a branch of the stochastic finite element method has been adopted. This is a useful tool to determine the response of systems subjected to uncertain parameters. Structures containing randomly heterogeneous materials have been extensively analysed using this method including timber [Moshtaghin *et al.* 2016], concrete [Most and Bucher 2007] and soil [Ghiocel and Ghanem 2002]. Pierce-Brown *et al.* [2018] studied the error induced by the midpoint approximation, which is often utilized to estimate parameters of the random field, for the case of effective modulus of elasticity, *E*. The analytical study focused on tensile loading and 3 and 4-point bending of a timber beam. Monte Carlo simulation was used to affect a random modulus along the member length. The study concluded that the midpoint approximation is not appropriate for tension loading (unsurprisingly) but was effective in modeling the bending tests.

The use of a random field allows for the generation of a random variable (e.g. modulus of elasticity) while accounting for its natural variability (Gaussian distribution) and spatial dependency (grading function through and along culm wall, both parallel and longitudinal to fibers). This approach has been applied to a number of problems, which exhibit high variability and spatial gradation including roadway pavements [Caro et al 2014], soils [Kim 2005] and ground water modelling [El-Kadi and Williamson 2000] but are not known to be applied to bamboo or similar natural materials.

This approach will be used to capture the characteristics of the microstructure of bamboo components on the mechanical response of bamboo under uncertainty without measuring the individual constitutive phases of the components. This involves three major stages: 1) identifying

the bamboo geometry and parameter of interest; 2) generating a probable spatial distribution of the parameter; and, 3) implementing this in a finite element (FE) model as will be described in Chapter 6. The outcome from the image analysis described in Chapters 3 and 4 will be incorporated here in order to develop a methodology which takes into account the effect of uncertainty when modeling bamboo. The variation of the fiber volume distribution, V_f through the culm wall is the primary material property considered for analysis in this study. As has been described in previous chapters, this radial variation can be correlated to other properties such as the elastic modulus, E, modulus of rupture, f_r, and the shear strength, f_v.

Assessing the impact of uncertainty in bamboo material on the calibration of eventual design equations is critical to the full understanding and eventual adoption of bamboo as a construction material. The proposed methodology will include the variations in material and mechanical properties as part of the mechanical response of bamboo structures. This will combine a stochastic technique with FE modelling. In order to achieve this representation, a two-dimensional matrix decomposition technique is used in addition to the random fields to model uncertainty in full-culm bamboo behavior. The matrix decomposition technique was adopted because it can model the statistically correlated random field with very clear relationships between the given statistical parameters and the corresponding random field, including a preselected correlation length [Kim 2005].

5.2 Implementation

The proposed implementation of the random field is described in this section and illustrated schematically in Figure 5.1. The culm geometry is chosen to be a radially symmetric cylindrical material with an outer diameter *D* and thickness *t*. The parameter of interest for this illustration is the radially-oriented elastic modulus, E_T (Equation 5-1) which is hypothesized to be a function of the fiber volume ratio, V_f and therefore varies radially through the bamboo culm wall. For the random fields approach, the mean value, covariance and spatial dependency (i.e. correlation length of the random field) of E_T, determined from empirical formulae and image analysis, are required.

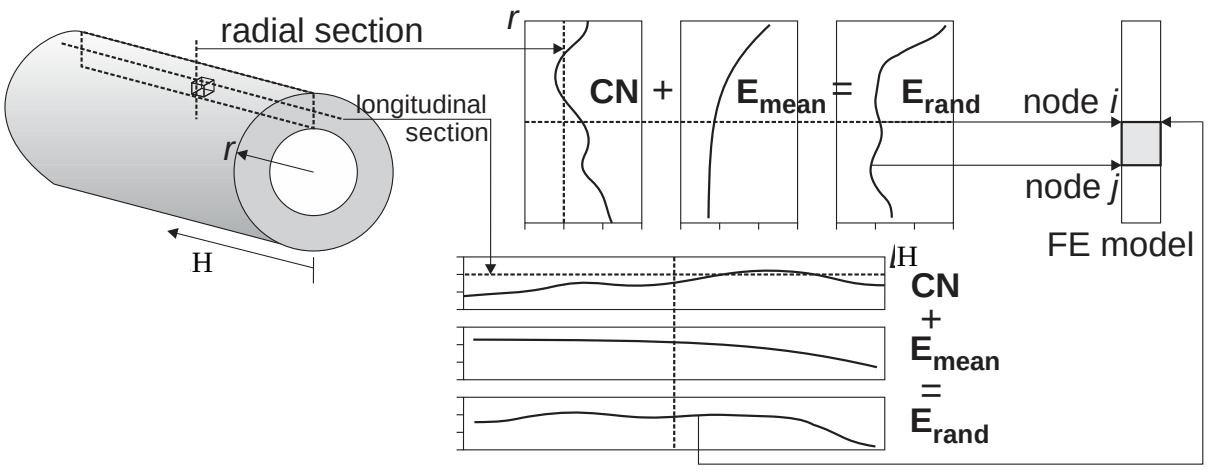

Figure 5.1: Schematic representation of random fields representing modulus.

The covariance matrix decomposition technique adopted to generate the random field of E_T is defined as:

$$\mathbf{E_{T,rand}} = \mathbf{CN} + \mathbf{E_{T,mean}} \tag{5-1}$$

where, $\mathbf{E_{T,rand}}$ is the vector containing the values of E_T for the discretized space considered; **N** is a vector of normally distributed random values between 0 and 1 (i.e., N[0,1]) and $\mathbf{E_{T,mean}}$ is the mean vector of experimentally measured E_T for the discretized space.

The technique is based on the assumption that the parameter of interest follows a Guassian distribution (confirmed in Chapter 4) and that the spatial correlation can be adequately characterized by a given correlation function. ***C*** is the autocorrelation matrix obtained from the covariance matrix of the random field **A**, as:

$$\mathbf{A} = \mathbf{C}\mathbf{C}^{\mathbf{T}} \tag{5-2}$$

The Cholesky decomposition matrix technique [Agarwal and Mehra 2014] can be applied to obtain **C** from **A**. The technique is used to decompose the matrix **A** which must be symmetric and positive-definite into an upper and lower triangular matrix of which **C** is the lower. The covariance matrix, **A**, contains information of both the standard deviation, σ, and spatial correlation, $\rho_{i,j}$, of E_T and is defined as:

$$A_{ij} = \sigma^2 \rho_{ij} \tag{5-3}$$

where $\rho_{i,j}$ = autocorrelation function between each couple of spatial points *i* and *j*.

The relationship for fiber volume ratio through the culm wall thickness for *P. edulis* was found to have a cubic regression function (Table 3.1):

$$V_f = 1.41x^3 - 1.23x^2 + 0.50x + 0.10 \quad (5\text{-}4)$$

where x is the normalized culm wall dimension (0 = interior surface and 1 = exterior) in the radial direction.

It should be noted that although the vector of mean values, $\mathbf{E_{T,mean}}$, is reported to be a cubic function with a constant mean value, the actual distribution that results from the stochastic realization in Equation 5-1 will not necessarily have this shape or mean. Various correlation functions have been adopted in literature and their selection is found to be problem specific. A summary of commonly used functions can be found in Chiles and Delfiner [2012]. Of all the summarized correlation functions, the exponential function is the most commonly used [Abrahamsen 1997]. Other significant functions include the spherical and the cubic functions which were also considered in this study.

Based on the regression function of V_f given in Equation 5-4, the spatial correlation of E_T is also assumed to be adequately characterized by the cubic correlation function. The isotropic form of the cubic correlation function, ρ, is:

$$\rho_{ij} = 1 - 7\left(\frac{d^r{}_{i,j}}{L_r}\right)^2 + \frac{35}{4}\left(\frac{d^r{}_{i,j}}{L_r}\right)^3 - \frac{7}{2}\left(\frac{d^r{}_{i,j}}{L_r}\right)^5 + \frac{3}{4}\left(\frac{d^r{}_{i,j}}{L_r}\right)^7 \text{ for } L_r \geq d^r \quad (5\text{-}5a)$$

$$\rho_{ij} = 0 \qquad \text{for } L_r \leq d^r \quad (5\text{-}5b)$$

where L_r is the correlation distance in the radial direction and $d^r{}_{i,j}$ is the radial component of the distance between points i and j.

The correlation function would include different correlation distances for each direction if an anisotropic random field were being generated. This is useful for a material such as bamboo in which property distributions are known to be highly anisotropic. In this study however, the variation of properties in the longitudinal direction is not considered due to the relatively short length of the material test specimens being modelled and the transverse distribution is assumed to radially symmetric. Extending this approach to address more complex variation along the culm and around the culm wall is an aspect for future investigation.

The resulting spatial variation of E_T is applied to obtain a solution to the FE model reported in Chapter 6. Repeating this process for different variables provides a means of assessing the impact of uncertainty and therefore helping to inform eventual design calibrations.

An example application is illustrated here for clarity. Existing measured data from experiments are used to generate a vector representing the random field of the subdivided layer of E_T. Figure 5.2 shows the geometry of the bamboo wall. Data for *P. edulis*-C through he culm wall thickness reported in Chapter 3 was used with E_T selected as the parameter of study in this example. The radial section was divided into 10 concentric sections of thickness 0.1t having negligible width in the circumferential direction.

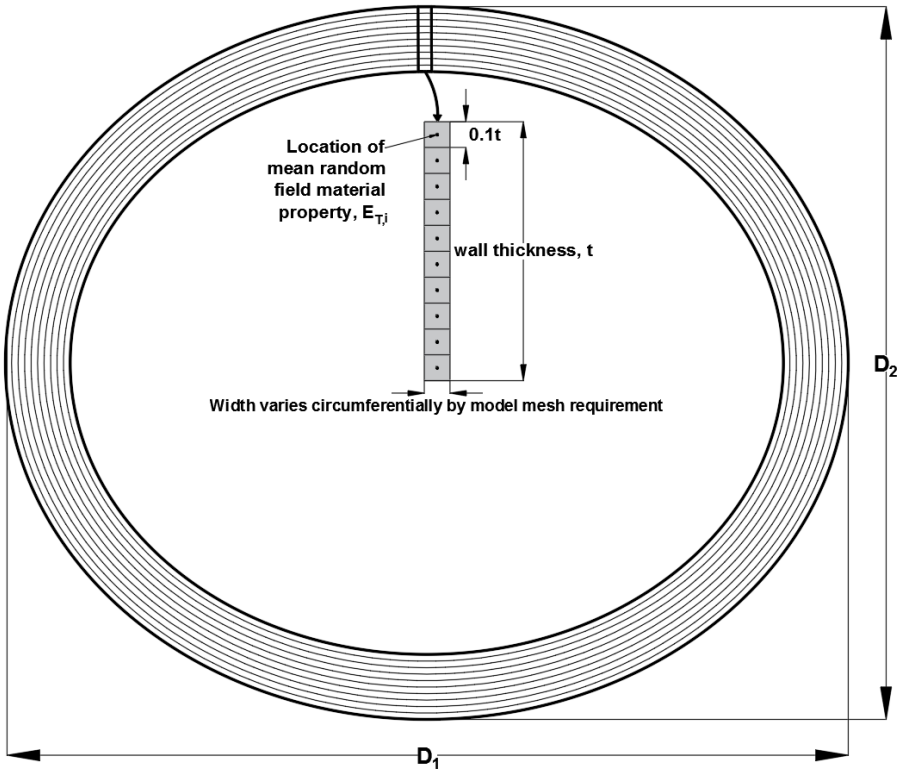

Figure 5.2: Geometry of the culm wall

The data available is the mean of V_f of *P. edulis*-C bamboo samples. The initial value of E_T was calculated using the Rule of Mixtures, with the Halpin-Tsai correction as given in Equation 3.3 using representative mechanical properties E_f = 35 GPa and E_m = 1.8 GPa reported by Janssen [2000] (see Section 3.3). Based on results shown in Figure 4.5, for *P. edulis*, variation of the function described by Equation 5-4 can be assumed to have a Gaussian distribution.

The random field procedure described was implemented using a MATLAB script (see Appendix B). The resulting vectors which contain values of the parameter, E_T for the discretized space considered are shown graphically in Figures 5.3a to 5.3c for a total of 10 randomly selected $\mathbf{E_{Trand}}$. It can be seen that there is a high level of dispersion in the random fields data around the

measured mean values (bold lines). This scatter is reduced as the correlation distance, L_r is increased; that is, the variation through the culm wall thickness becomes smoother as the value of L_r increases. While there is no available literature providing typical values of correlation length for bamboo, different values were considered here to determine the impact of the final distribution from the use of this stochastic technique. Qualitative comparison of the images in Figure 5.3 to the measured fiber volume distributions shown in Figures 3.3, 3.4 and 4.4 shows that a realistic distribution of E through the culm wall thickness is achieved as the correlation length approaches the culm wall thickness, t. This observation is in agreement with the findings of a similar one-dimensional random fields application presented by Caro *et al.* [2014]. Hence, a correlation distance $L_r = t$ is adopted in this study (Figure 5.3b).

Choosing one output data from Figure 5.3b (thicker red line), an example of the construction procedure used to generate the random fields $\mathbf{E}_{\mathbf{T,rand}}$ with all components required in Equation 5-1 is illustrated in Figure 5.3d.

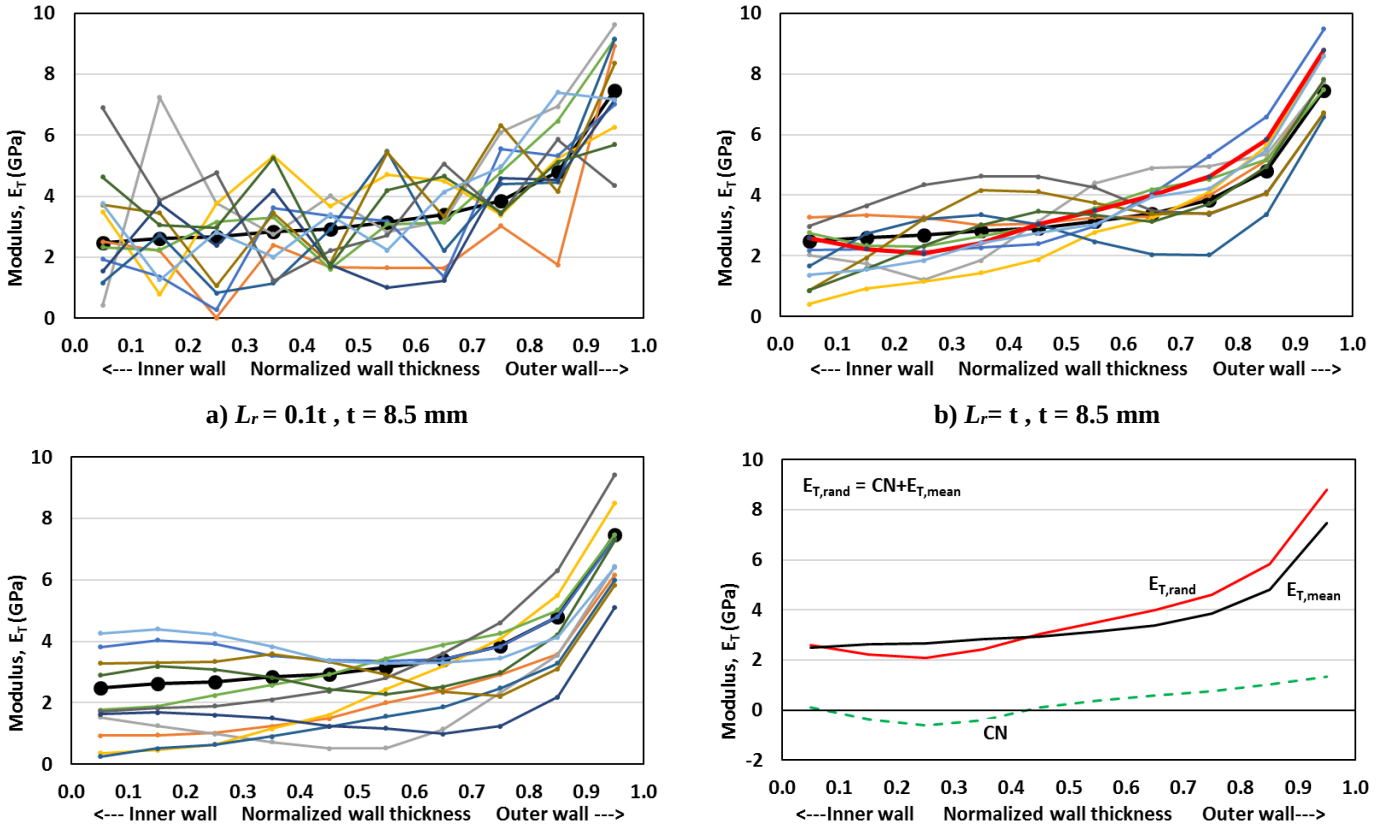

Figure 5.3: Profiles of $E_{T,rand}$ and the measured values $E_{T,mean}$ (shown in black) at varying L_r.

5.3 Summary

The random field analysis method was introduced as a means of quantifying the measured uncertainty of bamboo with respect to the mechanical characterization of its full-culm state. Such an approach has been reportedly used on other randomly heterogeneous materials to determine the response of systems subjected to uncertain paramaters but this is its first known application to bamboo. The approach to capture the characteristics of bamboo components without measuring the individual phases of the components involves three major stages: 1) identifying the bamboo

geometry and parameter of interest (as was done in Chapters 3 and 4); 2) generating a probable spatial distribution of the parameter (this Chapter); and, 3) implementing this in an FE model (Chapter 6).

An example of the implementation of the covariance matrix decomposition technique was illustrated with radially-oriented elastic modulus E_T as the parameter of interest hypothesized to be a function of the fiber volume ratio, V_f . Other data needed for the computation include the mean value, covariance and spatial dependency (i.e. correlation length of the random field) of the parameter of interest, E_T, determined from empirical formulae and image analysis. An initial assumption made is that the parameter of interest follows a Gaussian distribution which was confirmed in Chapter 4 and that the spatial correlation can be adequately characterized by a cubic correlation function. A correlation function of E_T for the analysis and a correlation distance equal to the bamboo wall thickness was selected.

This methodology relies on the availability of data – in this case, outcome of the image analysis which had been introduced in previous chapters – taking into account the effect of uncertainty when modeling bamboo. The output from this exercise will be used as input to demonstrate a numerical simulation of bamboo using ABAQUS in Chapter 6.

6.0 Numerical Modelling

6.1 Numerical Analysis of Bamboo

Bamboo is a transversely anisotropic material with differing properties in the longitudinal, radial and circumferential directions. Together, radial and circumferential properties are often referred to as transverse properties. This is partially because a number of experimental studies using small specimens to assess these properties have not adequately differentiated between the radial and circumferential orientations. Due to their dominance, properties in the longitudinal direction have typically been the focus of research studies and material test methods. Nonetheless, transverse properties are known to be equally (or perhaps more) important to structural behavior but more difficult to obtain. Occasionally, the finite element (FE) method has been adopted to assess transverse mechanical properties.

Torres *et al.* [2007] proposed a transversely isotropic model to simulate bamboo in a circumferential compression test (see Section 2.3.4). In this model, the transverse plane perpendicular to the longitudinal axis of the culm was considered to be isotropic and the mechanical properties in the radial direction were assumed equal to those in the circumferential direction. With the transversely isotropic model, the five independent elastic constants[9] required were the Young's moduli in the transverse plane (E_T) and in the axial direction (E_L), the Poisson's ratio in the transverse plane (radial-circumferential or out-of-plane Poisson's ratio, υ_{RC}), the circumferential-axial Poisson's ratio (υ_{CL}) and the circumferential-axial shear modulus G_{CL}

[9] see Figure 1.3 for orientation and notation conventions

[Christensen 2012]. This approach however neglects the functionally-graded nature of bamboo in the radial direction which is of importance to its characterization [Silva *et al.* 2006; Martínez-Pañeda 2019]. García *et al.* [2012] carried out both experimental and numerical simulations to determine the elastic properties of *G.angustifolia*. Specifically, the radial-circumferential Poisson ratio, circumferential Young's modulus and the circumferential-axial shear modulus were determined. The FE analysis conducted used experimentally-determined mechanical properties [Ghavami and Marinho 2005] and the simulation was similar to that presented by Torres *et al.* [2007].

This Chapter focuses on capturing the functionally-graded nature of the bamboo material in FE modelling. The approaches adopted have been used to model other functionally-graded materials but few works have been found on bamboo. The first known numerical modeling of full culm bamboo as a graded material was that of Silva *et al.* [2006] who used graded finite elements to capture the varying material property distribution through the bamboo culm wall. Silva *et al.* compared results from a spatially-varying Young's modulus, an averaged Young's modulus, and orthotropic constitutive properties obtained from homogenization. It was found that other than the homogenization technique which requires additional computational effort, the elastic modulus resulting from the other two methods provided suitable numerical accuracy for capturing the "global" deflection response of a bamboo structure. In addition, Silva *et al.* concluded that to accurately estimate local features in the material, for all three material model used, it is necessary to employ a numerical procedure that accurately models material gradients through the culm wall.

More recently, Martínez-Pañeda and Gallego [2015] investigated and presented another approach by which functionally graded materials (FGM) could be included in numerical modelling. The study reviews different methods by which FGMs have been modelled in the past

and concluded that the UMAT and USDFLD user subroutines in the ABAQUS software were most versatile. The USDFLD subroutine permits the assignment of material variables on an integration point-by-integration point basis. Bao and Wang [1995] assigned element properties both individually and by dividing a structure into multiple areas and then assigning properties to these areas but this was found to be inappropriate in failure analysis where local stress values may be of importance. Santare and Lambros [2000] and Kim and Paulino [2002] developed a formulation which automatically interpolates mechanical properties within the element. Santare and Lambros sampled the mechanical properties directly at the Gauss integration points of the element – the same approach programmed into the USDFLD subroutine. On the other hand, Kim and Paulino adopted a generalized isoparametric formulation. Both studies found that the solution quality was improved based on the same mesh density, especially for higher-order graded elements. Assigning spatially varying properties at integration points by defining properties as a function of temperature was demonstrated by Rousseau and Tippur [2000]. This technique, however, was not found to be able to define a non-linear continuous variation of the elastic properties in most FE codes and does not allow for differences in the gradient profile of different properties: Young's modulus and Poisson's ratio, for instance.

Due to the availability and versatility of the ABAQUS [2017] software, it was selected to conduct the numerical analysis presented here. Similar to the work of Martínez-Pañeda and Gallego [2015] and Burlayenko and Sadowski [2019], the bamboo material gradient is implemented in this work through either the USDFLD or UMAT user subroutines. Each subroutine handles the assignment of graded properties differently; by comparing both approaches, a recommendation of which to adopt for bamboo can be made. Material elastic properties are defined by functions whose variation in the specimen is programmed in the subroutines. Two additional

techniques, one which uses a gross section elastic Young's modulus and the other which divides the culm into concentric rings and applies individual properties to each ring will also be modelled. Finally, closed-form equations based on Castigliano's theorem suitable for homogeneous materials are applied; these are the formulation upon which the analysis of experimental results is founded (Chapter 2.3.4). The output of all methods is compared with the experimental data collected in this study using the digital image correlation method (Chapter 2.3.5) which allowed for accurate measurements of displacement and strain fields.

6.2 Modelling the Bamboo Culm Wall

A finite element model of full-culm bamboo is developed and implemented using ABAQUS [2017]. In this work, the models have the objective of modeling material test specimen behavior; specifically, that of the circumferential compression test (see Section 2.3.4). The models will be calibrated using data from Chapter 2 and validated using additional data from Chapter 3 and results from circumferential compression tests. The models consider non-homogeneous test specimen geometry and capture the functionally-graded nature of bamboo (Chapter 3) and uncertainty (Chapter 5). An example of the model implementation is described in this Chapter.

A user-defined subroutine for constitutive modelling which allows the relevant mechanical properties of bamboo to be defined with continuous spatial variation in all directions is developed using ABAQUS user-defined formulations. A naturally isoparametric formulation similar to the one described by Kim and Paulino [2002] is implemented using ABAQUS for linear [and eventually can be extended to non-linear] static analysis.

A linear three-dimensional continuum 8-node brick element (C3D8) is used as a base element. For the graded element analysis, the spatial variation of the material parameters is achieved by coding either the user-defined field subroutine USDFLD or the user-defined material subroutine UMAT. The inclusion of the graded element was adopted because it incorporates varying mechanical properties at integration points [Kim and Paulino 2002]. This approach was selected over a homogeneous element due to its continuous material property distribution in the numerical simulation which leads to smoothly varying and more accurate stress results. A reduced integration element (C3D8R) was initially considered but this was found to not fully capture the material strains at the extreme edges of the culm wall. A twenty-node quadratic brick element (C3D20) was also tried. Negligible differences in results between the eight and twenty node element models were observed. Therefore, the eight node element (C3D8) was selected in the simulation in order to optimize computation time. A hexahedral mesh was chosen due to its better convergence over tetrahedral [Tadepalli *et al.* 2011]; mesh size of approximately 0.1t (ten elements through culm wall thickness) was also selected in order to maintain uniformity in the comparison of all considered models.

The USDFLD subroutine was selected as an option for comparison in order to make use of the material models which are already available in ABAQUS. USDFLD is used to introduce solution-dependent mechanical properties as field variables and is called at all integration points of elements for which the material definition includes user-defined field variables. With USDFLD, the variation of the material elastic properties through the specimen culm wall thickness is programmed in the subroutine which is shown in Appendix C.

UMAT is used to program a 3D brick graded finite element having a smooth variation of elastic properties. The material is assumed to be transversely isotropic with mechanical properties

varying through the wall thickness in accordance with the estimated material variation function. UMAT can be used to define the mechanical constitutive behavior of a material which will be called at all material calculation points of elements for which the material definition includes a user-defined material behavior [ABAQUS 2017]. The associated code programmed for this subroutine is presented in Appendix D.

Linear static FE analyses of the circumferential compression tests (Section 2.3.4) are developed using the results presented in Chapter 2 to validate the procedure. The few tests that used digital image correlation (DIC) to obtain full field strain data (Chapter 2.6) are used as the data source for the validation. The FE model complexity is considered using four modelling scenarios in addition to a theoretical approach and all results are compared.

Model 0: Theoretical evaluation in which Castigliano's second theorem as described in Article 9.2 of *Roark's Formulas for Stress and Strain* [7th edition, Young *et al.* 2002] for a thin-walled ring subject to diametrically oriented compression was applied to the circumferential compression test specimens modeled. The equations, presented in this thesis as Eqs. 2-5 to 2-12 assume homogenous transverse material properties. Corrections are made for axial and shear deformations assuming thin-walled behavior with factors k_1 and k_2. Model 0 is presented since this is the same approach used to process test data. Model 0 is also a hand-calculation validation of Model 1 which should yield similar results.

Model 1: FE model in which uniform transversely isotropic mechanical properties are assigned. Gross section mechanical properties in different orientations are calculated using the rule of mixtures presented in Chapter 3 (Eqs 3-1 to 3-5) using the average fiber volume ratios. This is an improvement on a standard isotropic material, as it takes into account the expected material

property variation of bamboo in different directions but does not capture the graded nature of the culm wall. Model 1 is illustrated schematically in Figure 6.1b.

Model 2: FE model which divides the culm wall into ten concentric annular ring sections and assigns to each ring uniform transversely isotropic mechanical properties based on rule of mixtures refined for volume fractions determined for the concentric sections as described by the image analysis in Chapter 3 (see Figures 3.4 and 3.5). Model 2 is illustrated schematically in Figure 6.1c. The calculated elastic modulus is averaged over each annular section and assigned as the transverse modulus of elasticity for that section. This results in distribution of properties through the culm wall thickness represented by ten discrete steps.

Model 3: FE model which assigns mechanical properties through the culm wall using a continuum approach (graded elements) assigning properties to the integration points through the culm wall thickness using the USDFLD subroutine. This approach mitigates some of the errors anticipated using discrete steps in Model 2 and will lead to smoother strain fields [Silva *et al.* 2006].

Model 4: FE model which implements user-defined mechanical properties (UMAT) through the culm wall using a defined mechanical constitutive law for bamboo as a transversely isotropic material. The approach updates the stress and strain vectors, and other solution dependent variables over the element volume and assigns the material parameters directly at the integration points of the element [ABAQUS 2017].

Models 3 and 4, while implemented in a different manner, are both illustrated schematically in Figure 6.1d.

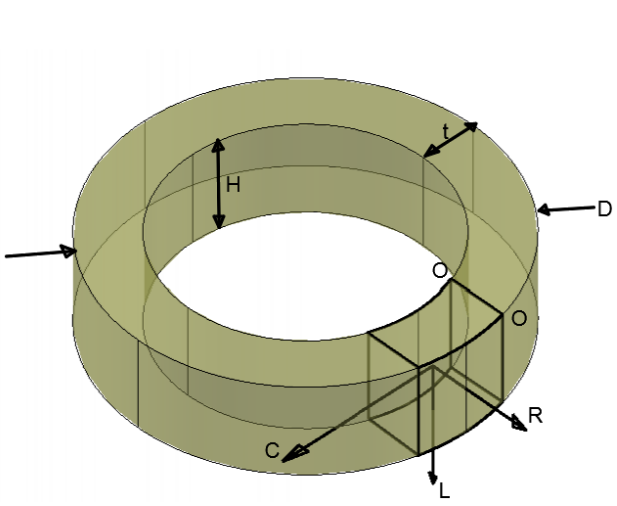

(a) Section through a bamboo culm wall

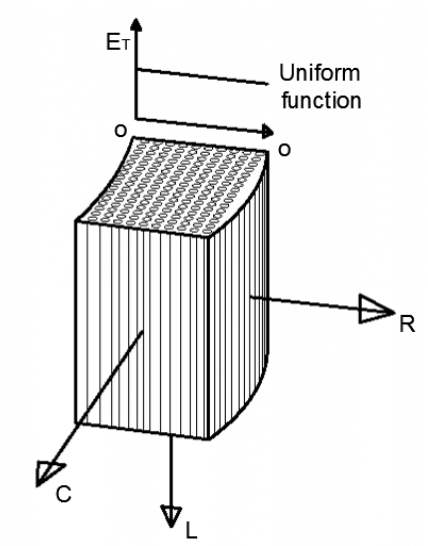

(b) Model 1

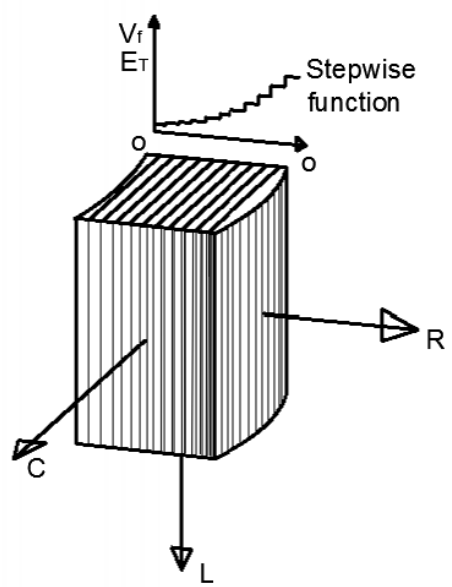

(c) Model 2

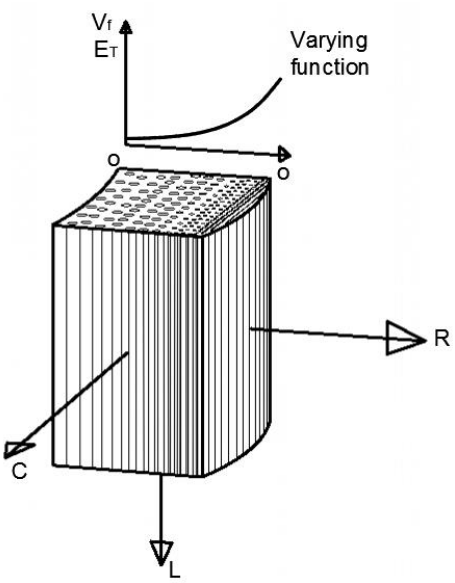

(d) Models 3 and 4

Figure 6.1: Modeling bamboo as a transversely isotropic material

6.2.1 Constitutive Equations for Bamboo Analysis

Bamboo is a functionally graded material assumed to be transversely isotropic with varying properties in the radial direction (see Figure 6.1). Figure 6.1a illustrates a cut o-o through a typical bamboo culm wall with local Cartesian coordinates defined as follows: *R* is the radial direction, *C* is the circumferential direction and *L* is the longitudinal direction. This local coordinate system will be used through the remainder of this discussion. Figure 6.1b shows a schematic illustration of Model 1 as an orthotropic material with *L* as the axis of symmetry. Model 2 is illustrated in Figure 6.1c with the culm wall divided into 10 annular ring sections each having an individual orthotropic material property. Figure 6.1d illustrates both Models 3 and 4 with the material property represented with a varying function through the culm wall thickness.

The constitutive equation of an elastic orthotropic material is governed by Hooke's law:

$$\boldsymbol{\sigma} = \mathbf{K}\boldsymbol{\varepsilon} \tag{6.1}$$

where σ is the stress, ε is the strain and **K** is the elasticity tensor (stiffness matrix) represented as [Bower 2009]:

$$\mathbf{K} = \begin{bmatrix} K_{11} & K_{12} & K_{13} & 0 & 0 & 0 \\ . & K_{11} & K_{13} & 0 & 0 & 0 \\ . & . & K_{33} & 0 & 0 & 0 \\ . & . & . & K_{44} & 0 & 0 \\ . & sym & . & . & K_{44} & 0 \\ . & . & . & . & . & (K_{11} - K_{12})/2 \end{bmatrix} \tag{6.2}$$

For an orthotropic material, there are nine independent material constants resulting in the following symmetric stiffness matrix [Bower 2009]:

$$\mathbf{K} = \begin{bmatrix} E_R(1-\upsilon_{CL}\upsilon_{LC})\emptyset & E_R(v_{CR}+\upsilon_{LR}v_{CL})\emptyset & E_R(v_{LR}+\upsilon_{RC}v_{LR})\emptyset & 0 & 0 & 0 \\ . & E_C(1-\upsilon_{RL}v_{LR})\emptyset & E_C(v_{LC}+\upsilon_{RC}v_{LR})\emptyset & 0 & 0 & 0 \\ . & . & E_L(1-\upsilon_{RC}v_{CR})\emptyset & 0 & 0 & 0 \\ . & . & . & G_{CL} & 0 & 0 \\ . & symmetric & . & . & G_{RL} & 0 \\ . & . & . & . & . & G_{RC} \end{bmatrix} \quad (6\text{-}3)$$

$$\emptyset = \frac{1}{1 - v_{RC}v_{CR} - v_{CL}v_{LC} - v_{LR}v_{RL} - 2v_{CR}v_{LC}v_{RL}} \quad (6\text{-}4)$$

$$G_{CL} = G_{RL} = \frac{E_L}{2(1+\upsilon_{CL})} \quad (6\text{-}5)$$

$$G_{RC} = \frac{E_C}{2(1+\upsilon_{RC})} \quad (6\text{-}6)$$

In this study, as described previously, we consider bamboo as a transversely isotropic material, in which case there are five independent elastic constants: Young's modulus and Poisson's ratio in the radial-circumferential plane, E_T and υ_T; and Young's modulus, Poisson's ratio and shear modulus in the longitudinal direction, E_L , v_{TL} and G_{TL}. That is, the following equivalencies are adopted:

$E_C = E_R$ and is represented by E_T as the transverse modulus,

$\upsilon_{RC} = \upsilon_{CR}$ and is represented by υ_T for the transverse Poisson's ratio.

$\upsilon_{LR} = \upsilon_{LC}$ and is represented by υ_{LT} for the axial-transverse Poisson's ratio

$\upsilon_{RL} = \upsilon_{CL}$ and is represented by υ_{TL} for the transverse-axial Poisson's ratio

$E_{L,}$ the longitudinal modulus, remains unchanged

The Poisson's ratios are not symmetric but satisfies the condition, $\frac{\upsilon_{TL}}{E_T} = \frac{\upsilon_{LT}}{E_L}$ for the derivation of the axial-transverse and the transverse-axial Poisson's ratios. The stiffness matrix in Eq. 6-3 is thereby simplified as:

$$\mathbf{K} = \begin{bmatrix} E_T(1-\upsilon_{TL}\upsilon_{LT})\emptyset & E_T(\upsilon_T+\upsilon_{TL}\upsilon_{LT})\emptyset & E_T(\upsilon_{LT}+\upsilon_T\upsilon_{LT})\emptyset & 0 & 0 & 0 \\ . & E_T(1-\upsilon_{TL}\upsilon_{LT})\emptyset & E_T(\upsilon_{LT}+\upsilon_T\upsilon_{LT})\emptyset & 0 & 0 & 0 \\ . & . & E_L(1-{\upsilon_T}^2)\emptyset & 0 & 0 & 0 \\ . & . & . & G_{TL} & 0 & 0 \\ . & symmetric & . & . & G_{TL} & 0 \\ . & . & . & . & . & G_T \end{bmatrix} \quad (6\text{-}7)$$

$$\emptyset = \frac{1}{1-{\upsilon_T}^2-2\upsilon_{TL}\upsilon_{LT}-2\upsilon_T\upsilon_{TL}\upsilon_{LT}} \quad (6\text{-}8)$$

$$G_{TL} = \frac{E_L}{2(1+\upsilon_{TL})} \quad (6\text{-}9)$$

$$G_T = \frac{E_T}{2(1+\upsilon_T)} \quad (6\text{-}10)$$

For a fiber-reinforced graded material, both E_L and E_T are dependent on the fiber volume ratio through the culm wall as previously described in Chapters 3 and 5. The stiffness matrix in Eq. 6-3 is in a form easily adopted to the material definitions in the USDFLD and UMAT subroutines that represent bamboo as a FGM material for the FE analysis

6.2.2 Parametric Definition and Calibration

In order to determine values of modulus required for the constitutive models, the rule of mixtures, with the Halpin-Tsai correction as given in Equation 3-3 was used along with experimentally determined fiber volume ratios. Initially, representative fiber and matrix moduli recommended by Janssen [2000] were used: E_f = 35 GPa and E_m = 1.8 GPa (see Sections 3.3 and 5.2). The numerical modeling campaign described in the following section was carried out using these values. Results – parallel to those reported in Section 6.3 – are provided in Appendix E. This initial analysis, resulted in a modeled behavior that was stiffer than the experimentally observed values by a factor of about 1.7.

The representative properties reported by Janssen were derived based on longitudinal material properties which are modeled well using the rule of mixtures (Section 3.2) and are dominated by the value of E_f. On the other hand, the transverse behavior considered in this study is very sensitive to the value of E_m. For these reasons, an evaluation of behavior – using only Models 1 and 4 – was undertaken in which E_f = 35 GPa and E_m is calibrated such that the stiffness of the models better matches the experimental data. A value of E_m = 1.0 GPa was found to be appropriate for the *P. nigra* material considered and was adopted for the analyses reported in the remainder of this Chapter.

6.3 Modeling the Circumferential Compression Test

To validate the modeling approaches, tested specimens are modelled individually as summarized in Table 6.1. The output of the experiments including the surface transverse strains

and displacement obtained using DIC are available for comparison. Three *P. nigra* specimens PN5B2C, PN5B2C and PN5B2C (Table 2.6) as well as consolidated data from a group of specimens, PN (Table 2.1) were selected to run the models for the validation process. The fiber volume ratios reported in Table 6.1 were determined for each specimen as the average of distributions obtained at the four quadrants of the particular specimen. The average value for PN given in Table 3.1 was obtained from seven samples (four quadrant measurements of each) as described in Chapter 3.4.2. Following initial calibration (see Section 6.2.2), values of E_L and E_T are calculated using the rule of mixtures (Eqs 3-1 and 3-3, respectively) using E_f = 35 GPa and E_m = 1 GPa.

Table 6.1: Geometric parameters of bamboo specimens used for modelling validation (see Table 2.1 and 2.6)

	PN5B2C	PN5B3C	PN5B4C	PN
D (mm)	91.0	90.8	90.5	93.5
H (mm)	17.2	18.2	19.3	18.7
t (mm)	8.35	8.40	8.10	6.74
std. dev. of t (mm)	0.40	0.10	0.30	1.27
ovality[a]	0.09	0.10	0.10	0.08
V_f	$V_f = 1.29x^3 - 1.28x^2 + 0.57x + 0.10$	$V_f = 0.81x^3 - 0.53x^2 + 0.28x + 0.10$	$V_f = 1.09x^3 - 0.90x^2 + 0.40x + 0.10$	$V_f = 0.94x^3 - 0.63x^2 + 0.36x + 0.06$
E_L (GPa)	$E_L = 43.9x^3 - 43.5x^2 + 19.4x + 4.2$	$E_L = 27.5x^3 - 18.0x^2 + 9.5x + 4.4$	$E_L = 37.1x^3 - 30.6x^2 + 13.6x + 4.5$	$E_L = 32x^3 - 21.4x^2 + 12.2x + 3.0$
E_T (GPa)	$E_T = 21.7x^3 - 23.7x^2 + 7.4x + 1.1$	$E_T = 17.2x^3 - 17.6x^2 + 5.3x + 1.1$	$E_T = 24.1x^3 - 25.9x^2 + 7.7x + 1.1$	$E_T = 33x^3 - 35.7x^2 + 10.6x + 0.8$
[a] ovality, $d_o = 2(D_{max} - D_{min})/(D_{max} + D_{min})$ [ISO 19624-2018]				

The FE model was created using a 3D deformable solid extrusion; units of Newtons and millimeters were used. Measured dimensions of the specimens from Table 6.1 were used to create each Model. The local Cartesian coordinate transformation was applied directly to the mechanical properties using the 'material orientation' option in ABAQUS. A snapshot of this is shown in

Figure 6.2 where the yellow arrows show the local Cartesian orientation also given in Figure 6.1. All FE results are reported in this local coordinate system.

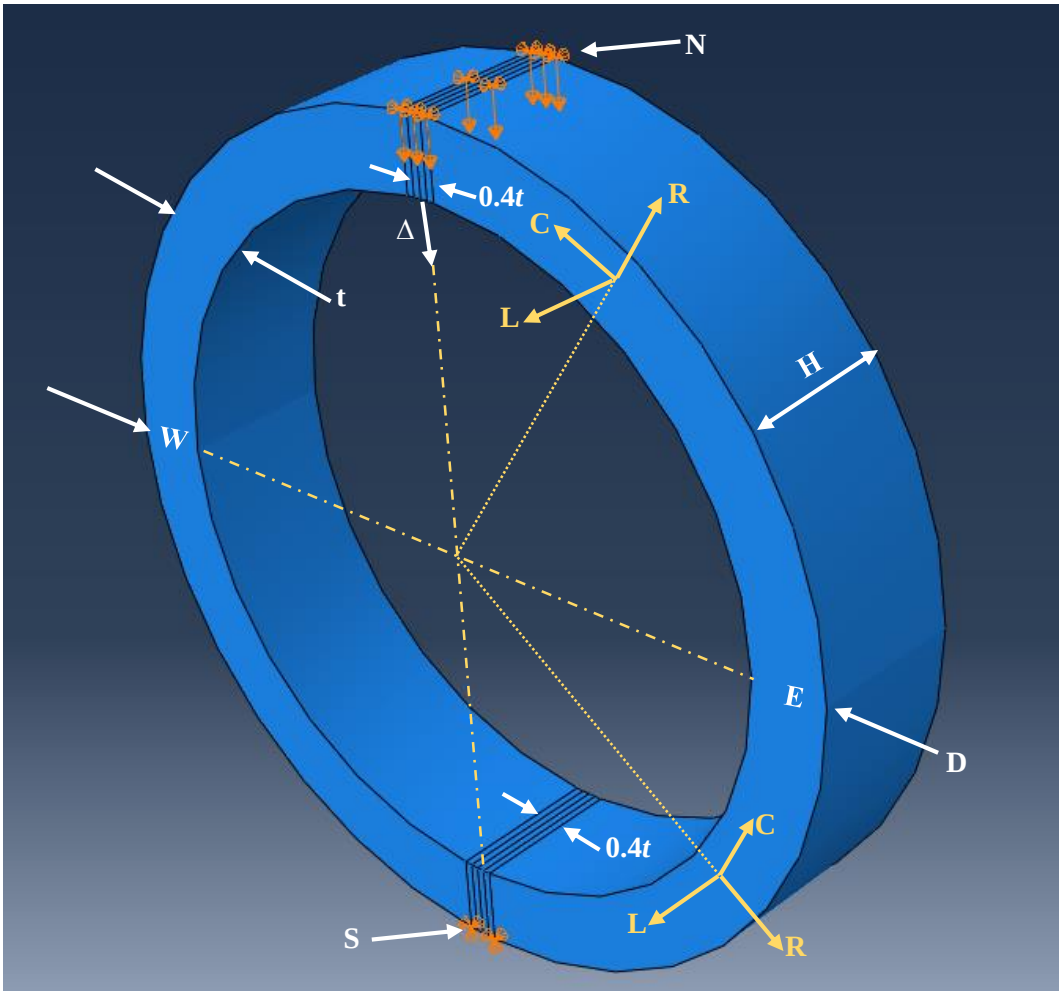

Figure 6.2: Image showing boundary conditions and orientation applied to ABAQUS modelling of the circumferential compression test

6.3.1 Model 1

Starting with Model 1, having uniform mechanical properties through the culm wall thickness, the material constants shown in Eq. 6-1 were calculated using the formulae in Eq. 6-7.

This leads to the input values for Model 1 shown in Table 6.2; these values represent the 'average' properties for the culm wall. The assumption made for the properties is that both the Poisson's ratio and the moduli of elasticity for the circumferential and the radial directions are equal.

Table 6.2: FEA model input for Model 1

Parameter	PN5B2C	PN5B3C	PN5B4C	PN
Gross section fiber volume fraction, V_f	0.28	0.27	0.28	0.27
Transverse Modulus $E_{T,}$ MPa	2473	2320	2513	2680
Longitudinal Modulus $E_{L,}$ Mpa	10748	10413	10793	10410
Transverse Poisson's ratio, $\nu_T = \nu_{LT}$ [Janssen 1981]	0.30	0.30	0.30	0.30
Longitudinal Poisson's ratio, $\nu_{TL} = \nu_{LT}E_T/E_L$	0.07	0.07	0.07	0.08
Shear Modulus, G_{TL} Mpa	5027	4880	5044	4832
$\emptyset$	1.2	1.2	1.2	1.2
$K_{11} = K_{22}$, Mpa	2828	2650	2875	3081
K_{33}, Mpa	11423	11045	11480	11148
$K_{12} = K_{21}$, Mpa	926	866	943	1019
$K_{13} = K_{23} = K_{31} = K_{32}$, Mpa	1126	1055	1145	1230
$K_{44} = K_{55}$, Mpa	5027	4880	5044	4832
$G_T = K_{66}$, Mpa	951	892	966	1031

6.3.2 Model 2

In Model 2, the bamboo culm wall is partitioned into ten concentric annular ring sections each having properties assigned in the same fashion as the entire culm wall in Model 1. Based on the fiber volume ratio variation through the section (Table 6.1), the properties at the midpoints of the ten sections (x in Table 6.3) are calculated. Tables 6.3a-d show the material input for the four specimens using Model 2.

Table 6.3a: FEA model input for Model 2 (PN5B2C)

Parameter	PN5B2C									
x	0.05	0.15	0.25	0.35	0.45	0.55	0.65	0.75	0.85	0.95
V_f	0.12	0.16	0.18	0.19	0.21	0.24	0.28	0.35	0.45	0.59
$E_{T,}$ MPa	1413	1750	1808	1717	1608	1611	1856	2473	3593	5346
$E_{L,}$ MPa	5067	6279	7017	7543	8122	9015	10487	12802	16221	21010
$\upsilon_T = \upsilon_{LT}$	0.30	0.30	0.30	0.30	0.30	0.30	0.40	0.25	0.30	0.30
$\upsilon_{TL} = \upsilon_{LT}E_T/E_L$	0.08	0.08	0.08	0.07	0.06	0.05	0.07	0.05	0.07	0.08
G_{TL} MPa	2338	2897	3257	3531	3833	4278	4897	6106	7605	9760
Ø	1.18	1.18	1.18	1.17	1.16	1.15	1.31	1.10	1.17	1.18
$K_{11} = K_{22}$, MPa	1631	2020	2078	1963	1829	1826	2371	2693	4104	6142
K_{33}, MPa	5458	6764	7515	8012	8557	9449	11580	13228	17201	22481
$K_{12} = K_{21}$, MPa	544	673	688	642	592	587	1045	714	1340	2030
$K_{13} = K_{23} = K_{31} = K_{32}$, MPa	653	808	830	782	726	724	1366	852	1633	2451
$K_{44} = K_{55}$, MPa	2338	2897	3257	3531	3833	4278	4897	6106	7605	9760
$G_T = K_{66}$, MPa	544	673	695	660	619	620	663	989	1382	2056

Table 6.3b: FEA model input for Model 2 (PN5B3C)

Parameter	PN5B3C									
x	0.05	0.15	0.25	0.35	0.45	0.55	0.65	0.75	0.85	0.95
V_f	0.11	0.13	0.15	0.17	0.19	0.23	0.28	0.35	0.45	0.58
$E_{T,}$ MPa	1323	1557	1594	1536	1488	1553	1833	2431	3452	4998
$E_{L,}$ MPa	4833	5513	6080	6699	7536	8755	10522	13002	16358	20758
$\upsilon_T = \upsilon_{LT}$	0.30	0.30	0.30	0.30	0.30	0.30	0.30	0.30	0.30	0.30
$\upsilon_{TL} = \upsilon_{LT}E_T/E_L$	0.08	0.08	0.08	0.07	0.06	0.05	0.05	0.06	0.06	0.07
G_{TL} MPa	2233	2541	2818	3134	3557	4157	5000	6155	7692	9680
Ø	1.18	1.18	1.18	1.17	1.16	1.15	1.15	1.15	1.16	1.17
$K_{11} = K_{22}$, MPa	1526	1798	1834	1757	1692	1759	2075	2759	3935	5728
K_{33}, MPa	5199	5945	6519	7119	7939	9174	11016	13658	17297	22128
$K_{12} = K_{21}$, MPa	508	600	608	575	548	565	666	889	1279	1883
$K_{13} = K_{23} = K_{31} = K_{32}$, MPa	610	720	732	700	672	697	822	1095	1564	2283
$K_{44} = K_{55}$, MPa	2233	2541	2818	3134	3557	4157	5000	6155	7692	9680
$G_T = K_{66}$, MPa	509	599	613	591	572	597	705	935	1328	1922

Table 6.3c: FEA model input for Model 2 (PN5B4C)

Parameter	PN5B4C									
x	0.05	0.15	0.25	0.35	0.45	0.55	0.65	0.75	0.85	0.95
V_f	0.12	0.15	0.16	0.18	0.20	0.23	0.28	0.36	0.46	0.60
$E_{T,}$ MPa	1423	1754	1783	1656	1516	1510	1781	2473	3733	5703
$E_{L,}$ MPa	5108	5977	6567	7102	7804	8896	10600	13139	16736	21612
$\upsilon_T = \upsilon_{LT}$	0.30	0.30	0.30	0.30	0.30	0.30	0.30	0.30	0.30	0.30
$\upsilon_{TL} = \upsilon_{LT}E_T/E_L$	0.08	0.09	0.08	0.07	0.06	0.05	0.05	0.06	0.07	0.08
G_{TL} MPa	2357	2747	3036	3319	3687	4232	5046	6218	7843	10013
Ø	1.18	1.19	1.18	1.17	1.16	1.15	1.15	1.15	1.17	1.18
$K_{11} = K_{22}$, MPa	1642	2029	2055	1895	1723	1708	2014	2808	4264	6564
K_{33}, MPa	5502	6464	7060	7555	8215	9302	11079	13807	17754	23185
$K_{12} = K_{21}$, MPa	548	680	683	621	557	547	644	905	1393	2177
$K_{13} = K_{23} = K_{31} = K_{32}$, MPa	657	813	821	755	684	677	798	1114	1697	2622
$K_{44} = K_{55}$, MPa	2357	2747	3036	3319	3687	4232	5046	6218	7843	10013
$G_T = K_{66}$, MPa	547	674	686	637	583	581	685	951	1436	2193

Table 6.3d: FEA model input for Model 2 (PN)

Parameter	PN									
x	0.05	0.15	0.25	0.35	0.45	0.55	0.65	0.75	0.85	0.95
V_f	0.08	0.10	0.13	0.15	0.18	0.22	0.29	0.37	0.49	0.64
$E_{T,}$ MPa	1245	1698	1734	1552	1348	1321	1669	2591	4283	6944
$E_{L,}$ MPa	3561	4457	5213	6021	7073	8561	10677	13613	17561	22713
$\upsilon_T = \upsilon_{LT}$	0.30	0.30	0.30	0.30	0.30	0.30	0.30	0.30	0.30	0.30
$\upsilon_{TL} = \upsilon_{LT}E_T/E_L$	0.10	0.11	0.10	0.08	0.06	0.05	0.05	0.06	0.07	0.09
G_{TL} MPa	1611	2000	2370	2794	3345	4091	5099	6439	8182	10402
Ø	1.21	1.22	1.20	1.18	1.16	1.14	1.14	1.16	1.17	1.19
$K_{11} = K_{22}$, MPa	1456	1998	2022	1784	1531	1491	1884	2942	4911	8054
K_{33}, MPa	3912	4941	5700	6448	7437	8914	11124	14313	18736	24650
$K_{12} = K_{21}$, MPa	498	692	688	590	494	475	600	949	1617	2713
$K_{13} = K_{23} = K_{31} = K_{32}$, MPa	586	807	813	712	607	590	745	1167	1958	3230
$K_{44} = K_{55}$, MPa	1611	2000	2370	2794	3345	4091	5099	6439	8182	10402
$G_T = K_{66}$, MPa	479	653	667	597	518	508	642	996	1647	2671

6.3.3 Model 3

In Model 3, the user-defined field function USDFLD in ABAQUS was used to directly program the cubic polynomial functions reported in Table 6.1. The cubic function of two

independent field variables for E_L and E_T were defined related to the solution of the elasticity tensor, which provides the input for the USDFLD function in ABAQUS. The USDFLD subroutine script is provided in Appendix C. Figure 6.3 provides a summary of the subroutine.

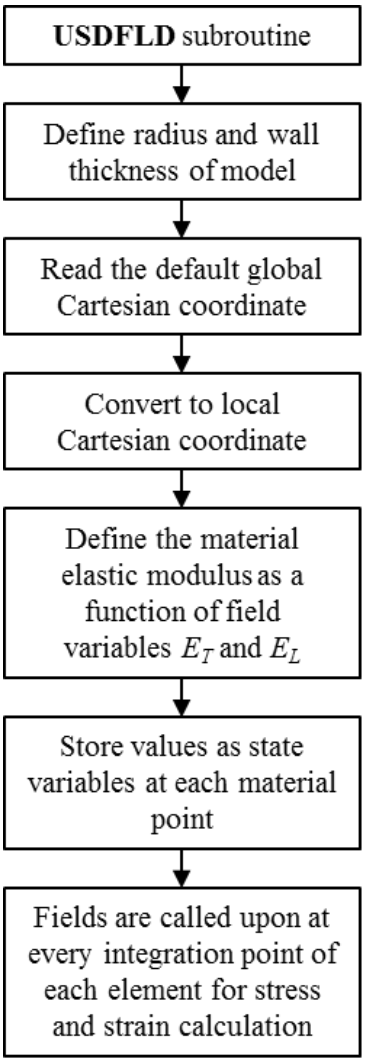

Figure 6.3: USDFLD subroutine summary

The dependence of modulus on the field variable that is specified in the USDFLD subroutine is defined using tabular input in the ABAQUS software. A screen shot of this is shown in Figure 6.4.

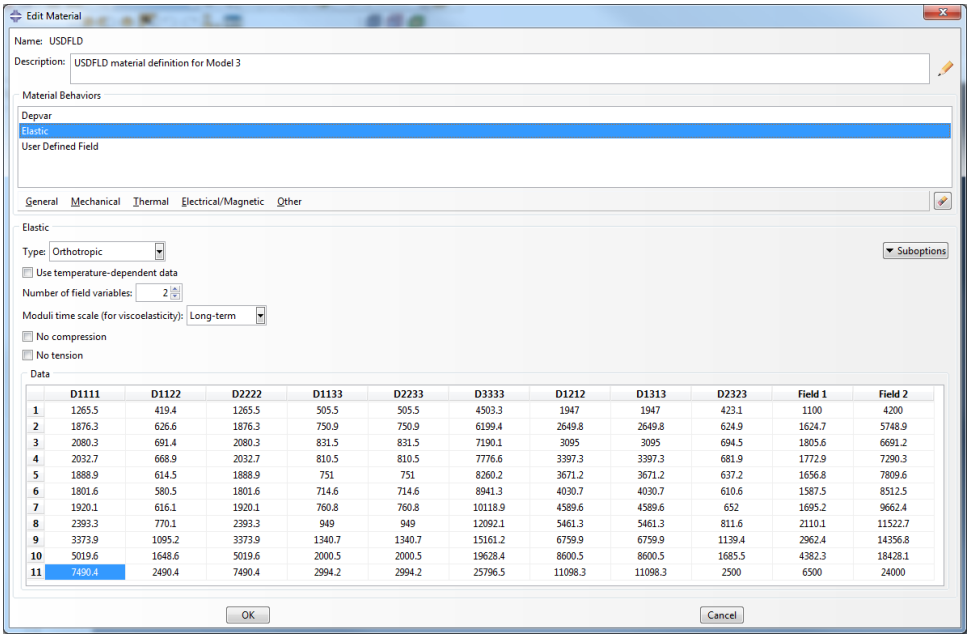

Figure 6.4: Example ABAQUS input of elastic modulus dependence on field variable (PN5B2C)

6.3.4 Model 4

The UMAT subroutine used in Model 4 has both E_L and E_T defined as a polynomial input to account for the graded material property through the culm wall thickness. The UMAT subroutine script is provided in Appendix D. Figure 6.5 provides a summary of the subroutine.

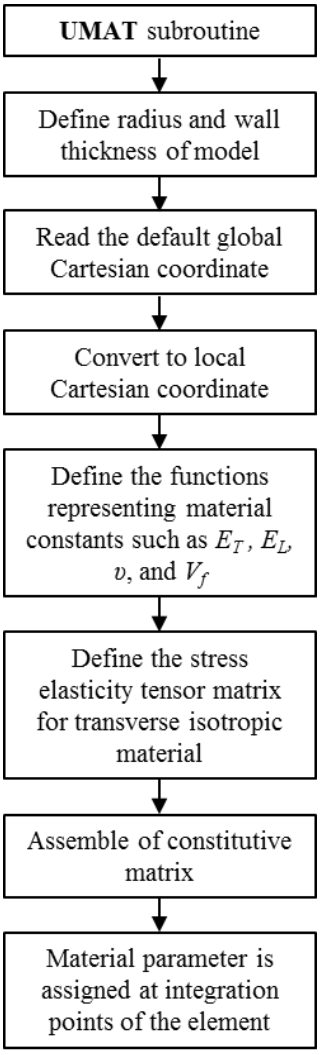

Figure 6.5: UMAT subroutine summary

As shown in Figure 6.5 and Appendix D, various properties (PROPS) defined in the subroutine need to be added as an input to the ABAQUS software. This was done manually and a screenshot of the output is shown in Figure 6.6.

- PROPS (1) is the transverse coefficient v_T and v_{LT}
- PROPS (2) – PROPS (5) are the coefficient of the cubic function of V_F
- PROPS (6) – PROPS (9) are the coefficient of the cubic function of E_L
- PROPS (10) – PROPS (13) are the coefficient of the cubic function of E_T

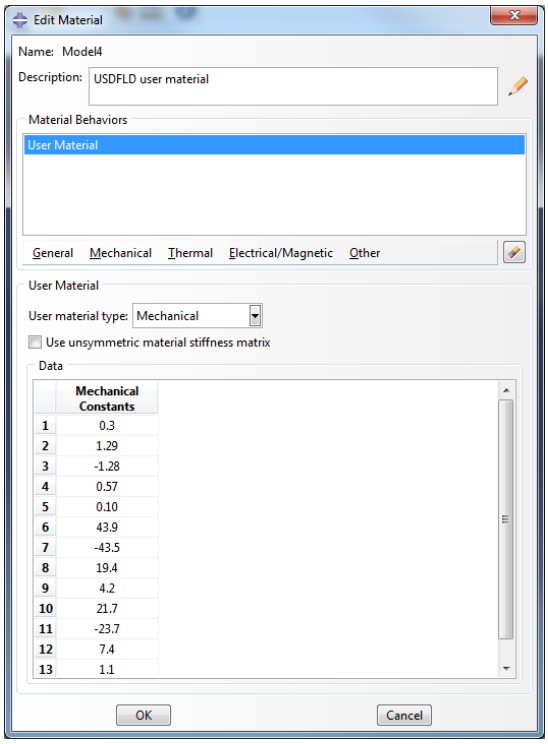

Figure 6.6: Example ABAQUS input of material property defined in UMAT subroutine (PN5B2C)

6.4 Model Implementation

All FE models used ABAQUS C3D8 eight-node linear brick elements with hexahedral mesh described earlier. The boundary conditions are described below with reference to a typical model image shown in Figure 6.2.

- Model restraint was provided by applying a 0.4*t* wide fixed boundary condition at the outer face of the lower part of the ring (point S in Figure 6.2).
- A prescribed displacement of 1.5 mm was assigned to all nodes within a width of approximately 0.4t located at the outer face of the upper part of the culm wall ring (point N in Figure 6.2). This simulates an experiment condition occurring before the ultimate capacity of the modeled tests was reached (Δ in Table 2.6).

6.4.1 FE Results

A summary of the FE model results and associated experimental results (see Table 2.6 and Figures 2.13 and 2.14 for the latter) is given in Table 6.4. The models simulated a deflection Δ = 1.5 mm, which is about 70% of the maximum displacement reported. Specimen PN represents the average material with dimensions presented in Table 2.1. DIC strain data is available for all specimens except PN.

Table 6.4: Stresses and strains from the E-W quadrant of the FEA at a prescribed displacement Δ = 1.5 mm

		Experimental	Model 0	Model 1	Model 2	Model 3	Model 4
Applied load to cause Δ = 1.5 mm, N	PN5B2C	293.7	288.5	310.8	305.7	305.0	306.0
	PN5B3C	300.0	294.3	307.2	296.7	296.2	297.2
	PN5B4C	315.0	303.4	326.3	321.5	320.7	321.9
	PN	-	152.9	184.5	169.1	167.7	168.9
Compressive strain at E-W quadrant, ε_{yy} με	PN5B2C	-4498	-	-5108	-6115	-6154	-6144
	PN5B3C	-4562	-	-5029	-6060	-6093	-6084
	PN5B4C	-4185	-	-4957	-6002	-6040	-6031
	PN	-	-	-3957	-4894	-4937	-4922
Tensile strain at E-W quadrant, ε_{yy} με	PN5B2C	2832	-	3757	2768	2732	2741
	PN5B3C	3064	-	3692	2672	2642	2650
	PN5B4C	3256	-	3698	2660	2622	2633
	PN	-	-	3529	2239	2197	2209
Neutral axis location, x	PN5B2C	0.54*t*	0.52*t*	0.52*t*	0.65*t*	0.65*t*	0.65*t*
	PN5B3C	0.56*t*	0.52*t*	0.52*t*	0.64*t*	0.64*t*	0.64*t*
	PN5B4C	0.50*t*	0.52*t*	0.52*t*	0.65*t*	0.65*t*	0.65*t*
	PN	-	0.52*t*	0.52*t*	0.67*t*	0.67*t*	0.67*t*
Compressive stress in E-W, $\sigma_{,yy}$ MPa (Eq. 2-10b)	PN5B2C	-12.9	-12.7	-12.4	-8.5	-6.8	-6.9
	PN5B3C	-12.1	-12.1	-11.5	-7.9	-6.7	-6.8
	PN5B4C	-12.9	-12.5	-12.3	-8.4	-6.7	-6.8
	PN	-	-9.7	-10.5	-6.0	-4.0	-4.1
Tensile stress at E-W quadrant, $\sigma_{,yy}$ MPa (Eq. 2-10a)	PN5B2C	9.40	9.2	9.1	14.4	17.1	17.1
	PN5B3C	8.93	8.7	8.4	13.0	15.0	15.3
	PN5B4C	9.53	9.2	9.1	14.8	17.7	17.7
	PN	-	7.6	9.3	15.1	18.3	18.3
Average circumferential modulus, $E_{m,90}$ MPa (Eq. 2-5)	PN5B2C	2623	2578	2777	2731	2725	2734
	PN5B3C	2354	2432	2539	2452	2448	2456
	PN5B4C	2658	2614	2811	2770	2763	2773
	PN	-	2700	3257	2986	2961	2982

Figure 6.7 shows the deformed shapes and the strain in the circumferential-direction for each model at a displacement $\Delta = 1.5$ mm for Specimen PN5B2C. Similar behavior was observed in all models with the location of the maximum tensile strain at the inner surface of the N-S quadrant while the maximum compressive strain occurred at inner surface of the E-W quadrant as expected (note that the color scales in each image vary somewhat). At the E (or W, the models are symmetric) quadrant, the maximum compressive strain values ranged from -5000 με in Model 1 and increased in the other models, all having similar values of approximately -6100 με. These values all exceeded the DIC-measured values of about -4500 με. The maximum tensile strain value at the E quadrant ranged from about 3700 με in Model 1 and decreased to similar values of approximately 2700 με in models 2, 3 and 4 – very close to the values measured using DIC which averaged about 2800 με. As shown in Table 6.4, the greater compressive strain and similar tensile strain result in a greater predicted shift in the neutral axis toward the outer culm wall. Model 1 predicts a neutral axis location of 0.52*t*, Models 2, 3 and 4 predict 0.64*t* while the experimentally observed behavior ranges from 0.50*t* to 0.56*t*.

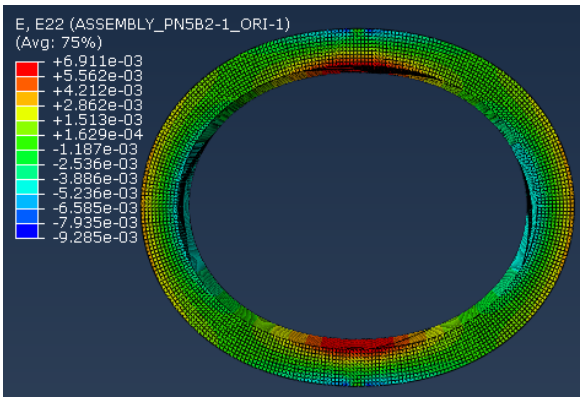

(a) Model 1

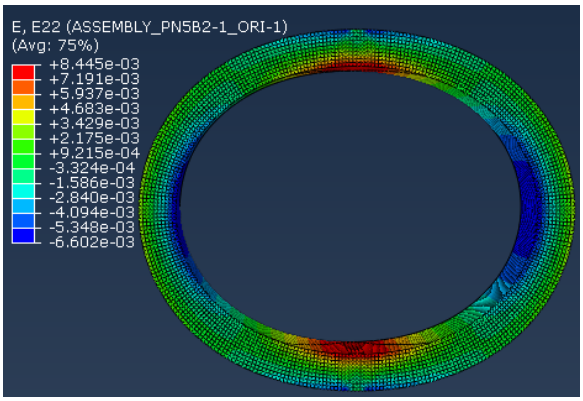

(b) Model 2

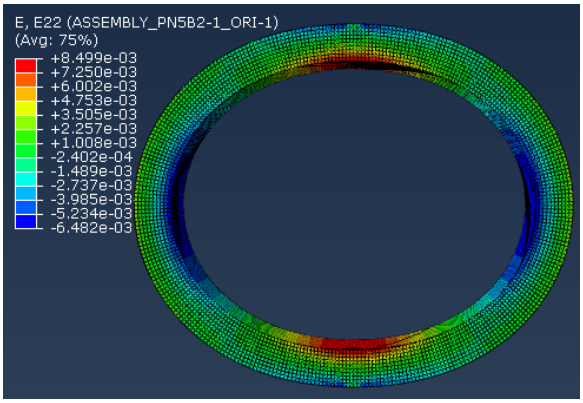

(c) Model 3

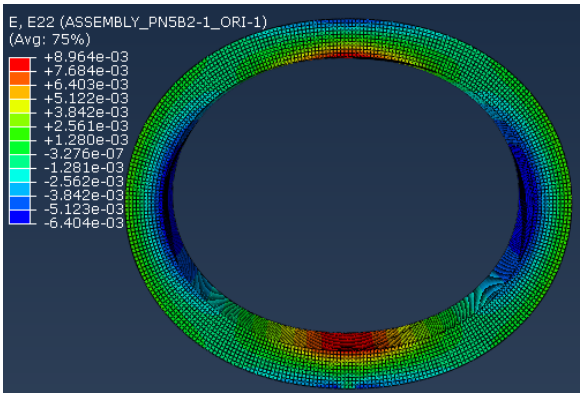

(d) Model 4

Figure 6.7: Circumferential strain distribution contours in modelled culm PN5B2C at Δ = 1.5 mm

The circumferential stress contours and deformed shapes for specimen PN5B2C are shown for all models in Figure 6.8. Once again, the output focuses on the stresses in the E quadrant (yellow line of Figure 6.8a). This region shows a range of compressive stresses (inner culm wall surface; $x = 0$) with a value of -12.4 MPa in Model 1 falling to approximately -8.5 MPa in Models 2 and -7.0 MPa in Models 3 and 4. Similarly, the maximum tensile stress (outer culm wall surface; $x = 1$) was 9.1 MPa in Model 1, increasing to 14.4 MPa in Models 2 and 17 MPa in Models 3 and 4. Using fundamental mechanics [Young *et al.* 2002 and ISO 22157-19], the calculated (Eq. 2-10)

stresses in specimen PN5B2C were -12.9 MPa and 9.4 MPa from the experiment and -12.7 MPa and 9.2 MPa for Model 0. The models were calibrated such that the circumferential moduli of the model and that obtained from the experiment were essentially the same. Despite the differences in strains and stresses, the average circumferential modulus, $E_{m,90}$ determined from the experiment (Eq. 2-5) is similar to that determined from the models with an error ranging from approximately 2% in Model 0 to 4% in Models 2 – 4 and 6% in Model 1.

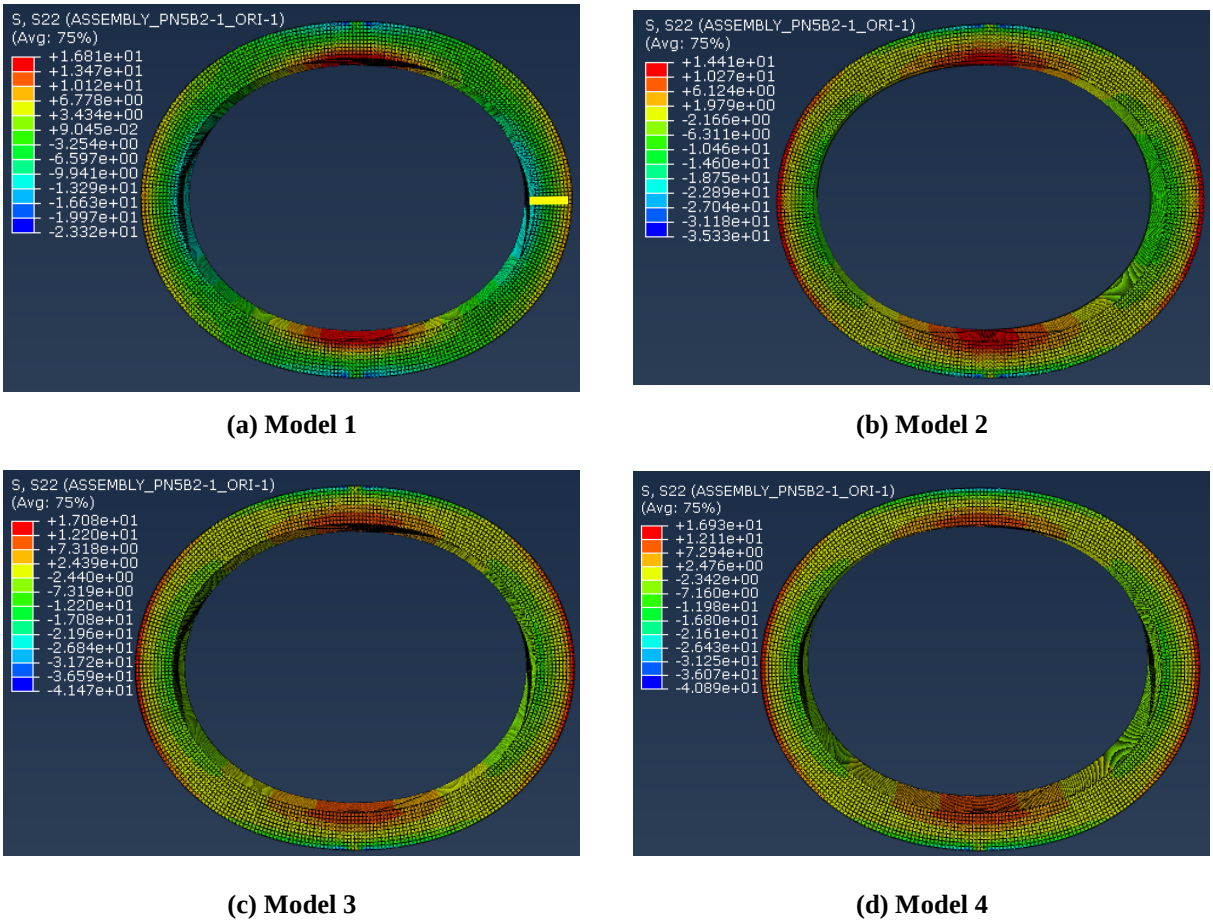

(a) Model 1 **(b) Model 2**

(c) Model 3 **(d) Model 4**

Figure 6.8: Variation of circumferential stress distribution contours in modelled culm PN5B2C at Δ = 1.5 mm

The circumferential strain distributions at the E quadrant of all models are shown in Figures 6.9a-d for all specimens considered. In terms of strain distribution, Model 1 has lower values than the experimental data at the inner culm wall and higher values at the outer wall although with only a slight shift in the resulting neutral axis location. Essentially Model 1 predicts similar behavior but a 'steeper' strain gradient. In the present experimental study and those reported in literature [Sharma *et al.* 2013; Moran *et al.* 2017], the circumferential strain profiles were generally found to shift towards the outer wall. This behavior was captured in the FE analysis. Models 2, 3 and 4 behave similarly with essentially identical values although all strains are shifted toward compression and, as a result, the neutral axis location is shifted further toward the outer culm wall. All FE models, predict a 'steeper' strain gradient (in terms of Figures 6.9a-d) than the experimental data. Such behavior suggests the FE model is 'softer' in transverse compression and 'stiffer' in transverse tension than the experimental data reveals. Nonetheless, the behavior exhibited in Figures 6.9a-d is promising and shows a relatively good comparison with experimental data after only limited calibration. The greatest difference between experimental results and the FE models was about 1500 με.

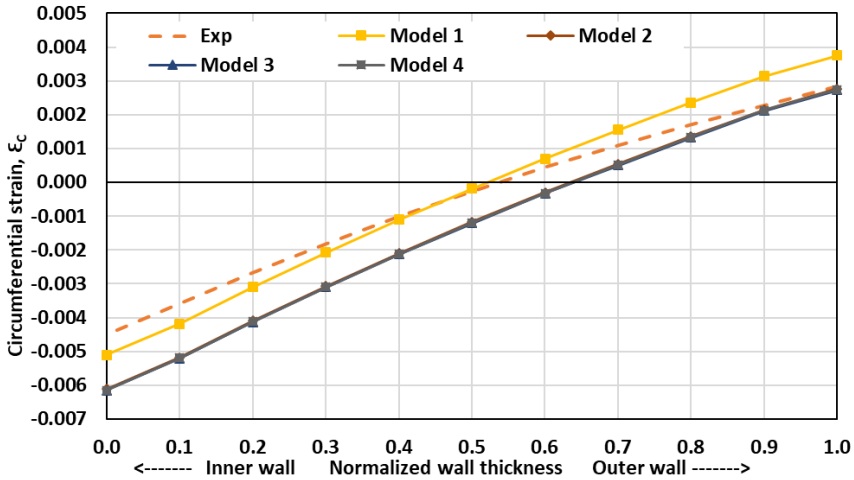

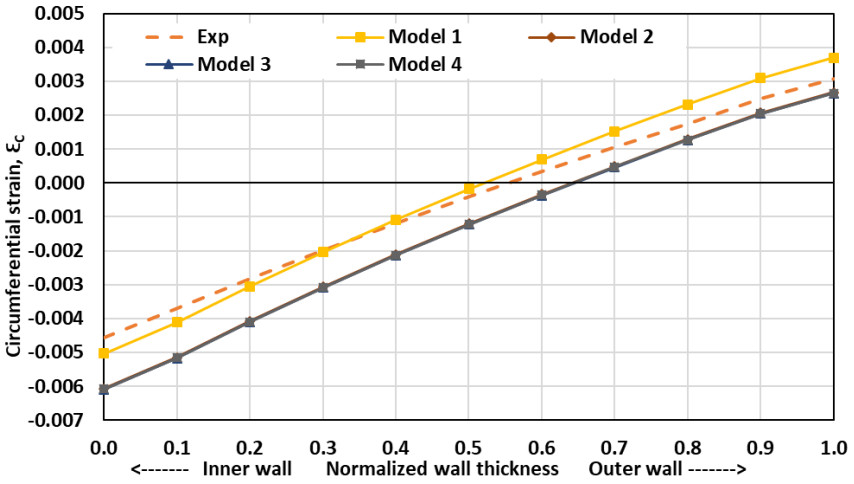
Exp
Model 1
Model 2
Model 3
Model 4
Circumferential strain, ε_c
0.005
0.004
0.003
0.002
0.001
0.000
-0.001
-0.002
-0.003
-0.004
-0.005
-0.006
-0.007
0.0 0.1 0.2 0.3 0.4 0.5 0.6 0.7 0.8 0.9 1.0
<------- Inner wall Normalized wall thickness Outer wall ------->
Figure 6.9b: Circumferential strain distribution comparison in E quadrant of culm PN5B3C

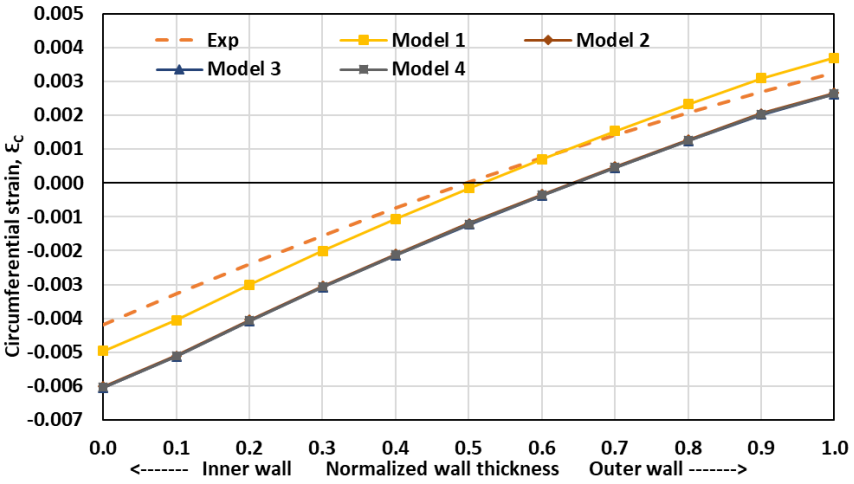
Exp
Model 1
Model 2
Model 3
Model 4
Circumferential strain, ε_c
0.005
0.004
0.003
0.002
0.001
0.000
-0.001
-0.002
-0.003
-0.004
-0.005
-0.006
-0.007
0.0 0.1 0.2 0.3 0.4 0.5 0.6 0.7 0.8 0.9 1.0
<------- Inner wall Normalized wall thickness Outer wall ------->
Figure 6.9c: Circumferential strain distribution comparison in E quadrant of culm PN5B4C

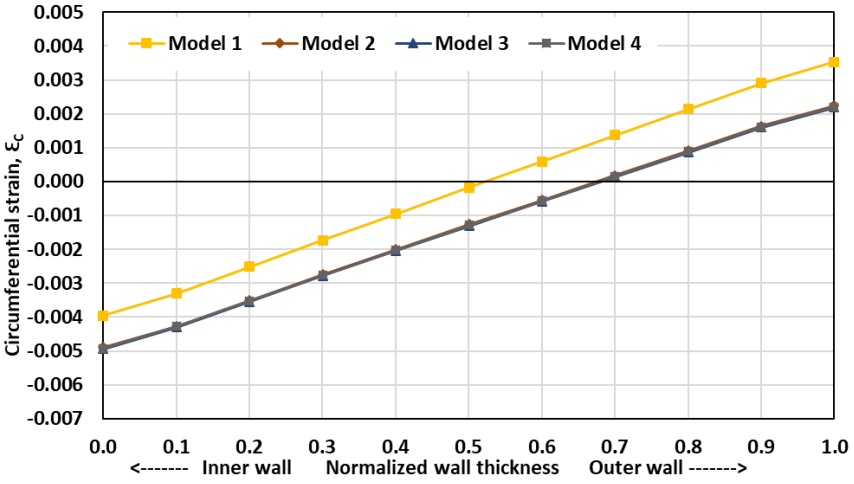
Model 1
Model 2
Model 3
Model 4
Circumferential strain, ε_c
0.005
0.004
0.003
0.002
0.001
0.000
-0.001
-0.002
-0.003
-0.004
-0.005
-0.006
-0.007
0.0 0.1 0.2 0.3 0.4 0.5 0.6 0.7 0.8 0.9 1.0
<------- Inner wall Normalized wall thickness Outer wall ------->
Figure 6.9d: Circumferential strain distribution comparison in E quadrant of culm PN

There are a number of simplifications inherent in the FE models which are likely to contribute to the efficacy of the specimen-specific models used in this validation. The FE specimens are simplified as round hollow cylinders having constant wall thickness. The experimental specimens exhibit some degree of ovality (defined as in ISO 19624) and variation in wall thickness as given in Table 6.1. Both will result in variation from the ideal culm. Similarly, the distribution of fiber volume ratio is assumed to be uniform around the entire culm circumference. As described in Section 3.4.3, the *P. nigra* specimens exhibited the greatest variation of measured fiber volume ratio.

Finally, as described in Section 3.5.2 and will be discussed further in Chapter 7, the application of the rule of mixtures using measured fiber volume distribution, especially for transverse properties, may not be appropriate.

Nonetheless, the output from the simulations are relatively close to the values reported from the experiments. Model 1 results – which consider the bamboo as a homogeneous transversely isotropic material – correlate well with Model 0 calculations based on Castigliano's theorem [Young *et al.* 2002] which serves as the basis for Equation 2-5 in which $E_{m,90}$ is equivalent to E_T. Similarly, Models 2, 3 and 4, which considered the effect of the fiber gradation through the culm wall yielded similar results. However, the graded models appear to result in a shift toward compression strains and, as a result, a more pronounced shift in the neutral axis toward the outer culm wall than was observed in the experiments.

With this in mind, the UMAT subroutine in Model 4 which requires the input of the coefficient of the representative cubic functions of V_f, E_L and E_T was selected to represent the simulation of the graded material and was used for all additional analysis conducted. It is clear that

there is little difference in Models 2 through 4; the UMAT subroutine of Model 4 is most easily implemented.

It is also important to note the effect of specimen dimension and distribution of the fiber volume ratio through the culm wall. The circumferential stress and strain variation through the culm wall obtained from Model 4 is shown in Figures 6.10 and Figure 6.11, respectively. Since specimens from the same culm were used in PN5B2C, PN5B3C and PN5B4C, it is expected that the fiber volume ratio, although slightly different in each specimen, would be close enough to have a similar behavior under testing. This was confirmed in the experimental tests conducted (Table 2.6) and is illustrated in Figure 6.10. PN however is a prototype obtained from the average geometry and fiber distributions of multiple *P. nigra* specimens (Table 2.1). The behavior differs only marginally from the specimen-specific data: the 'slope' of the circumferential strain profile is shallower. A notable difference between the three modeled test specimens and the prototypical PN model is that PN has a notable thinner wall. The wall thickness ratio, *D/t* of the three PN5B specimens is approximately 10.9 whereas that for PN is 13.9. Both are 'thin-walled' (typically defined for tubes as $D/t > 10$ and proposed for bamboo as $D/t > 8$ [Harries *et al.* 2017]), justifying the use of Eqs 2-6 to 2-12. However, a greater *D/t* ratio will lead to the stress distribution at the E or W quadrant being proportionally more dominated by the culm wall flexural response than the compression stress also passing through the section at this location – these are the first and second terms, respectively, of Eq. 2-9.

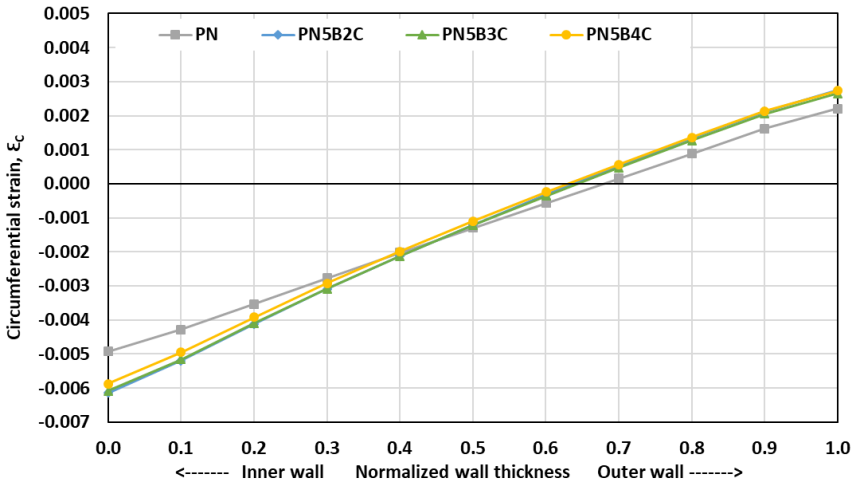

Figure 6.11 shows a similarity in the stress profiles of all PN5 specimens with the PN specimen varying slightly in the compressive region near the inner wall face. Using the PN specimen without experimental verification has shown that the procedure reported in this thesis can be used to predict full-culm bamboo test specimen behavior with reasonable reliability.

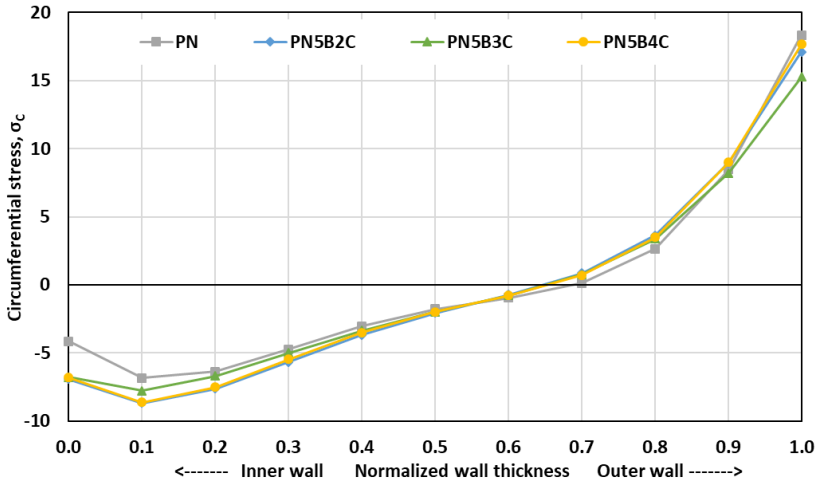

6.4.2 Sensitivity Study - Analysis of Parameters

The reasonable predictive capacity of the closed form solutions of Model 0 permit a rapid assessment of the sensitivity of results to various input parameters, Using the PN model culm the following geometric and material properties were each varied incrementally up to ±20% to investigate model sensitivity: diameter D, culm wall thickness t, specimen length H, shear modulus G, transverse modulus E_T, and longitudinal modulus E_L. This sensitivity analysis was carried out using the equations of Model 0 except for E_L where Model 1 was used. The result is shown in Figure 6.12 as normalized values representing the stiffness at a displacement of 1.5 mm plotted against the variation of each parameter.

The result shows that the specimen stiffness is most sensitive to a change in culm wall thickness, t, varying essentially in proportion to t^3 (that is, in proportion the moment of inertia of the wall section t x H). Specimen stiffness increases 80% with a 20% increase in wall thickness and decreases 50% as the thickness decreases by 20%. Similarly, specimen stiffness varies in an approximately inverse relationship proportional to $1/D^3$. This results in a 44% decrease in stiffness as the diameter increases by 20% and a 105% increase in stiffness as the diameter is reduced by 20%. Both E_T and H exhibited linearly proportional impacts on culm stiffness. The effect of E_L was minimal with a maximum of 2% change in stiffness for a 20% increase or decrease in E_L. G had no effect on the stiffness of the specimen over the 20% variation considered. The behavior again illustrates the importance of wall slenderness, D/t, to culm behavior. All other parameters being equal, a constant value of D/t results in the same stiffness. It is noted that fundamental behavior is expected to change as the culm dimensions transition from thin- to thick-walled at

around D/t = 8 to 10. In the present study, the *P. nigra* modelled has $D/t \approx 14$ and only *B. stenostachya* would be classified as thick-walled, having $D/t \approx 5.4$ (Table 2.1).

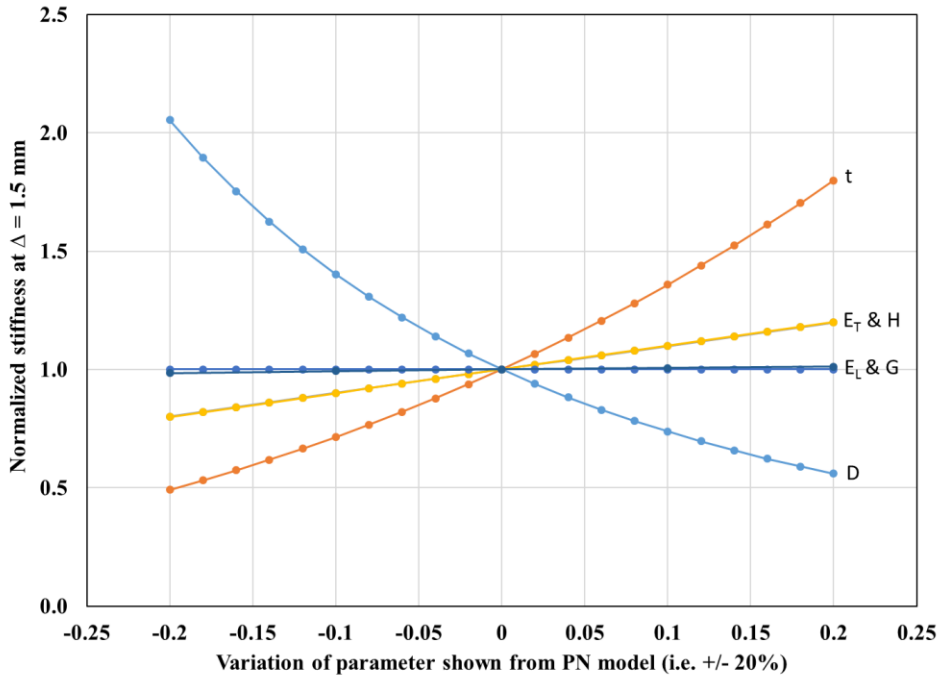

Figure 6.12: Sensitivity of bamboo material properties on stiffness using Specimen PN

6.5 Inclusion of Random Field Variables

In order to illustrate the impact of considering material variability as described in Chapter 5, Models 1 and 4 were re-run using sample PN5B2C including the effect of random field generated values of E_T. To achieve this, the data in Figure 5.3d were reconstructed using the values of E_m = 1 GPa and E_f = 35 GPa in the rule of mixtures to calculate the $\mathbf{E_{Tmean}}$ (Eq. 5-1). Five different random field outputs are then extracted as shown in Figure 6.13 denoted as RFE1 to RFE5.

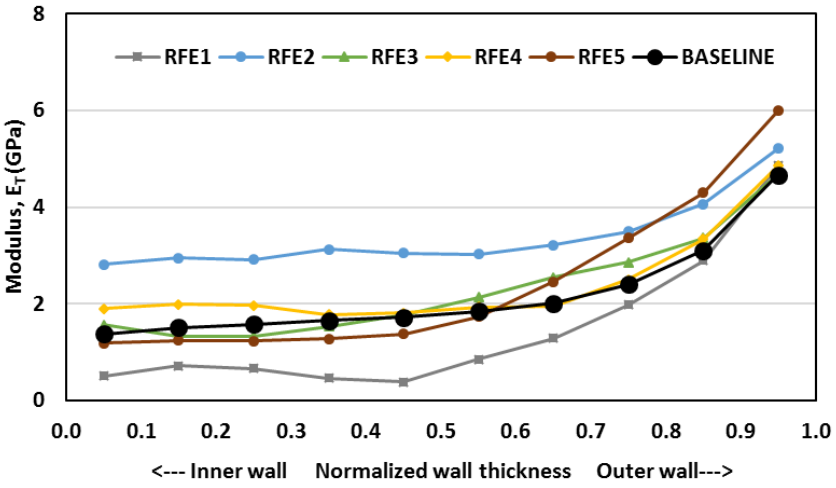

The corresponding cubic functions for E_T are given in Table 6.5. The longitudinal modulus, E_L is calculated directly using the rule of mixtures (Eq. 3-1). While E_L is also a material property in which the random field technique could be used to develop variations through the culm wall thickness, this has not been done in this study which models only short ($H = 0.2D$) test specimens for which the longitudinal properties have little impact (see Section 6.4.2). Additionally, since only very short material test specimens are modeled, variation along their length should be negligible.

Table 6.5: Model in input parameters E_T (PN5B2C)

Parameter	Model 1	Model 4
V_f	0.28	$V_f = 1.29x^3 - 1.28x^2 + 0.57x + 0.10$ (GPa)
E_L	10748 MPa	$E_L = 43.9x^3 - 43.5x^2 + 19.4x + 4.20$ (GPa)
E_T modelled in 6.4.1	2473 MPa	$E_T = 21.7x^3 - 23.7x^2 + 7.4x + 1.1$ (GPa)
RFE1	1634 MPa	$E_T = 14.58x^3 - 11.76x^2 + 2.58x + 0.45$ (GPa)
RFE2	3469 MPa	$E_T = 12.14x^3 - 13.47x^2 + 4.57x + 2.56$ (GPa)
RFE3	2534 MPa	$E_T = 15.41x^3 - 15.31x^2 + 3.87x + 1.72$ (GPa)
RFE4	2579 MPa	$E_T = 8.56x^3 - 3.00x^2 + 0.13x + 1.21$ (GPa)
RFE5	2417 MPa	$E_T = 2.56x^3 + 1.85x^2 - 0.87x + 1.50$ (GPa)

The same FE analysis described previously using only Models 1 and 4 was performed using the values of V_f , E_L and E_T given in Table 6.5. The results for Specimen PN5B2 are shown in Table 6.6; both the experimental and previously reported baseline (Table 6.4) results are included for comparison. Circumferential strain distributions resulting from Model 4 are shown in Figure 6.14. Similar to the results presented in Section 6.4.1 and Table 6.4, changes in stresses, strains and circumferential moduli was noticed for each randomly generated value of E_T. Each polynomial (Figure 6.13 and Table 6.5) is reviewed with its corresponding result to better explain the predicted behavior. In the descriptions, all data is compared to that of the baseline model described in Section 6.4.1.

Table 6.6: Summary of stresses and strain with Model 1 and 4 on five random field generated E_T for PN5B2

	Exp.	**Model**	**baseline (Table 6.4)**	**RFE1**	**RFE2**	**RFE3**	**RFE4**	**RFE5**
Applied load to cause Δ = 1.5 mm, N	293.7	1	-310.8	-209.3	-430.2	-318.2	-323.6	-304.0
		4	-306.0	-151.2	-439.1	-330.6	-270.7	-280.9
Compressive strain at E-W quadrant, ε_{yy} με	-4498	1	-5108	-5156	-5065	-5108	-5106	-5114
		4	-6144	-7081	-5510	-5868	-6569	-6161
Tensile strain at E-W quadrant, ε_{yy} με	2832	1	3757	3752	3761	3758	3759	3758
		4	2741	1868	3315	3000	2342	2738
Neutral axis location, x	0.54*t*	1	0.52*t*	0.52*t*	0.52*t*	0.52*t*	0.52*t*	0.52*t*
		4	0.65*t*	0.75*t*	0.57*t*	0.60*t*	0.69*t*	0.65*t*
Compressive stress in E-W, $\sigma_{,yy}$ MPa (Eq. 2-10b)	-12.9	1	-12.4	-8.3	-17.0	-12.7	-13.0	-12.2
		4	-6.9	-3.3	-14.2	-10.2	-7.9	-9.2
Tensile stress at E-W quadrant, $\sigma_{,yy}$ MPa (Eq. 2-10a)	9.4	1	9.11	6.00	12.79	9.34	9.50	8.90
		4	17.10	10.35	18.60	16.45	15.5	13.34
Circumferential modulus, $E_{m,90}$ MPa (Eq. 2-5)	2623	1	2777	1870	3843	2843	2891	2716
		4	2734	1351	3923	2954	2418	2510

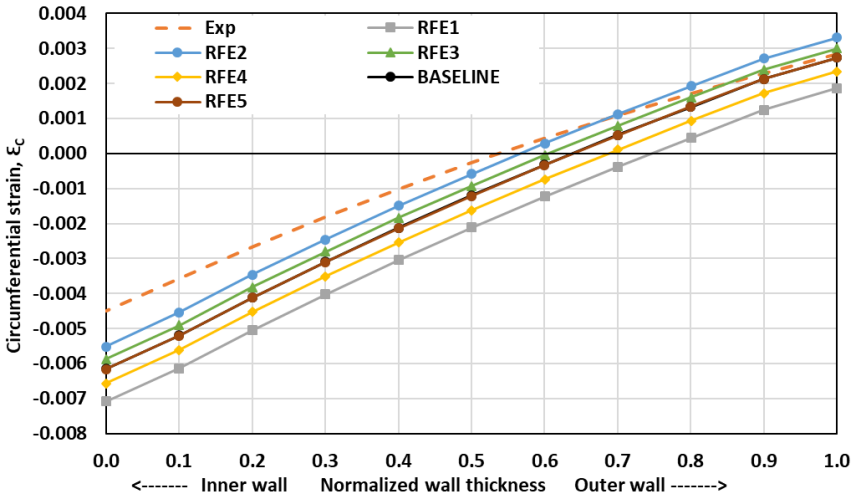

Figure 6.14: Circumferential strain distribution with Model 4 on five random field generated E_T for PN5B2

Because the model deformation is constant (Δ = 1.5 mm) and Model 1 is transversely isotropic, Model 1 strains are not expected to vary from the baseline case while stresses are proportional to E_T; this is shown in Table 6.7 which summarizes the differences from the baseline of results for the five random cases modeled using Model 1. Model 4, however, captures the effects of varying distribution of E_T.

RFE1 exhibits a lower value of E_T at the inner culm wall (x = 0) extending across most of the culm wall and then projects to a marginally higher value towards the outer culm wall (x = 1). As a result of the lower average modulus (the average used in Model 1 is 66% of that of the baseline model as shown in Table 6.7), a lower force is required to achieve the 'prescribed' displacement Δ = 1.5 mm. Because of the softer response across most of the culm wall, a shift in strains toward compression is observed (Figure 6.14) resulting in a significant shift of the neutral axis to 0.75t.

Consistent observations were made for the RFE2 case that has relatively higher modulus values across the culm wall (140% of that of the baseline model). In this case, a stiffer compressive

response is predicted resulting a shift in the strains toward tension and the neutral axis shifting back toward the center of the wall (0.57*t*).

RFE5 is also interesting in that E_T is lower at the inner culm compressive region and higher in the outer culm wall tensile region. This distribution results in a steeper gradient across the culm wall although a similar average modulus as the baseline case (98%). Despite the deviation in gradient, because the average strain was similar, the predicted strains are close to those of the baseline case (Figure 6.14). The local stresses are then proportional to the modulus.

RFE3 and RFE4 had very little variation from the baseline case in terms of input and model results. Table 6.7 summarizes the differences from the baseline of results for the five random cases modeled using Model 4. As described above, strains are proportional, and stresses are inversely proportional to modulus. As seen in Table 6.7, the effect of variation through the culm wall can significantly affect the ratios observed although maintains the same expected proportionalities.

Table 6.7: Ratio of random field results from Models 1 and 4 to those of the baseline Model

	Model 1					**Model 4**				
	RFE1	**RFE2**	**RFE3**	**RFE4**	**RFE5**	**RFE1**	**RFE2**	**RFE3**	**RFE4**	**RFE5**
average E_T (Table 6.5)	0.66	1.40	1.02	1.04	0.98	0.66	1.40	1.02	1.04	0.98
Applied load to cause Δ = 1.5 mm	0.67	1.38	1.02	1.04	0.98	0.49	1.43	1.08	0.88	0.92
Compressive strain at E-W quadrant, ε_{yy}	1.01	0.99	1.00	1.00	1.00	1.15	0.90	0.96	1.07	1.00
Tensile strain at E-W quadrant, ε_{yy}	1.00	1.00	1.00	1.00	1.00	0.68	1.21	1.09	0.85	1.00
Neutral axis location, x	no change	no change	no change	no change	no change	+0.10*t*	-0.07*t*	-0.05*t*	+0.04*t*	no change
Compressive stress in E-W, $\sigma_{,yy}$	0.67	1.37	1.02	1.05	0.98	0.48	2.05	1.47	1.14	1.33
Tensile stress at E-W quadrant, $\sigma_{,yy}$	0.66	1.40	1.03	1.04	0.98	0.61	1.09	0.96	0.91	0.78
Circumferential modulus, $E_{m,90}$	0.67	1.38	1.02	1.04	0.98	0.49	1.43	1.08	0.88	0.92

6.6 Summary

The inadequacy of knowledge of the transverse behavior of bamboo compared to its longitudinal properties was a motivation of this study. Previous use of FE analyses in studying longitudinal, let alone transverse behavior is limited. Few studies have modeled bamboo as an isotropic material while a few others modelled it as a transverse isotropic material both without and with consideration for the functionally graded nature of the material. The latter is the focus of this chapter which adopts a model of bamboo as a transversely isotropic material with functionally graded material properties in the radial direction. A summary of the complete analysis process for bamboo specimens described in this thesis is shown in the flowchart in Figure 6.15.

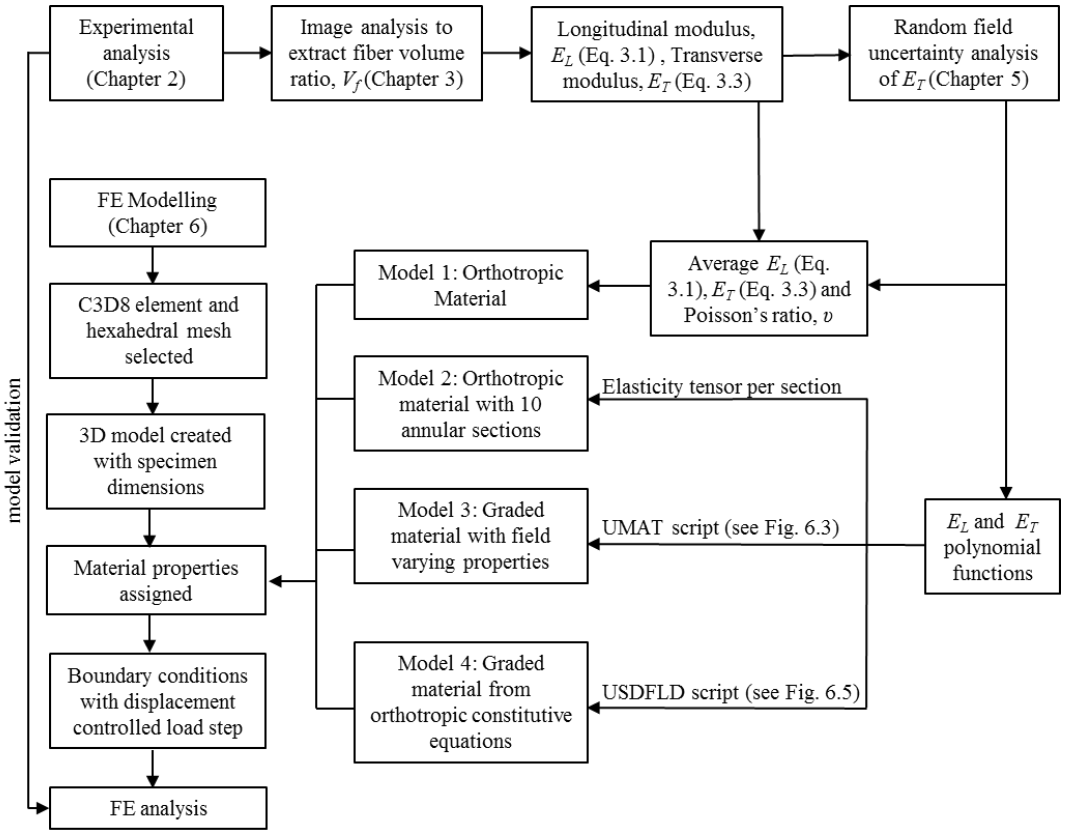

Figure 6.15: Summary flowchart of processes involved in FEM of bamboo

Five approaches to model the behavior of circumferential compression tests were used in this analysis and all modeling was implemented in ABAQUS. Model 0 consists of a theoretical evaluation based on Castigliano's theorem presented in a closed form. Model 1 assigns the orthotropic mechanical properties of bamboo in a FE analysis without capturing the graded nature of the culm wall. Model 2 captures the transverse gradation of properties by individually assigning average orthotropic mechanical properties to a culm wall divided into ten concentric annular ring sections for FE analysis. Model 3 assigns the graded material properties in a FE analysis using the continuum approach with the user-defined USDFLD subroutine in ABAQUS. Model 4 uses another user-defined UMAT subroutine in ABAQUS to define a transversely isotropic graded material with properties assigned at integration points of each element. Output from each model is compared, calibrated and validated with DIC and experimental results presented earlier in the study.

An initial set of analyses was run using the representative fiber and matrix moduli (E_f = 35 GPa and E_m = 1.8 GPa respectively) recommended by Janssen [2000] in combination with the rule of mixtures using the Halpin-Tsai correction for the transverse modulus calculations. This produced a model stiffer than the experimentally observed values by a factor of about 1.7. This model was therefore refined to produce a modelled behavior which better matched the experimental data using updated representative properties (E_f = 35 GPa and E_m = 1 GPa).

Following calibration, all models represented observed bamboo behavior reasonably well although there was a universally observed shift toward compression strains at the inner regions of the culm wall thickness while tension strains were well predicted. This resulted in the models exhibiting a "steeper" strain gradient and a greater shift in the predicted neutral axis location

toward the outer culm wall compared to that observed in the experiments as seen in Figure 6.9 and elsewhere. Despite the differences in strains and stresses, the average circumferential modulus, $E_{m,90}$ determined from the experiment (Eq. 2-5) is similar to that determined from the models.

Models 0 and 1, based on average material properties without considering a gradient, captured experimental data better than the more complex FE models. This observation needs to be understood in context. All models were calibrated to average values of E_T. The FE models then distributed the modulus using the rule of mixtures maintaining the calibrated average value. The fact that the FE models predicted gross section behavior (average behavior) relatively well but failed to capture observed local effects calls into question the assumptions involved in distributing the graded material properties using the rule of mixtures based on measured fiber volume ratio.

The sensitivity of circumferential compression test results to the individual input parameters from the geometry and material properties were considered using the PN specimen and Model 0. Each parameter - D, t H, G, E_T and E_L - was varied by ±20% and the effect on the stiffness of the specimen shown. It was found that the culm wall thickness t impacts stiffness proportionally to t^3 (the moment of inertia of the culm wall in the circumferential compression test) and the culm diameter impacts stiffness proportionally to $1/D^3$. Thus, all other parameters being equal, a constant value of D/t results in the same stiffness. E_T and H affected stiffness in a linearly proportional manner while E_L and G had essentially no effect on the test specimen stiffness.

The modelling procedure was repeated to demonstrate the random field methodology (Chapter 5) and to investigate the effect of uncertainty on bamboo transverse behavior. This was demonstrated using Models 1 and 4 to differentiate the behavior between uniform and functionally graded material responses. The intent of the inclusion of random fields is to capture the potential variation of material behavior for bamboo specimens having a similar range of fiber volume ratio

such as is likely in a single batch of a single species. As expected, it is observed that strains are proportional, and stresses are inversely proportional to modulus. The effect of variation through the culm wall can significantly affect the prediction of experimental results although the expected proportionalities are maintained.

The FE models developed will permit further investigation of observations made in this dissertation. Each of Models 2, 3 and 4 performed equally well. Model 2 is a 'brute force' approach ill-suited to a robust modeling campaign although useful in validating the numerically more complex Models 3 and 4. Model 4 was considered easier to implement than Model 3 and is recommended for adoption for further analysis studies.

The primary conclusion of this study is that the mechanical behavior of bamboo is greatly influenced by its transverse properties, which are not easily measured by experiment. The random field technique applying the rule of mixtures was proposed to address this deficiency. While the models developed are robust, their application has drawn into question the fundamental hypothesis that the functionally graded behavior of bamboo can be captured using the rule of mixtures.

7.0 Discussion, Conclusions and Recommendations for Future Research

The main objective of this dissertation was to develop a framework and the tools required to evaluate the material and mechanical properties of bamboo in its full-culm form. This framework brought together work conducted in the area of bamboo characterization to develop a correlation with the mechanical properties. This required an understanding of the behavior of the material at both macro and micro scales. To accomplish this, several studies were completed ranging from experimental work, to digital imaging and numerical simulations. These are summarized in the following sections. This study focused primarily on thin-walled (i.e., $D/t > 8$) bamboo species. Although a single thick-walled species is included in the study, the conclusions presented are intended for thin-walled species.

7.1 Full-culm Bamboo Material Properties

An experimental campaign to assess bamboo mechanical properties is described in Chapters 2 and 3. Four established test methods were conducted to quantify the mechanical properties of full culm bamboo in different directions. Both the longitudinal direction parallel to fibers (full-culm compression, f_c and full-culm shear, f_v), and the transverse direction (flat ring flexure, $f_{r\alpha}$ and the circumferential compression test, $f_{m,90}$) were considered using six species sourced from different locations: *P. edulis*, *P. bambusoides*, *P. meyeri*, *P. nigra*, *B. stenostachya*, and *D. barbatus*.

The material variation inherent in bamboo was evident. The compression strength parallel to the culm, f_c ranged from 36.2 MPa to 59.3 MPa across all species. The average single species coefficient of variation over all compression tests was 16%. Similarly, the shear strength f_v ranged from 9.9 MPa for the thick-walled *B. stenostachya* to 18.1 MPa for *P. edulis*-C and an average single species coefficient of variation of 13% was observed. The transverse modulus of rupture, $f_{r\alpha}$ from the flat ring flexure test also varied amongst species with values ranging from 9.4 MPa for the thick-walled *B. stenostachya* to 20 MPa for the thin walled *P. meyeri* with a 20% average single species coefficient of variation. Lower material strength was exhibited by the thick walled species in comparison to the thin walled species; this is partially attributed to the lower density of the thick-walled species.

The variation in mechanical properties from species to species was less significant within the same genus (*Phyllostachys*). However, significant differences were observed between batches of *P. edulis* sourced from Brazil and China. This reinforces the hypothesis that mechanical property variation in bamboo occurs between species and even amongst the same species with different growth conditions.

P. nigra specimens were selected for additional circumferential compression and flat ring flexure testing using digital image correlation (DIC). Both strain and displacement fields were captured in order to better understand the behavior of the through culm wall flexural response of the specimens. All specimens in the flat ring flexure tests were found to exhibit linear behavior at all load levels (i.e. plane sections remain plane) and there was also an apparent shift in the neutral axis towards the tension face. Circumferential compression DIC data was used to validate the finite element (FE) models developed in Chapter 6. The result of the tests conducted gave a better indication of the mechanical properties of bamboo and their variation. The aim of representing

these with relatively simple parameters such as the fiber volume variation in the culm section was considered in subsequent Chapters.

7.2 Digital Imaging to Assess Bamboo Fiber Volume Ratio

Image analysis together with a purpose-written MATLAB script was used to differentiate the bamboo fibers in a cross section and conduct fiber volume calculations and analyses of specimens used in the experimental campaign; this is described in Chapter 3. The analysis indicated a fiber distribution having a third-order polynomial distribution and that culm-wall fiber distribution differs significantly among bamboo genera but less so among species in the same genera (*Phyllostachys*). The need for a third order representation was primarily to account for nonlinearity in fiber volume variation at the extreme edges of the culm wall.

In Chapter 4, images of *P. edulis* bamboo obtained from two commercially available glue-laminated bamboo beam products were used to quantify the distribution of fiber volume ratio, V_f, in the strips. In total, 58 beam cross sections containing more than 3500 19 x 6 mm strips were analyzed. Simple digital manipulation techniques were found to work well in establishing fiber volume data from the 1200 dpi source images.

Although all bamboo was Chinese *P. edulis* and batches were likely from similar or identical source material (feedstock), variation was observed: the measured fiber volume ratio for each strip was 0.23 for Batch M and 0.19 for Batch P; the coefficient of variation observed was 12% and 19%, respectively. The imaged strips contained only the middle portion of the culm wall, without the extreme outer and inner faces. As such, both batches could be modelled as having a

linear distribution of V_f through their thickness although the gradient was different in each case: 0.025/mm and 0.032/mm for Batch M and P, respectively. These observations indicate significantly different bamboo source material for the two batches. Indeed, many factors may affect the properties of strips used even by the same manufacturer. Bamboo suppliers, harvest conditions, and location of strips along the culm length; all may result in variation of strip properties.

7.3 Numerical Modeling of Full-culm Bamboo

In Chapter 5, the random field analysis method was introduced as a means of quantifying the measured uncertainty of bamboo with respect to the mechanical characterization of its full-culm state. The approach to capture the characteristics of bamboo components without measuring the individual phases of the components involves three major stages: 1) identifying the bamboo geometry and parameter of interest (as was done in Chapters 3 and 4); 2) generating a probable spatial distribution of the parameter (Chapter 5); and, 3) implementing this in a finite element (FE) model (Chapter 6).

An example of the implementation of the covariance matrix decomposition technique was illustrated with radially-oriented elastic modulus E_T as the parameter of interest hypothesized as a function of the fiber volume ratio, V_f. An initial assumption made is that the fiber volume follows a Gaussian distribution which was confirmed in Chapter 4 and that the spatial correlation can be adequately characterized by a correlation function. A cubic correlation function was found to

adequately characterize the spatial correlation function of E_T and a correlation distance equal to the bamboo wall thickness was selected.

In Chapter 6, the study adopts an approach to modelling bamboo as a transversely isotropic material with the inclusion of a functionally graded material property in the radial direction. Five approaches to model the behavior of circumferential compression tests were used in this analysis and all modeling was implemented in ABAQUS. Model 0 consists of a theoretical evaluation based on Castigliano's theorem presented in a closed-form. Model 1 assigns the transversely isotropic mechanical properties of bamboo in a FE analysis without capturing the graded nature of the culm wall. Model 2 captures the transverse gradation of properties by individually assigning average transversely isotropic mechanical properties to a culm wall divided into ten concentric annular ring sections. Models 3 and 4 assign the graded material properties in FE analyses using the continuum approach implemented with the user-defined USDFLD or UMAT subroutines, respectively. Output from each model is compared, calibrated and validated with DIC and experimental results presented earlier in the study.

An initial set of analyses was run using the representative fiber and matrix moduli (E_f = 35 GPa and E_m = 1.8 GPa respectively) recommended by Janssen [2000] in combination with the rule of mixtures. This produced a model stiffer than that observed experimentally by a factor of about 1.7. The representative properties reported by Janssen were derived based on longitudinal material properties which are modeled well using the rule of mixtures and are dominated by the value of E_f. On the other hand, the transverse behavior considered in this study is very sensitive to the value of E_m. For these reasons, an evaluation of behavior was undertaken in which E_f = 35 GPa and E_m is calibrated such that the stiffness of the models better matches the experimental data. A

value of E_m = 1.0 GPa was found to be appropriate for the *P. nigra* material considered and was adopted.

Following calibration, all models represented observed bamboo behavior reasonably well although there was a universally observed shift toward compression strains at the inner regions of the culm wall thickness while tension strains were well predicted. This resulted in the models exhibiting a "steeper" strain gradient and a greater shift in the predicted neutral axis location toward the outer culm wall compared to that observed in the experiments.

Models 0 and 1, based on average material properties without considering a gradient, captured experimental data better than the more complex FE models. This observation needs to be understood in context. All models were calibrated to average values of E_T. The FE models then distributed the modulus using the rule of mixtures maintaining the calibrated average value. The fact that the FE models predicted gross section behavior relatively well but failed to capture observed local effects calls into question the assumptions involved in distributing the graded material properties using the rule of mixtures based on the measured fiber volume ratio.

The sensitivity of circumferential compression test results to the individual input parameters from the geometry and material properties were considered. Each parameter – D, t H, G, E_T and E_L – was varied ±20% and the effect on the stiffness of the specimen was investigated. It was found that the culm wall thickness t impacts stiffness proportionally to t^3 (the moment of inertia of the culm wall in the circumferential compression test) and the culm diameter impacts stiffness proportionally to $1/D^3$. Thus, all other parameters being equal, a constant value of D/t results in the same stiffness. E_T and H affected stiffness in a linearly proportional manner while E_L and G had essentially no effect on the test specimen stiffness.

The modelling procedure was repeated to demonstrate the random field methodology (Chapter 5) and to investigate the effect of uncertainty on bamboo transverse behavior. This was demonstrated using Models 1 and 4 to differentiate the behavior between uniform and functionally graded material responses. As expected, it is observed that strains are proportional, and stresses are inversely proportional to modulus. The effect of variation through the culm wall can significantly affect the prediction of experimental results although expected proportionalities are maintained.

Each of Models 2, 3 and 4 performed equally well. Model 2 is a 'brute force' approach ill-suited to a robust modeling campaign although useful in validating the numerically more complex Models 3 and 4. Model 4 was considered easier to implement than Model 3 and is recommended for adoption for further analytical studies.

The primary conclusion of this study (see Section 7.4) is that the mechanical behavior of bamboo is greatly influenced by its transverse properties, which are not easily measured by experiment. The random field technique applying the rule of mixtures was proposed to address this deficiency. While the models developed are robust, their application has drawn into question the fundamental hypothesis that the functionally graded behavior of bamboo can be captured using the rule of mixtures.

7.4 Rule of Mixtures

Bamboo is often referred to as a fiber reinforced material in which the longitudinal properties may be obtained from a rule of mixtures approach (Eq. 3-1). The dominant failure mode

of bamboo, however, is longitudinal splitting with a mode II shear failure. In this study, the Halpin-Tsai correction to the rule of mixtures (Eq. 3-3) was applied for the estimation of the transverse properties through the culm wall thickness. Various results from this study indicate that considering the transverse behavior of bamboo in this manner is not appropriate.

In order to implement the rule of mixtures, the modulus of elasticity of both the matrix, E_m and the fibers E_f are required. A summary of both values reported in literature is given in Table 3.1. Due to the very large ratio of fiber to matrix moduli (E_f/E_m is typically greater than 20), longitudinal behavior is dominated by fiber properties. Assuming the fiber volume is correctly assessed (see discussion of Dixon and Gibson [2014] and in Section 3.4.1), it is believed that longitudinal culm behavior is reasonably modelled by the rule of mixtures as given by Eq. 3-1. This has been confirmed in a number of studies as reported in Chapter 3.

In the transverse direction, the rule of mixtures (Eq 3-2 or 3-3) is dominated by matrix properties. A critical assumption is that the approach assumes the individual components to be isotropic and homogeneous. Indeed, the Halpin-Tsai correction to the transverse rule of mixtures (Eq. 3-3) is an attempt to address the fact that fiber elements, in particular, are not isotropic. Halpin-Tsai, however is an empirical correction found to work well with conventional fiber reinforced polymer materials [Halpin and Kadros 1976]. The bamboo parenchyma does not resemble, nor does it behave as a polymer. As described in the following sections, the outcomes of the present study support the need for another approach to modeling the transverse behavior of bamboo.

7.4.1 Experimental Results

Modifications to the flat-ring flexure test were conducted to isolate portions of the culm wall cross-section to measure the transverse tensile capacity of the bamboo and investigate its variation through the culm wall thickness (Section 3.5). Each specimen had reduced ("clipped") sections of 0.2*t* or 0.25*t* wall thickness in the constant moment region. The modulus of rupture determined from the clipped tests, show a significant variation through the culm wall thickness. The variation had a generally parabolic shape with higher modulus at both the inner and outer walls compared to the middle of the culm wall. Comparison of this behavior to the fiber volume ratio and the predicted distribution of modulus of rupture using the Halpin-Tsai rule of mixtures (Figure 3.7) suggests that bamboo does not behave as a classic fiber-reinforced composite material in the transverse direction. This counterintuitive observation prompted the need for further examination of the results using microscopic imaging techniques.

7.4.2 Imaging Results

The failure planes of some tested full-culm control specimens were selected for further analysis using SEM (Section 3.7). The surface of the failure plane did not require any preparation, allowing the observation to be imaged in as close to their as-is condition as possible. Significantly different visual characteristics of the failure plane – varying from the inner culm wall to the outer culm wall – were observed (Figures 3.11 and 3.13). The longitudinal aspect ratio of the parenchyma cells is observed to be different in the outer and inner regions of the culm wall. Furthermore, Zeng *et al.* [2019] identified significantly different morphology of parenchyma cell

walls through the culm wall thickness of *P. edulis* specimens (Figure 3.12). It is unclear how these differences impact the behavior exhibited in this study but it is evident that parenchyma is not homogeneous through the cross section.

Additionally, the SEM images revealed the presence of intra-fibril cracks within the fiber bundles (Figure 3.10). This observation draws into question the assumption of isotropic fiber properties. These cracks are hypothesized to be a result of shrinkage due to drying or treatment of the bamboo and to potentially be a source of eventual cracks through the parenchyma when the bamboo is under load. Although prior studies have shown the presence of such intra-fibril cracks, none described their source. This phenomenon requires further investigation.

7.4.3 Numerical Results

As described in Section 7.3, while robust, the finite element models that included a gradient of material properties did not capture the through culm wall effects of loading observed in the experiments and recorded using DIC. Models 2 through 4, having material gradients, captured local strains near the fiber-rich outer face of the culm wall of the specimens relatively well but exhibited a significant shift toward compression nearer the inner culm wall. This behavior suggests that the culm wall may exhibit two regions of behavior: an outer region reasonably well modeled using the rule of mixtures, and an inner region where the rule of mixtures collapses. Once again, this is seen experimentally in Figure 3.7. Tan *et al.* [2011] report a toughening effect –fiber bridging – in areas of lower fiber volume; this may also affect the behavior observed. Mathematically, the FE models could be made more predictive by increasing the value of E_m nearer

the inner culm wall, although there is no empirical (or otherwise) basis for assuming that this is true.

7.4.4 Variation of Parenchyma and Fiber Material Properties

Although not specifically addressed in this work, the following hypotheses require further study in order to better understand the relationship between the fiber-reinforced nature of bamboo and its material properties.

1. The value of E_m varies through the culm-wall thickness; that is, $E_m(x)$.
2. The matrix and fiber moduli, E_m and E_f are anisotropic, requiring transverse values for the determination of transverse culm properties.

The component fiber and matrix moduli are estimated from longitudinal tests. The value of E_f (Table 3.1) is commonly measured from nanoindentation of a single fiber or from fiber bundle tension tests from which E_m is then estimated using the rule of mixtures (thereby presupposing the validity of the rule of mixtures). A limitation of the nanoindentation technique described in Section 3.3 is its dependence on the assumptions of isotropy and homogeneity between the fibers [Yu *et al.* 2007]. The inter-fibril cracking observed (Figures 3.10) draws this assumption into question to some degree.

It is more clear that the parenchyma properties are likely to vary through the culm wall thickness. Although reported in the literature, nanoindentation results of parenchymal cells will be very sensitive to location (cell wall or cell wall interstices) and cell condition (Figures 3.11-3.15). Indeed, reported values of E_m vary from 200 to 7000 MPa (Table 3.1). Additionally, there is some evidence that the density of the parenchyma varies based on fiber content (Figures 3.14 and 3.15).

In natural materials, relative strength and stiffness are typically proportional to density. This all supports at least the second hypothesis.

7.4.5 Bond Between Parenchyma and Fiber Bundles

The rule of mixtures assumes that there is continuity or "perfect bond" between the matrix and the fibers and that the two components are isotropic. The SEM images presented in Chapter 3 illustrate fractures or separations through all surfaces/interfaces present: a) inter-fibril cracking (Figure 3.10); b) cracking through fiber bundle-parenchyma interface; c) cracking around parenchyma cell boundaries; and d) cracking through parenchyma cells. The latter three cases are seen in Figures 3.11 to 3.13. This observation further supports those of the previous section. The rule of mixtures does not capture this complex behavior.

7.4.6 Conclusion

Using an empirically corrected form of the rule of mixtures to obtain the transverse modulus of bamboo in this study has not attained the anticipated results. Different approaches were explored to better understand the reason for the discrepancies of bamboo not behaving like a unidirectional fiber reinforced material and conforming to the rule of mixtures as is uniformly described in the literature. A combination of experimental, SEM imaging and numerical approaches has identified possible causes of the deviation of the observed behavior. A realization from this study is the importance of an alternative approach to the determination of the component properties used in the definition of the fiber-reinforced composite nature of bamboo, E_f and E_m, their interaction and spatial relationship. The observations made from failure plane images and the

'clipped' flat ring flexure tests suggest that the components should be considered as non-homogeneous and transversely isotropic. Although further research is necessary, a modeling framework has been identified and demonstrated that is expected to further improve the understanding of bamboo material characterization.

7.5 Recommendation for Future Work

It is necessary to extend the test method modeling effort to other tests. Data in this study should permit validation using flat ring flexure test data. Additional DIC data, not reported here, is also available for *P. edulis*-B samples for a number of other test arrangements [Gauss *et al.* 2019]. A database of DIC-supported tests results should be established as a 'benchmark library'.

As described in this Chapter, the work presented in this thesis has raised a number of questions and new hypotheses of bamboo behavior. The characteristics of bamboo vary through the culm wall. The framework presented provides a vehicle for numerically modeling this variation but additional experimental data is required. An understanding of the possibly orthotropic natures of E_f and E_m is required. This would provide additional modulus values such as E_{fL}, E_{mL}, E_{fT}, E_{mT} as illustrated in Figure 7.1. An approach to obtaining this could be a nano-indentation campaign focused on obtaining data sufficiently dense to permit differentiation of parenchyma morphology (differentiate the cell wall from its interstices). Such an approach would need to be carried out in longitudinal and transverse orientations as schematically shown in Figure 7.1.

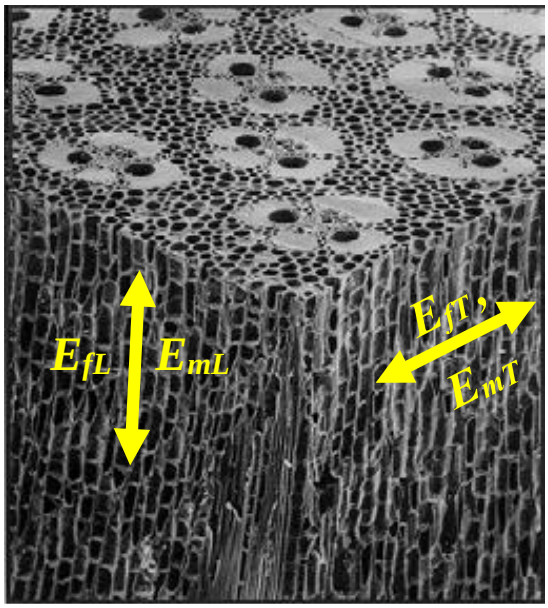

Figure 7.1: Proposed transverse and longitudinal modulus measurement. Original image from Liese [1998]

Further morphological study of bamboo to understand the causes – if they are not naturally occurring phenomena – of observed variation in parenchyma properties and intra-fibril cracking are recommended. These phenomena may result from drying and/or treatment and therefore may be controllable to some extent. Additionally, an internally consistent image analysis which correlates the mechanical properties from the experimental and numerical results to the microstructure analysis of the fracture surface is recommended. This should take into consideration the internal variation in local structure (shape and size) of the bamboo fiber and parenchyma cell morphology through the culm wall thereby addressing the potential for fiber bridging in areas with lower fiber density observed by Tan *et al.* [2011].

The approaches explored in this thesis are focused mainly on the use of bamboo within the research community. Nonetheless, some observations may have impact on the bamboo construction community if expanded upon and validated over a broader range of parameters. The approach to establishing variation of morphology in the components of glue-laminated beams has

potential for both quality control for such elements and for optimizing their performance. While not included in this dissertation, Akinbade *et al.* [2020] provides some initial insight into both these domains. A second serendipitous discovery was the "toughening" effect observed in the "shaved" flat ring flexure tests. The observed phenomenon is not well understood but the result could potentially be leveraged in bamboo connection detailing. If the bamboo indeed has greater resistance to splitting when the hard siliceous outer layer is removed; bolted and doweled connections could be made similarly more resistant. This requires further investigation. In most areas, a combination of data with a better understanding of the material properties will give rise to the acceptance and inclusion of bamboo as a 'proven' structural material.

Appendix A – Image Analysis Script

This appendix shows the MATLAB script used in bamboo culm wall image analysis. This was described in Section 3.4.2 and Section 4.4. Note that any line that starts with a "%" is a comment line and is not a part of the script.

```
clear
clc
close all

%% IMPORT THE IMAGE + INITIAL EDITS

%Prompt user for filename
FileName = input('Image File Name: ','s');

%Import the image using filename and imread
Im = imread(FileName);

%Store info about image using filename
ImINFO = imfinfo(FileName);

%convert Im to greyscale
Im = rgb2gray(Im);
%Smooth image
Im = imgaussfilt(Im,1);


%% SEPARATE IMAGE

%Store the size of the image into a rows/cols matrix
%h = height, w = width, cbands = number of color bands
[h,w,cbands] = size(Im);
%store just the height and width in a matrix
ImSize = [h w];

%Prompt for amount of divisions of picture
%For now we are just going to make it 10 for convenience
DivNum = 10;

%Establish height of individual heights
```

```
Newh = h/DivNum;

%Divide each image into equal heights of 10
Im10 = Im(1:Newh,1:w);
Im9 = Im((1 + Newh):(1 + 2*Newh),1:w);
Im8 = Im((1 + 2*Newh):(1 + 3*Newh),1:w);
Im7 = Im((1 + 3*Newh):(1 + 4*Newh),1:w);
Im6 = Im((1 + 4*Newh):(1 + 5*Newh),1:w);
Im5 = Im((1 + 5*Newh):(1 + 6*Newh),1:w);
Im4 = Im((1 + 6*Newh):(1 + 7*Newh),1:w);
Im3 = Im((1 + 7*Newh):(1 + 8*Newh),1:w);
Im2 = Im((1 + 8*Newh):(1 + 9*Newh),1:w);
Im1 = Im((1 + 9*Newh):h,1:w);


%% EDIT INDIVIDUAL STRIPS
%Enhance contrast
%Adjust threshold
%Save to individual image file
%Images numbered 1 - 10 from the inside out


%10
Im10 = imadjust(Im10,[.1 1],[]);
level = graythresh(Im10);
Im10 = im2bw(Im10,level);
imwrite(Im10,'Im10.jpg');

%9
Im9 = imadjust(Im9,[.1,.8],[]);
level = graythresh(Im9);
Im9 = im2bw(Im9,level);
imwrite(Im9,'Im9.jpg');

%8
Im8 = imadjust(Im8,[.1,.8],[]);
level = graythresh(Im8);
Im8 = im2bw(Im8,level);
imwrite(Im8,'Im8.jpg');

%7
Im7 = imadjust(Im7,[.1,.8],[]);
level = graythresh(Im7);
Im7 = im2bw(Im7,level);
imwrite(Im7,'Im7.jpg');
```

```
%6
Im6 = imadjust(Im6,[.1,.8],[]);
level = graythresh(Im6);
Im6 = im2bw(Im6,level);
imwrite(Im6,'Im6.jpg');

%5
Im5 = imadjust(Im5,[.1,.8],[]);
level = graythresh(Im5);
Im5 = im2bw(Im5,level);
imwrite(Im5,'Im5.jpg');

%4
Im4 = imadjust(Im4,[.1,.8],[]);
level = graythresh(Im4);
Im4 = im2bw(Im4,level);
imwrite(Im4,'Im4.jpg');

%3
Im3 = imadjust(Im3,[.1,.8],[]);
level = graythresh(Im3);
Im3 = im2bw(Im3,level);
imwrite(Im3,'Im3.jpg');

%2
Im2 = imadjust(Im2,[.1,.8],[]);
level = graythresh(Im2);
Im2 = im2bw(Im2,level);
imwrite(Im2,'Im2.jpg');

%1
Im1 = imadjust(Im1,[.1,.8],[]);
level = graythresh(Im1);
Im1 = im2bw(Im1,level);
imwrite(Im1,'Im1.jpg');


%% VIEW THE SUM OF ALL STRIPS

%Ask User if they would like to view the image
Viewim = input('Press 1 if you would like to view your edited images: ');

if Viewim == 1

%Show each image using imshow
```

```
imshow(Im10);
%Ask user to view next image
disp('Section 10: Press any key to continue ');

pause;

imshow(Im9);
%Ask user to view next image
disp('Section 9: Press any key to continue ');

pause;

imshow(Im8);
%Ask user to view next image
disp('Section 8: Press any key to continue ');

pause;

imshow(Im7);
%Ask user to view next image
disp('Section 7: Press any key to continue ');

pause;

imshow(Im6);
%Ask user to view next image
disp('Section 6: Press any key to continue ');

pause;

imshow(Im5);
%Ask user to view next image
disp('Section 5: Press any key to continue ');

pause;

imshow(Im4);
%Ask user to view next image
disp('Section 4: Press any key to continue ');

pause;

imshow(Im3);
%Ask user to view next image
disp('Section 3: Press any key to continue ');
```

```
pause;

imshow(Im2);
%Ask user to view next image
disp('Section 2: Press any key to continue ');

pause;

imshow(Im1);
%Ask user to view next image
disp('Section 1: Press any key to continue ');

pause;

end


%Ask user to close image and continue funciton
disp('Please press any key to continue ');

pause;

close all;



%% ANALYZE THE FIBER AREA

%initialize an empty matrix for future storage of percentage values
PercentA = zeros(10,1);

%use bware to calculate the percent of the white area and use that to find
%the percent for each individual strip
% **Would eventually like to make this into a loop**

%10
%determine the total area of the strip
[h10,w10] = size(Im10);
A10 = h10*w10;
RatioA10 = 1 - bwarea(Im10)/A10;
PercentA(10) = RatioA10;

%9
%determine the total area of the strip
[h9,w9] = size(Im9);
A9 = h9*w9;
```

```
RatioA9 = 1 - bwarea(Im9)/A9;
PercentA(9) = RatioA9;

%8
%determine the total area of the strip
[h8,w8] = size(Im8);
A8 = h8*w8;
RatioA8 = 1 - bwarea(Im8)/A8;
PercentA(8) = RatioA8;

%7
%determine the total area of the strip
[h7,w7] = size(Im7);
A7 = h7*w7;
RatioA7 = 1 - bwarea(Im7)/A7;
PercentA(7) = RatioA7;

%6
%determine the total area of the strip
[h6,w6] = size(Im6);
A6 = h6*w6;
RatioA6 = 1 - bwarea(Im6)/A6;
PercentA(6) = RatioA6;

%5
%determine the total area of the strip
[h5,w5] = size(Im5);
A5 = h5*w5;
RatioA5 = 1 - bwarea(Im5)/A5;
PercentA(5) = RatioA5;

%4
%determine the total area of the strip
[h4,w4] = size(Im4);
A4 = h4*w4;
RatioA4 = 1 - bwarea(Im4)/A4;
PercentA(4) = RatioA4;

%3
%determine the total area of the strip
[h3,w3] = size(Im3);
A3 = h3*w3;
RatioA3 = 1 - bwarea(Im3)/A3;
PercentA(3) = RatioA3;

%2
```

```
%determine the total area of the strip
[h2,w2] = size(Im2);
A2 = h2*w;
RatioA2 = 1 - bwarea(Im2)/A2;
PercentA(2) = RatioA2;

%1
%determine the total area of the strip
[h1,w1] = size(Im1);
A1 = h1*w1;
RatioA1 = 1 - bwarea(Im1)/A1;
PercentA(1) = RatioA1;

%% EXPORT DATA TO A TEXT FILE
newfile = fopen('newfile.txt','w');
fprintf(newfile,'%6.5f\n',PercentA);
fclose(newfile);
```

Appendix B – Random Field Script

This section details the MATLB script used for the random field analysis approach described in Chapter 5. An example is illustrated in Section 5.2 Note that any line that starts with a "%" is a comment line and is not a part of the script.

```
% Random field Spatial Decomposition method on ET
clc
clear all
tic;

% Radial dimension of specimen measure from wall interior
Rd = [ 0.05 0.15 0.25 0.35 0.45 0.55 0.65 0.75 0.85 0.95]';

% volume fiber ratio derived from image analysis
% vf input format is = [a b c d e f g h I j]';

vf = input ('enter fiber volume ratio matrix:');
Ef = input ('enter modulus of fiber:');
Em = input ('enter modulus of matrix:');
t = input ('enter thickness of culm wall:');

% Halpin-Tsai radial Modulus of Elasticity(GPa)
% Using Halpin-Tsai to convert the measured Vf into radial E
% rz = empirical constant

rz = zeros(size(vf));              % Make another array to fill up.
for ii = 1:numel(vf)
   if vf(ii)<0.5
      rz(ii) = 2;
   else
      rz(ii) =2+(40*(vf(ii).^10));
   end
end

% n = rule of mixture constant equation

n=zeros(size(vf));
for ii = 1:numel(vf)
n=((35/1.8)-1)./((35/1.8)+rz);
```

```
end

% Halpin-Tsai equation
mu= (1.8*(1+(rz.*n.*vf)))./(1-(n.*vf));
see=plot(mu);

% mu=[2.42 2.6 2.66 2.8 2.97 3.17 3.6 4.29 5.95 10.28]';
%Correlation distances in the x-direction
lx=t;

% thickness of Bamboo wall
r=t;

%variance of the radial Elasticity
s=var(mu);

%standard deviation of fiber volume ratio
sd=s^(1/2);

%Condition for isotropic material consideration
ly=lx;

% needed if wanting to make random value fixed
%rng(0,'twister');

% S.D of normally distributed random value
a=1;

 % mean of normally distributed random value
b=0;

%normally distributed random values generator
y=(a.*randn(10,1)+b)

%mean of random values
z=mean(y);

% The generation of the radial component of the distances between points
dx1j=[0 0.1*r 0.2*r 0.3*r 0.4*r 0.5*r 0.6*r 0.7*r 0.8*r 0.9*r];
dx2j=[0.1*r 0 0.1*r 0.2*r 0.3*r 0.4*r 0.5*r 0.6*r 0.7*r 0.8*r];
dx3j=[0.2*r 0.1*r 0 0.1*r 0.2*r 0.3*r 0.4*r 0.5*r 0.6*r 0.7*r];
dx4j=[0.3*r 0.2*r 0.1*r 0 0.1*r 0.2*r 0.3*r 0.4*r 0.5*r 0.6*r];
dx5j=[0.4*r 0.3*r 0.2*r 0.1*r 0 0.1*r 0.2*r 0.3*r 0.4*r 0.5*r];
dx6j=[0.5*r 0.4*r 0.3*r 0.2*r 0.1*r 0 0.1*r 0.2*r 0.3*r 0.4*r];
dx7j=[0.6*r 0.5*r 0.4*r 0.3*r 0.2*r 0.1*r 0 0.1*r 0.2*r 0.3*r];
dx8j=[0.7*r 0.6*r 0.5*r 0.4*r 0.3*r 0.2*r 0.1*r 0 0.1*r 0.2*r];
```

```
dx9j=[0.8*r 0.7*r 0.6*r 0.5*r 0.4*r 0.3*r 0.2*r 0.1*r 0 0.1*r];
dx10j=[0.9*r 0.8*r 0.7*r 0.6*r 0.5*r 0.4*r 0.3*r 0.2*r 0.1*r 0];
dx=[dx1j; dx2j; dx3j; dx4j; dx5j; dx6j; dx7j; dx8j; dx9j; dx10j;]';

% The generation of the longitudinal component of the distances between points
dy1j=[0 0 0 0 0 0 0 0 0 0];
dy2j=[0 0 0 0 0 0 0 0 0 0];
dy3j=[0 0 0 0 0 0 0 0 0 0];
dy4j=[0 0 0 0 0 0 0 0 0 0];
dy5j=[0 0 0 0 0 0 0 0 0 0];
dy6j=[0 0 0 0 0 0 0 0 0 0];
dy7j=[0 0 0 0 0 0 0 0 0 0];
dy8j=[0 0 0 0 0 0 0 0 0 0];
dy9j=[0 0 0 0 0 0 0 0 0 0];
dy10j=[0 0 0 0 0 0 0 0 0 0];
dy=[dy1j; dy2j; dy3j; dy4j; dy5j; dy6j; dy7j; dy8j; dy9j; dy10j;]';

% Condition for the Spherical and Cubic corr functions when needed
% rm is the autocorrelation function between points i and j
% Make another array to fill up.
rm = zeros(size(dx));
for ii = 1:numel(dx)
  if dx(ii)>=lx
      rm(ii) = 0;
  else
      rm(ii) =1-(7*(dx(ii)/lx)^2)+(35/4*(dx(ii)/lx)^3)-(7/2*(dx(ii)/lx)^5)+(3/4*(dx(ii)/lx)^7);
  end
end

% Conventional cubic (Polynomial line of best fit)
% rm=1.6+(13.56*(dx/lx))+(38.67*(dx/lx)^3)-(41.86*(dx/lx)^2)
% Spherical Model
% rm=1-((3/2*(dx/lx))+(1/2*(dx/lx)^3));
% Cubic Model
% rm=1-(7*(dx/lx)^2)+(35/4*(dx/lx)^3)-(7/2*(dx/lx)^5)+(3/4*(dx/lx)^7);
% Exponential Model
% rm=exp(-(dx/lx));

% Covariance Matrix
A=(sd^2)*rm;

% Lower bound of the Cholesky decomposition A=CC'
C=chol(A,'LOWER')

% Vector containing the spatial value of Er
E10=(C*y)+mu;
```

```
C*y
mu
E10
plot(E10)

% Generate the specimen data.
Y = [E10'];
X = [Rd'];

% Find the coefficients.
coeffs = polyfit(X, Y, 3)
plot(X, Y, 'ro', 'MarkerSize', 5)

toc;
```

Appendix C - USDFLD Subroutine

This section illustrates a typical USDFLD subroutine script described in Section 6.3.3. Dimensions are shown for Specimen PN5B2C. Note that any line that starts with a "!" is a comment line and is not a part of the subroutine.

```
      SUBROUTINE USDFLD (FIELD,STATEV,PNEWDT,DIRECT,T,
          1 CELENT,TIME,DTIME,CMNAME,ORNAME,NFIELD,
          2 NSTATV,NOEL,NPT,LAYER,KSPT,KSTEP,KINC,NDI,
          3 NSHR,COORD,JMAC,JMATYP,MATLAYO,
          4 LACCFLA)
c
      INCLUDE 'ABA_PARAM.INC'
c
      CHARACTER*80 CMNAME,ORNAME
      CHARACTER*8 FLGRAY(15)

      DIMENSION FIELD(NFIELD),STATEV(nSTATV),DIRECT(3,3),
          1 T(3,3),TIME(2),COORD(*),JMAC(*),JMATYP(*)
      DIMENSION ARRAY(15),JARRAY(15)

       REAL :: r0,r1
! r0 is inner radius of bamboo specimen and r1 is outer radius
              r0 = 37.15
              r1 = 45.5
! read x and y coordinate
        X = COORD(1)
        Y = COORD(2)
! Bamboo thickness calculation
        rB = (sqrt((X**2) + (Y**2)) - r0)
! normalized thickness
        rBn = rB/(r1-r0)
! calculate Young modulus
! FIELD(1) = ET
! FIELD(2) = EL
! define depend state variable (E(y))

        FIELD(1)= 1000*(21.7*rBn**3-23.7*rBn**2+7.4*rBn+1.1)
        FIELD(2)= 1000*(43.9*rBn**3-43.5*rBn**2+19.4*rBn+4.2)
```

```
! save E value for state dependent variable

      STATEV(1)= 1000*(21.7*rBn**3-23.7*rBn**2+7.4*rBn+1.1)
      STATEV(2)= 1000*(43.9*rBn**3-43.5*rBn**2+19.4*rBn+4.2)
! Use the GETVRM subroutine to get stress and strain values for validation
           CALL GETVRM('S', ARRAY, JARRAY, FLGRAY, JRCD,
         1 JMAC, JMATYP, MATLAYO, LACCFLA)
     S11 = ARRAY(1)
           S22 = ARRAY(2)
           S12 = ARRAY(4)
           CALL GETVRM('E', ARRAY, JARRAY, FLGRAY, JRCD,
         1 JMAC, JMATYP, MATLAYO, LACCFLA)
     E12 = ARRAY(4)
! Write output values to .DAT file for random element 100:
           IF (NOEL.eq.100) THEN
           WRITE(6,*) 'check',KSTEP, KINC, NOEL, NPT, S11, S22, S12, E12, rBn
           ENDIF
! Write output values to .DAT file for random element 1250:
           IF (NOEL.eq.1250) THEN
           WRITE(6,*) 'check',KSTEP, KINC, NOEL, NPT, S11, S22, S12, E12, rBn
           ENDIF
! If error, write comment to .DAT file:
           IF(JRCD.NE.0)THEN
     WRITE(6,*) 'REQUEST ERROR IN USDFLD FOR ELEMENT NUMBER
',NOEL,'INTEGRATION POINT NUMBER ',NPT
      ENDIF
!    USER CODE END
     END
```

Appendix D – UMAT Subroutine

This section illustrates a typical UMAT subroutine script described in Section 6.3.4. Dimensions are shown for Specimen PN5B2C. Note that any line that starts with a "!" is a comment line and is not a part of the subroutine.

```
      SUBROUTINE UMAT(STRESS,STATEV,DDSDDE,SSE,SPD,SCD,RPL,
          1 DDSDDT,DRPLDE,DRPLDT,STRAN,DSTRAN,TIME,DTIME,TEMP,DTEMP,
          2 PREDEF,DPRED,CMNAME,NDI,NSHR,NTENS,NSTATV,PROPS,NPROPS,
          3 COORDS,DROT,PNEWDT,CELENT,DFGRD0,DFGRD1,NOEL,NPT,LAYER,
          4 KSPT,KSTEP,KINC)
c
      INCLUDE 'ABA_PARAM.INC'
c
      CHARACTER*8 CMNAME

      DIMENSION STRESS(NTENS), STATEV(NSTATV), DDSDDE(NTENS, NTENS),
          1 DDSDDT(NTENS), DRPLDE(NTENS), STRAN(NTENS), DSTRAN(NTENS),
          2 PREDEF(1), DPRED(1), PROPS(NPROPS), COORDS(3), DROT(3, 3),
          3 DFGRD0(3, 3), DFGRD1(3, 3)
            DIMENSION EELAS(6), EPLAS(6), FLOW(6)

            PARAMETER (ZERO=0.D0, ONE=1.D0, TWO=2.D0, THREE=3.D0, SIX=6.D0,
          1 ENUMAX=.4999D0, NEWTON=10, TOLER=1.0D-6)

! UMAT FOR TRANSVERSELY ISOTROPIC ELASTIC WITH CUBIC VARYING
! MODULI - CANNOT BE USED FOR PLANE STRESS
! coords_1_ is X-coordinate of gauss points.
! coords_2_ is Y-coordinate of gauss points.
! coords_3_ is Z-coordinate of gauss points.
! Props is defined by users in Abaqus.
                    REAL :: r0,r1
           ! r0 is inner radius of bamboo specimen and r1 is outer radius
              r0 = 37.15
                    r1 = 45.5
!read x and y coordinate
       X = COORDS(1)
       Y = COORDS(2)
! Bamboo thickness calculation
       rB = (sqrt((X**2) + (Y**2)) - r0)
```

```
 ! normalized thickness
       rBn = rB/(r1-r0)
! Define constants for material property input
         ANU = PROPS(1)
         VF = PROPS(2)*rBn**3+PROPS(3)*rBn**2+PROPS(4)*rBn+ PROPS(5)
         EL = 1000*(PROPS(6)*rBn**3+ PROPS(7)*rBn**2+ PROPS(8)*rBn+ PROPS(9))
         ET = 1000*(PROPS(10)*rBn**3+ PROPS(11)*rBn**2+ PROPS(12)*rBn+
PROPS(13))
         ANU2=ANU**TWO
         ANUL=(ET/EL)*ANU
         DELTA=(ONE/(ONE-ANU2-(TWO*ANUL*ANU)-(TWO*ANU2*ANUL)))
         GL=EL/(TWO*(ONE+ANUL))
         GT=ET/(TWO*(ONE+ANU))

! PROPS(1) is the transverse coefficient VT and VLT
! PROPS(2) - PROPS(5) are the coefficient of the cubic function of VF
! PROPS(6) - PROPS(9) are the coefficient of the cubic function of ET
! PROPS(10) - PROPS(13) are the coefficient of the cubic function of ET
! CALCULATE STRESS
                          DO I=1, NTENS
                           DO J=1, NTENS
                           DDSDDE(I,J)=ZERO
                           END DO
                          END DO
                          DDSDDE(1,1)=DELTA*ET*(ONE-(ANUL*ANU))
                          DDSDDE(2,2)=DELTA*ET*(ONE-(ANUL*ANU))
                          DDSDDE(3,3)=DELTA*EL*(ONE-ANU2)
                          DDSDDE(4,4)=GL
                          DDSDDE(5,5)=GL
                          DDSDDE(6,6)=GT
                          DDSDDE(1,2)=DELTA*ET*(ANU+(ANUL*ANU))
                          DDSDDE(1,3)=DELTA*ET*(ANU+ANU2)
                          DDSDDE(2,3)=DELTA*ET*(ANU+ANU2)
                          DDSDDE(2,1)=DELTA*ET*(ANU+(ANUL*ANU))
                          DDSDDE(3,1)=DELTA*ET*(ANU+ANU2)
                          DDSDDE(3,2)=DELTA*ET*(ANU+ANU2)
                          DO I=1,NTENS
                           DO J=1,NTENS
                           STRESS(I)=STRESS(I)+DDSDDE(I,J)*DSTRAN(J)
                           ENDDO
                          ENDDO
                IF (NOEL.eq.8360) THEN
           WRITE(6,*) 'check',KSTEP, KINC, NOEL, rBn
           ENDIF
       RETURN
                END
```

Appendix E – Initial FEM summary

This Appendix shows output tables parallel to those reported in Section 6.3 for the initial modelling using material properties E_f = 35 GPa and E_m = 1.8 GPa as proposed by Janssen [2000]. As described in Section 6.2.2, the resulting model was too stiff and E_m was re-calibrated.

Table E1: Geometric parameters of bamboo specimens used for modelling validation (see Table 2.1 and 2.6)

	PN5B2C	PN5B3C	PN5B4C	PN
D (mm)	91.0	90.8	90.5	93.5
H (mm)	17.2	18.2	19.3	18.7
t (mm)	8.35	8.40	8.10	6.70
std. dev. of *t* (mm)	0.40	0.10	0.30	1.27
ovality[a]	0.09	0.10	0.10	0.08
V_f	$V_f = 1.29x^3 - 1.28x^2 + 0.57x + 0.10$	$V_f = 0.81x^3 - 0.53x^2 + 0.28x + 0.10$	$V_f = 1.09x^3 - 0.90x^2 + 0.40x + 0.10$	$V_f = 0.94x^3 - 0.63x^2 + 0.36x + 0.06$
E_L (GPa)	$E_L = 42.8x^3 - 42.5x^2 + 18.9x + 5.0$	$E_L = 26.9x^3 - 17.6x^2 + 9.3x + 5.1$	$E_L = 36.2x^3 - 29.9x^2 + 13.3x + 5.2$	$E_L = 31.2x^3 - 20.9x^2 + 12.0x + 3.8$
E_T (GPa)	$E_T = 30.5x^3 - 33.0x^2 + 10.4x + 2.0$	$E_T = 24.1x^3 - 24.2x^2 + 7.4x + 2.1$	$E_T = 33.0x^3 - 34.9x^2 + 10.5x + 2.0$	$E_T = 42.8x^3 - 45.4x^2 + 13.6x + 1.6$
[a] ovality, $d_o = 2(D_{max} - D_{min})/(D_{max} + D_{min})$ (ISO 19624-2018)				

Table E2: FEA model input for Model 1

Parameter	PN5B2C	PN5B3C	PN5B4C	PN
Gross section fiber volume fraction, V_f	0.28	0.27	0.27	0.27
Transverse Modulus $E_{T,}$ MPa	4038	3958	4110	4280
Longitudinal Modulus $E_{L,}$ MPa	11345	10988	11340	11065
Transverse Poisson's ratio, $\nu_T = \nu_{LT}$ [Janssen 1981]	0.30	0.30	0.30	0.30
Longitudinal Poisson's ratio, $\nu_{TL} = \nu_{LT}E_T/E_L$	0.11	0.11	0.11	0.12
Shear Modulus, G_{TL} MPa	5125	4958	5114	4957
Ø	1.2	1.2	1.2	1.2
$K_{11} = K_{22}$, MPa	4727	4637	4818	5041
K_{33}, MPa	12488	12109	12505	12287
$K_{12} = K_{21}$, MPa	1622	1593	1657	1749
$K_{13} = K_{23} = K_{31} = K_{32}$, MPa	1905	1869	1942	2037
$K_{44} = K_{55}$, MPa	5125	4958	5114	4957
$G_T = K_{66}$, MPa	1553	1522	1581	1646

Table E3a: FEA model input for Model 2 (PN5B2C)

Parameter	PN5B2C									
x	0.05	0.15	0.25	0.35	0.45	0.55	0.65	0.75	0.85	0.95
V_f	0.120	0.156	0.178	0.193	0.210	0.236	0.279	0.347	0.447	0.587
$E_{T,}$ MPa	2441	2920	3014	2905	2777	2812	3194	4105	5728	8247
$E_{L,}$ MPa	5744	6923	7638	8144	8699	9560	10983	13225	16543	21194
$\upsilon_T = \upsilon_{LT}$	0.30	0.30	0.30	0.30	0.30	0.30	0.30	0.30	0.30	0.30
$\upsilon_{TL} = \upsilon_{LT}E_T/E_L$	0.13	0.13	0.12	0.11	0.10	0.09	0.09	0.09	0.10	0.12
G_{TL} MPa	2547	3073	3415	3678	3969	4392	5051	6049	7493	9489
Ø	1.23	1.23	1.22	1.21	1.20	1.19	1.19	1.19	1.21	1.22
$K_{11} = K_{22}$, MPa	2897	3463	3555	3402	3229	3254	3694	4765	6695	9718
K_{33}, MPa	6449	7766	8500	8966	9477	10342	11870	14372	18160	23551
$K_{12} = K_{21}$, MPa	1019	1217	1237	1167	1093	1091	1237	1607	2288	3374
$K_{13} = K_{23} = K_{31} = K_{32}$, MPa	1175	1404	1438	1371	1296	1304	1479	1912	2695	3928
$K_{44} = K_{55}$, MPa	2547	3073	3415	3678	3969	4392	5051	6049	7493	9489
$G_T = K_{66}$, MPa	939	1123	1159	1117	1068	1082	1228	1579	2203	3172

Table E3b : FEA model input for Model 2 (PN5B3C)

Parameter	PN5B3C									
x	0.05	0.15	0.25	0.35	0.45	0.55	0.65	0.75	0.85	0.95
V_f	0.113	0.133	0.150	0.168	0.192	0.228	0.281	0.354	0.453	0.582
$E_{T,}$ MPa	2411	2741	2804	2745	2708	2837	3278	4175	5672	7914
$E_{L,}$ MPa	5524	6190	6745	7352	8172	9366	11096	13523	16809	21114
$\upsilon_T = \upsilon_{LT}$	0.30	0.30	0.30	0.30	0.30	0.30	0.30	0.30	0.30	0.30
$\upsilon_{TL} = \upsilon_{LT}E_T/E_L$	0.13	0.13	0.12	0.11	0.10	0.09	0.09	0.09	0.10	0.11
G_{TL} MPa	2442	2732	2999	3306	3717	4293	5097	6189	7632	9490
Ø	1.24	1.24	1.23	1.22	1.20	1.19	1.19	1.19	1.20	1.22
$K_{11} = K_{22}$, MPa	2867	3263	3321	3224	3156	3289	3795	4845	6618	9300
K_{33}, MPa	6223	6985	7553	8133	8933	10158	12009	14689	18406	23367
$K_{12} = K_{21}$, MPa	1012	1155	1164	1113	1073	1106	1273	1633	2255	3212
$K_{13} = K_{23} = K_{31} = K_{32}$, MPa	1164	1326	1346	1301	1268	1319	1520	1943	2662	3754
$K_{44} = K_{55}$, MPa	2442	2732	2999	3306	3717	4293	5097	6189	7632	9490
$G_T = K_{66}$, MPa	927	1054	1078	1056	1041	1091	1261	1606	2182	3044

Table E3c: FEA model input for Model 2 (PN5B4C)

Parameter	PN5B4C									
x	0.05	0.15	0.25	0.35	0.45	0.55	0.65	0.75	0.85	0.95
V_f	0.120	0.145	0.163	0.178	0.199	0.231	0.281	0.356	0.461	0.604
$E_{T,}$ MPa	2442	2901	2959	2815	2665	2708	3142	4166	5976	8771
$E_{L,}$ MPa	5795	6644	7222	7744	8429	9493	11154	13628	17134	21887
$\upsilon_T = \upsilon_{LT}$	0.30	0.30	0.30	0.30	0.30	0.30	0.30	0.30	0.30	0.30
$\upsilon_{TL} = \upsilon_{LT}E_T/E_L$	0.13	0.13	0.12	0.11	0.09	0.09	0.08	0.09	0.10	0.12
G_{TL} MPa	2572	2937	3216	3491	3849	4372	5142	6242	7755	9769
Ø	1.23	1.24	1.23	1.21	1.20	1.19	1.18	1.19	1.21	1.23
$K_{11} = K_{22}$, MPa	2895	3450	3501	3300	3097	3129	3628	4831	6987	10358
K_{33}, MPa	6499	7485	8072	8543	9175	10245	12025	14791	18822	24402
$K_{12} = K_{21}$, MPa	1017	1219	1225	1135	1047	1046	1211	1627	2391	3611
$K_{13} = K_{23} = K_{31} = K_{32}$, MPa	1174	1401	1418	1331	1243	1253	1452	1938	2813	4191
$K_{44} = K_{55}$, MPa	2572	2937	3216	3491	3849	4372	5142	6242	7755	9769
$G_T = K_{66}$, MPa	939	1116	1138	1083	1025	1042	1209	1602	2298	3374

Table E3d : FEA model input for Model 2 (PN)

Parameter	PN									
x	0.05	0.15	0.25	0.35	0.45	0.55	0.65	0.75	0.85	0.95
V_f	0.077	0.103	0.125	0.149	0.180	0.224	0.286	0.372	0.488	0.639
$E_{T,}$ MPa	2172	2763	2831	2634	2427	2467	3012	4319	6643	10242
$E_{L,}$ MPa	4352	5235	5981	6777	7811	9269	11338	14206	18060	23088
$\upsilon_T = \upsilon_{LT}$	0.30	0.30	0.30	0.30	0.30	0.30	0.30	0.30	0.30	0.30
$\upsilon_{TL} = \upsilon_{LT}E_T/E_L$	1.26	1.27	1.25	1.22	1.19	1.18	1.18	1.19	1.21	1.24
G_{TL} MPa	1892	2260	2619	3035	3572	4292	5251	6509	8133	10188
Ø	1.22	1.22	1.22	1.21	1.20	1.20	1.20	1.20	1.20	1.21
$K_{11} = K_{22}$, MPa	2615	3346	3392	3103	2817	2841	3468	5007	7796	12197
K_{33}, MPa	4992	6057	6810	7530	8489	9950	12169	15411	19947	26061
$K_{12} = K_{21}$, MPa	944	1221	1214	1077	950	943	1151	1685	2686	4319
$K_{13} = K_{23} = K_{31} = K_{32}$, MPa	1068	1370	1382	1254	1130	1135	1386	2008	3144	4955
$K_{44} = K_{55}$, MPa	1892	2260	2619	3035	3572	4292	5251	6509	8133	10188
$G_T = K_{66}$, MPa	835	1063	1089	1013	933	949	1159	1661	2555	3939

Table E4 : Stresses and strains from the E-W quadrant of the FEA at a prescribed displacement Δ = 1.5 mm

		Experimental Data at Δ = 1.5 mm	Model 0	Model 1	Model 2	Model 3	Model 4
Applied load to cause Δ = 1.5 mm, N	PN5B2C	293.7	288.5	498.7	494.0	493.6	494.8
	PN5B3C	300.0	294.3	511.6	500.4	502.1	501.6
	PN5B4C	315.0	303.4	525.0	518.7	518.3	519.8
	PN	-	152.9	284.8	266.8	265.6	267.0
Compressive Strain at E-W quadrant, ε_{yy} με	PN5B2C	-4498	-	-5045	-5956	-5997	-5984
	PN5B3C	-4562	-	-4961	-5871	-5899	-5893
	PN5B4C	-4185	-	-4889	-5843	-5880	-5870
	PN	-	-	-3943	-4696	-4735	-4722
Tensile Strain at E-W quadrant, ε_{yy} με	PN5B2C	2832	-	3759	2861	2831	2836
	PN5B3C	3064	-	3698	2796	2764	2775
	PN5B4C	3256	-	3707	2760	2727	2735
	PN	-	-	3366	2309	2272	2281
Neutral Axis location	PN5B2C	0.54 t	0.52 t	0.52 t	0.62 t	0.62 t	0.62t
	PN5B3C	0.56 t	0.52 t	0.52 t	0.62 t	0.63 t	0.63 t
	PN5B4C	0.50 t	0.52 t	0.52 t	0.62 t	0.62 t	0.62 t
	PN	-	0.52 t	0.53 t	0.65 t	0.65 t	0.65 t
Compressive Stress in E-W, $\sigma_{,yy}$ MPa	PN5B2C	-12.9	-12.7	-20.0	-14.4	-12.0	-12.1
	PN5B3C	-12.1	-12.1	-19.2	-14.0	-12.3	-12.4
	PN5B4C	-12.9	-12.5	-20.0	-14.1	-11.8	-11.9
	PN	-	-9.7	-16.6	-10.1	-7.6	-7.8
Tensile Stress at E-W quadrant, $\sigma_{,yy}$ MPa	PN5B2C	9.4	9.2	14.9	23.0	27.0	27.1
	PN5B3C	8.93	8.7	14.3	21.6	25.1	25.0
	PN5B4C	9.53	9.2	14.9	23.6	27.9	28.0
	PN	-	7.6	14.1	23.0	27.6	27.6
Average Circumferential Modulus, $E_{m,90}$ MPa (Eq. 2-5)	PN5B2C	2623	2578	4455	4413	4410	4421
	PN5B3C	2354	2432	4228	4136	4150	4146
	PN5B4C	2658	2614	4523	4469	4465	4478
	PN	-	2700	5028	4711	4689	4714

Appendix F – Individual Specimen Test Data

This appendix provides individual test data supporting the aggregated data presented in Tables 2.1, 2.2 and 3.2.

Table F1: Individual flat ring flexure test data for *P. edulis*-C

Flat Ring Flexure (*P. edulis*-C)						
Table 2.1 and 2.2 Full specimen						
Specimen ID	**Culm**	***D* (mm)**	***t* (mm)**	**β**	**α**	**$f_{r\alpha}$ (MPa)**
PE2E6	2	105.9	8.6	0.00	1.00	18.1
PE2E1	2	106.6	8.5	0.00	1.00	16.1
PE2D5	2	106.8	8.7	0.00	1.00	15.2
PE2D4	2	106.4	8.7	0.00	1.00	19.1
PE2D3	2	106.6	8.6	0.00	1.00	19.8
PE2C6	2	109.5	9.0	0.00	1.00	22.3
PE2C5	2	109.4	8.8	0.00	1.00	13.5
PE2B7	2	112.1	9.3	0.00	1.00	21.7
PE2B6	2	112.1	9.2	0.00	1.00	21.1
PE2B5	2	112.0	9.4	0.00	1.00	18.7
PE2B4	2	113.9	9.6	0.00	1.00	18.8
PE2B3	2	114.5	9.6	0.00	1.00	17.6
PE2B2	2	114.4	9.6	0.00	1.00	13.7
PE2B1	2	114.6	9.6	0.00	1.00	18.4
PE2A4	2	114.5	9.6	0.00	1.00	23.4
PE2A3	2	114.3	9.4	0.00	1.00	23.1
PE3A1	3	125.5	11.3	0.00	1.00	11.5
PE3A2	3	125.9	11.2	0.00	1.00	13.3
PE3A3	3	126.0	11.6	0.00	1.00	16.4
PE3A4	3	126.3	11.3	0.00	1.00	16.6
PE3B1	3	125.5	11.3	0.00	1.00	19.0
PE3B3	3	124.4	11.3	0.00	1.00	12.8
PE3B4	3	124.4	11.2	0.00	1.00	12.5
PE3B5	3	124.0	11.1	0.00	1.00	16.0
PE3B6	3	124.2	11.1	0.00	1.00	17.1
PE3B7	3	123.9	11.0	0.00	1.00	17.2
PE3C2	3	121.5	10.9	0.00	1.00	13.6
PE3C4	3	121.6	10.7	0.00	1.00	14.8
PE3C5	3	121.9	10.7	0.00	1.00	18.6
PE3D2	3	120.8	10.5	0.00	1.00	19.1
PE3D3	3	120.0	10.6	0.00	1.00	17.7

Table F1 (continued)

Specimen ID	Culm	*D* (mm)	*t* (mm)	β	α	$f_{r\alpha}$ (MPa)
PE3D4	3	119.9	10.5	0.00	1.00	15.8
PE3G1	3	116.9	9.8	0.00	1.00	19.4

Table F2: Individual compression parallel to fibers test data for *P. edulis*-C

Full-culm Compression Parallel to Fibers (*P. edulis*-C)					
Table 2.2					
Specimen ID	**Culm**	***D* (mm)**	***t* (mm)**	**P (N)**	$f_{c,0}$ **(MPa)**
PE1A1	1	109.2	10.2	112815	35.6
PE1B1	1	106.8	9.8	117720	39.3
PE1C1	1	105.1	9.6	115268	39.9
PE2A1	2	115.0	9.6	176580	55.6
PE2B5	2	111.5	9.2	129983	43.8
PE2D2	2	107.4	8.8	161865	59.4
PE3G2	3	114.8	10.3	176580	52.3
PE3G3	3	113.1	9.5	181485	58.7

Table F3: Individual shear parallel to fibers test data for *P. edulis*-C

Full-culm Shear Parallel to Fibers (*P. edulis*-C)					
Table 2.2					
Specimen ID	**Culm**	***D* (mm)**	***t* (mm)**	**P (N)**	f_v **(MPa)**
PE1B2	1	106.7	9.5	58860	13.8
PE1C2	1	104.6	9.5	58370	13.7
PE1D2	1	102.9	9.2	54446	13.7
PE2A2	2	114.5	9.6	68670	15.2
PE2C1	2	110.5	9.1	66218	16.4
PE2D1	2	107.4	8.8	71123	17.8

Table F4: Individual clipped flat ring flexure test data for *P. edulis*-C

Table 3.2 - Clipped specimens (*P. edulis*-C)						
Specimen ID	**Culm**	***D* (mm)**	***t* (mm)**	**β**	**α**	**f_r (MPa)**
PE1A4	1	109.2	10.3	0.00	0.22	17.1
PE2E5	2	104.9	8.1	0.00	0.30	17.0
PE3F5	3	117.1	10.2	0.00	0.20	16.1
PE3F10	3	117.4	10.3	0.00	0.20	23.1
PE2E4	2	106.0	8.2	0.25	0.28	19.4
PE1A5	1	109.0	10.1	0.25	0.25	13.0
PE3F8	3	116.8	9.4	0.40	0.21	12.5
PE2E3	2	105.8	8.4	0.50	0.26	13.4
PE3F2	3	118.1	10.2	0.60	0.20	18.8
PE3F7	3	117.3	10.0	0.60	0.20	23.0
PE2E2	2	105.9	8.4	0.75	0.29	27.9
PE3F1	3	117.4	10.2	0.80	0.20	33.3
PE3F6	3	117.1	10.2	0.80	0.20	33.7

Table F5: Individual flat ring flexure test data for *P. edulis*-B

Flat Ring Flexure (*P. edulis*-B)						
Table 2.1 and 2.2 Full specimen						
Specimen ID	***D* (mm)**	***t* (mm)**	**β**	**α**	$f_{r\alpha}$ **(MPa)**	ρ_{12} **(g/cm^3)**
CR26	80.8	7.7	0.00	1.00	8.9	0.701
CR26	80.8	7.8	0.00	1.00	8.0	0.690
CR26	80.9	7.9	0.00	1.00	7.4	0.678
CR26	78.0	7.9	0.00	1.00	7.7	0.703
CR26	80.6	8.0	0.00	1.00	7.4	0.676
CR28	80.7	8.0	0.00	1.00	14.0	0.791
CR28	80.3	8.0	0.00	1.00	10.2	0.794
CR28	80.4	8.2	0.00	1.00	11.3	0.772
CR28	80.0	8.2	0.00	1.00	14.5	0.782
CR23	85.7	8.1	0.00	1.00	14.9	0.733
CR23	85.1	8.0	0.00	1.00	9.9	0.736
CR23	84.7	8.2	0.00	1.00	14.4	0.730
CR23	84.8	8.1	0.00	1.00	10.4	0.741
DOT2	78.4	7.5	0.00	1.00	12.3	0.730
DOT2	77.1	6.7	0.00	1.00	12.0	0.781
DOT2	76.9	6.6	0.00	1.00	12.8	0.796
DOT2	76.9	6.7	0.00	1.00	13.8	0.790
DOT2	77.2	6.6	0.00	1.00	12.7	0.796
DOT2	77.3	6.7	0.00	1.00	13.5	0.782
DOT2	77.0	6.6	0.00	1.00	16.1	0.786
CCB10	76.2	6.5	0.00	1.00	15.1	0.793
CCB10	76.1	6.5	0.00	1.00	12.7	0.798
CCB10	75.9	6.4	0.00	1.00	13.1	0.801
CCB10	74.8	6.2	0.00	1.00	9.3	0.841
CCB10	75.1	6.5	0.00	1.00	14.4	0.813
CCB10	75.0	6.5	0.00	1.00	10.4	0.807
CCB10	73.4	6.4	0.00	1.00	12.8	0.820
CCB10	73.3	6.3	0.00	1.00	18.5	0.827

Table F6: Individual compression parallel to fibers test data for *P. edulis*-B

Full-culm Compression Parallel to Fibers (*P. edulis*-B)			
Table 2.2			
Specimen ID	***D* (mm)**	***t* (mm)**	**$f_{c,0}$ (MPa)**
A10CP1	78.1	6.5	55.9
A10CP2	76.4	6.5	59.8
A1CP1N	76.3	7.0	56.0
A1CP2	76.6	6.8	62.4
A1CP3	77.1	6.9	62.2
A1CP4	77.0	7.1	62.2
A1CP5N	77.1	7.0	61.6
A3CP1N	78.2	7.1	49.3
A3CP2	77.5	7.0	50.8
A3CP3	77.7	6.8	58.1
A3CP4	78.2	6.6	53.2
A3CP5N	77.6	6.9	60.4
A5CP1	77.6	7.2	60.4
A5CP2	77.3	6.8	60.6
A7CP3	77.4	6.4	62.2
A7CP4	77.4	6.7	54.8
B1CP1	80.0	7.8	58.5
B1CP2	78.5	7.6	48.5
B1CP3	78.0	7.4	56.6
B1CP4	78.5	7.5	54.9
B2CP1	75.5	6.5	53.3
B2CP2	75.2	6.5	58.1
B3CP1	74.6	6.4	53.4
B3CP2	74.5	6.4	56.8
B3CP3	74.2	6.3	54.0
B3CP4	74.1	6.5	54.3
B3CP5N	75.0	6.6	57.2
B7CP1	79.9	7.2	51.9

Full-culm Compression Parallel to Fibers (*P. edulis*-B)			
Table 2.2			
Specimen ID	***D* (mm)**	***t* (mm)**	**$f_{c,0}$ (MPa)**
B7CP2	80.4	6.9	48.6
B7CP3	80.6	7.0	56.3
B7CP4N	80.4	7.2	61.0
C10CP1N	80.5	8.3	60.4
C10CP2	80.1	8.3	57.9
C11CP1N	74.6	6.7	69.0
C11CP2	75.0	6.6	63.2
C11CP3	74.5	6.6	66.1
C1CP1	81.5	6.8	69.2
C1CP2N	81.3	7.0	64.9
C2CP1	83.2	8.0	62.0
C2CP2	82.7	8.2	62.0
C3CP1	85.7	8.7	52.6
C3CP2	85.3	8.5	47.3
C4CP1	75.1	8.4	57.9
C4CP2N	75.0	8.3	59.0
C5CP1	80.7	7.2	59.9
C5CP2N	81.7	7.4	59.8
C6CP1	76.1	7.7	64.2
C6CP2	75.7	7.6	64.8
C7CP1	77.0	7.3	56.4
C7CP2N	77.1	7.3	60.7
C8CP1	77.9	7.4	61.9
C8CP2N	79.0	7.6	62.1
C9CP1	82.1	8.2	51.3
C9CP2N	82.7	8.2	50.9
C9CP3	83.2	8.3	51.6

Table F7: Individual shear parallel to fibers test data for *P. edulis*-B

Full-culm Shear Parallel to Fibers (*P. edulis*-B)				
Table 2.2				
Specimen ID	**D (mm)**	**t (mm)**	**P (N)**	**f_v (MPa)**
A10SP1	76.3	6.8	37346	17.6
A10SP2	77.4	6.5	30585	16.3
A10SP3N	76.7	6.7	37376	18.4
A1SP1N	78.2	7.5	41956	18.4
A1SP2	76.7	7.2	37670	17.3
A1SP3	77.2	7.2	43226	19.6
A1SP4	76.7	7.0	41801	19.8
A3SP1N	77.4	7.0	37855	17.6
A3SP2	77.7	6.7	37312	18.1
A3SP3	77.5	6.8	40954	19.4
A3SP4	77.1	7.0	37322	17.0
A5SP1	77.4	7.0	36467	17.2
A7SP2	77.8	6.7	36621	17.2
A7SP3	77.8	6.8	38597	18.6
A7SP4N	77.7	6.7	40752	19.6
B1SP3	77.8	7.3	44050	19.3
B1SP4	77.7	7.5	48104	20.5
B2SP1	75.2	6.4	40915	21.0
B2SP2	75.6	6.9	37214	17.5
B2SP3N	76.9	7.0	41207	19.8
B3SP1	75.5	6.8	37734	18.9
B3SP2	75.5	6.5	37283	19.5
B3SP3	75.5	6.5	37922	19.8
B3SP4	76.0	6.4	38888	20.2
C10SP1N	81.3	8.3	48914	18.3

Full-culm Shear Parallel to Fibers (*P. edulis*-B)				
Table 2.2				
Specimen ID	**D (mm)**	**t (mm)**	**P (N)**	**f_v (MPa)**
C10SP2	79.9	8.1	43144	16.6
C10SP3N	79.9	8.1	45809	17.7
C11SP1N	75.1	7.0	40643	19.4
C11SP2	75.7	6.9	39380	18.5
C11SP3	74.8	6.9	37828	18.1
C1SP1	80.3	6.9	40226	18.1
C1SP2	80.3	6.7	40667	19.3
C2SP1N	83.1	8.2	50046	18.8
C2SP2	82.7	8.3	42937	16.1
C3SP1N	85.3	8.5	46801	16.4
C3SP2	85.1	8.4	44860	16.6
C4SP1	74.3	8.2	48381	19.5
C4SP2	74.7	8.3	43563	17.9
C5SP1	82.7	7.4	41068	17.2
C5SP2	82.8	7.8	36863	14.8
C6SP1	75.5	7.7	39395	17.0
C7SP1	77.1	7.2	41630	18.6
C7SP2	77.5	7.2	35678	15.9
C7SP3N	77.6	7.5	39177	16.8
C8SP1	77.8	7.2	41019	18.9
C8SP2	77.9	7.5	37042	16.0
C8SP3N	78.4	7.6	41481	18.6
C9SP1	82.3	7.9	40126	15.7
C9SP2N	81.5	7.9	40082	15.6

Table F8: Individual flat ring flexure test data for *P. bambusoides*

Flat Ring Flexure (*P. bambusoides*)						
Table 2.1 and 2.2 Full specimen						
Specimen ID	**Culm**	***D* (mm)**	***t* (mm)**	**β**	**α**	**$f_{r\alpha}$ (MPa)**
PB2H5	2	88.4	7.3	0.00	1.00	23.1
PB2H3	2	88.7	7.5	0.00	1.00	21.1
PB2H2	2	88.7	7.5	0.00	1.00	20.1
PB2G6	2	92.3	7.8	0.00	1.00	18.2
PB2G5	2	92.3	7.7	0.00	1.00	19.5
PB2F4	2	87.6	8.1	0.00	1.00	16.0
PB2F3	2	90.7	8.1	0.00	1.00	18.9
PB2E3	2	88.3	9.2	0.00	1.00	20.6
PB2D3	2	89.5	10.2	0.00	1.00	16.8
PB2A3	2	91.4	13.8	0.00	1.00	19.6
PB2A2	2	92.4	14.3	0.00	1.00	15.1
PB3B1	3	100.4	7.8	0.00	1.00	13.6
PB3B2	3	99.2	7.7	0.00	1.00	13.9
PB3B4	3	97.6	7.6	0.00	1.00	13.6
PB3B5	3	97.2	7.4	0.00	1.00	13.9
PB3C2	3	96.6	7.4	0.00	1.00	14.7
PB3C4	3	98.2	7.5	0.00	1.00	13.5
PB3C5	3	98.5	7.2	0.00	1.00	15.5
PB3C6	3	99.5	7.8	0.00	1.00	14.6
PB3D1	3	100.6	7.8	0.00	1.00	10.9
PB3D2	3	100.5	7.4	0.00	1.00	13.5
PB3D3	3	100.9	7.3	0.00	1.00	15.0
PB3D4	3	100.7	7.6	0.00	1.00	13.9
PB3D5	3	100.4	7.7	0.00	1.00	10.3
PB3E2	3	99.2	7.1	0.00	1.00	11.7
PB3E3	3	99.4	7.3	0.00	1.00	14.0
PB3E4	3	100.1	7.5	0.00	1.00	12.7

Table F9: Individual compression parallel to fibers test data for *P. bambusoides*

Full-culm Compression Parallel to Fibers (*P. bambusoides*)					
Table 2.2					
Specimen ID	**Culm**	**D (mm)**	**t (mm)**	**P (N)**	**$f_{c,0}$ (MPa)**
PB1B1	1	94.0	6.6	85838	47.2
PB1C5	1	90.8	6.1	76028	46.6
PB2D2	2	89.0	10.3	125078	49.2
PB2E1	2	88.7	9.0	122625	54.6
PB2F1	2	88.6	8.1	105458	51.3
PB3C1	3	63.7	7.9	117720	85.1
PB3E1	3	64.4	6.7	98100	81.0

Table F10: Individual shear parallel to fibers test data for *P. bambusoides*

Full-culm Shear Parallel to Fibers (*P. bambusoides*)					
Table 2.2					
Specimen ID	**Culm**	***D* (mm)**	***t* (mm)**	**P (N)**	**f_v (MPa)**
PB1B2	1	92.6	6.5	30902	12.1
PB1C6	1	91.0	6.1	27468	11.5
PB3B6	3	97.6	7.8	41693	13.6
PB2D1	2	89.3	10.0	52484	14.5
PB2E2	2	88.4	9.0	48069	14.6
PB2F2	2	87.9	7.8	58762	21.3

Table F11: Individual clipped flat ring flexure test data for *P. bambusoides*

Table 3.2 Clipped specimen (*P. bambusoides*)						
Specimen ID	**Culm**	***D* (mm)**	***t* (mm)**	**β**	**α**	**f_r (MPa)**
PB1C4	1	92.4	6.2	0.00	0.29	18.7
PB2C5	2	88.5	11.1	0.00	0.29	21.6
PB3F4	3	99.6	7.0	0.00	0.20	28.0
PB3F9	3	100.1	8.6	0.00	0.22	18.1
PB1C7	1	91.5	6.0	0.25	0.26	14.8
PB2C4	2	88.4	11.0	0.25	0.24	10.4
PB3F2	3	100.3	7.3	0.40	0.21	12.4
PB2C3	2	88.6	10.9	0.50	0.28	19.1
PB3F1	3	100.7	7.5	0.60	0.20	21.4
PB3F6	3	98.7	7.1	0.60	0.20	16.0
PB2C2	2	88.6	10.8	0.75	0.28	15.5
PB1C9	1	91.1	6.0	0.75	0.31	16.1
PB3E5	3	100.4	7.6	0.80	0.21	18.7
PB3F5	3	99.0	7.0	0.80	0.20	27.3

Table F12: Individual flat ring flexure test data for *P. nigra*

Flat Ring Flexure (*P. nigra*)						
Table 2.1 and 2.2 Full specimen						
Specimen ID	**Culm**	***D* (mm)**	***t* (mm)**	**β**	**α**	**$f_{r\alpha}$ (MPa)**
PN2D2	2	91.4	8.1	0.00	1.00	17.1
PN2D1	2	92.0	8.2	0.00	1.00	20.7
PN2C6	2	92.8	8.2	0.00	1.00	14.1
PN2C4	2	92.5	8.1	0.00	1.00	11.7
PN2B7	2	96.0	8.7	0.00	1.00	14.5
PN2B6	2	96.0	8.6	0.00	1.00	19.5
PN2B4	2	96.1	8.4	0.00	1.00	20.2
PN2A7	2	99.6	9.1	0.00	1.00	17.0
PN2A6	2	99.1	8.9	0.00	1.00	18.7
PN2D11-2	2	89.4	7.6	0.00	1.00	13.9
PN2D11-3	2	89.3	7.5	0.00	1.00	19.8
PN2D11-4	2	89.4	7.6	0.00	1.00	15.1
PN3B3	3	93.6	5.7	0.00	1.00	13.8
PN3B4	3	93.7	5.8	0.00	1.00	15.4
PN3B5	3	94.2	5.8	0.00	1.00	14.7
PN3B7	3	94.3	5.7	0.00	1.00	12.0
PN3B8	3	93.9	5.8	0.00	1.00	16.3
PN3B9	3	94.6	5.8	0.00	1.00	14.9
PN3B10	3	94.3	6.1	0.00	1.00	15.7
PN3B11	3	94.9	6.0	0.00	1.00	13.6
PN3B12	3	94.8	6.4	0.00	1.00	15.2
PN3D3	3	92.7	5.7	0.00	1.00	13.1
PN3D4	3	93.2	6.0	0.00	1.00	14.2
PN3D5	3	93.1	5.7	0.00	1.00	14.9
PN3D6	3	93.0	5.6	0.00	1.00	14.7
PN3D7	3	92.9	5.7	0.00	1.00	14.6
PN3D8	3	92.8	5.6	0.00	1.00	14.3
PN3D9	3	92.3	5.6	0.00	1.00	15.4
PN3D10	3	92.3	5.6	0.00	1.00	16.4
PN3D11	3	92.1	5.6	0.00	1.00	16.7
PN3D13	3	91.5	6.1	0.00	1.00	16.0

Table F13: Individual compression parallel to fibers test data for *P. nigra*

Table 2.2 Full-culm Compression Parallel to Fibers (*P. nigra*)					
Specimen ID	**Culm**	***D* (mm)**	***t* (mm)**	**P (N)**	**$f_{c,0}$ (MPa)**
PN1B1	1	96.3	8.1	88290	39.1
PN1C1	1	95.6	8.5	85838	37.1
PN1D1	1	90.0	7.7	79706	40.0
PN3C12	3	93.4	5.8	78480	49.3
PN3C13	3	92.6	7.0	76028	40.6
PN3D1	3	94.0	5.8	80933	50.3
PN3D2	3	93.2	5.7	66218	42.3
PN2B1	2	98.1	8.6	122625	50.5
PN2B3	2	96.3	8.4	122625	53.1
PN2C1	2	94.8	8.4	112815	49.5

Table F14: Individual shear parallel to fibers test data for *P. nigra*

Table 2.2 Full-culm Shear Parallel to Fibers (*P. nigra*)					
Specimen ID	**Culm**	***D* (mm)**	***t* (mm)**	**P (N)**	**f_v (MPa)**
PN1B2	1	95.8	7.9	39240	13.0
PN1C2	1	92.4	7.5	34335	11.9
PN1D2	1	88.9	7.5	33354	12.0
PN2A1	2	99.4	8.7	44734	12.2
PN2B2	2	96.9	8.5	54544	15.8
PN2C2	2	93.7	8.2	53955	17.2
PN2C3	2	93.3	8.2	56506	18.3
PN3B1	3	93.4	5.7	32373	15.5
PN3B2	3	93.9	5.6	31883	15.5

Table F15: Individual clipped flat ring flexure test data for *P. nigra*

Table 3.2 Clipped specimen (*P. nigra*)						
Specimen ID	**Culm**	***D* (mm)**	***t* (mm)**	**β**	**α**	**f_r (MPa)**
PN1C7	1	90.8	7.5	0.00	0.26	15.2
PN2D9	2	89.6	7.6	0.00	0.30	21.4
PN3C4	3	93.3	5.7	0.00	0.25	18.2
PN3C8	3	92.7	5.8	0.00	0.25	22.1
PN1C8	1	91.4	7.5	0.25	0.25	16.7
PN2D8	2	90.8	7.6	0.25	0.35	11.5
PN3C3	3	93.1	5.8	0.25	0.24	18.4
PN3C7	3	93.5	5.7	0.25	0.25	20.1
PN3C10	3	93.4	5.8	0.50	0.24	20.7
PN1C9	1	91.4	7.5	0.50	0.27	18.5
PN3C2	3	93.3	5.9	0.50	0.25	20.1
PN3C6	3	93.2	5.8	0.50	0.24	20.2
PN1C10	1	91.5	7.8	0.75	0.25	22.1
PN3C1	3	93.4	6.1	0.75	0.24	22.4
PN3C5	3	93.3	5.7	0.75	0.25	20.2
PN3C9	3	92.9	5.8	0.75	0.25	14.9

Table F16: Individual flat ring flexure test data for *P. meyeri*

Flat Ring Flexure (*P. meyeri*)						
Table 2.1 and 2.2 Full specimen						
Specimen ID	**Culm**	***D* (mm)**	***t* (mm)**	**β**	**α**	**$f_{r\alpha}$ (MPa)**
PM1D12	1	54.2	4.6	0.00	1.00	17.1
PM1C6	1	57.5	4.7	0.00	1.00	18.0
PM1C12	1	55.8	5.0	0.00	1.00	13.7
PM1B6	1	58.6	5.1	0.00	1.00	17.0
PM1B2	1	58.9	5.3	0.00	1.00	19.1
PM1B13	1	58.0	5.0	0.00	1.00	18.1
PM1B12	1	58.3	5.3	0.00	1.00	13.8
PM1B11	1	58.4	5.0	0.00	1.00	14.5
PM1B10	1	58.4	4.9	0.00	1.00	14.7
PM2F4	2	72.8	6.2	0.00	1.00	12.6
PM2F2	2	72.8	6.3	0.00	1.00	19.5
PM2E8	2	74.1	6.8	0.00	1.00	17.7
PM2E7	2	73.4	6.9	0.00	1.00	21.4
PM2D8	2	73.9	7.0	0.00	1.00	20.4
PM2D7	2	74.4	7.0	0.00	1.00	24.4
PM2D6	2	74.3	6.8	0.00	1.00	21.5
PM2D5	2	74.1	6.9	0.00	1.00	22.9
PM2D4	2	74.3	6.8	0.00	1.00	22.5
PM2D3	2	74.8	6.9	0.00	1.00	21.4

Table F16 (continued)

Flat Ring Flexure (*P. meyeri*)						
Table 2.1 and 2.2 Full specimen						
Specimen ID	**Culm**	***D* (mm)**	***t* (mm)**	**β**	**α**	**$f_{r\alpha}$ (MPa)**
PM2C5	2	74.0	6.9	0.00	1.00	21.8
PM2C4	2	74.2	7.0	0.00	1.00	20.4
PM2C3	2	74.2	6.9	0.00	1.00	21.8
PM2B7	2	73.6	7.0	0.00	1.00	21.3
PM2B6	2	73.6	7.0	0.00	1.00	25.1
PM2A7	2	72.1	7.2	0.00	1.00	23.1
PM2B1-2	2	75.2	7.3	0.00	1.00	14.7
PM3A2	3	61.4	9.4	0.00	1.00	24.0
PM3A3	3	61.7	9.3	0.00	1.00	20.5
PM3B1	3	63.1	9.2	0.00	1.00	20.3
PM3B2	3	63.4	8.6	0.00	1.00	25.6
PM3B3	3	62.8	8.5	0.00	1.00	25.5
PM3B4	3	61.3	8.6	0.00	1.00	21.9
PM3C2	3	62.9	7.8	0.00	1.00	21.7
PM3C3	3	62.2	7.6	0.00	1.00	23.9
PM3C4	3	61.5	7.7	0.00	1.00	22.3
PM3C5	3	62.1	7.7	0.00	1.00	20.1
PM3C6	3	61.9	7.8	0.00	1.00	24.5
PM3C7	3	62.0	8.2	0.00	1.00	22.4
PM3G6	3	61.8	5.9	0.00	1.00	18.7
PM3G7	3	61.8	5.9	0.00	1.00	16.7
PM3G8	3	61.6	5.9	0.00	1.00	16.4
PM3G9	3	61.8	5.7	0.00	1.00	18.6
PM3G10	3	61.5	5.7	0.00	1.00	19.2
PM3G11	3	61.6	5.9	0.00	1.00	19.4
PM3H1	3	61.4	5.8	0.00	1.00	16.7
PM3H2	3	61.4	5.7	0.00	1.00	20.1
PM3H3	3	61.6	5.9	0.00	1.00	18.2
PM3H4	3	61.6	5.8	0.00	1.00	20.6
PM3H5	3	61.7	6.2	0.00	1.00	21.6

Table F17: Individual compression parallel to fibers test data for *P. meyeri*

Table 2.2 Full-culm Compression Parallel to Fibers (*P. meyeri*)					
Specimen ID	**Culm**	***D* (mm)**	***t* (mm)**	**P (N)**	**$f_{c,0}$ (MPa)**
PM1B7	1	58.7	4.9	42183	50.8
PM1C10	1	56.8	4.6	46107	60.7
PM1D5	1	55.3	4.4	44145	62.2
PM2A1	2	72.9	7.7	80933	51.5
PM2C1	2	74.6	6.8	78480	54.3
PM2D1	2	74.9	6.8	63765	43.8
PM3C1	3	63.7	7.9	79706	57.6
PM3D9	3	62.4	7.1	78480	63.2
PM3E1	3	64.4	6.7	71123	58.7
PM3F11	3	61.6	6.5	61313	54.7

Table F18: Individual shear parallel to fibers test data for *P. meyeri*

Table 2.2 Full-culm Shear Parallel to Fibers (*P. meyeri*)					
Specimen ID	**Culm**	***D* (mm)**	***t* (mm)**	**P (N)**	**f_v (MPa)**
PM1B8	1	58.0	4.9	20111	17.0
PM1B9	1	58.3	4.9	18639	16.0
PM1C11	1	56.1	4.7	19620	17.0
PM1D6	1	55.5	4.5	18149	16.9
PM2A2	2	71.6	7.1	34826	17.6
PM2D2	2	74.4	7.1	31883	15.1
PM2E1	2	72.7	6.7	31883	16.0
PM3A1	3	62.3	9.3	37769	15.1
PM3B5	3	61.6	8.4	34335	15.1

Table F19: Individual clipped flat ring flexure test data for *P. meyeri*

Table 3.2 Clipped specimen (*P. meyeri*)						
Specimen ID	**Culm**	***D* (mm)**	***t* (mm)**	**β**	**α**	**f_r (MPa)**
PM2A6	2	71.5	7.2	0.00	0.30	27.8
PM2E6	2	73.9	6.5	0.00	0.26	32.2
PM3F4	3	63.0	6.3	0.00	0.25	27.3
PM3F8	3	61.7	6.3	0.00	0.23	24.7
PM2E5	2	73.2	6.7	0.25	0.33	12.3
PM3F3	3	63.0	6.5	0.25	0.25	22.0
PM3F7	3	61.7	6.2	0.25	0.25	18.2
PM1C7	1	57.4	4.7	0.50	0.22	17.8
PM2A4	2	71.6	7.1	0.50	0.32	14.1
PM2E4	2	73.9	6.6	0.50	0.30	9.1
PM3F2	3	63.3	6.6	0.50	0.24	20.6
PM3F6	3	62.1	6.4	0.50	0.24	16.5
PM3F10	3	61.6	6.4	0.50	0.24	18.6
PM2A3	2	71.3	7.1	0.75	0.28	20.5
PM2E3	2	73.0	7.0	0.75	0.27	16.5
PM3F1	3	62.6	7.1	0.75	0.24	25.9
PM3F5	3	62.1	6.2	0.75	0.25	17.1
PM3F9	3	61.6	6.2	0.75	0.24	17.4
PM1B1	1	58.6	5.8	0.75	0.29	15.1
PM1C8	1	57.3	4.7	0.75	0.23	20.9

Table F20: Individual flat ring flexure test data for *B. stenostachya*

Flat Ring Flexure (*B. stenostachya*)						
Table 2.1 and 2.2 Full specimen						
Specimen ID	**Culm**	***D* (mm)**	***t* (mm)**	**β**	**α**	**$f_{r\alpha}$ (MPa)**
BS1A8	1	84.1	8.6	0.00	1.00	9.2
BS1E3	1	80.8	10.3	0.00	1.00	10.9
BS1D4	1	80.8	9.4	0.00	1.00	6.7
BS1D2	1	81.4	9.6	0.00	1.00	10.5
BS1C5	1	82.2	9.0	0.00	1.00	10.8
BS1C4	1	82.4	8.8	0.00	1.00	10.0
BS1C3	1	83.1	8.8	0.00	1.00	11.4
BS1F3	1	81.0	11.2	0.00	1.00	7.5
BS1F2	1	81.0	10.9	0.00	1.00	7.4
BS1F1	1	81.2	10.6	0.00	1.00	10.3
BS1D8	1	80.0	10.0	0.00	1.00	7.9
BS1D1-2	1	82.0	9.7	0.00	1.00	9.6
BS1D1-3	1	81.2	9.8	0.00	1.00	6.9
BS1D1-4	1	84.1	10.3	0.00	1.00	10.0
BS2F6	2	82.2	9.4	0.00	1.00	11.1
BS2C4	2	78.3	11.5	0.00	1.00	11.9
BS2C3	2	78.6	11.6	0.00	1.00	9.2
BS2C2	2	78.5	12.0	0.00	1.00	9.2
BS2C1	2	79.8	12.5	0.00	1.00	9.0
BS2B4	2	80.9	12.6	0.00	1.00	7.4
BS2C6-1	2	82.7	16.3	0.00	1.00	8.8
BS2C6-4	2	80.6	11.7	0.00	1.00	9.0
BS3A1	3	74.4	21.0	0.00	1.00	10.9
BS3B1	3	74.8	20.1	0.00	1.00	8.3
BS3B2	3	73.5	19.3	0.00	1.00	9.0
BS3B3	3	73.9	20.2	0.00	1.00	9.4
BS3B4	3	73.6	19.5	0.00	1.00	10.6
BS3B5	3	73.1	20.3	0.00	1.00	8.9
BS3B6	3	72.7	20.3	0.00	1.00	8.8
BS3B7	3	72.8	20.2	0.00	1.00	9.1
BS3B8	3	72.6	20.2	0.00	1.00	9.3
BS3B9	3	73.0	20.3	0.00	1.00	9.8
BS3D3	3	71.9	18.2	0.00	1.00	10.3
BS3D5	3	71.3	18.3	0.00	1.00	9.6
BS3D6	3	71.3	18.3	0.00	1.00	11.7

Table F20 (continued)

Flat Ring Flexure (*B. stenostachya*)						
Table 2.1 and 2.2 Full specimen						
Specimen ID	**Culm**	***D* (mm)**	***t* (mm)**	**β**	**α**	**$f_{r\alpha}$ (MPa)**
BS3D7	3	71.1	18.0	0.00	1.00	8.9
BS3D8	3	71.5	18.4	0.00	1.00	9.7
BS3D9	3	71.5	18.1	0.00	1.00	9.1
BS3D10	3	71.8	18.3	0.00	1.00	9.5

Table F21: Individual compression parallel to fibers test data for *B. stenostachya*

Full-culm Compression Parallel to Fibers (*B. stenostachya*)					
Table 2.2					
Specimen ID	**Culm**	***D* (mm)**	***t* (mm)**	**P (N)**	**$f_{c,0}$ (MPa)**
BS1A7	1	86.8	8.5	98100	47.0
BS1B7	1	83.7	9.8	105458	46.5
BS2A1	2	77.7	12.7	103005	39.8
BS2B1	2	78.7	11.6	103005	42.1
BS2C5	2	79.2	11.7	95648	38.5
BS3B10	3	74.6	20.5	156960	45.1
BS3F3	3	72.7	18.7	171675	54.1
BS3G1	3	70.3	16.6	147150	52.5
BS3G2	3	74.5	17.7	154508	48.8

Table F22: Individual shear parallel to fibers test data for *B. stenostachya*

Full-culm Shear Parallel to Fibers (*B. stenostachya*)					
Table 2.2					
Specimen ID	**Culm**	***D* (mm)**	***t* (mm)**	**P (N)**	**f_v (MPa)**
BS1B6	1	84.3	9.5	24525	7.7
BS1C1	1	82.6	9.1	29430	9.2
BS2B2	1	79.1	11.9	37769	10.2
BS2D1	1	79.8	11.4	40908	11.0
BS2F1	2	81.3	9.7	33256	10.7
BS3F1	2	70.0	16.6	48069	9.9
BS3F2	2	70.3	16.9	50522	10.5

Table F23: Individual clipped flat ring flexure test data for *B. stenostachya*

Table 3.2 Clipped specimen (*B. stenostachya*)						
Specimen ID	**Culm**	***D* (mm)**	***t* (mm)**	**β**	**α**	**f_r (MPa)**
BS1D3	1	81.3	9.2	0.00	0.24	13.2
BS2E4	2	81.4	10.4	0.00	0.30	15.6
BS3E3	3	71.9	17.9	0.00	0.19	17.2
BS3E8	3	70.5	17.9	0.00	0.19	17.1
BS3E2	3	72.7	18.1	0.20	0.19	12.7
BS3E7	3	70.7	17.8	0.20	0.19	11.3
BS2E3	2	80.9	10.0	0.25	0.28	10.9
BS1D5	1	80.1	9.4	0.25	0.24	6.7
BS3E1	3	74.2	18.4	0.40	0.19	8.0
BS3E6	3	70.8	17.9	0.40	0.19	8.5
BS2E2	2	79.6	9.8	0.50	0.28	7.5
BS3D12	3	73.5	18.5	0.60	0.19	8.3
BS3E5	3	71.1	17.9	0.60	0.18	9.5
BS1D7	1	79.9	9.9	0.75	0.24	8.2
BS2E1	2	79.2	10.2	0.75	0.27	12.4
BS3D11	3	72.6	18.6	0.80	0.19	12.5
BS3E4	3	71.3	17.7	0.80	0.19	15.0

Table F24: Individual flat ring flexure test data for *D. barbatus*

Flat Ring Flexure (*D. barbatus*)						
Table 2.1 and 2.2 Full specimen						
Specimen ID	**Culm**	***D* (mm)**	***t* (mm)**	**β**	**α**	**$f_{r\alpha}$ (MPa)**
M1-02-01	2	78.5	11.0	0.00	1.00	8.3
M1-02-02	2	78.5	9.3	0.00	1.00	8.0
M3-04-01	4	79.5	7.5	0.00	1.00	10.6
M4-04-01	4	78.8	10.5	0.00	1.00	9.2
M13-01-02	1	79.5	8.3	0.00	1.00	6.5
M14-01-01	1	76.3	15.8	0.00	1.00	6.0
M11-05-01	5	80.3	18.7	0.00	1.00	7.1

Table F25: Individual compression parallel to fibers test data for *D. barbatus*

Full-culm Compression Parallel to Fibers (*D. barbatus*)					
Table 2.2					
Specimen ID	**Culm**	***D* (mm)**	***t* (mm)**	**P (N)**	**$f_{c,0}$ (MPa)**
M1-03-1	3	79.0	9.7	73385	34.9
M2-01-2	1	78.1	5.6	37011	29.3
M3-01-1	1	79.5	7.2	57092	34.8
M4-02-1	2	77.7	9.5	78953	38.7
M5-02-1	2	80.1	9.0	60010	29.9
M3-04-01(N)	4	82.4	9.1	96212	46.1
M4-04-01(N)	4	80.6	10.9	92641	38.8
M10-02-01(N)	2	81.3	9.4	93056	43.7
M11-01-01(N)	1	82.2	12.5	82598	30.2
M11-02-01(N)	2	82.3	13.5	102596	35.2
(N) - Includes Node					

Table F26: Individual shear parallel to fibers test data for *D.barbatus*

Full-culm Shear Parallel to Fibers (*D. barbatus*)						
Table 2.1 and 2.2 (density)						
Specimen ID	**Culm**	***D* (mm)**	***t* (mm)**	**P (N)**	**f_v (MPa)**	**ρ_{12} (g/cm^3)**
M1-2-2	2	77.7	8.8	36500	13.5	0.528
M3-1-2	1	79.9	7.3	28300	12.9	0.879
M3-2-2	2	79.9	7.5	29600	13.0	0.879
M4-2-2	2	75.8	8.9	30700	11.3	0.898
M4-3-2	3	76.6	9.2	33900	12.1	0.898
M5-1-1	1	70.1	9.8	26300	8.8	0.546
M5-3-1	3	79.8	9.4	29000	10.4	0.546
M1-5-1	5	77.8	8.1	27200	11.3	0.528
M10-1-1	1	80.3	9.1	35200	13.0	0.689
M11-3-1	3	81.6	15.7	43200	9.3	0.596
M11-4-1	4	83.1	17.7	49600	9.3	0.596

Bibliography

Abrahamsen, P. (1997). A review of Gaussian Random Fields and Correlation Functions. *Tech. Rep, 917 Norwegian Computing Center, Box 114, Blindern, N0314 Oslo, Norway*.

Agarwal, M., and Mehra, R. (2014). Review of Matrix Decomposition Techniques for Signal Processing Applications. *Int. Journal of Engineering Research and Applications* SSN : 2248-9622, Vol. 4, Issue 1(Version 4), pp.90-93

AIS (Asociacon Colombiana de Ingenieria Sismica), (2010). NSR-10-Reglamento colombiano de construccion sismo resistente – Capitulo G.12: Estructuras de guadua. AIS, Bogota, Colombia.

Akinbade, Y., Harries, K.A., Sharma, B., Nettleship, I. and Ramage, M. (2020). Variation of through-culm wall morphology in P. edulis bamboo strips used in glue-laminated bamboo beams, *Construction and Building Materials*, 232**,** 117248.

Akinbade, Y., Harries, K.A., Flower, C., Nettleship, I., Papadopoulos, C., and Platt, S.P. (2019). Through-Culm Wall Mechanical Behaviour of Bamboo, *Construction and Building Materials*, Vol. 216, pp 485-495.

Akinlabi, E. T., Anane-Fenin, K., and Akwada, D. R. (2017). Bamboo taxonomy and distribution across the globe. In *Bamboo* (pp. 1-37). Springer, Cham.

Alder, R.J. and Taylor, J.E. (2010). *Random Fields and Geometry*, Springer Monographs in Mathematics, New York

Amada S., and Untao, S. (2001). Fracture properties of bamboo. *Composites Part B* 32, 451.

Amada, S. (1995). Hierarchical gradient structures of bamboo, barley and corn. *MRS Bulletin*, 20, 35-36

Amada, S., Ichikawa, Y., Munekata, T., Nagase,Y. and Shimizu,H.(1997). Fiber texture and mechanical graded structure of bamboo. *Compos. Part B-Eng*. 28, 13–20.

Amada, S., Munekata, T., Nagase, Y., Ichikawa, Y., Kirigai, A., and Yang, Z. (1996). The mechanical structures of bamboos in viewpoint of functionally gradient and composite materials. *Journal of Composite Materials*, 30(7), 800–819.

Arce-Villalobos, O.A. (1993). Fundamentals of the Design of Bamboo Structures (Doctoral dissertation). Retrieved from Eindhoven University of Technology website: http://alexandria.tue.nl/extra3/proefschrift/PRF9B/9303473.pdf

Archila, H., Kaminski, S., Trujillo, D., Zea Escamilla, E. and Harries, K.A. (2018). Bamboo Reinforced Concrete – a Critical Review, *Materials and Structures* 51:102.

Bamboo Phylogeny Group [BPG]. (2012). An updated tribal and subtribal classification of the bamboos (Poaceae: Bambusoideae). In: Gielis J, Potters G (eds) *Proceedings of the 9th world bamboo congress, Antwerp, Belgium*, 10–12 Apr 2012, pp 3–27

Bao, G., and Wang,L. (1995). Multiple cracking in functionally graded ceramic/metal coatings. *Int. J. Solids. Struct.* 32(19), 2853–2871

Bower, A. F. (2009). *Applied mechanics of solids*. CRC press.

Burlayenko, V. N., and Sadowski, T. (2019). Free vibrations and static analysis of functionally graded sandwich plates with three-dimensional finite elements. *Meccanica*, 1-18.

Canavan, S., Richardson, D. M., Visser, V., Le Roux, J. J., Vorontsova, M. S., and Wilson, J. R. (2016). The global distribution of bamboos: assessing correlates of introduction and invasion. *AoB Plants*, *9*(1), plw078.

Caro, S., Castillo, D., and Sanchez-Silva, M. (2014). Methodology for Modeling the Uncertainty of Material Properties in Asphalt Pavements. *ASCE Journal of Materials in Civil Engineering*, Vol. 26, No. 3, pp 440-448.

Chen G., Luo H., Yang H., Zhang, T. and Li, S. (2018). Water effects on the deformation and fracture behaviors of the multi-scaled cellular fibrous bamboo. *Acta Biomaterialia* 65, 203-215

Chiles, J.P, and Delfiner.P. (2012). *Geostastistics, Modeling spatial uncertainty* Wiley, New Jersey and Canada

Christensen, R. M. (2012). *Mechanics of composite materials*. Courier Corporation.

Chung, K. F., and Yu, W. K. (2002). Mechanical properties of structural bamboo for bamboo scaffoldings. *Engineering structures*, *24*(4), 429-442.

Clark L.G., Londoño X., and Ruiz-Sanchez E. (2015). Bamboo Taxonomy and Habitat. In: Liese W., Köhl M. (eds) Bamboo. Tropical Forestry, vol 10. Springer, Cham

Correal, D., Francisco, J., and Arbeláez, C. (2010). Influence of age and height position on Colombian Guadua angustifolia bamboo mechanical properties. *Maderas. Ciencia y tecnología*, 12(2), 105-113.

Cousins, W. J., Armstrong, R. W., and Robinson, W. H. (1975). Young's modulus of lignin from a continuous indentation test. *Journal of Materials Science*, *10*(10), 1655-1658.

Cruz, M. L. S. (2002). Caracteriza*a*o fisicae mec*a*nica de colmosinteiros do bambu da esp*e*ciephyllostachysaurea: comportamento*a* flambagem. *M.S. thesis, Pontificia Universidade Catolica - Rio de Janeiro,Brazil* (in Portuguese).

Dixon, P.G., Ahvenainen, P., Aijazi, A.N., Chen, S.H., Lin, S., Augusciak, P.K., Borrega, M., Svedstrom, K. and Dixon, L.J. (2015). Comparison of the structure and flexural properties of Moso, Guadua and Tre Gai bamboo, *Construction and Building Materials*, 90, 11-17.

Dixon, P.G., and Gibson, L.J. (2014). The structure and mechanics of Moso bamboo material. *Journal of the Royal Society Interface* Vol 11: 20140321.

Dransfield, S. (1992). The bamboos of Sabah. *Sabah forest records no. 14. Forestry Department*, Sabah, Malaysia, p 94

Dransfield, S. (1998). *Valiha* and *Cathariostachys*, two new bamboo genera (Gramineae-Bambusoideae) from Madagascar. *Kew Bull* 53:375–397

Dransfield S, and Widjaja EA (eds) (1995). Plant resources of South-East Asia No. 7: bamboos. *Backhuys, Leiden*, p 189

El-Kadi, A.I., and Williams, S.A. (2000). Generating two-dimensional fields of autocorrelated, normally distributed parameters by the matrix decomposition method. *Ground Water*, Vol. 38, No. 4, pp 530-532.

Fang, C. H., Jiang, Z. H., Sun, Z. J., Liu, H. R., Zhang, X. B., Zhang, R., and Fei, B. H. (2018). An overview on bamboo culm flattening. *Construction and Building Materials*, *171*, 65-74.

Food and Agriculture Organization of the United Nations, FAO. (2007). World Bamboo Resources. *Non-Wood Forest Products*, Rome.

García, J. J., Rangel, C., and Ghavami, K. (2012). Experiments with rings to determine the anisotropic elastic constants of bamboo. *Construction and building materials*, *31*, 52-57.

Gauss, C., Savastano Jr, H., and Harries, K. A. (2019). Use of ISO 22157 mechanical test methods and the characterisation of Brazilian P. edulis bamboo. *Construction and Building Materials*, *228*, 116728.

Ghavami, K. and Marinho, A.B. (2005). Propriedades físicas e mecânicas do colmo inteiro do bambu da espécie Guadua angustifolia. *Revista Brasileira de Engenharia Agrícola e Ambiental*, 9(1), 107-114. (in Portuguese)

Ghavami, K., Rodriques, C.S., and Paciornik, S., (2003). Bamboo: Functionally Graded Composite Material. *Asian Journal of Civil Engineering (Building and Housing)*, 4(1), 1-10.

Ghiocel, D. M., and Ghanem, R. G. (2009). Stochastic finite-element analysis of seismic soil–structure interaction. Journal of Engineering Mechanics, 128(1), 66-77.

Grass Phylogeny Working Group [GPWG] II (2012). New grass phylogeny resolves deep evolutionary relationships and discovers C4 origins.. *New Phytol* 193:304–312

Habibi, M.K., and Lu, Y. (2014). Crack Propagation in Bamboo's Hierarchical Cellular Structure. *Sci. Rep*. 4, 5598; DOI:10.1038/srep05598

Habibi, M.K., Samaei, A.T., Gheshlaghi, B., Lu, J. and Lu, Y. (2015). Asymmetric flexural behavior from bamboo's functionally graded hierarchical structure: Underlying mechanisms. *Acta Biomaterialia*, 16, 178-186.

Halpin, J.C., and Kardos, J.L. (1976). The Halpin-Tsai Equations: A Review. *Polymer Engineering and Science* 16(5), 344-352

Harries, K.A., Sharma, B. and Richard, M.J. (2012). Structural Use of Full Culm Bamboo: The Path to Standardization. *International Journal of Architecture, Engineering and Construction* 1, 66–75.

Harries, K.A., Bumstead, J., Richard, M.J. and Trujillo, D. (2017). Geometric and Material Effects on Bamboo Buckling Behaviour, *ICE Structures and Buildings Themed issue on bamboo in structures and buildings*, Vol. 170, No. 4. pp 236-249

Hewitt, R.L. and Malherbe, M.C. (1970). An Approximation for the Longitudinal Shear Modulus of Continuous Fiber Composites. *Composite Materials*, 4, 280.

Hoaglin, D.C. (2003). John W. Tukey and Data Analysis, *Statistical Science* 18(3), 311-318.

Holttum R.E. (1956). The classification of bamboos. *Phytomorphology* 6:73–90

ISO (2004a). *ISO 22156: Bamboo - Structural design*. International Standards Organization, Geneva, Switzerland.

ISO (2018). *ISO 19624*: *Bamboo structures -- Grading of bamboo culms -- Basic principles and procedures*. International Standards Organization, Geneva, Switzerland.

ISO (2019). *ISO 22157: Bamboo structures -- Determination of physical and mechanical properties of bamboo culms.* International Standards Organization, Geneva, Switzerland.

Jain, S. (1992). Mechanical behavior of bamboo and bamboo composite. *J. Mat. Sci.*, 27, 4598-4604. 'Quoted in Amada *et al.* (1997)'

Janssen, J., (1981). Bamboo in Building Structures. *Doctoral Thesis*. Eindhoven University of Technology, Netherlands.

Janssen, J.A. (2000). Designing and Building with Bamboo. *International Network for Bamboo and Rattan*, Technical Report No. 20

Judziewicz, E.J., Clark, L.G., Londoño, X., and Stern, M.J. (1999). American bamboos. *Smithsonian Institution*, Washington, DC, p 392

Kim, H. (2005). Spatial Variability of Soils: Stiffness and Strength. *PhD Dissertation*, Georgia Tech.

Kim, J. H., and Paulino, G.H. (2002). Isoparametric Graded Finite Elements for Nonhomogeneous Isotropic and Orthotropic Materials. *Journal of Applied Mechanics.* Vol. 69/513

Krause, J.Q., Andrade Silva, F., Ghavami, K., Gomes, O.F.M. and Toledo Filho, R.D. (2016). On the influence of Dendrocalamus giganteus bamboo microstructure on its mechanical behavior. Construction and Building Materials, 127, 199-209.

Li, H., Shen, S. (2011). The mechanical properties of bamboo and vascular bundles. *J. Mater. Res*., Vol. 26, No. 21.

Li, S. H., Fu, S.Y., Zhou, B. L., Zeng, A.Y. and Bao, X. R. (1994). Reformed bamboo and reformed bamboo/aluminum composite. *J. Mat. Sci.* 29, 5990-5996

Liese, W. (1987). Research on bamboo. *Wood Science and Technology*, *21*(3), 189-209.

Liese, W. (1998). The anatomy of bamboo culms. *International Network for Bamboo and Rattans (INBAR)*, Beijing, Tech rep no. 18

Liese, W., and Weiner, G. (1996). Ageing of bamboo culms. A review. *Wood Science and Technology*, *30*(2), 77-89.

Liese, W., and Kohl, M. (2015). *Bamboo: the plant and its uses*. Tropical Forestry. Springer, Cham; http://link.springer.com/10.1007/978-3-319-14133-6

Limaye, V.D., (1952). Strength of bamboo (Dendr. strictus). *Indian Forest Records, New Series, Timber Mechanics* 1 (1), 17. 'Quoted in Janssen (1981)'.

Low, I. M., Che, Z. Y. and Latella, B. A. (2006). Mapping the structure, composition and mechanical properties of bamboo. *J. Mater. Res*. 21, 1969–1976.

Lu, X., Wang, K., Yi, X., Liou, J., and He, J., (1985). A study on the physic-mechanical properties of culm wood of Phyllostachys Glauca of Shandong. *Journal of Bamboo Research*, Zhejiang Forestry Science Research Institute, Hangzhou, China 4 (2), Quoted in Janssen (1991).

Mallick, P. K. (2008). Fiber-reinforced composites: materials, manufacturing, and design. (third edition). *CRC press*.

Mannan, S., Paul Knox, J., and Basu, S. (2017). Correlations between axial stiffness and microstructure of a species of bamboo. *Royal Society open science*, *4*(1), 160412.

Mannan, S., Zaffar, M., Pradhan, A., and Basu, S. (2016). Measurement of microfibril angles in bamboo using Mueller matrix imaging. *Applied optics*, *55*(32), 8971-8978.

Martínez-Pañeda, E., and Gallego, R. (2015). Numerical analysis of quasi-static fracture in functionally graded materials. *International Journal of Mechanics and Materials in Design*, *11*(4), 405-424.

Martínez-Pañeda, E., and Gallego, R. (2015). Numerical analysis of quasi-static fracture in functionally graded materials. *International Journal of Mechanics and Materials in Design*, *11*(4), 405-424.

McClure, F.A. (1966). The bamboos: a fresh perspective. *Harvard University*, Cambridge, MA, p 347

Mitch, D., Harries, K. A., and Sharma, B. (2010). Characterization of splitting behavior of bamboo culms. *ASCE Journal of Materials in Civil Engineering*, 22, 1195–1199.

Moran, R., Webb, K., Harries, K., and García, J. J. (2017). Edge bearing tests to assess the influence of radial gradation on the transverse behavior of bamboo. *Construction and Building Materials*, *131*, 574-584.

Moreira, L. E. (1991). Desenvolvimento de estruturastreliadasespaciais de bamboo. *Ph.D. thesis*, Pontif*i*cia Universidade Cato*l*ica, Rio de Janeiro, Brazil (in Portuguese).

Moshtaghin, A. F., Franke, S., Keller, T., and Vassilopoulos, A. P. (2016). Random field-based modeling of size effect on the longitudinal tensile strength of clear timber. *Structural safety*, 58, 60-68.

Most, T., and Bucher, C. (2007). Probabilistic analysis of concrete cracking using neural networks and random fields. *Probabilistic engineering mechanics*, 22(2), 219-229.

National Building code of India (NBCI) (2005). Part 6: Structural design, Section 3 Timber and Bamboo: 3B Bamboo.

Nogata, F., and Takahashi, H. (1995). Intelligent functionally graded material: Bamboo. *Compos. Eng.* 5, 743.

Obataya, E., Kitin, P., and Yamauchi, H. (2007). Bending characteristics of bamboo (Phyllostachys pubescens) with respect to its fiber–foam composite structure. *Wood science and technology*, *41*(5), 385-400.

Ohrnberger, D. (1999). The bamboos of the world: annotated nomenclature and literature of the species and the higher and lower taxa. *Elsevier*, Amsterdam, p 585

Osorio, L., Trujillo, E., Van Vuure, A. W., and Verpoest, I. (2011). Morphological aspects and mechanical properties of single bamboo fibers and flexural characterization of bamboo/epoxy composites. *Journal of reinforced plastics and composites*, *30*(5), 396-408.

Osorio, L., Trujillo, E., Lens, F., Ivens, J., Verpoest, I., and Van Vuure, A. W. (2018). In-depth study of the microstructure of bamboo fibres and their relation to the mechanical properties. *Journal of Reinforced Plastics and Composites*, *37*(17), 1099-1113.

Ota, M. (1952). Studies on the properties of bamboo stem (part 9). On the relation between compressive strength parallel to grain and moisture content of bamboo splint. *Bulletin of Kyushu University of Forestry* 22 87-108. 'Quoted by Janssen (1981)'.

Palombini, F. L., Kindlein Jr, W., de Oliveira, B. F., and de Araujo Mariath, J. E. (2016). Bionics and design: 3D microstructural characterization and numerical analysis of bamboo based on X-ray microtomography. *Materials Characterization*, *120*, *357-368*.

Pan, B., Qian, K., Xie, H., and Asundi, A. (2009). Two-dimensional digital image correlation for in-plane displacement and strain measurement: a review. *Measurement science and technology*, *20*(6), 062001.

Pan, B., Wu, D., and Yu, L. (2012). Optimization of a three-dimensional digital image correlation system for deformation measurements in extreme environments. *Applied optics*, *51*(19), 4409-4419.

Penellum, M., Sharma, B., Shah, D. U., Foster, R. M., and Ramage, M. H. (2018). Relationship of structure and stiffness in laminated bamboo composites. *Construction and Building Materials*, *165*, 241-246.

Pierce-Brown, J., Neves, L. C., and Brown, D. L. (2018). Uncertainty quantification for random fields estimated from effective moduli of elasticity.

Rabin, B. H. and Shiota, K. (1995). Functionally gradient materials. *MRS bulletin* 20, 14-18. 'Quoted in Amada *et al.* (1997)'

Rahman, M. M., Rashid, M. H., Hossain, M. A., Hasan, M. T., and Hasan, M. K. (2011). Performance evaluation of bamboo reinforced concrete beam. *Int J Eng Technol*, *11*(4), 142-146.

Rawat, J. K., and Khanduri, D. C. (1999). The status of Bamboo and Rattan in India. *International Network for Bamboo and Rattan*.

Richard, M.J., (2013). Assessing the Performance of Bamboo Structural Components. *Doctoral dissertation*, University of Pittsburgh, PA, USA.

Richard, M.J., and Harries, K.A., (2015). On Inherent Bending in Tension Tests of Bamboo. *Wood Science and Technology*. Vol 49, No.1, pp 99-119

Richard, M. J., Gottron, J., Harries, K. A., and Ghavami, K. (2017). Experimental evaluation of longitudinal splitting of bamboo flexural components. *Proceedings of the Institution of Civil Engineers-Structures and Buildings*, *170*(4), 265-274.

Rousseau, C.E., and Tippur, H.V. (2000). Compositionally graded materials with cracks normal to the elastic gradient. *Acta. Mater*. 48, 4021–4033

Sakaray, H., Togati, N. V. K., and Reddy, I. R. (2012). Investigation on properties of bamboo as reinforcing material in concrete. *International Journal of Engineering Research and Application, 2*, 077-083.

Santare, M.H., and Lambros, J. (2000). Use of graded finite elements to model the behaviour of nonhomogeneous materials. J. Appl. Mech. Trans. ASME. 67, 819–822

Sattar, M. A., Kabir, M. F., and Bhattacharjee, D. K. (1990). Effect of age and height position of muli (Melocanna baccifera) and borak (Bambusa balcooa) bamboos on their physical and mechanical properties. *Bangladesh Journal of Forest Science, 19*(1/2), 29-37.

Seethalakshmi, K. K., and Kumar, M. S. M. (1998). Bamboos of India: a compendium. Kerala Forest Research Institute, Peechi, India and International Network for Bamboo and Rattan, New Delhi, p 342.

Sekhar, A. C., and Bhartari, R. K. (1960). Studies on strength of bamboos: a note on its mechanical behavior. *Indian Forest*. 86: 296–301

Shao, Z. P., Fang, C. H., and Tian, G. L. (2009). Mode I interlaminar fracture property of moso bamboo (Phyllostachys pubescens). *Wood Sci Technol* 45(5–6):527–536.

Shao, Z.P., Fang, C.H, Huang, S.X., and Tian, G.L. (2010). Tensile properties of Moso bamboo (Phyllostachys pubescens) and its components with respect to its fiber-reinforced composite structure. *Wood Sci. Technol*. 44, 655–666. doi: 10.1007/s00226-009- 0290-1

Shao, Z., and Wang, F. (2018). Mechanical Characteristics of Bamboo Structure and Its Components. *In The Fracture Mechanics of Plant Materials* (pp. 125-146). Springer, Singapore.

Sharma, B. (2010). Performance based design of bamboo structures. *Ph.D. thesis*, University of Pittsburgh, Pittsburgh, United States.

Sharma, B., Harries, K.A. and Ghavami, K. (2013). Methods of Determining Transverse Mechanical Properties of Full-Culm Bamboo. *Journal of Construction and Building Materials*, Vol 38, pp 627-637.

Sharma, B., Gatoo, A., Bock, M., and Ramage, M. H. (2015a). Engineered bamboo for structural applications. *Construction and Building Materials* 81, 66–73.

Sharma, B., Gatoo, A., and Ramage, M. H. (2015b). Effects of processing methods on the mechanical properties of engineered bamboo, *Construction and Building Materials 83,* 95–101.

Sharma, B., Bauer, H., Schickhofer, G., and Ramage, M. H. (2017). Mechanical characterization of structural laminated bamboo, *ICE Structures B* 170 (4), 250–264.

Sharma, B., Shah, D. U., Beaugrand, J., Janecek, E. R., Scherman, O. A., and Ramage, M. H. (2018). Chemical composition of processed bamboo for structural applications, *Cellulose* 25, 3255-3266.

Shigematsu, Y., (1958). Analytical investigation of the stem form of the important species of bamboo. *Bulletin of the Faculty of Agriculture* University of Miyazaki 3: 124–135 (in Japanese). [partially translated in 2016 by Ms Mutsuko Grant of the Natural Materials and Structures research group at the University of Cambridge]

Silva, E. C. N., Walters, M. C., and Paulino, G. H. (2006). Modeling bamboo as a functionally graded material: lessons for the analysis of affordable materials. *Journal of Materials Science*, *41*(21), 6991-7004.

Simulia, ABAQUS. V. 6.12(2017). Computer Software. *Dassault Systemes, Providence, RI, USA*.

Soderstrom, T. R. (1985). Bamboo yesterday, today and tomorrow. *J Am Bamb Soc* 6:4–16

Stapleton, C. M. A. (1994a). The bamboos of Nepal and Bhutan Part I: *Bambusa, Dendrocalamus, Melocanna, Cephalostachyum, Teinostachyum,* and *Pseudostachyum* (Gramineae: Poaceae, Bambusoideae). Edinb J Bot 51:1–32

Stapleton, C. M. A. (1994b). The bamboos of Nepal and Bhutan Part II: Arundinaria, Thamnocalamus, Borinda and Yushania (Gramineae: Poaceae, Bambusoideae). *Edinb J Bot* 51:275–295

Stapleton, C. M. A. (1994c). The bamboos of Nepal and Bhutan Part III: Drepanostachyum, Himalayacalamus, Ampelocalamus, Neomicrocalamus and Chimonoba mbusa. *Edinb J Bot* 51:301–330

Tadepalli, S. C., Erdemir, A., and Cavanagh, P. R. (2011). Comparison of hexahedral and tetrahedral elements in finite element analysis of the foot and footwear. *Journal of biomechanics*, 44(12), 2337-2343.

Tan, T., Rahbar, N., Allameh, S. M., Kwofie, S., Dissmore, D., Ghavami, K., and Soboyejo, W.O. (2011) 'Mechanical properties of functionally graded hierarchical bamboo structures'. *ActaBiomaterialia 7 (2011) 3796–3803*

Torres, L. A., Ghavami, K., and Garcia, J. J. (2007). A transversely isotropic law for the determination of the circumferential young's modulus of bamboo with diametric compression tests. *Latin American applied research*, *37*(4), 255-260.

Trujillo, D., Jangra, S., and Gibson, J., (2017). Flexural properties as a basis for bamboo strength grading, *ICE Structures and Building* Themed issue on bamboo in structures and buildings, Vol. 170, No. 4. pp 284-294

Vaessen, M. J. and Janssen, J. A. (1997). Analysis of the critical length of culms of bamboo in four-point bending tests. *HERON*, 42(2), 113-124.

Van Der Lugt, P., Van den Dobbelsteen, A. A. J. F., and Abrahams, R. (2003). Bamboo as a building material alternative for Western Europe? A study of the environmental performance, costs and bottlenecks of the use of bamboo (products) in Western Europe. *Journal of Bamboo and Rattan*, *2*(3), 205-223.

Virgo, J., Moran, R., Harries, K.A., Garcia, J. J., and Platt, S. (2017). Flat Ring Flexure Test for Full-Culm Bamboo. *Proceedings of 17th International Conference on Non-Conventional Materials and Technologies (17th NOCMAT),* Yucatán, México.

Vittouris, A., and Richardson, M. (2011). Designing vehicles for natural production: growing a velomobile from bamboo. *In Australasian transport research forum,* Adelaide, South Australia (pp. 28-30).

Vorontsova, M. S., Clark, L. G., Dransfield, J., Govaerts, R., and Baker, W. J. (2016). *World Checklist of Bamboos and Rattans: In Celebration of INBAR's 20th Anniversary*. Beijing.

Wang, H., Wang, H., Li, W., Ren, D., and Yu, Y. (2013). Effects of moisture content on the mechanical properties of moso bamboo at the macroscopic and cellular levels. *Bioresources*, *8*(4), 5475-5484.

Wei, X., Zhou, H., Chen, F., and Wang, G. (2019). Bending Flexibility of Moso Bamboo (Phyllostachys Edulis) with Functionally Graded Structure. *Materials*, *12*(12), 2007.

Widjaja, E. A., (1987). A revision of Malesian *Gigantochloa* (Poaceae-Bambusoideae). *Reinwardtia* 10:291–389.

Wong, K. M. (1993). Four new genera of bamboos (Gramineae: Bambusoideae) from Malesia. *Kew Bull* 48:517–532.

Wong, K. M. (1995). The morphology, anatomy, biology and classification of Peninsular Malaysian bamboos. *Univ Malaya Bot Monogr* 1:1–189.

Wong, K. M. (2005). *Mullerochloa*, a new genus of bamboo (Poaceae: Bambusoideae) from North-east Australia and notes on the circumscription of *Bambusa*. *Blumea* 50:425–441.

Xu, Q., Harries, K., Li, X., Liu, Q., and Gottron, J. (2014). Mechanical properties of structural bamboo following immersion in water. *Engineering Structures*, *81*, 230-239.

Yi, T. P., Shi, J. Y., Ma, L. S., Wang, H. T., and Yang, L. (2008). Iconographia Bambusoide arum Sinicarum. *Science Press*, Beijing, p 766.

Young, W. C., Budynas, R. G., and Sadegh, A. M. (2002). *Roark's formulas for stress and strain* (Vol. 7). New York: McGraw-Hill.

Yu, W. K., Chung, K. F., and Chan, S. L. (2003). Column buckling of structural bamboo. *Engineering Structures*, *25*(6), 755-768.

Yu, Y., Fei, B., Zhang, B., and Yu, X. (2007). Cell-wall mechanical properties of bamboo investigated by in-situ imaging nanoindentation. *Wood and Fiber Science*, *39*(4), 527-535.

Yu, H., Fei, B., Ren, H., and Jiang, Z. (2008). Variation in tensile properties and relationship between tensile properties and air-dried density for moso bamboo. *Frontiers of Forestry in China*, *3*(1), 127-130.

Yu, Y., Tian, G., Wang, H., Fei, B., and Wang, G. (2011a). Mechanical characterization of single bamboo fibers with nanoindentation and microtensile technique. *Holzforschung* 65(1), 113–11

Yu, Y., Jiang, Z., Fei, B., Wang, G., and Wang, H. (2011b). An improved microtensile technique for mechanical characterization of short plant fibers: a case study on bamboo fibers. *Journal of Materials Science*, *46*(3), 739-746.

Yu, Y., Wang, H., Lu, F., Tian, G., and Lin, J. (2014). Bamboo fibers for composite applications: a mechanical and morphological investigation. *Journal of materials science*, *49*(6), 2559-2566.

Zeng, Q., Zhang, Q., Lu, Q., Zhou, Y., Chen, N., Rao, J., and Fan, M. (2019). Wetting behavior and laminate bonding performance of profiled tangential surfaces of moso bamboo. *Indust. Crops Products*.

Zhang, Q., Jiang, S., and Tang, Y. (2001). Industrial Utilization on Bamboo. *INBAR Technical report* No. 26 .8.5.

Zhang, K., Wang, F., Liang, W., Wang, Z., Duan, Z., and Yang, B. (2018). Thermal and mechanical properties of bamboo fiber reinforced epoxy. *composites. Polymers, 10*(6), 608.

Zhang, Q. S. (2003). Attaching importance to science and innovation in the processing and utilization of bamboo timber in China. *J. Zhejiang For. Coll*. 20: 1–4.

Zhou, G. M., Wu, J. S., and Jiang, P. K. (2006). Effects of different management models on carbon storage in Phyllostachys pubescens forests. *J. Beijing Forestry Univ*. 28: 51–55.

Zhu, S. L., Ma, N. X., and Fu, M. Y., (1994). A compendium of Chinese bamboo. *China Forestry Publication House,* Beijing, p 241.

Zou, L., Jin, H., Lu, W. Y., and Li, X. (2009). Nanoscale structural and mechanical characterization of the cell wall of bamboo fibers. *Materials Science and Engineering: C*, *29*(4), 1375-1379.